TECHNISCHE UNIVERSITÄT MÜNCHEN
Lehrstuhl T31 für Theoretische Elementarteilchenphysik

The Fourth Generation: A Comprehensive Analysis

Christoph Promberger

Vollständiger Abdruck der von der Fakultät für Physik der Technischen Universität München zur Erlangung des akademischen Grades eines

Doktors der Naturwissenschaften (Dr. rer. nat.)

genehmigten Dissertation.

Vorsitzender:		Univ.-Prof. Dr. Stefan Schönert
Prüfer der Dissertation:	1.	Univ.-Prof. Dr. Andrzej J. Buras
	2.	Univ.-Prof. Dr. Alejandro Ibarra

Die Dissertation wurde am 24.5.2011 bei der Technischen Universität München eingereicht und durch die Fakultät für Physik am 6.6.2011 angenommen.

Zusammenfassung

Gegenstand dieser Arbeit ist eine systematische phänomenologische Analyse der als SM4 bezeichneten Standardmodell-Erweiterung durch eine vierte Generation von Quarks und Leptonen. In diesem Rahmen behandeln wir neben direkten Messungen der beteiligten Parameter vor allem elektroschwache Präzisionstests sowie Flavor- und CP-verletzende Observablen im Quark- wie im Lepton-Sektor.

Unsere Analyse elektroschwacher Präzisionstests widerlegt die weit verbreitete Annahme, eine vierte Generation würde durch solche Messungen bereits ausgeschlossen. Allerdings wird der verfügbare Parameterraum dadurch stark eingeschränkt, insbesondere die Mischung zwischen Quarks der dritten und vierten Familie sowie die möglichen Massendifferenzen innerhalb der neuen Quark- und Lepton-Duplets.

Im Weiteren berechnen wir mehr als 30 Prozesse im Quark- und Lepton-Sektor, in denen flavor-ändernde neutrale Ströme und/oder Verletzungen der CP-Symmetrie auftreten. Es wird gezeigt, wie im SM4 die bestehenden Anomalien im Unitaritätsdreieck sowie in den CP Asymmetrien $S_{\psi\phi}$ und $S_{\phi K_S}$ gleichzeitig behoben werden können. Eine globale numerische Untersuchung aller behandelter Observablen schränkt den Parameterraum weiter ein und offenbart charakteristische Korrelationsmuster zwischen bestimmten Messgrößen. Die hierdurch erhaltenen phänomenologischen Signaturen erlauben es, das SM4 eindeutig von anderen Modellen neuer Physik zu unterscheiden.

Abstract

The subject of this thesis is a systematic phenomenological analysis of the SM4, the standard model of particle physics extended by a fourth generation of quarks and leptons. In this framework we study the impact of direct measurements of the involved parameters, electroweak precision tests, as well as flavor and CP violation observables in the quark and lepton sector.

The analysis of electroweak precision tests disproves the commonly held assumption that a fourth generation would be excluded by these constraints. Yet, they impose severe bounds on the involved parameter space, particularly the quark mixing between the third and fourth family and the possible mass differences within the new quark and lepton doublets.

Subsequently, we calculate more than 30 flavor changing neutral current and CP-violating processes in the quark and lepton sector. It is shown how the existing anomalies in the unitarity triangle fits as well as in the CP asymmetries $S_{\psi\phi}$ and $S_{\phi K_S}$ can be explained simultaneously in the SM4. A global numerical analysis of all calculated observables further constrains the parameter space and reveals characteristic patterns of correlation between certain measurable quantities. The phenomenological signatures obtained in this way allow to clearly distinguish the SM4 from other new physics scenarios.

Contents

1. Introduction

The world around us is composed of only three types of basic elementary particles: *Up*- and *down-quarks* are the principal components of all atomic nuclei, and *electrons* constitute the atomic shells. In addition, there is the *electron neutrino* first postulated by Pauli in 1931 [1] and discovered in 1956 [2], which is too volatile to act as a constituent of matter. These four fermions – two quarks and two leptons – comprise what we call today the *first generation*.

The first indication that this is not the end of the story came from the discovery of the *muon* in 1937 [3,4], which is approximately 200 times heavier than the electron but identical in all other properties. The surprise which this particle caused in the physical community is probably best captured by I.I. Rabi's famous question: "Who ordered that?" [5]. Throughout the following decades, the *muon neutrino* was established as an individual particle (1962, [6]) and also further quarks were discovered: The *strange quark* occurring in strange particles (1944, [7,8]) and the *charmed quark*, predicted in 1970 [9] and verified in 1974 [10–13]. These four particles form the *second generation* and are basically similar to their first generation counterparts, differing only by their masses.

Very soon, it turned out that two generations cannot be the final truth either, when the *tau lepton* was discovered in 1975 [14], followed by the *bottom quark* in 1977 [15, 16]. The *third generation* was finally established by the detection of the unusually heavy *top quark* in 1995 [17, 18], and the identification of the *tau neutrino* in 2001 [19].

Today, these three generations of fermions form the basic building blocks of the most comprehensive and successful physical theory that has ever been conceived: the standard model of particle physics (SM). It describes three fundamental forces – the strong, weak and electromagnetic force – as so-called gauge interactions in a unified quantum field theory. In this intriguing theory, interactions arise from local (gauged) symmetries and are mediated by corresponding *gauge bosons*.

Among the successes of the SM are the predictions of several particles before they were observed – such as the W and Z boson, the gluon, the top and charm quark. Several properties of these particles have been predicted with good accuracy, and many other high precision measurements can be accommodated in the SM. In fact, today there is no experimental result directly contradicting the SM.

Nonetheless, the SM is far from being perfect since it suffers from several shortcomings of theoretical and experimental nature:

- First of all, it is not a complete theory as it does not contain gravity, the fourth fundamental force. This interaction is conclusively described by Einstein's theory of general relativity, which still cannot be cast into a quantum field theoretical framework.

- The SM cannot accommodate the large amount of dark matter (DM) in the universe that is required by astronomic observations. Furthermore, the predicted cosmological

constant which is assumed to be responsible for dark energy is more than 100 orders of magnitudes too large. Also the observed baryon asymmetry of the universe (BAU) requires an amount of CP violation which cannot be accounted for in the framework of the SM.

- Measurements of neutrino oscillations imply that these particles have tiny masses, which is not explained satisfactorily within the SM.

- One of the most important open issues of the SM is the Higgs mechanism which provides mass to the particles via the Higgs boson. The existence of this particle is of vital importance for the SM, but has not been proven yet and the current lower bounds on the Higgs mass create a strong tension on the SM parameter fits. Intensive efforts are being made to discover this particle in the coming years at the LHC.

- Although being theoretically self-consistent, the SM has several unnatural properties evoking riddles such as the hierarchy problem and the strong CP problem.

- Also the large number of 19 unrelated and arbitrary parameters (or even 28 when incorporating neutrino masses) in the SM is very unsatisfactory from a theoretical point of view. Most of these parameters occur in the *flavor sector*, i.e. they are related to the duplication of fermions in generations. Especially the masses and mixings of the quarks exhibit pronounced hierarchies which are not explained in the SM.

- Over the last years, certain tensions have been observed in the SM unitarity triangle fits and particularly in the CP asymmetries $S_{\psi\phi}$ and $S_{\phi K_S}$. These so-called flavor anomalies could be a hint for new physics (NP) beyond the SM, and will be treated thoroughly in the further course of this work.

Many of the problems of the SM are related with *flavor physics*, i.e. with the different types (flavors) of fermions, their arrangement in generations and their masses and mixings. But above all these open issues, the central question of flavor physics reads:

Why are there three generations of fermions?

Throughout the last decades, several attempts have been made to answer this question[1], but none has been satisfactory. In this work, we want to take another approach. We will not try to find an answer, but rather reply with a counter-question:

What if not?

Or in more detail:

What would be the consequences of adding another, fourth generation (4G) and what properties would it need to have?

[1] For example, the so-called 331 models [20–23] use an extended gauge group and the requirement of anomaly cancellation to predict the number of generations to be a multiple of 3.

The idea of a standard model extended by such a fourth generation (SM4) is probably as old as the SM itself, and has experienced a rather turbulent history since then. The most severe setback for the SM4 came in 1989 from the measurements of the Z boson width at SLAC [24, 25] and CERN [26–28]. These experiments determined the number of light neutrinos, into which the Z boson could decay, to be unambiguously equal to three. It is often claimed that this result would constrain the number of generations, but in fact it is rather a statement about the possible mass of new neutrinos which has to be above $\frac{M_Z}{2} \approx 45$ GeV. Of course, in times when the three SM neutrinos were assumed to be massless, such a heavy fourth neutrino appeared very unnatural. Therefore, the fourth generation was declared dead until the turn of the century that marked another turning point in this story: The detection of neutrino oscillations [29–32] proved that these particles are massive. Given the fact that the SM offers no convincing theory for the tiny neutrino masses, it became clear that the exclusion of the fourth generation due to its unnaturally heavy neutrino could have been slightly premature. However, another serious threat for the idea of four generations came from electroweak precision measurements at SLAC, LEP and Tevatron, which put very stringent bounds on any model of particle physics. Particularly the so-called oblique parameters extracted from this data were the basis for several papers by Erler and Langacker who claimed that under certain assumptions the SM4 would be excluded with up to 6 σ [33–35]. On the other hand, a certain resurrection of the fourth generation was initiated by Maltoni et al. in 1999 [36], followed by a number of works [36–41] objecting Erler and Langacker and pointing out that the SM4 is in good agreement with electroweak precision data when some assumptions are relaxed. In the last few years, this has led to a considerable revival of the fourth generation with more than 50 papers on this subject published over the last three years[2]. Among the most important topics studied were the impact of a 4G on Higgs physics [39], electroweak precision tests [38–41] and flavor physics [44–50]. In this context, Lenz et al. [49,51] have studied the constraint on the mixing between the fourth and third generation by using flavor changing neutral current (FCNC) processes and electroweak precision data, deriving interesting bounds on this mixing which we will also address in the course of our work.

The keen interest in the fourth generation might come as a surprise taking into account that the SM4 does not tackle any of the known hierarchy and naturalness problems mentioned above[3]. But apart from being the most simple extension of the SM (hereafter also referred to as SM3), the inclusion of a fourth generation has a number of profound implications that make it interesting to consider:

1. A fourth generation can remove the tension between the SM3 fit and the lower bound on the Higgs mass from LEP II. Indeed, as pointed out in [37, 39, 52], a heavy Higgs boson does not contradict EWPT as soon as the 4G exists.

2. $SU(5)$ gauge coupling unification could in principle be achieved without supersymmetry [53], although the present lower bound on the masses of 4G quarks and the appearance of Landau poles in Yukawa couplings well below the GUT scales practi-

[2] A good overview is given in [42, 43], for instance.

[3] This holds at least in the setup with perturbative Yukawa couplings which we will assume throughout this work.

cally excludes this possibility if one wants to stay within a perturbative framework at short-distance scales.

3. The inclusion of a fourth generation can enhance the amount of CP violation by a factor of up to 10^{13} as compared to the SM3. This effect could enable electroweak baryogenesis and explain the large baryon asymmetry of the universe which cannot be accommodated in the SM [54–56].

4. Dynamical breaking of electroweak symmetry might be triggered by the presence of 4G quarks [57–63]. However, since it is in the very nature of non-perturbative Yukawa couplings to defy direct calculations, there is no explicit model for this scenario up to now.

5. The neutrino of the fourth generation is a possible dark matter candidate [39, 64, 65]. However, the required stability and existing direct search limits would necessitate unnaturally small mixing and a very high mass of the fourth neutrino. This problem could be solved by introducing a new $B - 4L_4$ gauge symmetry, as recently shown in [64].

6. The structure of the lepton sector in the SM4 can be interesting as shown in [66]: a heavy (mostly Dirac) 4G neutrino in addition to very light (mostly Majorana) neutrinos can be obtained in a setup with electroweak symmetry breaking in warped extra dimensions.

7. Most importantly, from the point of view of the present work, certain anomalies present in flavor-changing processes could in principle be resolved [45–47, 67].

In this thesis, we will present a detailed analysis of the SM4 including direct measurements and electroweak precision tests as well as flavor and CP violation in the quark and lepton sector. It is based on our publications about fourth generation effects on flavor violation [67], the charm system [68] and lepton flavor violation [69] and extends these works. Our work is comprehensive in the sense that we cover all active constraints on the SM4 and treat all relevant flavor and CP violation observables known today.[4] In particular:

- We will analyze the latest data from direct searches for fourth generation fermions and tree-level CKM measurements in order to derive constraints on the involved parameters.

- From the study of electroweak precision tests (oblique and non-oblique corrections) we will infer important bounds on the parameters of the SM4. Especially the analysis of possible mass splittings and their dependence on the 3-4 mixing s_{34} goes beyond the results that can be found in the literature.

[4] As we have seen above, there are many possible fields of application in the vicinity of a fourth generation which we do not discuss. Most of these possible virtues of the SM4 – for instance gauge coupling unification, electroweak baryogenesis, dynamical electroweak symmetry breaking and a 4G dark matter candidate – are only hypothetical and need further assumptions in order to constrain the SM4.

- We will present a straightforward way to generalize the known SM3 expressions and give the detailed SM4 formulae for a large number of flavor and CP observables in the quark and lepton sector.

- We will establish a number of correlations between various observables that should allow us to distinguish this NP scenario from the Littlest Higgs model with T-parity (LHT), the Randall-Sundrum model with custodial protection (RSc) and supersymmetric flavor models that have been analyzed in [70–75] recently. We will also carefully study how these correlations depend on the size of the 4G mixing angles and phases.

- For the most interesting observables, we will investigate the departures from models with (constrained) minimal flavor violation ((C)MFV), taking into account all existing constraints.

- We will demonstrate transparently how certain anomalies observed in the unitarity triangle fits and in the CP asymmetries $S_{\psi\phi}$ and $S_{\phi K_S}$ can be resolved simultaneously and how these solutions affect other observables.

- We will address the question how the additional five parameters of the 4×4 quark mixing matrix, θ_{14}, θ_{24}, θ_{34}, δ_{14} and δ_{24}, could — in principle — be determined by means of the mixing-induced CP asymmetries $S_{\psi\phi}$ and $S_{\psi K_S}$, the $B^0_{d,s} - \bar{B}_{d,s}$ mixing mass differences $\Delta M_{d,s}$, ϵ_K and the branching ratios for the rare decays $K^+ \to \pi^+ \nu\bar{\nu}$, $K_L \to \pi^0 \nu\bar{\nu}$, $B_{s,d} \to \mu^+\mu^-$, $B \to X_s \nu\bar{\nu}$.

- We will study the implications of bounds from lepton flavor violation (LFV) on the corresponding parameters in the lepton sector.

- On the theoretical side, we will introduce certain consistency conditions between the SM3 and SM4 mixing angles which can be used to eliminate "fine-tuned" values in parameter space. The remaining cases can be classified according to the scaling of the 4G mixing angles with the Cabibbo angle, and for each individual case an SM4 generalization of the Wolfenstein parametrization can be constructed.

Our work is organized as follows: In Section 2, we will introduce the SM4 with its new particles and parameters and discuss the impact of direct measurements on the corresponding masses and mixing matrix elements. Section 3 is dedicated to the analysis of electroweak precision observables in the presence of four generations. This will allow us to derive further important constraints on the involved parameters. In Section 4, we will calculate a large number of flavor and CP observables both in the quark and the lepton sector. These observables will be analyzed numerically in Section 5, under particular consideration of correlations between various quantities. There we will also estimate approximate upper bounds on several observables, study the anatomy of flavor effects in the SM4 and outline an efficient procedure to constrain the new mixing angles. Finally, in Section 6 we summarize our main findings. The effective one-loop vertices and functions used throughout this work are collected in the appendix.

2. The SM4

2.1. Particles and Properties

2.1.1. Extending the SM

The standard model of particle physics (SM) has been very successful in predicting and explaining measurements at high precision while on the theoretical side, it is of captivating conceptual simplicity. Nevertheless, as discussed in the introduction, it has its shortcomings and therefore physicists are eager to go beyond and extend the SM to a more general new physics (NP) model. Many of these extensions have been conceived and studied throughout the last decades, most of them requiring the inclusion of additional fermions from general principles, for instance supersymmetry (SuSy), extra dimensions (ED) or grand unified theories (GUTs). Instead of this top-down perspective, one can also follow the bottom-up approach and study the possibilities to add extra fermions, i.e. spin-$\frac{1}{2}$-particles to the SM [42]. These can be characterized by their behaviour under the electroweak gauge group $\mathrm{SU}(2)_L \times \mathrm{U}(1)$: *Chiral fermions* have left- and right-handed components transforming differently under $\mathrm{SU}(2)_L \times \mathrm{U}(1)$. All fermions present in the SM are of this type, with the left-handed components transforming as doublets, while the right-handed parts are singlets under $\mathrm{SU}(2)_L$. In some models one also adds mirror chiral doublets, where the right handed components transform as doublets while the left-handed are invariant under $\mathrm{SU}(2)_L$. Chiral fermions are strictly massless before the electroweak symmetry breaking. On the other hand, *non-chiral* (also known as *vector-like*) fermions have left- and right- handed components transforming similarly under the electroweak gauge group. So far only chiral fermions have been observed, and therefore it appears most natural to take this type when including new fermions.

When treating chiral doublets or singlets, one is in constant danger of evoking chiral anomalies. In the SM these are cancelled spectacularly within each generation of quarks and leptons, and in this work we will make use of this mechanism by introducing a full, sequential generation[1]. The particles included in this fourth generation (4G) will be denoted as

$$b', \qquad t', \qquad \ell_4, \qquad \nu_4, \tag{2.1}$$

where the up- and down-like quarks (t', b') and leptons (ν_4, ℓ_4) have the same quantum numbers as their standard model partners.

[1] It is worth mentioning that there are several models treating the problems of chiral anomalies in a more creative way. For example, the so-called 331 models [20–23] use an extended gauge group and the requirement of anomaly cancellation to predict the number of generations to be 3.

In the further course of this section we will study the most basic properties of these particles, such as their masses and mixings, and give the experimental bounds on these parameters.

2.1.2. Direct Searches and Mass Limits

2.1.2.1. Mass Limits for Fourth Generation Quarks

The most straightforward way to look for fourth generation quarks is the analysis of collider data with respect to distinctive signatures arising from these intermediate particles. Numerous of such studies have been performed with data from LEP and CDF, and even the first LHC results obtained from the CMS experiment have been analyzed in this sense [76]. Since the amount of data collected at CDF is still larger than that from CMS, we will restrict our discussion to the former.

There are basically three CDF data samples from $\sqrt{s} = 1.96$ TeV $p\bar{p}$ collisions that are taken as possible signatures for new heavy quarks [77]:

The $\ell + 4j$ sample, requiring a single lepton and at least four jets in the detector, tracks the decay $t' \to W\{q = d, s, b\}$, which occurs in the process

$$p\bar{p} \to t'\bar{t}' \to (W \to \ell\nu)q(W \to qq')q\,. \tag{2.2}$$

Analyzing 4.6 fb^{-1} of data, CDF found $m_{t'} > 335$ GeV [78] under the assumption that $\mathrm{Br}(t' \to W\{q = d, s, b\}) = 100\%$.

The $\ell + 5j$ sample is generated by the decay $b' \to Wt$, occurring in

$$p\bar{p} \to b'\bar{b}' \to WtW\bar{t} \to WWbWW\bar{b} \to (\ell^{\pm}\nu)(qq')b(qq')(qq')\bar{b}\,, \tag{2.3}$$

which is identified by the detection of one or more leptons, at least five jets (one with a b tag) and missing transverse energy of more than 20 GeV. Analyzing 4.8 fb^{-1} of data, CDF found $m_{b'} > 385$ GeV [79], assuming $\mathrm{Br}(b' \to Wt) = 100\%$.

The $\ell^{\pm}\ell^{\pm}jb\not{E}_T$ sample is defined by two same-charge leptons, at least two jets (at least one with a b tag) and missing transverse energy of at least 20 GeV, generated by

$$p\bar{p} \to b'\bar{b}' \to WtW\bar{t} \to WWbWW\bar{b} \to (\ell^{\pm}\nu)(qq')b(qq')(\ell^{\pm}\nu)\bar{b}\,. \tag{2.4}$$

Searching in 2.7 fb^{-1} of data and assuming $\mathrm{Br}(b' \to Wt) = 100\%$, CDF [80] found $m_{b'} > 338$ GeV.

Obviously, none of these studies has found evidence for new heavy quarks, but the stated lower mass bounds are important inputs for our study of the fourth generation. However, these numbers have to be handled with care since it is often assumed that new quarks decay exclusively via certain channels, which does not hold in general. In order to obtain reliable bounds on $m_{b'}$ and $m_{t'}$, we will therefore follow the recent study of Flacco et al. [77]. Combining data from the three samples introduced above, one is able to derive lower bounds

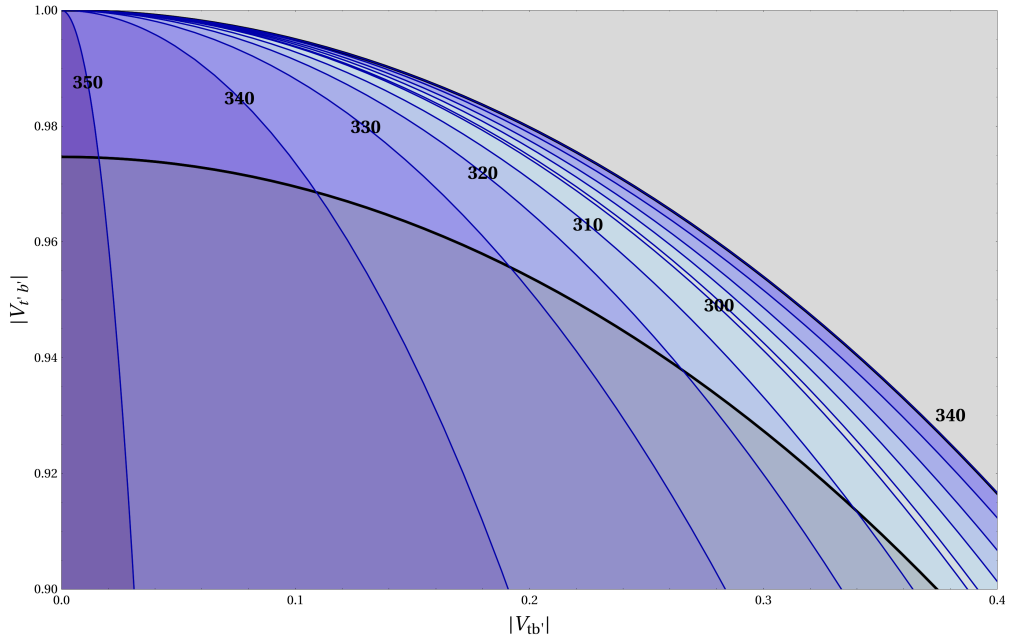

Figure 2.1.: Lower limits on $m_{b'}$ (in GeV) depending on the mixing matrix elements $|V_{tb'}|$ and $|V_{t'b'}|$, for a mass splitting of $m_{t'} - m_{b'} \approx 50$ GeV. The gray regions are excluded by unitarity in combination with $0 \leq |V_{ub'}|^2 + |V_{cb'}|^2$ (upper bound) and $|V_{ub'}|^2 + |V_{cb'}|^2 \lesssim 0.22^2$ (lower bound, s. (2.30)).

on the new quark masses in dependence on the mixing matrix elements $V_{tb'}$ and $V_{t'b'}$. We reproduced these results as shown in Fig. 2.1.

The picture shows that $m_{b'} \gtrsim 300$ GeV for a mass splitting of $m_{t'} - m_{b'} \approx 50$ GeV, which is preferred by electroweak precision data (s. Section 3.2.3). It has been demonstrated in [77] that for different mass splittings the parameter dependence of the minimal b' mass does vary, but the lower bound of 300 GeV essentially remains unchanged. So for our further analysis we choose

$$m_{b'}, m_{t'} \geq 300 \text{ GeV} . \tag{2.5}$$

2.1.2.2. Mass Limits for Fourth Generation Leptons

The matter of fourth generation lepton masses is one of the most severe shortfalls of the SM4: Measurements of the Z boson width at LEP [81] allow for only three light neutrinos into which the Z can decay. This forces the mass of a potential fourth neutrino to be above $M_Z/2 \approx 45$ GeV, in strong contrast to the first three neutrinos with $m_{\nu_i} \lesssim 1$ eV. The smallness of these three masses can be explained by the so-called seesaw mechanism in which the existence of heavy Majorana neutrinos leads to a mass suppression of the observed neutrinos. While the usual Dirac masses could be of the order of the electroweak scale, the Majorana masses are assumed to be generated by effects at higher energies, for instance at the GUT scale. This is obviously beyond the scope of the SM, so the seesaw mechanism crucially depends on the assumption of new physics. The existence of a very massive fourth neutrino would certainly require major changes in the mechanism of neutrino mass generation. Although this would complicate the quest for a unified model, it would

surely be premature to exclude the fourth generation solely due to this fact.

The strongest bounds on 4G lepton masses are obtained from direct searches performed at the L3 detector at LEP [82]. The data obtained from e^+e^- collisions at $\sqrt{s} \approx 200$ GeV has been searched through for signatures from these particles due to the processes

$$e^+e^- \to \nu_4\bar{\nu}_4 \to \ell^+\ell^-(W^+ \to \ell^+\nu_\ell/q\bar{q}')(W^- \to \ell^-\bar{\nu}_\ell/q\bar{q}')\,, \tag{2.6a}$$

$$e^+e^- \to \ell_4^+\ell_4^- \to \nu_\ell\bar{\nu}_\ell(W^+ \to \ell^+\nu_\ell/q\bar{q}')(W^- \to \ell^-\bar{\nu}_\ell/q\bar{q}')\,. \tag{2.6b}$$

As in the hadronic case, LEP has not found evidence for new heavy particles, leading to lower limits on the hypothetic masses of

$$m_{\ell_4} > 110.8 \text{ GeV}\,, \qquad m_{\nu_4} > \begin{cases} 90.3 \text{ GeV for Dirac } \nu \\ 80.5 \text{ GeV for Majorana } \nu\,. \end{cases} \tag{2.7}$$

The fact that the mass bound is weaker in the case of a Majorana type neutrino is due to a different mass dependence of the cross section compared to the Dirac case.

2.1.2.3. Upper Mass Bounds from Perturbativity

We have seen above that stringent lower bounds on fourth generation fermion masses can be derived from direct measurements. On the other hand, no experimental result constrains these masses from above. Nevertheless, there is a theoretical argument providing such a bound: As argued in [83], the bound from partial wave unitarity is reached at some high fermion mass scale, which is around 500 GeV for quarks and 1 TeV for leptons. For such ultraheavy fermions, the weak interactions of the $\mathrm{SU}(2)_L \times \mathrm{U}(1)$ gauge theory would become strong and the perturbation expansion would fail. This does not mean that such high masses are excluded in principle, but the theory would not be predictive any more. For the further course of this work we will therefore set the upper bound on quarks and leptons to

$$m_{b'}, m_{t'}, m_{\ell_4}, m_{\nu_4} \leq 600 \text{ GeV}\,. \tag{2.8}$$

2.2. Fermion Mixing

The concept of fermion mixing, first introduced by Cabibbo in 1963 [84] and extended to three generations by Kobayashi and Maskawa [85], is a central element in our theory of elementary particles. Not only does it help to preserve the universality of the weak interactions in the SM, but it also offers a successful explanation for the origin of CP violation. In the SM and many of its extensions the fermion mixing matrices for quarks and leptons, V_{CKM} and U_{PMNS} respectively, are responsible for most of the free parameters and therefore are an essential ingredient for any calculation of observables. This is of course also the case in the SM4, where the number of mixing parameters is increased considerably compared to the case of three generations.

In the following, we will elaborate on the properties of the mixing matrices, i.e. their parametrization, measurements and several theoretical considerations which will be useful in the further course of our work.

2.2.1. The 4×4 Quark Mixing Matrix V_{SM4}

2.2.1.1. Parametrization and Unitarity

Parametrization

Considering a SM-like model with N quark generations, the mixing matrix is basically a $N \times N$ unitary matrix $V^{(N)} \in U(N)$. As we know from group theory, the number of parameters determining $V^{(N)}$ is N^2, consisting of $\frac{N(N-1)}{2}$ rotation angles and $\frac{N(N+1)}{2}$ complex phases. In the physical context, $2N-1$ of these phases are relative phases which can be rotated away, so there remains a total number of

$$(N-1)^2 \text{ CKM parameters} = \frac{N(N-1)}{2} \text{ angles} + \frac{(N-1)(N-2)}{2} \text{ phases}\,. \tag{2.9}$$

Applying this to the four generation case, one obtains for the 4×4 quark mixing matrix V_{SM4} a total number of

$$9 \text{ CKM parameters} = 6 \text{ angles} + 3 \text{ phases}\,, \tag{2.10}$$

as compared to the SM3 case with

$$4 \text{ CKM parameters} = 3 \text{ angles} + 1 \text{ phase}\,. \tag{2.11}$$

There are several ways to parametrize V_{SM4}, which are all valid but differ in their usability for phenomenological applications. We will use the standard parametrization of the SM4 mixing matrix introduced in [86,87], in which V_{SM4} is given by six rotations in the i-j plane $V_{ij} \in \mathrm{SU}(2)$, parametrized by the angles θ_{ij} $(i<j)$ and phases δ_{ij} $(i<j-1)$. The 4×4 CKM matrix then reads

$$\begin{aligned}
V_{\mathrm{SM4}} &= \underbrace{V_{34}V_{24}V_{14}}_{V^{(\mathrm{new})}_{\mathrm{SM4}}} \times \underbrace{V_{23}V_{13}V_{12}}_{V^{(4)}_{\mathrm{SM3}}} \\
&= \begin{pmatrix}
c_{14} & 0 & 0 & e^{-i\delta_{14}}s_{14} \\
-e^{i(\delta_{14}-\delta_{24})}s_{14}s_{24} & c_{24} & 0 & e^{-i\delta_{24}}c_{14}s_{24} \\
-e^{i\delta_{14}}c_{24}s_{14}s_{34} & -e^{i\delta_{24}}s_{24}s_{34} & c_{34} & c_{14}c_{24}s_{34} \\
-e^{i\delta_{14}}c_{24}c_{34}s_{14} & -e^{i\delta_{24}}c_{34}s_{24} & -s_{34} & c_{14}c_{24}c_{34}
\end{pmatrix} \\
&\quad \times \begin{pmatrix}
c_{12}c_{13} & c_{13}s_{12} & e^{-i\delta_{13}}s_{13} & 0 \\
-c_{23}s_{12} - e^{i\delta_{13}}c_{12}s_{13}s_{23} & c_{12}c_{23} - e^{i\delta_{13}}s_{12}s_{13}s_{23} & c_{13}s_{23} & 0 \\
s_{12}s_{23} - e^{i\delta_{13}}c_{12}c_{23}s_{13} & -e^{i\delta_{13}}c_{23}s_{12}s_{13} - c_{12}s_{23} & c_{13}c_{23} & 0 \\
0 & 0 & 0 & 1
\end{pmatrix}
\end{aligned} \tag{2.12a}$$

$$= \begin{pmatrix} c_{12}c_{13}c_{14} & c_{13}c_{14}s_{12} & c_{14}s_{13}e^{-i\delta_{13}} & s_{14}e^{-i\delta_{14}} \\ \begin{array}{c} -c_{23}c_{24}s_{12} - c_{12}c_{24}s_{13}s_{23}e^{i\delta_{13}} \\ -c_{12}c_{13}s_{14}s_{24}e^{i(\delta_{14}-\delta_{24})} \end{array} & \begin{array}{c} c_{12}c_{23}c_{24} - c_{24}s_{12}s_{13}s_{23}e^{i\delta_{13}} \\ -c_{13}s_{12}s_{14}s_{24}e^{i(\delta_{14}-\delta_{24})} \end{array} & \begin{array}{c} c_{13}c_{24}s_{23} \\ -s_{13}s_{14}s_{24}e^{-i(\delta_{13}+\delta_{24}-\delta_{14})} \end{array} & c_{14}s_{24}e^{-i\delta_{24}} \\ \begin{array}{c} -c_{12}c_{23}c_{34}s_{13}e^{i\delta_{13}} + c_{34}s_{12}s_{23} \\ -c_{12}c_{13}c_{24}s_{14}s_{34}e^{i\delta_{14}} \\ +c_{23}s_{12}s_{24}s_{34}e^{i\delta_{24}} \\ +c_{12}s_{13}s_{23}s_{24}s_{34}e^{i(\delta_{13}+\delta_{24})} \end{array} & \begin{array}{c} -c_{12}c_{34}s_{23} - c_{23}c_{34}s_{12}s_{13}e^{i\delta_{13}} \\ -c_{12}c_{23}s_{24}s_{34}e^{i\delta_{24}} \\ -c_{13}c_{24}s_{12}s_{14}s_{34}e^{i\delta_{14}} \\ +s_{12}s_{13}s_{23}s_{24}s_{34}e^{i(\delta_{13}+\delta_{24})} \end{array} & \begin{array}{c} c_{13}c_{23}c_{34} \\ -c_{13}s_{23}s_{24}s_{34}e^{i\delta_{24}} \\ -c_{24}s_{13}s_{14}s_{34}e^{i(\delta_{14}-\delta_{13})} \end{array} & c_{14}c_{24}s_{34} \\ \begin{array}{c} -c_{12}c_{13}c_{24}c_{34}s_{14}e^{i\delta_{14}} \\ +c_{12}c_{23}s_{13}s_{34}e^{i\delta_{13}} \\ +c_{23}c_{34}s_{12}s_{24}e^{i\delta_{24}} - s_{12}s_{23}s_{34} \\ +c_{12}c_{34}s_{13}s_{23}s_{24}e^{i(\delta_{13}+\delta_{24})} \end{array} & \begin{array}{c} -c_{12}c_{23}c_{34}s_{24}e^{i\delta_{24}} + c_{12}s_{23}s_{34} \\ -c_{13}c_{24}c_{34}s_{12}s_{14}e^{i\delta_{14}} \\ +c_{23}s_{12}s_{13}s_{34}e^{i\delta_{13}} \\ +c_{34}s_{12}s_{13}s_{23}s_{24}e^{i(\delta_{13}+\delta_{24})} \end{array} & \begin{array}{c} -c_{13}c_{23}s_{34} \\ -c_{13}c_{34}s_{23}s_{24}e^{i\delta_{24}} \\ -c_{24}c_{34}s_{13}s_{14}e^{i(\delta_{14}-\delta_{13})} \end{array} & c_{14}c_{24}c_{34} \end{pmatrix} , \tag{2.12b}$$

where we defined

$$s_{ij} = \sin\theta_{ij} , \qquad c_{ij} = \cos\theta_{ij} . \tag{2.13}$$

In the limiting case of vanishing mixing with the 4G quarks ($\theta_{i4} = \delta_{j4} = 0$), the standard parametrization of the 3×3 CKM matrix is recovered (second line in (2.12a)).

Note that in (2.12), just as in the SM3 case, all angles θ_{ij} can be chosen to lie in the interval $[0, \pi/2]$. This fact, which is sometimes forgotten (e.g. in [51]) can be shown in the following way [88]: In the above parametrization, $V_{\rm SM4}$ is a product of six matrices $V_{ij} \in SU(2)$, $i, j = 1, ..., 4$, consecutively mixing the different quark generations. The phases of each of these matrices can be factored out via

$$\begin{aligned} V_{ij} &= I_i(\alpha)\bar{V}_{ij}I_i(\beta)I_j(\gamma) = I_j(\alpha')\bar{V}_{ij}I_i(\beta')I_j(\gamma') \\ &= I_i(\alpha'')I_j(\beta'')\bar{V}_{ij}I_i(\gamma'') = I_i(\alpha''')I_j(\beta''')\bar{V}_{ij}I_j(\gamma''') , \end{aligned} \tag{2.14}$$

where

$$[I_i(\alpha)]_{jk} = \delta_{j,k}e^{i\alpha\delta_{i,j}} \tag{2.15}$$

are phase operators and $\bar{V}_{ij}$ are $SO(2)$ rotation matrices with angles θ_{ij} in the interval $[0, \pi/2]$. Each of the four sets of angles in (2.14) obeys one relation $\alpha + \beta + \gamma = 0$ etc., such that each V_{ij} has three parameters. Clearly, with 6×3 parameters $V_{\rm SM4}$ must have 9 redundant phases. However, these unphysical phases will either cancel or be rotated away by quark field redefinitions. To see this, write $V_{\rm SM4}$ as

$$V_{\rm SM4} = V_{34}V_{24}V_{14}V_{23}V_{13}V_{12} , \tag{2.16}$$

factor out the phases as done in (2.14), and rearrange the phase operators in that expression, repeatedly using $[I_i(\alpha), I_j(\beta)] = 0$ and (2.14). In doing so, all but three of those operators can be moved to the extreme left or right of $V_{\rm SM4}$, where they can be absorbed into phase redefinitions of the quark fields and one ends up with the standard parametrization

$$V_{\rm SM4} = \bar{V}_{34}I_4(\delta_{24})\bar{V}_{24}I_4(-\delta_{24})I_4(\delta_{14})\bar{V}_{14}I_4(-\delta_{14})\bar{V}_{23}I_3(\delta_{13})\bar{V}_{13}I_3(-\delta_{13})\bar{V}_{12} , \tag{2.17}$$

with all angles θ_{ij} in $[0, \pi/2]$ and phases δ_{ij} in $[0, 2\pi]$.

A thorough analysis of $V_{\rm CKM4}$ in the framework of minimal flavor violation (MFV) can be found in our work [67].

CKM Factors and Unitarity

In writing the formulae for the observables of interest, it is useful to use the unitarity of the matrix $V_{\rm SM4}$. To this end, we define the generalized CKM factors

$$\lambda_{u_i}^{(d_a d_b)} \equiv V_{u_i d_a} V_{u_i d_b}^* \,, \qquad \lambda_{d_i}^{(u_a u_b)} \equiv V_{u_b d_i} V_{u_a d_i}^* \,, \tag{2.18}$$

obeying the unitarity relations

$$\sum_{i=1}^{4} \lambda_{u_i}^{(d_a d_b)} = \delta^{ab} \,, \qquad \sum_{i=1}^{4} \lambda_{d_i}^{(u_a u_b)} = \delta^{ab} \,. \tag{2.19}$$

In our analysis of FCNC observables, we will especially be interested in mixing within the K, B and D system, so it is useful to define the corresponding special CKM factors

$$\lambda_i^{(K)} \equiv \lambda_i^{(ds)} = V_{is}^* V_{id} \,, \qquad \lambda_i^{(B_d)} = \lambda_i^{(db)} = V_{ib}^* V_{id} \,, \qquad \lambda_i^{(B_s)} = \lambda_i^{(ds)} = V_{ib}^* V_{is} \,, \tag{2.20a}$$

$$\lambda_j^{(D)} \equiv \lambda_j^{(cu)} = V_{cj}^* V_{uj} \,, \tag{2.20b}$$

with $i \in \{u, c, t, t'\}$ and $j \in \{d, s, b, b'\}$.

The unitarity relations are then written as

$$\lambda_u^{(A)} + \lambda_c^{(A)} + \lambda_t^{(A)} + \lambda_{t'}^{(A)} = 0 \,, \tag{2.21a}$$

$$\lambda_d^{(D)} + \lambda_s^{(D)} + \lambda_b^{(D)} + \lambda_{b'}^{(D)} = 0 \,, \tag{2.21b}$$

with $A \in \{K, B_d, B_s\}$. These relations allow to eliminate $\lambda_u^{(A)}$, respectively $\lambda_d^{(D)}$, in any given observable, so that only $\lambda_c^{(A)}$, $\lambda_t^{(A)}$ and $\lambda_{t'}^{(A)}$, respectively $\lambda_s^{(D)}$, $\lambda_b^{(D)}$ and $\lambda_{b'}^{(D)}$, enter the final expressions.

2.2.1.2. Tree Level CKM Constraints

Direct Measurements of CKM Matrix Elements

Depending on the model being studied, flavor and CP violation observables usually involve a number of different parameters simultaneously. The measurements of such observables provide rather complex bounds on the involved parameter space, which will be treated in later sections. But there are also several processes which are dominated by one single CKM element since they can proceed at tree level in the SM. The bounds arising from this type of observables, called *tree level constraints*, are presented in Table 2.1.

Most of the CKM elements shown in the table are independent from the considered model. However, for two quantities the situation is not so simple, which we will discuss in the following.

The first of these observables is $|V_{tb}|$, which is obtained from single top-quark production [99, 100] and extracted from the ratio

$$R = \frac{\mathcal{B}(t \to Wb)}{\mathcal{B}(t \to Wq)} \,. \tag{2.22}$$

Element	value	relative error	source
$\lvert V_{ud}\rvert$	0.97425 ± 0.00022	0.022%	Superallowed $0^+ \to 0^+$ nuclear β decays [89]
$\lvert V_{us}\rvert$	0.2252 ± 0.0009	0.40%	Semileptonic K-decays [90]
$\lvert V_{ub}\rvert$	$(3.89 \pm 0.44) \times 10^{-3}$	11%	Semileptonic B-decays [91]
$\lvert V_{cd}\rvert$	0.230 ± 0.011	4.8%	Semileptonic D-decays [92]
$\lvert V_{cs}\rvert$	1.023 ± 0.036	3.5%	(Semi-)Leptonic D-decays [93–98]
$\lvert V_{cb}\rvert$	$(40.6 \pm 1.3) \times 10^{-3}$	3.2%	Semileptonic B to charm decays [91]
$\lvert V_{tb}\rvert_{\rm SM3}$	(0.88 ± 0.07)	8.0%	Single top-quark production [99, 100]
γ	$(71^{+21}_{-25} \pm 2)^\circ$	38%	CKM fitter [101], + 2° error from 4th generation [102]

Table 2.1.: Direct Measurements of the CKM matrix elements [103]

In the SM3, this ratio is simply given by $R = |V_{tb}|^2$, and one obtains from the measurements

$$|V_{tb}|^{(\rm exp)}_{\rm SM3} = \sqrt{R^{(\rm exp)}} = (0.88 \pm 0.07)\,. \tag{2.23}$$

Including a fourth generation, the ratio is changed to

$$R = \frac{|V_{tb}|^2}{\sum_{q=b,s,d} |V_{tq}|^2} = \frac{|V_{tb}|^2}{1 - |V_{tb'}|^2}\,, \tag{2.24}$$

so the resulting matrix element is diminished by a factor of $\sqrt{1 - |V_{tb'}|^2}$,

$$|V_{tb}| = |V_{tb}|_{\rm SM3} \cdot \sqrt{1 - |V_{tb'}|^2}\,. \tag{2.25}$$

This subtlety has been missed in previous analyses, such as [49, 104].

In the SM3, the CKM phase

$$\gamma \equiv \mathrm{Arg}\left(-\frac{V_{ud}V^*_{ub}}{V_{cd}V^*_{cb}}\right)\,, \tag{2.26}$$

is simply equal to the CKM phase δ_{13}. Its value has been determined by CKM fitter [101],

$$\gamma = (71^{+21}_{-25})^\circ\,. \tag{2.27}$$

Introducing a fourth generation, the simple parameter dependence is lost. However, as shown in [102], the fitted value in (2.27) is only disturbed by an additional error of $\pm 2^\circ$.

Parameter Ranges

Taking the tree level constraints from Table 2.1 and using the unitarity of the 4×4 CKM matrix, one is able to constrain the unmeasured mixing matrix elements. Without any further constraints, it turns out that s_{34} can become as large as 0.8, which has been discussed in [49]. It will be shown in Section 3.2.2 that electroweak precision tests provide a strong bound on this mixing angle (3.31),

$$s_{34} \leq 0.24\,, \tag{2.28}$$

which we will consequently include in our analysis. Similar to [49], we allowed each of the 7 measured magnitudes of Table 2.1 to vary within $2\,\sigma$ and a total χ^2 of 14, corresponding to 95% confidence level. We generated 10^5 randomly distributed points fulfilling these constraints and derived the following bounds on the CKM angles:

$$s_{12} = 0.2252 \pm 0.0018\,, \qquad s_{13} = 0.00389 \pm 0.00088\,, \qquad s_{23} = 0.041 \pm 0.003 \tag{2.29a}$$

$$s_{14} \leq 0.042\,, \qquad s_{24} \leq 0.22\,, \qquad s_{34} \leq 0.24\,. \tag{2.29b}$$

This constrains the elements of $V_{\rm SM4}$ to the following magnitudes at 95% C.L.

$$|V_{\rm SM4}| = \begin{pmatrix} 0.97425 \pm 0.04\% & 0.2252 \pm 0.8\% & 3.89 \times 10^{-3} \pm 23\% & \leq 0.042 \\ 0.22 \pm 4\% & \geq 0.95 & 40.6 \times 10^{-3} \pm 6\% & \leq 0.22 \\ \leq 0.04 & \leq 0.09 & \geq 0.97 & \leq 0.24 \\ \leq 0.08 & \leq 0.21 & \leq 0.25 & \geq 0.94 \end{pmatrix} \tag{2.30}$$

2.2.1.3. Simplifications, Wolfenstein Expansion and Scaling Scenarios

Simplifications of $V_{\rm SM4}$

The entries in $V_{\rm SM4}$ can get rather complicated when displayed at full length as in (2.12b). Therefore, we want to discuss simplifications for these expressions in order to better understand the basic parametric dependencies.

The most natural simplification of the CKM matrix is obtained by setting all $c_{ij} = 1$. This is justified by the smallness of the mixing angles given in (2.29). In this limit the six mixing angles are directly determined by the moduli of the off-diagonal elements in the upper right corner of $V_{\rm SM4}$:

$$\begin{aligned} &s_{12} \simeq |V_{us}|\,, && s_{13} \simeq |V_{ub}|\,, && s_{23} \simeq |V_{cb}|\,, \\ &s_{14} \simeq |V_{ub'}|\,, && s_{24} \simeq |V_{cb'}|\,, && s_{34} \simeq |V_{tb'}|\,. \end{aligned} \tag{2.31}$$

Another simplification comes from considering the difference with respect to the SM3 CKM matrix. As we have seen in the previous sections, the fourth generation mixings are rather small and therefore the 4G contributions to $V_{\rm SM3}$ can be expected to be only minor. In order to quantify this effect, we introduce the 3×3 matrix $\Delta V_{\rm 4G}$ by

$$(V_{SM4})_{ij} = (V_{SM3})_{ij} \cdot (\Delta V_{\rm 4G})_{ij} \qquad (\text{no summation over } \; i,j = 1,2,3)\,. \tag{2.32}$$

Inserting the points which we generated in the analysis of the previous section, we find the following fourth generation contributions

$$\Delta V_{\rm 4G} = \begin{pmatrix} 1 & 1 & 1 \\ (0.95 - 1.01)\; e^{\pm i 2^\circ} & (0.97 - 1)\; e^{i \pm 0.1^\circ} & (0.97 - 1)\; e^{i \pm 0.04^\circ} \\ (0 - 4)\; e^{i \pm 180^\circ} & (0 - 2)\; e^{i \pm 180^\circ} & (0.97 - 1)\; e^{i \pm 0.1^\circ} \end{pmatrix}\,. \tag{2.33}$$

These numbers show clearly that in the tree level constrained CKM entries $(V_{u(d,s,b)}, V_{c(d,s,b)}, V_{tb})$ the contributions from the fourth family amount to not more than 5%. This means that for most applications, one can just use the SM3 expressions for these elements. In contrast, the not yet measured CKM entries (V_{td}, V_{ts}) can differ considerably from the SM3 expressions, not to mention the elements involving the fourth generation which are of course vanishing in the case of three generations.

Generalized Wolfenstein Expansion

In the SM3, the hierarchical structure of the CKM matrix is neatly described by the Wolfenstein expansion [105, 106]. It is an approximate parametrization in which each element is expanded as a power series in the parameter

$$\lambda = |V_{us}| = 0.2252\,. \tag{2.34}$$

As we have seen in the previous paragraph, the measured CKM elements are almost unaffected by the fourth generation, so the Wolfenstein parametrization of these entries will basically remain unchanged and we have

$$\lambda \equiv |V_{us}| \approx s_{12}\,, \quad A\lambda^2 \equiv |V_{cb}| \approx s_{23}\,, \quad A\lambda^3(\rho + i\eta) \equiv A\lambda^3\, z_\rho \equiv V_{ub} \approx s_{13} e^{i\delta_{13}}\,, \tag{2.35}$$

where the approximations are valid in the limit of $c_{ij} \approx 1$. The 4G mixings $V_{(u,c,t)b'}$ can then be parametrized by

$$\lambda^{n_1} z_\tau \equiv V_{ub'} = s_{14} e^{i\delta_{14}}\,, \quad \lambda^{n_2} z_\sigma \equiv V_{cb'} \approx s_{24} e^{i\delta_{24}}\,, \quad \lambda^{n_3} B \equiv V_{tb'} \approx s_{34}\,, \tag{2.36}$$

where A, B, z_i, z_i^* are coefficients of order one, and the exponents n_i are constrained due to the upper bounds (2.29b):

$$n_1 \geq 2\,, \qquad n_2 \geq 1\,, \qquad n_3 \geq 1\,. \tag{2.37}$$

Froggatt-Nielsen Approach and Scaling Scenarios

A particular way to realize a hierarchical CKM matrix is to consider a simple Froggatt-Nielsen (FN) setup [107], where the scaling of the mixing angles is controlled by different $U(1)$ charge factors b_i for the left-handed doublets of different generations, leading to

$$\theta_{ij} \sim \lambda^{|b_i - b_j|}\,. \tag{2.38}$$

Here λ is given by the VEV of some $U(1)$-breaking scalar field divided by a large UV-scale. The triangle inequalities for $|b_i - b_k| + |b_k - b_j|$ then guarantee that the consistency relations discussed in [108] always hold:

$$\theta_{ik}\theta_{jk} \;\lesssim\; \theta_{ij} \qquad (i,j,k = 1\ldots 4)\,. \tag{2.39}$$

Since (2.38) only involves charge *differences*, we may set $b_4 \equiv 0$, while the charges b_{1-3} and the related 4G mixing angles are not completely fixed. However, we can identify certain benchmark cases which may later be compared with the phenomenological constraints from EWPT, tree-level decays and rare decays of SM3 quarks: Scenarios with some 4G mixing angles being of order $\mathcal{O}(1)$ are already ruled out by tree-level quark decays (2.29) and EWPT (Section 3). Among the interesting scenarios with sufficiently small mixing angles, we identify:

$$\text{(a)} \quad b_3 = 1,\, b_2 = 3,\, b_1 = 4\text{:} \quad V_{\text{SM4}} \sim \begin{pmatrix} 1 & \lambda & \lambda^3 & \lambda^4 \\ \lambda & 1 & \lambda^2 & \lambda^3 \\ \lambda^3 & \lambda^2 & 1 & \lambda \\ \lambda^4 & \lambda^3 & \lambda & 1 \end{pmatrix}, \text{ with } (n_1, n_2, n_3) = (4, 3, 1)\,, \tag{2.40a}$$

which yields a very symmetric scaling pattern for the 4G mixing matrix, and shares the feature of the SM3 CKM matrix that more off-diagonal elements get smaller. Notice that of the 9 inequalities in (2.39) involving the 4G mixing angles, 3 are saturated, namely

$$\text{(a)} \quad \theta_{12}\theta_{24} \sim \theta_{13}\theta_{34} \sim \theta_{14}\,, \quad \theta_{24} \sim \theta_{23}\theta_{34}\,. \tag{2.40b}$$

Scenarios with even smaller mixing angles ($\theta_{i4} \to \lambda^n \theta_{i4}$) can simply be obtained from (2.40) by increasing $b_{1-3} \to b_{1-3} + n$. An FN example for a scenario with (relatively) large 4G mixing angles is given by

$$\text{(b)} \quad b_3 = 1, b_2 = -1, b_1 = -2\text{:} \quad V_{\text{SM4}} \sim \begin{pmatrix} 1 & \lambda & \lambda^3 & \lambda^2 \\ \lambda & 1 & \lambda^2 & \lambda \\ \lambda^3 & \lambda^2 & 1 & \lambda \\ \lambda^2 & \lambda & \lambda & 1 \end{pmatrix}, \text{ with } (n_1, n_2, n_3) = (2, 1, 1)\,, \tag{2.41a}$$

which meets the lower bounds on n_i given in (2.37). In this case, the saturated inequalities are

$$\text{(b)} \quad \theta_{14}\theta_{34} \sim \theta_{13}\,, \quad \theta_{24}\theta_{34} \sim \theta_{23}\,, \quad \theta_{12}\theta_{24} \sim \theta_{14}\,. \tag{2.41b}$$

For later use, we further identify two interesting non-FN scenarios. The first one is given by

$$\text{(c)} \quad V_{\text{SM4}} \sim \begin{pmatrix} 1 & \lambda & \lambda^3 & \lambda^2 \\ \lambda & 1 & \lambda^2 & \lambda^3 \\ \lambda^3 & \lambda^2 & 1 & \lambda \\ \lambda^2 & \lambda^3 & \lambda & 1 \end{pmatrix}, \text{ with } (n_1, n_2, n_3) = (2, 3, 1)\,, \tag{2.42a}$$

$$\text{saturating} \quad \theta_{14}\theta_{34} \sim \theta_{13}\,, \quad \theta_{12}\theta_{14} \sim \theta_{23}\theta_{34} \sim \theta_{24} \tag{2.42b}$$

In this case, the SM4 mixing matrix takes a very symmetric form, where the mixing angle θ_{14} between the fourth and first generation is larger than θ_{24}. Finally, for

$$\text{(d)} \quad V_{\text{SM4}} \sim \begin{pmatrix} 1 & \lambda & \lambda^3 & \lambda^3 \\ \lambda & 1 & \lambda^2 & \lambda^2 \\ \lambda^3 & \lambda^2 & 1 & \lambda \\ \lambda^3 & \lambda^2 & \lambda & 1 \end{pmatrix}, (n_1, n_2, n_3) = (3, 2, 1)\,, \tag{2.43a}$$

$$\text{saturating} \quad \theta_{12}\theta_{24} \sim \theta_{14}\,, \tag{2.43b}$$

we encounter the situation that the mixing of the fourth and third generation with the first and second one is similar in size, $\theta_{13} \sim \theta_{14}$, $\theta_{23} \sim \theta_{24}$.

2.2.1.4. CP-Violating Invariants

Throughout the last decade, B-factories have ultimately confirmed the Kobayashi-Maskawa model [85] as an explanation of CP violation in the SM3. However, this model does not

meet the Sakharov conditions necessary for generating the observed baryon asymmetry of the universe (BAU). For this discussion a quantity summarizing the amount of CP violation in the quark Yukawa sector is needed. In the SM3, this quantity is the well-known Jarlskog determinant which has been obtained from studying appropriate basis-independent invariants built from the Yukawa matrices [109, 110]. Its generalization to the SM4 case has, for instance, been discussed in [54, 111]. In the limit $m^2_{u,d,s,c} \ll m^2_b \ll m^2_{t,b',t'}$, the invariants reduce to one new CP-violating quantity,

$$\begin{aligned} I_1 &= \mathrm{Im\,tr}\left[(Y_U Y_U^\dagger)^2 (Y_D Y_D^\dagger)(Y_U Y_U^\dagger)(Y_D Y_D^\dagger)^2\right] \\ &\simeq -m_b^2 m_t^2 m_{b'}^4 m_{t'}^2 (m_{t'}^2 - m_t^2)\,(F_{2323} + F_{1313} + F_{2313} + F_{1323}) \\ &\simeq m_b^2 m_t^2 m_{b'}^4 m_{t'}^2 (m_{t'}^2 - m_t^2) \begin{cases} -\,s_{23} s_{24} s_{34} \sin\delta_{24}\,, \\ s_{34}\,(s_{13} s_{14} \sin(\delta_{13} - \delta_{14}) - s_{23} s_{24} \sin\delta_{24})\,, \end{cases} \end{aligned} \tag{2.44}$$

which can be related to the area of a quadrangle in the complex plane, described by the functions

$$F_{ijkl} = \mathrm{Im}\left(V_{ik} V_{jk}^* V_{il}^* V_{jl}\right)\,.$$

The first line in (2.44) refers to scenarios with $s_{24} \gtrsim s_{14}$, like (2.40,2.41,2.43). The second line is valid for $s_{24} \sim \lambda\, s_{14}$, like in case of (2.42). It has been stressed in [54] that the quark mass-dependent prefactor in (2.44) can lead to an enhancement of several orders of magnitude compared to the SM3 analogue.

The overall scaling with the Wolfenstein parameter λ is given by $I_1 \sim \lambda^{2+n_2+n_3}$, which can be as large as λ^4 for scenario (2.41). For the benchmark scenario (2.43) one obtains $I_1 \sim \lambda^5$, whereas (2.40,2.42) would lead to $I_1 \sim \lambda^6$. As we will illustrate in the numerical section below, the dependence of I_1 on the SM4 mixing parameters is directly correlated with the size of $S_{\psi\phi}$. Even though I_1 is enhanced by many orders of magnitude over the corresponding SM3 expression, it is not yet clear whether this can explain the observed baryon asymmetry of the universe.

2.2.2. The 4×4 Lepton Mixing Matrix U_{SM4}

Parametrization

The most general leptonic mixing matrix in the presence of four generations is determined by 12 parameters: 6 mixing angles, 3 Dirac phases and 3 Majorana phases. A standard parametrization is obtained by treating the mixing angles and Dirac phases in analogy to the quark sector with the Majorana phases contained in an additional diagonal matrix,

$$U_{\mathrm{SM4}} = U_{34}\, I_4(\delta^\ell_{24})\, U_{24}\, I_4(-\delta^\ell_{24})\, I_4(\delta^\ell_{14})\, U_{14}\, I_4(-\delta^\ell_{14})\, U_{23}\, I_3(\delta^\ell_{13})\, U_{13}\, I_3(-\delta^\ell_{13})\, U_{12}\, I_{\mathrm{Maj.}}\,, \tag{2.45}$$

where the matrices U_{ij} are rotations in the i-j plane analogous to the V_{ij} in (2.12). They are parametrized by corresponding mixing angles θ^ℓ_{ij} while

$$[I_i(\alpha)]_{jk} = \delta_{jk}\, e^{i\alpha\,\delta_{ij}}\,, \qquad I_{\mathrm{Maj.}} = \mathrm{diag}[e^{i\alpha_1}, e^{i\alpha_2}, e^{i\alpha_3}, 1]\,, \tag{2.46}$$

contain the Dirac and Majorana phases, respectively. The observables we will consider in the course of this work are insensitive to the Majorana phases α_i, which will therefore be dropped in the following.

PMNS Factors and Unitarity

In all observables studied throughout this work, the PMNS matrix elements only occur in the following combinations

$$\lambda_{\nu_i}^{(\ell_a \ell_b)} \equiv U_{\ell_b \nu_i} U_{\ell_a \nu_i}^* \,, \qquad \lambda_{\ell_i}^{(\nu_a \nu_b)} \equiv U_{\ell_i \nu_a} U_{\ell_i \nu_b}^* \,. \tag{2.47}$$

As in the quark case (2.19), the PMNS matrix is unitary and therefore the following unitarity relations hold

$$\sum_{i=1}^{4} \lambda_{\nu_i}^{(\ell_a \ell_b)} = \delta^{ab} \,, \qquad \sum_{i=1}^{4} \lambda_{\ell_i}^{(\nu_a \nu_b)} = \delta^{ab} \,. \tag{2.48}$$

Tri-Bi-Maximal Mixing

Concerning the mixing angles and Dirac phases, it is well known that the SM3 lepton sector behaves very differently as compared to the SM3 quark sector. In particular, the PMNS matrix for SM3 leptons is known to follow an approximate "tri-bi-maximal" mixing pattern [112], reading

$$U_{\rm SM3} \simeq U_{\rm SM3}^{\rm max} = \begin{array}{c} \\ e \\ \mu \\ \tau \end{array} \begin{array}{c} \begin{array}{cccc} \nu_1 & \nu_2 & \nu_3 \end{array} \\ \begin{pmatrix} \sqrt{\frac{2}{3}} & \frac{1}{\sqrt{3}} & 0 \\ -\frac{1}{\sqrt{6}} & \frac{1}{\sqrt{3}} & \frac{1}{\sqrt{2}} \\ \frac{1}{\sqrt{6}} & -\frac{1}{\sqrt{3}} & \frac{1}{\sqrt{2}} \end{pmatrix} \end{array} \,, \tag{2.49}$$

which is obtained by setting the 3G mixing angles to $s_{23} = 1/\sqrt{2}$, $s_{12} = 1/\sqrt{3}$, $s_{13} = 0$.

A priori, it is not clear whether such a pattern could or should be extended to an SM4 lepton-mixing matrix, leading to potentially large mixing angles between the new lepton generation and the SM3 ones. However, as we will see in more detail below, the current experimental situation already excludes large new mixing angles θ_{i4}^{ℓ} with the 4G leptons, and therefore we should rather consider

$$U_{\rm SM4} \approx U_{\rm SM4}^{\rm max} = \begin{pmatrix} \sqrt{\frac{2}{3}} & \frac{1}{\sqrt{3}} & 0 & 0 \\ -\frac{1}{\sqrt{6}} & \frac{1}{\sqrt{3}} & \frac{1}{\sqrt{2}} & 0 \\ \frac{1}{\sqrt{6}} & -\frac{1}{\sqrt{3}} & \frac{1}{\sqrt{2}} & 0 \\ 0 & 0 & 0 & 1 \end{pmatrix} \tag{2.50}$$

as a starting point.[2] The *deviations* from this mixing pattern can then be conveniently described in terms of an almost diagonal mixing matrix,

$$U_{\rm SM4} = V_{\rm SM4}^{\rm residual} \cdot U_{\rm SM4}^{\rm max} \cdot I^{\rm Maj.} \,, \tag{2.51}$$

[2] This ansatz reflects the special role of the fourth-generation neutrino, which requires some particular theoretical framework to be realized (see e.g. [66]).

where $V^{\rm residual}$ is parametrized in terms of small mixing angles Δ_{ij} and 3 Dirac phases, and can be treated in an analogous way as the 4G quark mixing matrix.

While the deviations from tri-bi-maximal mixing Δ_{ij} – with the present experimental bounds – can still be of order $10-20\%$, the radiative LFV decays (see Section 4.3) constrain the products

$$\begin{aligned}
\Delta_{14}\Delta_{24} &\lesssim 3.5\times 10^{-4}\,,\\
\Delta_{14}\Delta_{34} &\lesssim 1.8\times 10^{-2}\,,\\
\Delta_{24}\Delta_{34} &\lesssim 1.8\times 10^{-2}\,.
\end{aligned} \tag{2.52}$$

3. Electroweak Precision Tests

Electroweak Precision Tests (EWPT) provide some of the most stringent bounds on the fourth generation currently available. In the past, it has even been stated that they would completely rule out the SM4 [33–35, 113], but since then numerous analyses have objected this finding [36–41] and given rise to a veritable revival of the fourth generation throughout the last years.

In this section we want to introduce the electroweak observables (EWPO) which are putting the most severe constraints on the SM4, and analyze their impact on the given parameter space. We will find important bounds, especially for the mass splitting of the new fermion doublets and for the magnitude of the CKM matrix element $V_{tb'}$, which will be of great importance for our further analysis. Our results do not contradict but rather generalize and extend those found in previous works [39, 40, 49].

3.1. Electroweak Precision Observables

In the early 90's of the last century, experiments at the colliders *LEP* (at CERN) and *SLC* (at SLAC) collected large amounts of data from e^+e^- collisions, featuring extremely precise measurements of Z boson properties such as its mass, width, branching ratios and several asymmetries. *LEP 2*, running from 1995-2000, contributed further precision data on properties of the W boson and a lower bound on the Higgs mass, among others. The still running *Tevatron* program at Fermilab provided further measurements, such as the top quark and W boson mass. An overview of all these high precision experiments and their outcome is given in [113].

Altogether, a set of up to 35 independent precision observables can be used to constrain and test a given model of particle physics. Analyses of the SM showed that it does very well in meeting the requirements from EWPO. On the one hand this is fortunate because it suggests that particle physics is somehow "on the right way". On the other hand, from the perspective of any new physics (NP) model, it is a tough challenge since any new contribution to EWPO has to be very tiny, which constrains or even rules out many of these models.

Of course one could calculate all available precision observables (or a certain subset, chosen by criteria such as precision, involved scale etc.) and perform a corresponding fit for every new model being studied. Evidently this would be a very tedious procedure which fortunately is not always necessary. This is because a great deal of all electroweak precision effects in NP models arises from contributions to gauge boson self-energies only. These so-called *oblique corrections* can effectively be parametrized by a set of only 3 parameters [114], which will be studied in Section 3.1.1. However, there are also contributions that do not originate in self-energy corrections. These include the partial widths of the Z boson decaying into various fermions, which will be the subject of Section 3.1.2.

3.1.1. Oblique Parameters

3.1.1.1. General Introduction

The effects of oblique corrections are expressed in terms of gauge boson vacuum polarizations

$$\Pi_{ab}^{\mu\nu}(q) \equiv \Pi_{ab}(q^2) g^{\mu\nu} + (\dots q^\mu q^\nu) \,. \tag{3.1}$$

For a, b, one can either choose the set of mass and charge eigenstate gauge bosons $a, b \in \{W, Z, \gamma\}$, or the weak eigenstates $a, b \in \{1, 3, Q\}$ corresponding to W_1^μ, W_3^μ, A^μ. The two bases are related by [115]

$$\Pi_{\gamma\gamma} = e^2 \Pi_{QQ} \,, \tag{3.2a}$$

$$\Pi_{Z\gamma} = \frac{e^2}{s_W c_W} (\Pi_{3Q} - s_W^2 \Pi_{QQ}) \,, \tag{3.2b}$$

$$\Pi_{ZZ} = \frac{e^2}{s_W^2 c_W^2} (\Pi_{33} - 2 s_W^2 \Pi_{3Q} + s_W^4 \Pi_{QQ}) \,, \tag{3.2c}$$

$$\Pi_{WW} = \frac{e^2}{s_W^2} \Pi_{11} \,. \tag{3.2d}$$

Since the set $\{1, 3, Q\}$ yields simpler expressions, we will use it although their physical meaning might not be as intuitive as for $\{W, Z, \gamma\}$.

It has been argued in [116] that there are in principle six independent combinations of Π's, but if the new particles are considerably heavier than the electroweak scale, i.e. $m_{\mathrm{NP}} \gg M_Z$, only three of them remain. These three oblique parameters denoted by S, T and U were first defined by Peskin and Takeuchi [114, 115] in the following way:

$$\alpha S = 4 e^2 \left[\Pi'_{33}(0) - \Pi'_{3Q}(0) \right] \,, \tag{3.3a}$$

$$\alpha T = \frac{e^2}{s_W^2 c_W^2 M_Z^2} \left[\Pi_{11}(0) - \Pi_{33}(0) \right] \,, \tag{3.3b}$$

$$\alpha U = 4 e^2 \left[\Pi'_{11}(0) - \Pi'_{33}(0) \right] \,. \tag{3.3c}$$

T is related to the well-known ρ parameter [83, 117] by

$$\rho \equiv \frac{M_W^2}{c_W^2 M_Z^2} = 1 + \alpha T \,, \tag{3.4}$$

and therefore determined by the difference between the W and Z self energies at $q^2 = 0$. Likewise, S is connected to the difference between the Z self energies at $q^2 = M_Z^2$ and $q^2 = 0$ and $S + U$ describes the difference between the W self energy at $q^2 = M_W^2$ and $q^2 = 0$.

3.1.1.2. Oblique Parameters in the SM4

4G Contribution

In the SM4, the fermionic contributions to the oblique parameters in (3.3) are given by [37, 40, 51]

$$S^{\rm SM4} = \frac{N_c}{6\pi}\sum_{i=1}^{4}\left[1-\frac{1}{3}\log\frac{m_{u_i}^2}{m_{d_i}^2}\right]+\frac{1}{6\pi}\sum_{i=1}^{4}\left[1+\log\frac{m_{\nu_i}^2}{m_{\ell_i}^2}\right], \tag{3.5a}$$

$$\begin{aligned} T^{\rm SM4} &= \frac{N_c}{16\pi s_W^2 c_W^2 M_Z^2}\left[\sum_{i=1}^{4}(m_{u_i}^2+m_{d_i}^2)-\sum_{i,j=1}^{4}\left|V_{u_i d_j}\right|^2 F_T(m_{u_i}^2,m_{d_j}^2)\right] \\ &\quad+\frac{1}{16\pi s_W^2 c_W^2 M_Z^2}\left[\sum_{i=1}^{4}(m_{\nu_i}^2+m_{\ell_i}^2)-\sum_{i,j=1}^{4}\left|U_{\ell_j\nu_i}\right|^2 F_T(m_{\nu_i}^2,m_{\ell_j}^2)\right], \end{aligned} \tag{3.5b}$$

$$\begin{aligned} U^{\rm SM4} &= \frac{N_c}{3\pi}\left[\sum_{i,j=1}^{4}\left|V_{u_i d_j}\right|^2 F_U(m_{u_i}^2,m_{d_j}^2)-\frac{5}{6}\sum_{i=1}^{4}1\right] \\ &\quad+\frac{1}{3\pi}\left[\sum_{i,j=1}^{4}\left|U_{\ell_j\nu_i}\right|^2 F_U(m_{\nu_i}^2,m_{\ell_j}^2)-\frac{5}{6}\sum_{i=1}^{4}1\right], \end{aligned} \tag{3.5c}$$

where the auxiliary functions F_T and F_U are defined as

$$F_T(m_1^2,m_2^2)\equiv 2\frac{m_1^2 m_2^2}{m_1^2-m_2^2}\log\frac{m_1^2}{m_2^2}, \tag{3.6a}$$

$$F_U(m_1^2,m_2^2)\equiv 2\frac{m_1^2 m_2^2}{(m_1^2-m_2^2)^2}+\left(\frac{m_1^2+m_2^2}{2(m_1^2-m_2^2)}-\frac{m_1^2 m_2^2(m_1^2+m_2^2)}{(m_1^2-m_2^2)^3}\right)\log\frac{m_1^2}{m_2^2}. \tag{3.6b}$$

Since the parameter U is close to zero, all the neutral current and low energy observables depend only on S and T [115]. Subtracting the SM3 values of these parameters, we are left with the contributions due to the fourth generation

$$S^4 \equiv S^{\rm SM4}-S^{\rm SM3}=\frac{1}{3\pi}\left[2-\log\frac{m_{t'}m_{\ell_4}}{m_{b'}m_{\nu_4}}\right], \tag{3.7a}$$

$$\begin{aligned} T^4 &\equiv T^{\rm SM4}-T^{\rm SM3} \\ &= \frac{3}{16\pi s_W^2 c_W^2 M_Z^2}\left[m_{t'}^2+m_{b'}^2-\left|V_{t'b'}\right|^2 F_T(m_{t'}^2,m_{b'}^2)-\left|V_{tb'}\right|^2 F_T(m_t^2,m_{b'}^2)\right] \\ &\quad+\frac{1}{16\pi s_W^2 c_W^2 M_Z^2}\left[m_{\nu_4}^2+m_{\ell_4}^2-\left|U_{\ell_4\nu_4}\right|^2 F_T(m_{\nu_4}^2,m_{\ell_4}^2)\right] \\ &\gtrsim \frac{3}{16\pi s_W^2 c_W^2}\left[\delta m_{t'b'}+\left|V_{tb'}\right|^2\frac{F_T(m_{t'}^2,m_{b'}^2)-F_T(m_t^2,m_{b'}^2)}{M_Z^2}+\frac{1}{3}\delta m_{\nu_4\ell_4}\right], \end{aligned} \tag{3.7b}$$

where all negligible contributions to T^4 have been dropped[1], and in the last step we have left out small positive contributions proportional to $|V_{ub'}|^2, |V_{cb'}|^2$ and $(1-|U_{\ell_4\nu_4}|^2)$. Furthermore, we introduced the function

$$\delta m_{ij} \equiv \frac{1}{M_Z^2}\left(m_i^2 + m_j^2 - F_T(m_i^2, m_j^2)\right) , \tag{3.8}$$

which is minimized for $m_i = m_j$:

$$\delta m_{ii} = 0 . \tag{3.9}$$

Higgs Contribution

Additionally, one has to take into account the impact of a heavier Higgs on the oblique parameters [114, 115], which are finally given by

$$S = S^4 + S_H , \qquad T = T^4 + T_H . \tag{3.10}$$

A first approximation for the Higgs correction terms has been given in [114]:

$$S_H \approx \frac{1}{12\pi}\log\frac{m_H^2}{(117\text{GeV})^2} , \qquad T_H \approx -\frac{3}{16\pi c_W^2}\log\frac{m_H^2}{(117\text{GeV})^2} . \tag{3.11}$$

The full SM4 result calculated in [118] reads

$$\begin{aligned} S_H = -\frac{1}{12\pi}\Bigg[&\frac{2m_H^4+8M_Z^4}{\left(m_H^2-M_Z^2\right)^2} + \frac{m_H^6-3m_H^4M_Z^2+12m_H^2M_Z^4}{\left(m_H^2-M_Z^2\right)^3}\log\frac{M_Z^2}{m_H^2} \\ &- \frac{2m_R^4+8M_Z^4}{\left(m_R^2-M_Z^2\right)^2} - \frac{m_R^6-3m_R^4M_Z^2+12m_R^2M_Z^4}{\left(m_R^2-M_Z^2\right)^3}\log\frac{M_Z^2}{m_R^2}\Bigg] , \end{aligned} \tag{3.12a}$$

$$\begin{aligned} T_H = \frac{3}{16\pi s_W^2 M_W^2}\Bigg[&\frac{m_H^4\left(M_W^2-M_Z^2\right)}{\left(m_H^2-M_W^2\right)\left(m_H^2-M_Z^2\right)}\log\frac{m_H^2}{m_R^2} \\ &+ \left(m_H^2-m_R^2\right)\Bigg(\frac{M_W^4}{\left(m_H^2-M_W^2\right)\left(m_R^2-M_W^2\right)}\log\frac{M_W^2}{m_R^2} \\ &- \frac{M_Z^4}{\left(m_H^2-M_Z^2\right)\left(m_R^2-M_Z^2\right)}\log\frac{M_Z^2}{m_R^2}\Bigg)\Bigg] , \end{aligned} \tag{3.12b}$$

where the Higgs reference mass m_R is set to 117 GeV and the correction to U is negligible.

3.1.2. Non-Oblique Effects: $Zb\bar{b}$ Vertex

There have been several analyses of $Zb\bar{b}$ vertex corrections from a fourth family in the literature (e.g. [38, 104, 119]). Chanowitz stated in [40] that the constraints from $Z \to b\bar{b}$

[1] A numerical analysis involving the ranges of involved masses shows that the contribution from $F_T(m_{t'}^2, m_b^2)$ is below 5×10^{-3}. The terms involving lighter quarks, such as $F_T(m_t^2, m_b^2)$ are of course even smaller. Compared to the standard deviation of T from the SM3 fit (3.26), these contributions can safely be neglected.

were only minor compared to those from oblique corrections. However, performing a full analysis of both types of parameters, we found that this statement is not true in general. For example the bound on s_{34} obtained from $Zb\bar{b}$ can be stronger than the one from S and T, as we will see in the next section.

Following [120], the decay width of $Z \to q\bar{q}$ can be written as

$$\Gamma(Z \to q\bar{q}) = \frac{\hat{\alpha}}{16\hat{s}_W^2\hat{c}_W^2} m_Z(|a_q^2| + |v_q|^2)(1+\delta_q^{(0)})(1+\delta_{\mathrm{QED}}^q)(1+\delta_{\mathrm{QCD}}^q)(1+\delta_\mu^q) \times (1+\delta_{t\mathrm{QCD}}^q)(1+\delta^q)\,, \tag{3.13}$$

where $\hat{\alpha}$ is the electromagnetic fine structure constant, $\hat{s}_W$ and $\hat{c}_W$ the sine and cosine of the Weinberg angle, $a_q = 2I_3^q$ and $v_q = 2I_3^q - 4Q_q\hat{s}_W^2$ the axial and vector coupling constants of quark q, and the δ terms corrections due to various higher order loops. Quantities given in the $\overline{\mathrm{MS}}$ scheme at the scale $\mu = M_Z$ are denoted by a hat. Most of the δ corrections cancel by taking appropriate branching ratios. The most convenient ratio for our purpose is

$$R_h \equiv \frac{\Gamma(Z \to b\bar{b})}{\Gamma(Z \to \mathrm{hadrons})}\,, \tag{3.14}$$

in which all the δ's in the first line of (3.13) cancel, leaving only two relevant corrections:

- $\delta_{t\mathrm{QCD}}^q$ is an $\mathcal{O}(\alpha_s^2)$ correction to the axial-vector current induced rate, arising due to large mass splitting [121, 122]

$$\delta_{t\mathrm{QCD}}^q = -\frac{a_q}{v_q^2 + a_q^2}\left(\frac{\alpha_s}{\pi}\right)^2 \left[a_t f(\mu_t) + a_{t'} f(\mu_{t'}) + a_{b'} f(\mu_b')\right]\,, \tag{3.15}$$

  where $\mu_q^2 \equiv 4m_q^2/M_Z^2$ and the t' and b' contribution have been added to the corresponding formula of [120]. The function

$$f(\mu) \approx \log\frac{4}{\mu^2} - 3.083 + \frac{0.346}{\mu^2} + \frac{0.211}{\mu^4}\,, \tag{3.16}$$

  approximates the full function given in (3.5) of [122] with an accuracy better than 0.02% for 160 GeV $\leq m_q \leq$ 600 GeV.

- The correction δ^q is only nonzero for $q = b$. In this case, δ^b contains the interesting effects of the t and t' quark masses,

$$\delta^b \approx 10^{-2}\left[\left(-\frac{1}{2}\frac{m_t^2}{M_Z^2} + 0.2\right)|V_{tb}|^2 + \left(-\frac{1}{2}\frac{m_{t'}^2}{M_Z^2} + 0.2\right)|V_{t'b}|^2\right]\,. \tag{3.17}$$

  δ^b is the origin for the $m_{t'}$ dependence of the $Z \to b\bar{b}$ vertex. Increasing $m_{t'}$ decreases δ^b and therefore also decreases the ratio R_h.

When calculating R_h, one has to be aware of the high precision of the involved quantities and take extra care when handling the errors. The calculation of the central value yields

$$R_h = \left(1 + \frac{2}{R_s} + \frac{1}{R_c} + \frac{1}{R_u}\right)^{-1}\,, \tag{3.18}$$

with the ratios $R_q \equiv \Gamma(Z \to b\bar{b})/\Gamma(Z \to q\bar{q})$,

$$R_s = 0.99089\ g(m_{t'}, V_{t'b})\,, \tag{3.19a}$$

$$R_c = 1.27940\ \frac{1+\delta^b_{t\mathrm{QCD}}}{1+\delta^c_{t\mathrm{QCD}}}\ g(m_{t'}, V_{t'b})\,, \tag{3.19b}$$

$$R_u = 1.27799\ \frac{1+\delta^b_{t\mathrm{QCD}}}{1+\delta^u_{t\mathrm{QCD}}}\ g(m_{t'}, V_{t'b})\,. \tag{3.19c}$$

where we introduced the function

$$g(m_{t'}, V_{t'b}) = 1 + \frac{1}{100}\left(\frac{1}{5} - 6.0131 \times 10^{-5}\ m^2_{t'}\right)|V_{t'b}|^2 - 0.0137866\ (1 - |V_{t'b}|^2)\,. \tag{3.20}$$

and used unitarity together with the smallness of $|V_{cb}|$ and $|V_{ub}|$ (2.30),

$$|V_{tb}|^2 = 1 - |V_{t'b}|^2 - |V_{cb}|^2 - |V_{ub}|^2 \approx 1 - |V_{t'b}|^2\,. \tag{3.21}$$

The corrections $\delta^b_{t\mathrm{QCD}}$ and $\delta^c_{t\mathrm{QCD}} = \delta^u_{t\mathrm{QCD}}$ in R_c and R_u bear an additional $m_{b'}$ dependence which cannot be neglected. The most conservative bounds arise from $\Delta m = m_{t'} - m_{b'} = 0$. In this case we can further simplify the result to

$$R_h^{(\Delta m=0)} = \frac{0.38089\ g(m_{t'}, V_{t'b})}{1.37007 + 0.38089\ g(m_{t'}, V_{t'b})} \pm 0.00015\,, \tag{3.22}$$

where the theoretical error on R_h includes all uncertainties from the involved parameters.

On the experimental side, the measured values [103]

$$\mathrm{Br}(Z \to b\bar{b}) = (15.12 \pm 0.05) \times 10^{-2}\,, \quad \mathrm{Br}(Z \to \mathrm{hadrons}) = (69.91 \pm 0.06) \times 10^{-2}\,, \tag{3.23}$$

allow us to calculate

$$R_h = \frac{\mathrm{Br}(Z \to b\bar{b})}{\mathrm{Br}(Z \to \mathrm{hadrons})} = 0.21627 \pm 0.00074\,. \tag{3.24}$$

In the next section we will combine (3.22) and (3.24) in order to derive an upper bound on $s_{34} \approx V_{t'b}$, depending on $m_{t'}$.

3.2. Numerical Analysis of Electroweak Precision Tests in the SM4

3.2.1. Outline

For our analysis of the effects of oblique electroweak precision observables in the framework of a fourth generation, we will proceed as follows: We will take the χ^2 value for the observables S and T from (3.10), which is given by [123]

$$\chi^2_{ST} = \begin{pmatrix} S - S_0 \\ T - T_0 \end{pmatrix}^T \begin{pmatrix} \sigma_S^2 & \sigma_S\sigma_T\rho \\ \sigma_S\sigma_T\rho & \sigma_T^2 \end{pmatrix} \begin{pmatrix} S - S_0 \\ T - T_0 \end{pmatrix}\,, \tag{3.25}$$

where S_0, T_0 are the best fit values, σ_S, σ_T the standard deviations and ρ gives the statistic correlation of S and T. For these parameters we take the following values from the SM fit [124]

$$S_0 = 0.03\,, \qquad T_0 = 0.07\,, \qquad \sigma_S = 0.09\,, \qquad \sigma_T = 0.08\,, \qquad \rho = 0.867\,. \tag{3.26}$$

In the frequentist approach [123], χ^2 is related to the confidence level C by

$$F_{\chi^2}(\chi^2_{\max}, n) = C\,, \tag{3.27}$$

where the χ^2 cumulative distribution for $n = 2$ degrees of freedom is given as

$$F_{\chi^2}(\chi^2, n = 2) = 1 - e^{-\chi^2/2}\,. \tag{3.28}$$

So the χ^2 values corresponding to the 68%, 95% and 99% confidence levels for 2 degrees of freedom read

$$\chi^2_{\max} = 2.3 \text{ (68\% C.L.)}\,, \quad \chi^2_{\max} = 6.0 \text{ (95\% C.L.)}\,, \quad \chi^2_{\max} = 9.2 \text{ (99\% C.L.)}\,. \tag{3.29}$$

For the numerical analysis we scan through the possible parameter ranges of

$$m_{t'} \in [300, 600] \text{ GeV}\,,\ m_{\ell_4} \in [110, 600] \text{ GeV}\,,\ m_H \in [117, 1000] \text{ GeV}\,,\ V_{tb'} \in [0., 0.8]\,, \tag{3.30}$$

and for each point minimize χ^2_{ST} given in (3.25) with respect to $m_{b'}$ and m_{ν_4}, under the constraint that $m_{b'} > 300$ GeV and $m_{\nu_4} > 90$ GeV. In this way we create a set of more than 10^5 points distributed uniformly over the scanned parameter region, which we will analyze with respect to different questions in the following subsection.

3.2.2. Bound on s_{34}

It has been stated by Chanowitz [40] that the constraints from oblique parameters effectively constrain the SM4 and exclude large mixing scenarios which have been advocated in [49]. Table 3 of [40] shows a particularly interesting correlation between the maximum value for $|V_{tb'}| \approx s_{34}$ and the t' mass.

For our numerical analysis of oblique parameters, we minimized the values of χ^2_{ST} for each pair of $(m_{t'}, s_{34})$ and plotted the curves of constant χ^2 for the 95% confidence levels given in (3.29). The resulting upper bound on s_{34} (shown as blue line in Figure 3.1) is in good agreement with the results of Chanowitz' analysis (red line).

Simultaneously, we calculated the bounds arising from corrections to the $Zb\bar{b}$ vertex, which were discussed in the previous section. As one can see in Figure 3.1, the most conservative constraint at 95% C.L. (green line) is considerably stronger than the one from oblique parameters. For large $\Delta m \equiv m_{t'} - m_{b'} = 100$ GeV, this bound is even more severe (dashed green line). The overall maximum reads

$$s_{34} \leq 0.24\,, \tag{3.31}$$

which we already used to bound the CKM matrix elements in Sec. 2.2.1.

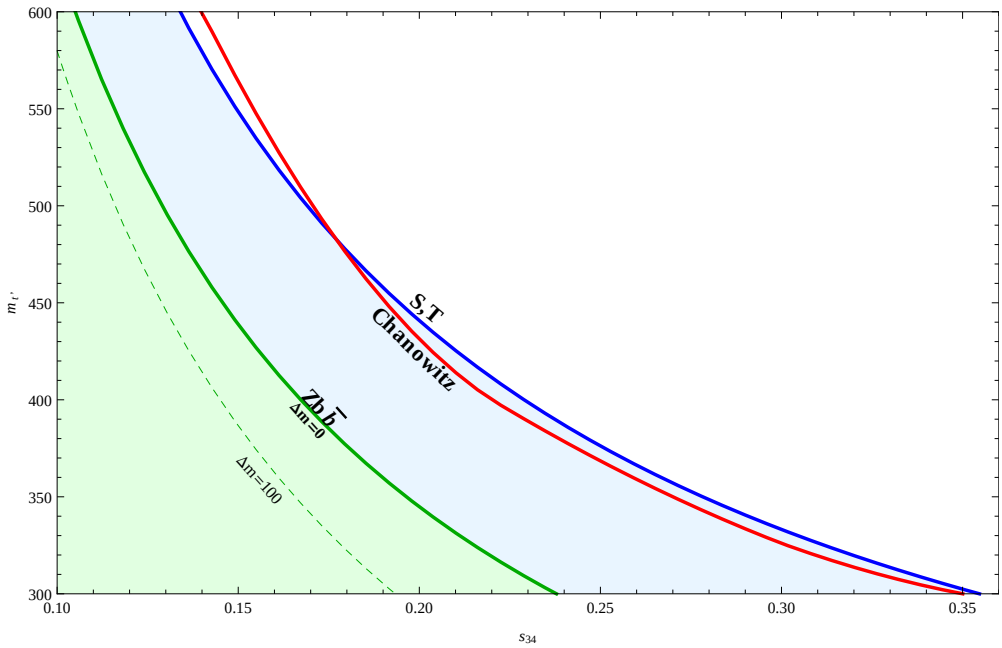

Figure 3.1.: Upper limits on $m_{t'}$ depending on $s_{34} \approx |V_{tb'}|$ obtained from our study of oblique parameters, at 95% C.L. Our bound from S and T (blue line) agrees very well with the one from Chanowitz [40] (red line), implying an upper limit on s_{34} of about 0.35. The constraint obtained from the nonoblique $Z \to b\bar{b}$ (green line) is stronger than the oblique one, implying $s_{34} \leq 0.24$. The dashed green line shows the $Z \to b\bar{b}$ bound for a mass splitting of $\Delta m = 100$, which is even more severe.

3.2.3. Mass Splitting

The mass splittings of the fourth generation quark and lepton doublets are important parameters of the SM4 that are strongly constrained by EWPT.

In their heavily cited analysis of EWPT effects on the fourth family, Kribs et al. [39] gave a very neat formula for the mass splittings $\Delta m_q \equiv m_{t'} - m_{b'}$ and $\Delta m_\ell \equiv m_{\ell_4} - m_{\nu_4}$ under the assumption of $V_{tb} = 1$:

$$\Delta m_q \approx \left(1 + \frac{1}{5} \log \frac{m_H}{117 \text{ GeV}}\right) \times 50 \text{ GeV}\,, \qquad \Delta m_\ell \approx 30 - 60 \text{ GeV}\,. \tag{3.32}$$

Our analysis shows that this assertion is basically right, but rather oversimplified.

In principle, Δm_q and Δm_ℓ are subject to competing forces due to S and T, as can be inferred from the expressions given in (3.7) together with the best fit values $T \approx S \approx 0$ in (3.26):

- The S parameter obtains a positive contribution of $S^4 = 0.21$ in the case of degenerate masses. Hence, from a sole analysis of the S parameter a mass ratio of $\frac{m_{t'}}{m_{b'}} \frac{m_{\ell_4}}{m_{\nu_4}} \approx 6$ would be favored.

- The T parameter has quite the opposite effect: Assuming vanishing fourth generation mixing, T^4 is proportional to $\delta m_{t'b'} + \frac{1}{3} \delta m_{\nu_4 \ell_4}$ and minimized by degenerate isospin doublets due to (3.9).

In the case of fourth generation quark mixing, i.e. $V_{tb'} > 0$, it is useful to rewrite the quark component of T^4 in (3.7b) by factoring out $m_{t'}^2$:

$$T_q^4 \propto m_{t'}^2 \; f_T(r_{b'}, r_t, |V_{t'_b}|)\,, \tag{3.33}$$

where we introduced the auxiliary function f_T depending on the quark mass ratios $r_{b'} \equiv \frac{m_{b'}^2}{m_{t'}^2}$, $r_t \equiv \frac{m_t^2}{m_{t'}^2}$ and the fourth generation mixing $V_{tb'} \approx s_{34}$. In comparison with $r_{b'}$, the dependence on r_t is rather weak and so we can neglect it for the following qualitative discussion. The minimum of f_T is increasing with s_{34} and therefore the minimal T^4 is no longer zero but proportional to the square of the involved mass scale, $m_{t'}^2$.

From this qualitative analysis of S and T, positive mass splittings $\Delta m_{q,\ell}$ are to be expected. For increasing s_{34}, the preferred Δm_q is supposed to decrease due to the rising influence of T, which prefers small positive mass splittings. This effect should even be enhanced by increasing $m_{t'}$. In addition, the overall χ^2 is supposed to increase due to the departure of T from its preferred value close to zero. These expectations are confirmed by the results of our combined numerical analysis:

The diagrams in Fig. 3.2 show that for most scenarios, χ^2_{ST} exhibits a Mexican-hat-like shape in the $m_{b'} - m_{\nu_4}$ plane, with an ellipse of minimal χ^2_{ST} around the point $(m_{b'}, m_{\nu_4}) = (m_{t'}, m_{l_4})$. This ellipse is tilted such that positive mass splittings $\Delta m_q, \Delta m_\ell > 0$ are preferred. The overall best fit points are given in red, while the best fits including the mass limits (2.5) and (2.7) are shown as green dots. From the first row in Fig. 3.2 ($s_{34} = 0$), one can see that these best fit points are basically in agreement with the ranges given by Kribs et al. (yellow bands), and also their positive correlation with the Higgs mass is reproduced. However, the diagrams show very clearly that there are several scenarios featuring rather extended 95% C.L. regions, so taking only the mass splitting corresponding to the best fit point as done in [39] is quite an oversimplification.

A point which has been mentioned for the first time in [51][2] and was completely neglected in previous analyses is the influence of nonzero 3-4 mixing s_{34}. As one can see in the second and third rows of Fig. 3.2, increasing s_{34} will decrease the maximum in the middle of the ellipse and therefore also decrease $|\Delta m_{q,\ell}|$. This means that s_{34} has basically the opposite effect on the shape of the allowed mass region as m_H. For s_{34} and $m_{t'}$ large enough, the Mexican hat will be deformed into a simple potential well, allowing even zero mass splittings at the 95% confidence level (see the diagrams with $s_{34} = 0.1, 0.2$ and $m_H = 117$ GeV in Fig. 3.2)! The fact that in the last row ($s_{34} = 0.2$) there are no more allowed regions for large top masses confirms our results for the correlation of s_{34} and $m_{t'}$ found in Sec. 3.2.2.

[2]While the authors of that paper come to the same conclusion that $s_{34} > 0$ allows for degenerate masses, they chose to display the points in the S-T-plane where the mass dependence shown in Fig. 3.2 is invisible.

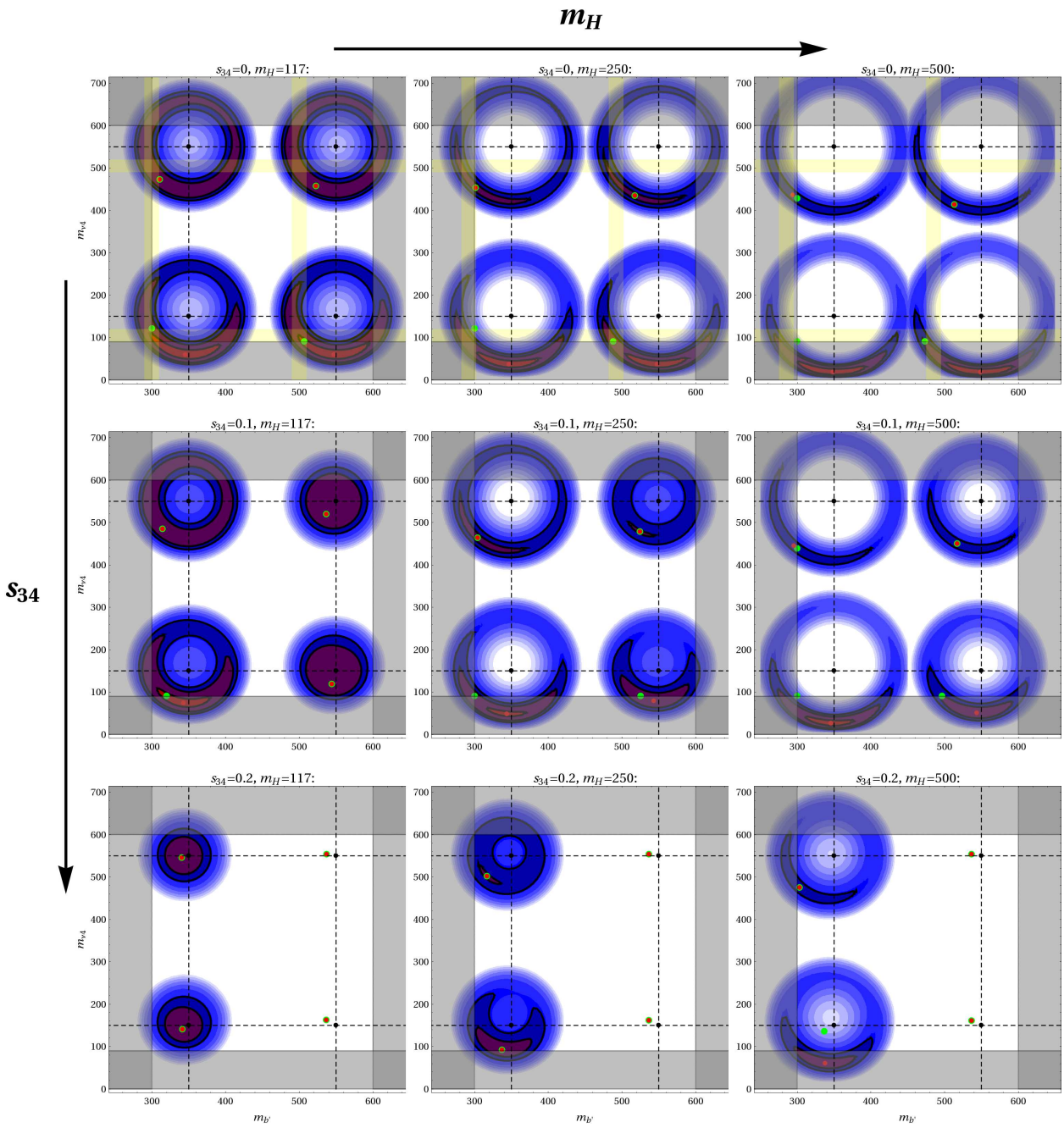

Figure 3.2.: Allowed regions of the masses $m_{b'}$ and m_{ν_4}, for different 3-4 mixing s_{34} and Higgs mass m_H. In each plot, the results are shown for four different combinations of $m_{t'} \in \{350\ \text{GeV}, 550\ \text{GeV}\}$ and $m_{\ell_4} \in \{150\ \text{GeV}, 550\ \text{GeV}\}$ (depicted by dashed lines). The three confidence levels 68%, 95% and 99% are given by the red, purple an dark blue areas, respectively, while higher χ^2 value are depicted by lighter shades of blue. The gray bands give the mass regions excluded by direct searches and perturbativity. While the red dot shows the overall χ^2 minimum, the minimum within the allowed mass region is displayed by the green dot. The light yellow bands in the first row indicate the mass splittings given by Kribs et al. [39].

4. Flavor and CP Violation Observables

4.1. Preliminaries: Effective Hamiltonians and Loop Functions

4.1.1. Introduction to Effective Field Theories

Effective field theories (EFT) are the method of choice for any serious phenomenology of weak decays. In this framework it is possible to describe physics at a given scale μ by a certain set of parameters, without knowledge of the processes at arbitrarily small distances. Due to the Operator Product Expansion (OPE) [125] the Hamiltonian of an effective theory has the following general structure

$$\mathcal{H}_{\text{eff}} = \mathcal{H}_{\text{light}} + \frac{G_F}{2} \sum_i V^i_{\text{CKM}} C_i(\mu) \mathcal{Q}_i \,, \tag{4.1}$$

where $\mathcal{Q}_i$ are the relevant local operators of the considered decay. The effective Hamiltonian $\mathcal{H}_{\text{eff}}$ in (4.1) can also be considered as a sum of effective vertices multiplied by effective coupling constants $C_i(\mu)$ and the Cabibbo-Kobayashi-Maskawa factors V^i_{CKM}. The part $\mathcal{H}_{\text{light}} = \mathcal{H}_{\text{QED}\times\text{QCD}}$ contains the interactions of the light particles whereas the heavy particles, such as W and Z bosons as well as the top quark and heavy new particles have been integrated out.

Eventually, after the determination of the effective Hamiltonian $\mathcal{H}_{\text{eff}}$ the decay amplitudes can be calculated. The transition amplitude for a decay of an initial state i, e.g. a K or B meson, into a final state f, e.g. $\ell^+\ell^-$ or $\pi\pi$, can then be specified by

$$\mathcal{A}(i \to f) = \langle f|\mathcal{H}_{\text{eff}}|i\rangle = \frac{G_F}{2} \sum_i V^i_{\text{CKM}} \; C_i(\mu) \; \langle f|\mathcal{Q}_i(\mu)|i\rangle \,, \tag{4.2}$$

where $\langle f|\mathcal{Q}_i(\mu)|i\rangle$ denote the hadronic matrix elements and $C_i(\mu)$ are the corresponding Wilson coefficients. Here two very important properties of the Operator Product Expansion are emphasized:

- The Wilson coefficients $C_i(\mu)$ contain all information of the contributions from scales higher than μ. Due to the asymptotic freedom of QCD they can be calculated within perturbation theory. The effect of these heavy particles such as Z, W-bosons and top quark are fully contained in the Wilson coefficients $C_i(\mu)$. Consequently $C_i(\mu)$ is a function of m_t, M_W, and also of the masses of new particles, if extensions of the Standard Model are considered.

- The hadronic matrix elements $\langle f|\mathcal{Q}_i(\mu)|i\rangle$ summarize the contributions of the amplitude $\mathcal{A}(i \to f)$ from scales lower than μ. Since the full amplitude of the decay may not depend on the scale μ, the μ-dependence of the couplings $C_i(\mu)$ must cancel the μ-dependence of the hadronic matrix elements $\langle f|\mathcal{Q}_i(\mu)|i\rangle$. However, in most cases it is not easy to calculate these matrix elements reliably and non-perturbative methods such as lattice calculations are required.

As we have seen, the OPE allows to separate the problem of calculating the amplitude $\mathcal{A}(i \to f)$ into two distinct parts: the short- distance (SD, perturbative) calculation of the couplings $C_i(\mu)$ and the long-distance (LD, generally non-perturbative) calculation of the hadronic matrix elements $\langle f|\mathcal{O}_i(\mu)|i\rangle$, both separated by the scale μ which can be chosen arbitrarily. For the evaluation of the matrix elements it is necessary to choose μ to be of the order of the mass of the decaying hadron. This is $\mathcal{O}(m_b)$ and $\mathcal{O}(m_c)$ for B decays and D decays respectively. In the case of K decays the typical choice is $\mu = \mathcal{O}(1 - 2GeV)$ instead of $\mathcal{O}(m_K)$, which is much too low for any perturbative calculation of the couplings $C_i(\mu)$.

Thus in an effective theory a process is properly described by shrinking the propagator of heavy particles and replacing it by an effective vertex. So formula (4.1) can be regarded as a generalization of the Fermi Theory. But in contrast to the Fermi theory, all known quarks and leptons as well as their strong and electroweak interactions coming from the SM are taken into account.

For non-leptonic B meson decays this generalization yields a list of relevant operators that can be found in [126]. Furthermore the formulation of weak decays in terms of effective Hamiltonians is well suited for the inclusion of new physics and is therefore very useful for testing extensions of the SM like the SM4.

In order to determine the Wilson coefficients one has to calculate the considered amplitude in the full theory and in the effective theory. Subsequently the full theory has to be matched to the effective theory, i.e. the following condition has to be imposed

$$\mathcal{A}_{full} = \mathcal{A}_{eff}. \tag{4.3}$$

After the calculation of the diagrams in the full theory which contribute to the considered operators and using the matching condition (4.3), one can extract the corresponding Wilson-coefficients by comparison. In the next section we will perform this task for several generic processes, identifying loop functions that occur repeatedly in all kinds of processes we will study subsequently.

4.1.2. Gauge Independent Loop and Master Functions in the SM4

In this section we present a generalized treatment of flavor changing neutral current processes in the SM4. In Section 4.1.2.1 we will first identify a set of gauge independent loop functions which correspond to the SM functions introduced in [127]. In Section 4.1.2.2 we will then introduce SM4 master functions that make it very easy to generalize the SM3 results for the studied flavor observables.

4.1.2.1. Gauge Independent Loop Functions

In Appendix A.1, we have computed all box and penguin diagrams needed for the observables in the following work. However, when calculating physical processes, it turns out that most of the diagrams do not occur alone but always in combination with other diagrams. Therefore it is not surprising that the loop functions corresponding to isolated diagrams – B_0, C_0, D_0 and H_0 – do not fulfill the requirements we impose on physical quantities. As shown in [127], these functions are in general dependent on the applied gauge scheme, wherefore a set of better suited gauge invariant functions X_0, Y_0 and Z_0 has been derived there.

In the SM4 these functions are modified due to SM simplifications which do not longer hold in the presence of a fourth generation. In Appendix A.2 we calculate the corresponding functions in a different way than in [127], where the gauge dependence has been calculated and cancelled explicitly. By contrast, we use the fact that the Wilson coefficients for the relevant vertices must be gauge invariant and we simply take these to identify the appropriate loop functions.

The results of the detailed calculation that can be found in Appendix A.2, are as follows: The basic loop functions which are already gauge invariant read

$$S_0(x_i, x_j)\,, \qquad E_0(x_i)\,, \qquad D_0'(x_i)\,, \qquad E_0'(x_i)\,, \qquad H_0'(x_i)\,. \tag{4.4a}$$

In contrast, the loop functions B_0, C_0, D_0 and H_0 are not gauge invariant and have to be replaced by

$$\bar{X}^f(x_i) = X_0(x_i) + \sum_{j=2}^{4} \lambda_j^{(ff)} F^{(-)}(x_i, x_j)\,, \tag{4.4b}$$

$$\bar{Y}^f(x_i) = Y_0(x_i) - \sum_{j=2}^{4} \lambda_j^{(ff)} F^{(+)}(x_i, x_j)\,, \tag{4.4c}$$

$$\bar{Z}^{(i)}(x_i) = C_0(x_i) + \frac{1}{4} D^{(i)}(x_i)\,, \tag{4.4d}$$

where the functions on the right hand side can be found in Appendix B and (A.14), and the generalized CKM factors $\lambda_j^{(ff)}$ are defined in (2.18, 2.47). While S_0 is relevant for $\Delta F = 2$ observables, the function $\bar{X}^f$ ($\bar{Y}^f$) occurs in $\Delta F = 1$ processes with outgoing fermions $f\bar{f}$ and weak isospin $+\frac{1}{2}$ ($-\frac{1}{2}$). $\bar{Z}^{(i)}$ is a charge-dependent contribution to $\Delta F = 1$ processes with loop fermions i.

4.1.2.2. Master Functions

In the following work, we will study a large number of flavor observables that have already been calculated in the SM3. Of course, recalculating all these processes including a fourth generation would be a rather tedious procedure. In this section we will therefore introduce a rather simple generalization which makes it very easy to adapt the well-known SM3 expressions for our purposes.

$\Delta F = 1$ *observables:* Beginning with $\Delta F = 1$ observables, in the SM3 they usually are of the form

$$\mathcal{O}^{\rm SM3}_{\Delta F=1} \propto \sum_{i=2}^{3} \lambda_{u_i}^{(A)} f(x_{u_i}) = \lambda_c^{(A)} f(x_c) + \lambda_t^{(A)} f(x_t)\,, \tag{4.5}$$

where $A \in \{K, B_d, B_s\}$[1] denotes the considered meson system and $f \in \{X_0, Y_0, Z_0, D_0', E_0^{(\prime)}, H_0'\}$ is an arbitrary, real and universal Inami-Lim function. The charm contribution on the right hand side can usually be neglected in the $B_{s,d}$ systems but not in the K system. In the SM4, $\mathcal{O}_{\Delta F=1}$ obtains an additional contribution from the new t' quark in the loop, leading to

$$\mathcal{O}^{\rm SM4}_{\Delta F=1} \propto \sum_{i=2}^{4} \lambda_{u_i}^{(A)} \bar{f}(x_{u_i}) = \lambda_c^{(A)} \bar{f}(x_c) + \lambda_t^{(A)} \bar{f}(x_t) + \lambda_{t'}^{(A)} \bar{f}(x_{t'})\,, \tag{4.6}$$

where the modified $\bar{f} \in \{\bar{X}^f, \bar{Y}^f, \bar{Z}^{(i)}, D_0', E_0^{(\prime)}, H_0'\}$ is one of the gauge independent SM4 functions in (4.4). As in the case of the LHT model [71], we can now introduce so-called *master functions*:

$$f_A \equiv \bar{f}(x_t) + \frac{\lambda_{t'}^{(A)}}{\lambda_t^{(A)}} \bar{f}(x_{t'})\,, \tag{4.7}$$

which are basically generalized Inami-Lim functions. In contrast to the latter, the f_A are complex and non-universal, that means dependent on the considered process. By introducing them, we recover the SM3 form of (4.5):

$$\mathcal{O}^{\rm SM4}_{\Delta F=1} \propto \lambda_c^{(A)} \bar{f}(x_c) + \lambda_t^{(A)} f_A\,. \tag{4.8}$$

$\Delta F = 2$ *observables:* In the case of $\Delta F = 2$ processes, the situation is a little more complex. Here, the SM3 observable can be written as

$$\begin{aligned}\mathcal{O}^{\rm SM3}_{\Delta F=2} &\propto \sum_{i=2}^{3}\sum_{j=2}^{3} \lambda_{u_i}^{(A)} \lambda_{u_j}^{(A)} \eta_{u_i u_j}^{(A)} S_0(x_{u_i}, x_{u_j}) \\ &= \left(\lambda_c^{(A)}\right)^2 \eta_{cc}^{(A)}\ S_0(x_c) + 2\lambda_c^{(A)}\lambda_t^{(A)}\eta_{ct}^{(A)}\ S_0(x_c, x_t) + \left(\lambda_t^{(A)}\right)^2 \eta_{tt}^{(A)}\ S_0(x_t)\,. \end{aligned} \tag{4.9}$$

As in the $\Delta F = 1$ case, we can define a master function

$$S_A \equiv S_0(x_t) + \frac{\eta_{t't'}^{(A)}}{\eta_{tt}^{(A)}} \left(\frac{\lambda_{t'}^{(A)}}{\lambda_t^{(A)}}\right)^2 S_0(x_{t'}) + 2\frac{\eta_{tt'}^{(A)}}{\eta_{tt}^{(A)}}\frac{\lambda_{t'}^{(A)}}{\lambda_t^{(A)}} S_0(x_t, x_t') + 2\frac{\eta_{ct}^{(A)}}{\eta_{tt}^{(A)}}\frac{\lambda_c^{(A)}\lambda_{t'}^{(A)}}{\lambda_t^{(A)2}} S_0(x_c, x_t')\,, \tag{4.10}$$

such that we simply recover the SM3 form (4.9) in the SM4:

$$\mathcal{O}^{\rm SM4}_{\Delta F=2} = \left(\lambda_c^{(A)}\right)^2 \eta_{cc}^{(A)}\ S_0(x_c) + 2\lambda_c^{(A)}\lambda_t^{(A)}\eta_{ct}^{(A)}\ S_0(x_c, x_t) + \left(\lambda_t^{(A)}\right)^2 \eta_{tt}^{(A)}\ S_A\,. \tag{4.11}$$

[1] In this section we will only cover the K and B systems in order to keep the discussion as simple as possible. Of course the procedure can easily be applied to the D system as well, with only minor modifications.

Assuming the following approximate relations for the 4G QCD corrections[2],

$$\eta_{tt}^{(i)} \approx \eta_{tt'}^{(i)} \approx \eta_{t't'}^{(i)}, \qquad \eta_{ct}^{(i)} \approx \eta_{ct'}^{(i)}\,, \tag{4.12}$$

the master function simplifies to

$$S_A \equiv S_0(x_t) + \left(\frac{\lambda_{t'}^{(A)}}{\lambda_t^{(A)}}\right)^2 S_0(x_{t'}) + 2\frac{\lambda_{t'}^{(A)}}{\lambda_t^{(A)}} S_0(x_t, x_t') + 2\frac{\eta_{ct}^{(A)}}{\eta_{tt}^{(A)}}\frac{\lambda_c^{(A)}\lambda_{t'}^{(A)}}{\lambda_t^{(A)2}} S_0(x_c, x_t')\,. \tag{4.13}$$

Altogether, we have the following eight rules for replacing SM3 expressions by master functions in the SM4:

$$S_0(x_t) \to S_A \equiv |S_A| e^{i\theta_S^A}\,, \qquad X_0(x_t) \to X_A^f \equiv |X_A^f| e^{i\theta_X^{f,A}}\,, \tag{4.14a}$$

$$Y_0(x_t) \to Y_A^f \equiv |Y_A^f| e^{i\theta_Y^{f,A}}\,, \qquad Z_0(x_t) \to Z_A^{(i)} \equiv |Z_A^{(i)}| e^{i\theta_Z^{i,A}}\,, \tag{4.14b}$$

$$E_0(x_t) \to E_A \equiv |E_A| e^{i\theta_E^A}\,, \qquad D_0'(x_t) \to D_A' \equiv |D_A'| e^{i\theta_{D'}^A}\,, \tag{4.14c}$$

$$E_0'(x_t) \to E_A' \equiv |E_A'| e^{i\theta_{E'}^A}\,, \qquad H_0'(x_t) \to H_A' \equiv |H_A'| e^{i\theta_{H'}^A}\,, \tag{4.14d}$$

where the functions S_A and $f_A \in \{X_A^f, Y_A^f, Z_A^{(i)}, E_A, D_A', E_A', H_A'\}$ are given in (4.13) and (4.7), respectively.

4.2. Quark Flavor and CP Violation

In the following, we will introduce all the flavor and CP violation observables which will be used in our study of the fourth generation. Their experimental values and theoretical input parameters which are not given here can be found in Table 5.1.

4.2.1. Particle-Antiparticle Mixing ($\Delta F = 2$) and Indirect CP Violation

4.2.1.1. $K^0 - \bar{K}^0$ Mixing ($\Delta S = 2$)

Effective Hamiltonian: The effective Hamiltonian for $\Delta S = 2$ transitions in the full theory ($\mu_{\text{high}} \approx m_{t'}$) can be obtained from the elementary box vertex (A.6) given in Appendix A:

$$\mathcal{H}_{\text{eff}}^{\Delta S=2}(\mu_{\text{high}}) = i$$

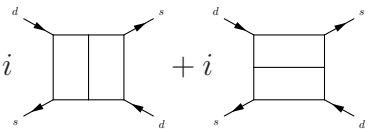

$$= \frac{G_F^2 M_W^2}{16\pi^2} \sum_{i,j=2}^{4} \lambda_{u_i}^{(K)} \lambda_{u_j}^{(K)} S_0(x_{u_i}, x_{u_j}) (\bar{s}d)_{\text{V-A}} (\bar{s}d)_{\text{V-A}} + \text{h.c.}\,, \tag{4.15}$$

[2]This approximation is justified as $m_{t'}$ is only by a factor of 2–3 larger than m_t, the anomalous dimension of the involved $(V-A)\otimes(V-A)$ operator is small, and the QCD corrections only very weakly depend on the actual value of $m_{t'}$ (where the t'–mass is defined as $m_{t'}(m_{t'})$).

with $u_{2,3,4} = c, t, t'$, $\lambda_{u_i}^{(K)} = V_{u_i s}^* V_{u_i d}$ defined in (2.20), $x_{u_i} = \frac{m_{u_i}^2}{M_W^2}$ and the loop function S_0 given in (B.1a).

For calculating observables, we need the effective Hamiltonian at the low scale $\mu \approx 1$ GeV:

$$\mathcal{H}_{\rm eff}^{\Delta S=2} = \frac{G_F^2 M_W^2}{16\pi^2} \sum_{i,j=2}^{4} \lambda_{u_i}^{(K)} \lambda_{u_j}^{(K)} \eta_{u_i u_j}^{(K)} S_0(x_{u_i}, x_{u_j}) \\ \times \left(\alpha_s^{(3)}(\mu)\right)^{-\frac{2}{9}} \left[1 + \frac{\alpha_s^{(3)}(\mu)}{4\pi} J_3\right] (\bar{s}d)_{\rm V-A} (\bar{s}d)_{\rm V-A} \tag{4.16}$$

where the QCD corrections obtained by renormalization group running from $\mu_{\rm high}$ to μ have been absorbed in the functions $\eta_{u_i u_j}^{(K)}$ and explicit factors of α_s.

Absorbing the contributions of the 4G quarks into a redefinition of the loop function $S_0(x_t)$ as discussed in Sec. 4.1.2.2, we can bring this Hamiltonian into the form known from the SM3,

$$\mathcal{H}_{\rm eff}^{\Delta S=2} = \frac{G_F^2 M_W^2}{16\pi^2} \left[\left(\lambda_c^{(K)}\right)^2 \eta_{cc}^{(K)} S_0(x_c) + \left(\lambda_t^{(K)}\right)^2 \eta_{tt}^{(K)} S_K + 2\lambda_t^{(K)} \lambda_c^{(K)} \eta_{ct}^{(K)} S_0(x_t, x_c) \right] \times \\ \times \left(\alpha_s(\mu)\right)^{-2/9} \left[1 + \frac{\alpha_s(\mu)}{4\pi} J_3\right] (\bar{s}d)_{\rm V-A} (\bar{s}d)_{\rm V-A}\,, \tag{4.17}$$

with the master function (4.13)

$$S_K = S_0(x_t) + \left(\frac{\lambda_{t'}^{(K)}}{\lambda_t^{(K)}}\right)^2 S_0(x_{t'}) + 2\frac{\lambda_{t'}^{(K)}}{\lambda_t^{(K)}} S_0(x_t, x_{t'}) + 2\frac{\eta_{ct}^{(K)}}{\eta_{tt}^{(K)}} \frac{\lambda_c^{(K)} \lambda_{t'}^{(K)}}{\lambda_t^{(K)2}} S_0(x_c, x_{t'})\,. \tag{4.18}$$

In writing this we have assumed the approximate relations (4.12) for the QCD corrections.

ΔM_K and ε_K: The off-diagonal element in the dispersive part of the amplitude for $K^0 - \bar{K}^0$ mixing is given by

$$2m_K \left(M_{12}^K\right)^* = \left\langle \bar{K}^0 | H_{\rm eff}^{\Delta S=2} | K^0 \right\rangle\,. \tag{4.19}$$

The usual procedure [128] then gives

$$M_{12}^K = \frac{G_F^2}{12\pi^2} F_K^2 \hat{B}_K m_K M_W^2 \overline{M}_{12}^K\,, \tag{4.20}$$

where

$$\overline{M}_{12}^K = \left(\lambda_c^{(K)*}\right)^2 \eta_{cc} S_0(x_c) + \left(\lambda_t^{(K)*}\right)^2 \eta_{tt}^{(K)} S_K^* + 2\eta_{ct}^{(K)} \lambda_t^{(K)*} \lambda_c^{(K)*} S_0(x_t, x_c), \tag{4.21}$$

and we have introduced the renormalization group invariant parameter

$$\hat{B}_K \equiv B_K(\mu) \left(\alpha_s(\mu)\right)^{-2/9} \left[1 + \frac{\alpha_s(\mu)}{4\pi} J_3\right]\,, \tag{4.22}$$

with

$$\left\langle \bar{K}^0|(\bar{s}d)_{\mathrm{V-A}}(\bar{s}d)_{\mathrm{V-A}}|K^0\right\rangle \equiv \frac{8}{3}B_K(\mu)F_K^2m_K^2\,. \tag{4.23}$$

Then

$$\Delta M_K = 2\mathrm{Re}\left(M_{12}^K\right)\,, \tag{4.24}$$

$$\varepsilon_K = \frac{\kappa_\varepsilon e^{i\varphi_\varepsilon}}{\sqrt{2}(\Delta M_K)_{\mathrm{exp}}}\mathrm{Im}\left(M_{12}^K\right)\,, \tag{4.25}$$

where the parameters $\varphi_\varepsilon = (43.51 \pm 0.05)^\circ$ and $\kappa_\varepsilon = 0.92 \pm 0.02$ [129] take into account that $\varphi_\varepsilon \neq \pi/4$ and include an additional effect from $\mathrm{Im}(A_0)$, the imaginary part of the isospin-0 amplitude in $K \to \pi\pi$. The result for κ_ε has recently been confirmed in [130][3]. The phase $2\varphi_K$ of the leading S_K^* term in (4.21) is given by

$$2\varphi_K = 2\bar{\beta} - 2\bar{\beta}_s - \theta_S^K\,, \tag{4.26}$$

with θ_S^K defined in (4.14) and the two phases β and β_s are given by

$$\beta \equiv -\mathrm{Arg}(V_{tb}^*V_{td}) \approx -\mathrm{Arg}(V_{td})\,, \qquad \beta_s \equiv -\mathrm{Arg}(V_{ts})\,. \tag{4.27}$$

Finally, we have to mention that concerning ΔM_K, the theory side cannot keep up with the very precise experimental measurements (s. Table 5.1). This is due to potentially large LD contributions to ΔM_K that – in spite of many efforts – are not well understood at present. Several analyses indicate that these contributions are positive and in the ballpark of 30% of the measured value [132–134]. This is supported by the fact that, in the SM3, the value of the SD box-diagram contributions ΔM_K^{SD} to ΔM_K amounts to only $(70 \pm 10)\%$ of the measured value.

4.2.1.2. $B_q^0 - \bar{B}_q^0$ Mixing ($\Delta B = 2$)

Effective Hamiltonian: In principle, (4.15) can be directly generalized to the B_d and B_s systems. In practice, the terms involving the charm quark mass are negligible and consequently ($q = d, s$)

$\mathcal{H}_{\mathrm{eff}}^{(B_q)} = i$ 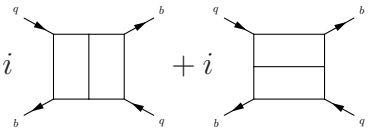 $+ i$

(4.28)

Again, we can retain the SM3 form by absorbing the t' contributions into a generalized Inami-Lim function S_q (4.13):

$$\mathcal{H}_{\mathrm{eff}}^{(B_q)} = \frac{G_F^2M_W^2}{16\pi^2}\eta_B\left(\lambda_t^{(q)}\right)^2 S_q\left[\alpha_s^{(5)}\right]^{-\frac{6}{23}}\left[1 + \frac{\alpha_s^{(5)}}{4\pi}J_5\right](\bar{b}q)_{\mathrm{V-A}}(\bar{b}q)_{\mathrm{V-A}}\,, \tag{4.29}$$

[3] The recent inclusion of additional long distance contributions modifies κ_ε to 0.94 ± 0.02 [131] without any visible impact on our numerical results.

$$S_q = S_0(x_t) + \frac{\eta_{t't'}^{(q)}}{\eta_{tt}^{(q)}} \left(\frac{\lambda_{t'}^{(q)}}{\lambda_t^{(q)}}\right)^2 S_0(x_{t'}) + 2\,\frac{\eta_{tt'}^{(q)}}{\eta_{tt}^{(q)}} \left(\frac{\lambda_{t'}^{(q)}}{\lambda_t^{(q)}}\right) S_0(x_t, x_{t'}) + 2\,\frac{\eta_{ct'}^{(q)}}{\eta_{tt}^{(q)}} \left(\frac{\lambda_c^{(q)}\lambda_{t'}^{(q)}}{\lambda_t^{(q)2}}\right) S_0(x_{t'}, x_c)\,, \tag{4.30}$$

where the relations (4.12) for QCD corrections have again been assumed. In contrast to the last term in (4.18), that can be relevant for certain values of the parameters involved, the last term in (4.30) turns out to be negligibly small.

$\Delta B = 2$ Observables: As in the K system (4.19), $B_q - \bar{B}_q$ mixing is described by the off-diagonal matrix element M_{12}^q $(q = d, s)$ given by

$$M_{12}^q = \frac{G_F^2}{12\pi^2} F_{B_q}^2 \hat{B}_{B_q} m_{B_q} M_W^2 \overline{M}_{12}^q\,, \tag{4.31}$$

where

$$\overline{M}_{12}^q = \left(\lambda_t^{(q)*}\right)^2 \eta_B S_q^*\,. \tag{4.32}$$

The contributions involving charm can be neglected. For the mass differences in the $B_{d,s}^0 - \bar{B}_{d,s}^0$ systems we have

$$\Delta M_q = 2\,|M_{12}^q|\,. \tag{4.33}$$

Indirect CP violation in the B_q system is determined by the phase $\varphi_{B_q}^{\rm tot}$, defined by

$$M_{12}^q = |M_{12}^q|\, e^{2i\varphi_{B_q}^{\rm tot}}. \tag{4.34}$$

In contrast to the K system, the different CP eigenstates B_q^0 and $\bar{B}_q^0$ do not decay in a distinctive manner, so the measurement of indirect CP violation is not that easy. However, in the SM3 it is a well-known fact [126] that the time-dependent CP asymmetries in the decays $B_d^0 \to \psi K_S$ and $B_s^0 \to \psi\phi$ are strongly dominated by the respective mixing phase. As we will argue in Section 4.2.5.3, this purity is somewhat weakened in the SM4, but nevertheless we still expect mixing to be the dominant source of CP violation. In this approximation, we can write the time-dependent CP asymmetries $S_{\psi K_S}$ and $S_{\psi\phi}$ by

$$S_{\psi K_S} = \sin 2\varphi_{B_d}^{\rm tot}\,, \qquad S_{\psi\phi} = -\sin 2\varphi_{B_s}^{\rm tot}\,. \tag{4.35}$$

A detailed discussion of the involved observables and phases can be found in Section 4.2.5.3.

Finally, we want to emphasize that in the SM4 the ratio $\Delta M_d/\Delta M_s$ does not determine directly the side R_t in the UT, since the UT does not close any more and there are non-MFV contributions. Therefore, the determination of the ratio $|V_{td}|/|V_{ts}|$ by means of

$$\frac{\Delta M_d}{\Delta M_s} = \frac{m_{B_d}}{m_{B_s}} \frac{\hat{B}_{B_d} F_{B_d}^2}{\hat{B}_{B_s} F_{B_s}^2} \left|\frac{V_{td}}{V_{ts}}\right|^2 \frac{|S_d|}{|S_s|}\,, \tag{4.36}$$

will clearly be affected since the last ratio is now generally different from unity.

4.2.1.3. $D^0 - \bar{D}^0$ Mixing ($\Delta C = 2$)

Effective Hamiltonian: The effective Hamiltonian for $\Delta C = 2$ transitions in the full theory can be obtained from the elementary box vertex (A.6)

$$\mathcal{H}_{\rm eff}^{\Delta C=2}(\mu_{\rm high}) = i$$ 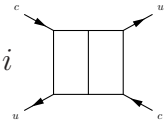 $$+ i$$ 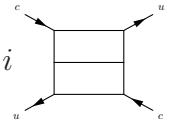

$$= \frac{G_F^2 M_W^2}{16\pi^2} \sum_{i,j=2}^{4} \lambda_{d_i}^{(D)} \lambda_{d_j}^{(D)} S(x_{d_i}, x_{d_j}) (\bar{u}c)_{\rm V-A} (\bar{u}c)_{\rm V-A} \,, \tag{4.37}$$

with the CKM factor defined in (2.20)

$$\lambda_{d_i}^{(D)} = V_{cd_i}^* V_{ud_i} \,. \tag{4.38}$$

Taking into account QCD corrections arising from RG running down to the scale μ, one obtains

$$\mathcal{H}_{\rm eff}^{\Delta C=2} = \frac{G_F^2 M_W^2}{16\pi^2} \sum_{i,j=2}^{4} \eta_{d_i d_j}^{(D)} \lambda_{d_i}^{(D)} \lambda_{d_j}^{(D)} S(x_{d_i}, x_{d_j}) \left[\alpha_s^{(4)}(\mu)\right]^{-\frac{6}{25}} \left[1 + \frac{\alpha_s^{(4)}(\mu)}{4\pi} J_4\right] (\bar{c}u)_{\rm V-A} (\bar{c}u)_{\rm V-A} \tag{4.39}$$

It should be remarked that with $m_{b'}$ defined as $m_{b'}(m_{b'})$ the QCD factors depend only weakly on $m_{b'}$. Moreover, the μ-dependent QCD corrections in (4.39) are absorbed in the renormalization group invariant parameter $\hat{B}_D$ defined by

$$\hat{B}_D = B_D(\mu) \left[\alpha_s^{(4)}(\mu)\right]^{-6/25} \left[1 + \frac{\alpha_s^{(4)}(\mu)}{4\pi} J_4\right] \,. \tag{4.40}$$

Lattice calculations [135–137] yield $B_D(\mu = 2\text{GeV}) = 0.845 \pm 0.024^{+0.024}_{-0.006}$, so together with $J_4 = 6719/3750$ [138] and $\alpha_s(M_Z) = 0.1184 \pm 0.0007$ [139], we find

$$\hat{B}_D = 1.18^{+0.07}_{-0.05} \,, \tag{4.41}$$

which will be used in our numerical calculations.

$\Delta C = 2$ Observables: The short distance (SD) contributions to the matrix element of the effective Hamiltonian (4.39) can be written as

$$\langle \bar{D}^0 | \mathcal{H}_{\rm eff}^{\Delta C=2} | D^0 \rangle_{\rm SD} \equiv \left| M_{12}^D \right| e^{2i\phi_D} = \left(M_{12}^D \right)^* \,, \tag{4.42}$$

where

$$M_{12}^D = \frac{G_F^2}{12\pi^2} F_D^2 \hat{B}_D m_D M_W^2 \overline{M}_{12}^D \,, \tag{4.43}$$

and

$$\overline{M}_{12}^{D} = \left(\lambda_s^{(D)*}\right)^2 \eta_{cc}^{(K)} S_0(x_s) + \left(\lambda_b^{(D)*}\right)^2 \eta_{cc}^{(K)} S_0(x_b) + \left(\lambda_{b'}^{(D)*}\right)^2 \eta_{tt}^{(K)} S_0(x_{b'}) + 2\lambda_b^{(D)*}\lambda_s^{(D)*}\eta_{cc}^{(K)} S_0(x_b, x_s) + 2\lambda_{b'}^{(D)*}\lambda_s^{(D)*}\eta_{ct}^{(K)} S_0(x_{b'}, x_s) + 2\lambda_{b'}^{(D)*}\lambda_b^{(D)*}\eta_{ct}^{(K)} S_0(x_{b'}, x_b)\,. \tag{4.44}$$

In contrast to [51] where the 4G mixing terms in $\overline{M}_{12}^{D}$ were neglected, we found that these terms can give important contributions and therefore such a simplification is not appropriate. For the QCD corrections we used the approximate relations

$$\eta_{b'b'}^{(D)} \approx \eta_{tt}^{(K)}\,, \qquad \eta_{b'b}^{(D)} \approx \eta_{b's}^{(D)} \approx \eta_{ct}^{(K)}\,, \qquad \eta_{ss}^{(D)} \approx \eta_{bb}^{(D)} \approx \eta_{bs}^{(D)} \approx \eta_{cc}^{(K)}\,, \tag{4.45}$$

which are found by comparing the size of QCD corrections in the $D^0 - \bar{D}^0$ and $K^0 - \bar{K}^0$ systems.

The full matrix elements are then given by

$$\langle \bar{D}^0 | \mathcal{H}_{\rm eff}^{\Delta C=2} | D^0 \rangle = \left(M_{12}^{D} + M_{12}^{\rm LD}\right)^* - \frac{i}{2}\Gamma_{12}^{\rm LD*}\,, \tag{4.46}$$

$$\langle D^0 | \mathcal{H}_{\rm eff}^{\Delta C=2} | \bar{D}^0 \rangle = \left(M_{12}^{D} + M_{12}^{\rm LD}\right) - \frac{i}{2}\Gamma_{12}^{\rm LD}\,. \tag{4.47}$$

Here $\Gamma_{12}^{\rm LD}$ and $M_{12}^{\rm LD}$ stand for long distance (LD) contributions with the former arising exclusively from SM3 dynamics. These contributions are very difficult to estimate and will be included in our phenomenological analysis using the strategy of [140, 141].

4.2.2. Leptonic Decays: $K_L \to \mu^+\mu^-$ and $B_{s,d} \to \mu^+\mu^-$

4.2.2.1. $K_L \to \mu^+\mu^-$

Effective Hamiltonian: Using (A.25) and the definitions thereafter, one finds for the effective Hamiltonian

$\mathcal{H}_{\rm eff}^{K_L\to\mu^+\mu^-} =$ 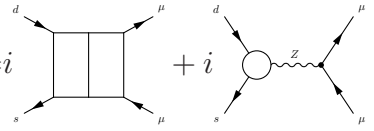 $+ i$

$$= -\frac{G_F}{\sqrt{2}}\frac{\alpha}{2\pi s_W^2}\sum_{i=2}^{4}\lambda_{u_i}^{(K)}\,\bar{Y}^{\mu}(x_{u_i})\,(\bar{s}d)_{\rm V-A}(\bar{\mu}\mu)_{\rm V-A}\,, \tag{4.48}$$

with the SM4 gauge independent loop function $\bar{Y}^{\mu}$ defined in (4.4c),

$$\bar{Y}^{\mu}(x_{u_i}) = Y_0(x_{u_i}) - \lambda_{\nu_4}^{(\mu\mu)} F^{(+)}(x_{u_i}, x_{\nu_4})\,, \tag{4.49}$$

where $\lambda_{\nu_4}^{(\mu\mu)} = |U_{\mu\nu_4}|^2$ (2.47) and the functions Y_0 and $F^{(+)}$ are given in Appendix B. Note that the charm contribution ($i = 2$) can be significant and therefore it cannot be neglected here. Again, we can rewrite this Hamiltonian in the form known from the SM3,

$$\mathcal{H}_{\rm eff}^{K_L\to\mu^+\mu^-} = -\frac{G_F}{\sqrt{2}}\frac{\alpha}{2\pi s_W^2}\left[\lambda_c^{(K)}\bar{Y}^{\mu}(x_c) + \lambda_t^{(K)} Y_K^{\mu}\right]\,, \tag{4.50}$$

by introducing the master function (4.7)

$$Y_K^\mu \equiv \bar{Y}^\mu(x_t) + \frac{\lambda_{t'}^{(K)}}{\lambda_t^{(K)}}\bar{Y}^\mu(x_{t'})\,. \tag{4.51}$$

Within the SM3, QCD corrections have been found to be tiny in the top quark part [142,143], so we will also neglect them for the t and t' contributions in the SM4. However, for the charm contributions QCD corrections are significant and have to be included [142,144]. However, it will be shown in Section 5.4 that $\lambda_{\nu_4}^{(\mu\mu)} \leq 0.025$ (s. Fig. 5.24). So the charm contribution will remain intact, which allows us to take the SM3 QCD corrections.

Branching Ratio and Experimental Status: In analogy to the SM3 case [144], the short distance contribution to the branching ratio is given in the SM4 by

$$\mathrm{Br}(K_L \to \mu^+\mu^-)_{\mathrm{SD}} = 2.08 \cdot 10^{-9} \left(\frac{\mathrm{Re}\lambda_c^{(K)}}{|V_{us}|} P_c(Y_K) + \frac{\mathrm{Re}(\lambda_t^{(K)} Y_K)}{|V_{us}|^5} \right)^2 , \tag{4.52}$$

where $P_c\,(Y_K) = 0.113 \pm 0.017$ [144].

Unlike $B_{s,d} \to \mu^+\mu^-$ which is discussed below, the SD part calculated here is only one part of a dispersive contribution to $K_L \to \mu^+\mu^-$ that is by far dominated by the absorptive part with two internal photon exchanges. Consequently, the SD contribution constitutes only a small fraction of the branching ratio. Moreover, because of long-distance (LD) contributions to the dispersive part of $K_L \to \mu^+\mu^-$, the extraction of the SD part from the data is subject to considerable uncertainties. The most recent estimate gives [145]

$$\mathrm{Br}(K_L \to \mu^+\mu^-)_{\mathrm{SD}} \leq 2.5 \cdot 10^{-9}\,, \tag{4.53}$$

to be compared with $(0.8 \pm 0.1) \cdot 10^{-9}$ in the SM3 [144].

4.2.2.2. $B_{s,d} \to \mu^+\mu^-$

Effective Hamiltonian: In analogy to (4.48), the effective Hamiltonian for $B_q \to \mu^+\mu^-$ ($q = s, d$) reads

$$\mathcal{H}_{\mathrm{eff}}^{B_q \to \mu^+\mu^-}(\mu_{\mathrm{high}}) = -\frac{G_F}{\sqrt{2}} \frac{\alpha}{2\pi s_W^2} \sum_{i=3}^{4} \lambda_{u_i}^{(B_q)}\; \bar{Y}^\mu(x_{u_i})\; (\bar{b}q)_{\mathrm{V-A}} (\bar{\mu}\mu)_{\mathrm{V-A}}\,, \tag{4.54}$$

where the negligible charm contributions have been dropped. This can again be rewritten into the SM3 form

$$\mathcal{H}_{\mathrm{eff}}^{B_q \to \mu^+\mu^-} = -\frac{G_F}{\sqrt{2}} \frac{\alpha}{2\pi s_W^2} \lambda_t^{(B_q)}\; Y_{B_q}\; (\bar{b}q)_{\mathrm{V-A}} (\bar{\mu}\mu)_{\mathrm{V-A}}\,, \tag{4.55}$$

with the master functions (4.7)

$$Y_{B_q}^\mu \equiv \bar{Y}^\mu(x_t) + \frac{\lambda_{t'}^{(B_q)}}{\lambda_t^{(B_q)}} \bar{Y}^\mu(x_{t'}) \tag{4.56}$$

Branching Ratio and Experimental Status: The two decays $B_{s,d} \to \mu^+\mu^-$ are helicity suppressed in the SM3 and CMFV models. Their branching ratios are proportional to the squares of the corresponding weak decay constants that still suffer from sizable uncertainties. However, using simultaneously the SM3 expressions for the very well measured mass differences $\Delta M_{s,d}$, these errors can be eliminated [146], leaving the hadronic parameters $\hat{B}_{B_s}$ and $\hat{B}_{B_d}$ as the only sources of theoretical uncertainty in $\mathrm{Br}(B_{s,d} \to \mu^+\mu^-)$. These parameters enter the branching ratios linearly and are already known from lattice calculations with $5-10\%$ precision, as seen in Table 5.1.

Translating this idea to the SM4, one finds with the help of the effective Hamiltonian (4.55),

$$\mathrm{Br}(B_q \to \mu^+\mu^-) = C\frac{\tau(B_q)}{\hat{B}_{B_q}}\frac{|Y_q|^2}{|S_q|}\Delta M_q\,, \qquad (q = s, d)\,, \tag{4.57}$$

where ΔM_q is supposed to be taken from experiment and the prefactor C is defined as

$$C = 6\pi\frac{\eta_Y^2}{\eta_B}\left(\frac{\alpha}{4\pi\sin^2\theta_W}\right)^2\frac{m_\mu^2}{M_{\mathrm{W}}^2} = 4.39\cdot 10^{-10}\,. \tag{4.58}$$

Consequently, the golden relation between $\mathrm{Br}(B_{d,s} \to \mu^+\mu^-)$ and $\Delta M_d/\Delta M_s$, valid in CMFV models [146], is modified as follows:

$$\frac{\mathrm{Br}(B_s \to \mu^+\mu^-)}{\mathrm{Br}(B_d \to \mu^+\mu^-)} = \frac{\hat{B}_{B_d}}{\hat{B}_{B_s}}\frac{\tau(B_s)}{\tau(B_d)}\frac{\Delta M_s}{\Delta M_d}\,r\,, \quad r = \left|\frac{Y_s}{Y_d}\right|^2\frac{|S_d|}{|S_s|}\,, \tag{4.59}$$

where $r = 1$ can now differ from unity.

The analogous SM3 expressions yield the rather precise predictions

$$\mathrm{Br}(B_s \to \mu^+\mu^-) = (3.2 \pm 0.2)\cdot 10^{-9}\,, \qquad \mathrm{Br}(B_d \to \mu^+\mu^-) = (1.0 \pm 0.1)\cdot 10^{-10}\,, \tag{4.60}$$

where the updated value of $\mathrm{Br}(B_s \to \mu^+\mu^-)$ has already been reported in [147]. These values should be compared to the 95% C.L. upper limits from CDF [148] and D0 [149] (in parentheses)[4]

$$\mathrm{Br}(B_s \to \mu^+\mu^-) \le 3.3\ (5.3)\cdot 10^{-8}\,, \qquad \mathrm{Br}(B_d \to \mu^+\mu^-) \le 1\cdot 10^{-8}\,. \tag{4.61}$$

The comparison of (4.60) and (4.61) reveals that a lot of space is still left for NP contributions in these channels. This gap could be closed soon as $\mathrm{Br}(B_s \to \mu^+\mu^-)$ is the subject of intensive research at LHCb. To show the power of this experiment, we also state the predicted exclusion limit [151] of

$$\mathrm{Br}(B_s \to \mu^+\mu^-)_{\mathrm{excl}} \approx 7\cdot 10^{-9} \qquad (\text{at } 90\%\ \text{C.L.})\,, \tag{4.62}$$

for an integrated luminosity of 1 fb^{-1}, which is expected by the end of 2011. With luck, even the more suppressed decay $B_d \to \mu^+\mu^-$ could soon be detected as well.

[4] The numbers given are updates presented at the EPS-HEP09 conference. More information is given by Punzi [150].

4.2.3. Semi-Leptonic Decays: $K \to \pi\nu\bar{\nu}$ and $B \to X_{d,s}\nu\bar{\nu}$

4.2.3.1. $K^+ \to \pi^+\nu\bar{\nu}$ and $K_L \to \pi^0\nu\bar{\nu}$

Effective Hamiltonian: Using the result for the general $\Delta F = 1$ effective Hamiltonian (A.25), we find for the decay of a $K = (K_L, K^+)$ into a corresponding $\pi = (\pi^0, \pi^+)$ meson and a pair of light neutrino mass eigenstates $\nu_l\bar{\nu}_l$ $(l = 1, 2, 3)$

$\mathcal{H}_{\rm eff}^{K\to\pi\nu_l\bar{\nu}_l} =$ 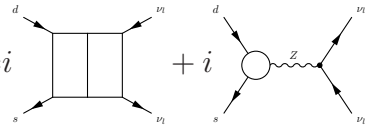 $+ i$

$$= \frac{G_F}{\sqrt{2}}\frac{\alpha}{2\pi s_W^2}\sum_{i=2}^{4}\lambda_{u_i}^{(K)}\ \bar{X}^{\nu_l}(x_{u_i})\ (\bar{s}d)_{\rm V-A}(\bar{\nu}_l\nu_l)_{\rm V-A}\,, \tag{4.63}$$

where the generalized SM4 gauge independent loop function $\bar{X}^i$ is defined in (4.4b),

$$\bar{X}^{\nu_l}(x_{u_i}) = X_0(x_{u_i}) + \sum_{j=3}^{4}\lambda_{\ell_j}^{(\nu_l\nu_l)}F^{(-)}(x_{u_i}, x_{\ell_j})\,, \tag{4.64}$$

with X_0 and $F^{(-)}$ given in Appendix B.

$\mathcal{H}_{\rm eff}$ can again be brought into the SM3 form [152]

$$\mathcal{H}_{\rm eff}^{K\to\pi\nu_l\bar{\nu}_l} = \frac{G_F}{\sqrt{2}}\frac{\alpha}{2\pi\sin^2\theta_W}\left[\lambda_c^{(K)}X_0(x_c) + \lambda_t^{(K)}X_K^{\nu_l}\right](\bar{s}d)_{V-A}(\bar{\nu}_l\nu_l)_{V-A}\,, \tag{4.65}$$

with (4.7)

$$X_K^{\nu_l} \equiv \bar{X}^{\nu_l}(x_t) + \frac{\lambda_{t'}^{(K)}}{\lambda_t^{(K)}}\bar{X}^{\nu_l}(x_{t'})\,. \tag{4.66}$$

Branching Ratios and Experimental Status: The SM4 generalization of the SM3 expressions for the branching ratios yields

$$\mathrm{Br}(K^+ \to \pi^+\nu_l\bar{\nu}_l) = \frac{\kappa_+}{3}\left[\left(\frac{\mathrm{Im}(\lambda_t^{(K)}X_K^{\nu_l})}{|V_{us}|^5}\right)^2 + \left(\frac{\mathrm{Re}\lambda_c^{(K)}}{|V_{us}|}P_c^{\nu_l}(X) + \frac{\mathrm{Re}(\lambda_t^{(K)}X_K^{\nu_l})}{|V_{us}|^5}\right)^2\right], \tag{4.67a}$$

$$\mathrm{Br}(K_L \to \pi^0\nu_l\bar{\nu}_l) = \frac{\kappa_L}{3}\left(\frac{\mathrm{Im}(\lambda_t^{(K)}X_K^{\nu_l})}{|V_{us}|^5}\right)^2, \tag{4.67b}$$

where the relevant hadronic matrix elements have been determined from tree-level leading K decays for $\lambda = 0.226$ [153]:

$$\kappa_+ = (5.36 \pm 0.026)\cdot 10^{-11}\,, \qquad \kappa_L = (2.31 \pm 0.01)\cdot 10^{-10}\,. \tag{4.68}$$

By summing over three light neutrinos ν_l in the final state, we then simply obtain

$$\mathrm{Br}(K^+ \to \pi^+\nu\bar{\nu}) = \sum_{l=1,2,3}\mathrm{Br}(K^+ \to \pi^+\nu_l\bar{\nu}_l)\,, \tag{4.69a}$$

$$\mathrm{Br}(K_L \to \pi^0 \nu\bar{\nu}) = \sum_{l=1,2,3} \mathrm{Br}(K_L \to \pi^0 \nu_l \bar{\nu}_l). \tag{4.69b}$$

In the case of small mixing of light neutrinos and heavy leptons, the l-dependence vanishes and the factors of $\frac{1}{3}$ in (4.67) simply drop out.

On the other hand, if the mixing with the 4G leptons is substantial, also the charm contribution will be affected. Taking this effect into account, one would also have to study the QCD corrections and electroweak corrections in the charm sector. Yet we do not think that this effort is worthwhile before the discovery of the fourth generation and we simply set

$$P_c^l(X) = P_c(X) = 0.42 \pm 0.03\,, \tag{4.70}$$

where $P_c(X)$ including the NNLO QCD corrections [154], electroweak corrections [155] and LD contributions [156] has been calculated in the SM3.

The most recent SM3 predictions read [154, 155]

$$\mathrm{Br}(K^+ \to \pi^+ \nu\bar{\nu})_{\mathrm{SM}} = (8.5 \pm 0.7)\cdot 10^{-11}\,, \qquad \mathrm{Br}(K_L \to \pi^0 \nu\bar{\nu})_{\mathrm{SM}} = (2.8 \pm 0.6)\cdot 10^{-11}\,, \tag{4.71}$$

where the errors are dominated by parametrical uncertainties, in particular by the CKM parameters. This is to be compared to the experimental values given by [157, 158]

$$\mathrm{Br}(K^+ \to \pi^+ \nu\bar{\nu}) = (17.3^{+11.5}_{-10.5}) \cdot 10^{-11}\,, \qquad \mathrm{Br}(K_L \to \pi^0 \nu\bar{\nu}) \le 6.7 \cdot 10^{-8}\,. \tag{4.72}$$

The experimental upper bound on $\mathrm{Br}(K_L \to \pi^0 \nu\bar{\nu})$ still surpasses the SM3 value by more than three orders of magnitude, but significant improvements are to be expected in the coming decade from E391a at KEK. In Section 5.1 we will see that the SM4 can accommodate spectacular enhancements of both branching ratios over their SM3 expectations.

4.2.3.2. $B \to X_{d,s}\nu\bar{\nu}$

Effective Hamiltonian: In analogy with (4.63), we find

$$\mathcal{H}_{\mathrm{eff}}^{B\to X_q \nu_l \bar{\nu}_l} = i$$

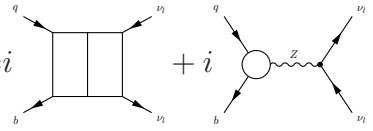

$$= \frac{G_F}{\sqrt{2}} \frac{\alpha}{2\pi s_W^2} \sum_{i=3}^{4} \lambda_{u_i}^{(B_q)}\ \bar{X}^{\nu_l}(x_{u_i})\ (\bar{b}q)_{\mathrm{V-A}} (\bar{\nu}_l \nu_l)_{\mathrm{V-A}}\,, \tag{4.73}$$

where the negligible charm contribution has again been dropped. This can be brought into the SM3 form [152]

$$\mathcal{H}_{\mathrm{eff}}^{B\to X_q \nu_l \bar{\nu}_l} = \frac{G_F}{\sqrt{2}} \frac{\alpha}{2\pi \sin^2\theta_W} \lambda_t^{(B_q)} X_{B_q}^{\nu_l}\ (\bar{b}q)_{V-A} (\bar{\nu}_l \nu_l)_{V-A}\,, \tag{4.74}$$

with the master function (4.7)

$$X_{B_q}^{\nu_l} \equiv \bar{X}^{\nu_l}(x_t) + \frac{\lambda_{t'}^{(B_q)}}{\lambda_t^{(B_q)}} \bar{X}^{\nu_l}(x_{t'})\,. \tag{4.75}$$

Branching Ratios and Experimental Status: For our analysis of the theoretically clean decays $B \to X_{s,d}\nu\bar{\nu}$, the most convenient quantities are the three ratios

$$\frac{\mathrm{Br}(B \to X_s\nu\bar{\nu})}{\mathrm{Br}(B \to X_s\nu\bar{\nu})_{\mathrm{SM3}}} = \frac{1}{3}\frac{\sum_{l=1,2,3}|X_{B_s}^{\nu_l}|^2}{|X_0(x_t)|^2} r_s\,, \qquad r_s = \frac{|V_{ts}|^2}{|V_{ts}|^2_{\mathrm{SM3}}}\,, \tag{4.76a}$$

$$\frac{\mathrm{Br}(B \to X_d\nu\bar{\nu})}{\mathrm{Br}(B \to X_d\nu\bar{\nu})_{\mathrm{SM3}}} = \frac{1}{3}\frac{\sum_{l=1,2,3}|X_{B_d}^{\nu_l}|^2}{|X_0(x_t)|^2} r_d\,, \qquad r_d = \frac{|V_{td}|^2}{|V_{td}|^2_{\mathrm{SM3}}}\,, \tag{4.76b}$$

$$\frac{\mathrm{Br}(B \to X_d\nu\bar{\nu})}{\mathrm{Br}(B \to X_s\nu\bar{\nu})} = \frac{\sum_{l=1,2,3}|X_{B_d}^{\nu_l}|^2}{\sum_{l=1,2,3}|X_{B_s}^{\nu_l}|^2}\left|\frac{V_{td}}{V_{ts}}\right|^2\,. \tag{4.76c}$$

It can be seen explicitly that the branching ratios are defined to include all three light neutrinos in the final state. The index SM3 reminds us that the extracted $|V_{td}|$ and $|V_{ts}|$ in the presence of 4G quarks can differ from those in the SM. Furthermore, we note that for $X_{B_d}^{\nu_l} \neq X_{B_s}^{\nu_l}$ the relation of the last ratio to $|V_{td}/V_{ts}|$ is modified with respect to MFV models.

Recent analyses of these decays within the SM3 and several NP scenarios can be found in [159, 160]. The recently improved SM3 prediction for $B \to X_s\nu\bar{\nu}$ reads [159]

$$\mathrm{Br}(B \to X_s\nu\bar{\nu})_{\mathrm{SM3}} = (2.7 \pm 0.2)\cdot 10^{-5}\,. \tag{4.77}$$

On the experimental side, the measurements of $B \to X_{s,d}\nu\bar{\nu}$ are even harder than those of the rare K decays discussed above. The experimental prospects for these decays at future Super-B machines are summarized in [161].

The formulae in (4.76) also apply to $B \to K^*\nu\bar{\nu}$, $B \to K\nu\bar{\nu}$ and various distributions discussed in [159, 162].

4.2.4. Radiative Decays: $B \to X_s\gamma$, $B \to X_s\ell^+\ell^-$ and $K_L \to \pi^0\ell^+\ell^-$

4.2.4.1. $B \to X_s\gamma$

The decay $B \to X_s\gamma$ is one of the most popular decays used to constrain NP contributions, for which the measured branching ratio [163]

$$\mathrm{Br}(B \to X_s\gamma)_{\mathrm{exp}} = (3.52 \pm 0.30)\cdot 10^{-4} \tag{4.78}$$

agrees well with the NNLO prediction in the SM3 [164],

$$\mathrm{Br}(B \to X_s\gamma)_{\mathrm{SM}} = (3.15 \pm 0.23)\cdot 10^{-4}\,. \tag{4.79}$$

Effective Hamiltonian and QCD Corrections: The effective Hamiltonian relevant for the decay $B \to X_s\gamma$ within the SM3 is given as follows,

$$\mathcal{H}_{\mathrm{eff}}^{\mathrm{SM}}(\bar{b} \to \bar{s}\gamma) = -\frac{G_F}{\sqrt{2}}\lambda_t^{(s)}\left[\sum_{i=1}^{6} C_i(\mu_b)Q_i + C_{7\gamma}(\mu_b)Q_{7\gamma} + C_{8G}(\mu_b)Q_{8G}\right]\,, \tag{4.80}$$

where Q_i are four-quark operators, $Q_{7\gamma}$ is the magnetic photon penguin operator and Q_{8G} the magnetic gluon penguin operator, contributing to $\bar{b} \to \bar{s}\gamma$ transitions.

In the LO approximation, the Wilson coefficients $C_{7\gamma}$ and C_{8G} at the renormalization scale $\mu_W = \mathcal{O}(M_W)$ are given by

$$C_{7\gamma}^{(0)}(\mu_W) = -\frac{1}{2}D'_s\,, \qquad C_{8G}^{(0)}(\mu_W) = -\frac{1}{2}E'_s\,, \tag{4.81}$$

with the master functions ($i = K, s, d$)

$$D'_i = D'_0(x_t) + \frac{\lambda_{t'}^{(i)}}{\lambda_t^{(i)}} D'_0(x_{t'})\,, \tag{4.82a}$$

$$E'_i = E'_0(x_t) + \frac{\lambda_{t'}^{(i)}}{\lambda_t^{(i)}} E'_0(x_{t'})\,. \tag{4.82b}$$

In view of the importance of QCD corrections in this decay, we will make sure that in the limit of neglecting 4G contributions the NNLO result in the SM3 (4.79) is reproduced. For this purpose, we will evaluate the known LO expressions for the relevant Wilson coefficients at an appropriately chosen renormalization scale, $\mu_{\rm eff}$, which turns out to equal 3.22GeV. The fact that this scale is somewhat lower than the bottom-quark mass, expresses the important role of QCD corrections, leading to an enhancement of the branching ratio. The 4G effects will then be included through the modification of the SM3 Wilson coefficients at $\mu = M_W$ without the inclusion of additional QCD corrections. Since the dominant QCD corrections to $\mathrm{Br}(B \to X_s\gamma)$ stem from the renormalization group evolution from M_W down to $\mu_{\rm eff}$, leading to dominant matrix elements of the operators Q_2 and $Q_{7\gamma}$ at $\mu_{\rm eff}$, these dominant corrections are common to the SM3 and the SM4. While not exact, this treatment of QCD corrections in the SM4 should be sufficient for our purposes.

Thus, in this approximate treatment the SM4 formulae for the relevant Wilson coefficients $C_{7\gamma}$ and C_{8G} are obtained by replacing $D'_0(x_t) \to D'_s$ and $E'_0(x_t) \to E'_s$ in the corresponding SM3 expressions evaluated at $\mu_{\rm eff} = 3.22$ GeV, yielding

$$C_{7\gamma}(\mu_{\rm eff}) = -(0.208 + 0.305D'_s + 0.052E'_s)\,, \qquad C_{8G}(\mu_{\rm eff}) = -(0.095 + 0.325E'_s)\,. \tag{4.83}$$

Branching Ratio: The explicit expression for the branching ratio $\mathrm{Br}(B \to X_s\gamma)$ resulting from (4.80), is very complicated and shall not be presented here (see [164] and references therein).

However, the ratio of SM4 to SM3 branching ratios can be expressed easily using the approximate $C_{7\gamma}$ from (4.83):

$$\frac{\mathrm{Br}(B \to X_s\gamma)}{\mathrm{Br}(B \to X_s\gamma)_{\rm SM}} = r_{bs\gamma}^2 \left| \frac{0.208 + 0.305D'_s + 0.052E'_s}{0.208 + 0.305D'_0(x_t) + 0.052E'_0(x_t)} \right|^2\,, \tag{4.84}$$

where $r_{bs\gamma}$, defined as

$$r_{bs\gamma} = \left(\frac{|V_{ts}^* V_{tb}|}{|V_{cb}|}\right) \Big/ \left(\frac{|V_{ts}^* V_{tb}|}{|V_{cb}|}\right)_{\rm SM}\,, \tag{4.85}$$

takes into account possible deviations of $V_{\rm SM4}$ from $V_{\rm SM3}$.

4.2.4.2. $B \to X_s \ell^+ \ell^-$

Theoretical Treatment: The decay $B \to X_s \ell^+ \ell^-$ proceeds very similar to $B \to X_s \gamma$ discussed in the previous section. Since the 4G effects in $B \to X_s \ell^+ \ell^-$ are not significant, we will only make sure that our numerical analysis is in accordance with the existing data. The theoretical expressions for the branching ratios and the forward-backward asymmetry in $b \to s\mu^+\mu^-$ [165–168] in the framework of the SM4 can again be obtained by taking the corresponding SM3 expressions and replacing the occurring master functions Y_s, Z_s, E_s, E' and D' by the SM4 master functions of Section 4.1.2.2. This replacement is demonstrated explicitly in Section 5.5 of [168]. Alternatively, all the formulae can be found in [169], so we chose not to repeat them here. The NNLO treatment can for instance be found in [170–173].

Experimental Status: Due to the presence of resonances there is no rigorous theoretical prediction for the whole q^2 range. Instead, theory and experiment are compared for a high q^2 cut, $q^2 > 14.4\,\mathrm{GeV}^2$, and a low q^2 range, $1\,\mathrm{GeV}^2 < q^2 < 6\,\mathrm{GeV}^2$. The BaBar [174] and Belle [175] collaboration published the following results for both ranges:

$$\mathrm{Br}(B \to X_s \ell^+ \ell^-)_{\mathrm{low}} = \begin{cases} \left(1.493 \pm 0.504^{+0.411}_{-0.321}\right) \cdot 10^{-6} & \text{Belle} \\ (1.8 \pm 0.7 \pm 0.5) \cdot 10^{-6} & \text{BaBar} \\ (1.6 \pm 0.5) \cdot 10^{-6} & \text{Average} \end{cases} \tag{4.86a}$$

$$\mathrm{Br}(B \to X_s \ell^+ \ell^-)_{q^2 > 14.4\mathrm{GeV}^2} = \begin{cases} \left(0.418 \pm 0.117^{+0.061}_{-0.068}\right) \cdot 10^{-6} & \text{Belle} \\ \left(0.5 \pm 0.25^{+0.08}_{-0.07}\right) \cdot 10^{-6} & \text{BaBar} \\ (0.44 \pm 0.12) \cdot 10^{-6} & \text{Average} \end{cases} \tag{4.86b}$$

For our numerical analysis we will use the averaged measurement. The NNLO prediction for the zero $\hat{s}_0$ of the forward-backward asymmetry A_{FB} in the SM3 is [171]

$$\hat{s}_0 = 0.162 \pm 0.008\,. \tag{4.87}$$

Note that according to [171], the NNLO contributions to $B \to X_s \ell^+ \ell^-$ are sizable and *negative*. To accommodate the NNLO effects, we matched our NLO result to the NNLO result given in [171] for the low and high q^2 ranges independently.

4.2.4.3. $K_L \to \pi^0 \ell^+ \ell^-$

Theoretical Status: Among the rare K meson decays, $K_L \to \pi^0 e^+ e^-$ and $K_L \to \pi^0 \mu^+ \mu^-$ belong to the theoretically cleanest, although they cannot compete with $K \to \pi\nu\bar{\nu}$. They are dominated by CP-violating contributions: In the SM3, the main contribution comes from the indirect (mixing-induced) CP violation and its interference with the direct CP-violating contribution [176–179]. The direct CP-violating contribution to the branching ratio is in the ballpark of $4 \cdot 10^{-12}$, while the CP-conserving contribution is at most $3 \cdot 10^{-12}$. Since the dominant indirect CP-violating contributions are practically determined by the measured decays $K_S \to \pi^0 \ell^+ \ell^-$ and the parameter ε_K, new physics contributions can only play a role in the subleading direct CP violation. Therefore the decays $K_L \to \pi^0 \ell^+ \ell^-$ are in general not as sensitive to new physics as $K_L \to \pi^0 \nu\bar{\nu}$. However, it has been pointed

out in [168] that in the presence of large new CP-violating phases, the direct CP-violating contribution can become dominant and enhance the branching ratios for $K_L \to \pi^0\ell^+\ell^-$ significantly, with a stronger effect in the case of $K_L \to \pi^0\mu^+\mu^-$ [178, 179]. Most recent discussions can be found in [180, 181].

Branching Ratios and Experimental Status: Adapting the formulae of [177–180] with the help of [168] to the SM4, we find

$$\mathrm{Br}(K_L \to \pi^0\ell^+\ell^-) = \left(C^\ell_{\mathrm{dir}} \pm C^\ell_{\mathrm{int}}\,|a_s| + C^\ell_{\mathrm{mix}}\,|a_s|^2 + C^\ell_{\mathrm{CPC}}\right)\cdot 10^{-12}\,, \tag{4.88}$$

where

$$C^e_{\mathrm{dir}} = (4.62 \pm 0.24)(\omega_{7V}^2 + \omega_{7A}^2)\,, \qquad C^\mu_{\mathrm{dir}} = (1.09 \pm 0.05)(\omega_{7V}^2 + 2.32\omega_{7A}^2)\,, \tag{4.89a}$$

$$C^e_{\mathrm{int}} = (11.3 \pm 0.3)\omega_{7V}\,, \qquad C^\mu_{\mathrm{int}} = (2.63 \pm 0.06)\omega_{7V}\,, \tag{4.89b}$$

$$C^e_{\mathrm{mix}} = 14.5 \pm 0.05\,, \qquad C^\mu_{\mathrm{mix}} = 3.36 \pm 0.20\,, \tag{4.89c}$$

$$C^e_{\mathrm{CPC}} \simeq 0\,, \qquad C^\mu_{\mathrm{CPC}} = 5.2 \pm 1.6\,, \tag{4.89d}$$

$$|a_s| = 1.2 \pm 0.2 \tag{4.89e}$$

with

$$\omega_{7V} = \frac{1}{2\pi}\left[P_0 + \frac{|Y^\ell_K|}{\sin^2\theta_W}\frac{\sin\beta^K_Y}{\sin(\beta-\beta_s)} - 4|Z^{(u)}_K|\frac{\sin\beta^K_Z}{\sin(\beta-\beta_s)}\right]\left[\frac{\mathrm{Im}\,\lambda_t^{(K)}}{1.4\cdot 10^{-4}}\right]\,, \tag{4.90a}$$

$$\omega_{7A} = -\frac{1}{2\pi}\frac{|Y^\ell_K|}{\sin^2\theta_W}\frac{\sin\beta^K_Y}{\sin(\beta-\beta_s)}\left[\frac{\mathrm{Im}\,\lambda_t^{(K)}}{1.4\cdot 10^{-4}}\right]\,. \tag{4.90b}$$

Here $P_0 = 2.88 \pm 0.06$ [182] includes NLO QCD corrections, Y^ℓ_K and $Z^{(u)}_K$ can be found in (4.7) and the corresponding phases are given as

$$\beta^{\ell,K}_Y = \beta - \beta_s - \theta^{\ell,K}_Y\,, \qquad \beta^{u,K}_Z = \beta - \beta_s - \theta^{u,K}_Z\,, \tag{4.91}$$

where $\theta^{\ell,K}_Y$ and $\theta^{u,K}_Z$ can be found in (4.14), and the phases β and β_s are defined in (4.27).

The new physics effects are mainly realized in ω_{7A}, since the corresponding contributions in ω_{7V} cancel each other to a large extent. The present experimental bounds [183, 184],

$$\mathrm{Br}(K_L \to \pi^0 e^+e^-) < 28\cdot 10^{-11}\,, \qquad \mathrm{Br}(K_L \to \pi^0\mu^+\mu^-) < 38\cdot 10^{-11}\,, \tag{4.92}$$

are still by one order of magnitude larger than the SM3 predictions, [180]

$$\mathrm{Br}(K_L \to \pi^0 e^+e^-)_{\mathrm{SM}} = 3.54^{+0.98}_{-0.85}\left(1.56^{+0.62}_{-0.49}\right)\cdot 10^{-11}\,, \tag{4.93a}$$

$$\mathrm{Br}(K_L \to \pi^0\mu^+\mu^-)_{\mathrm{SM}} = 1.41^{+0.28}_{-0.26}\left(0.95^{+0.22}_{-0.21}\right)\cdot 10^{-11}\,, \tag{4.93b}$$

where the values in parentheses correspond to the "$-$" sign in (4.88).

4.2.5. CP Violation in K and B Decays

4.2.5.1. Preliminaries

The observation of neutral K and B meson decays provides valuable information about CP violation (CPV), which occurs via two different mechanisms: Indirect CPV comes from mixing in the particular meson system and reflects the fact that mass eigenstates are not identical to CP eigenstates. In contrast to this, direct CPV occurs when the respective meson CP eigenstates decay into final states of different CP parity.

Since in the SM3 most CP asymmetries are predicted to be tiny and NP models could have rather large effects, these observables can provide a useful tool to test these models.

In this section we will examine the effects of a fourth generation on CP violation in several decays of B^0 and K^0 mesons.

4.2.5.2. Direct CP Violation in the K system: ε'/ε

The ratio ε'/ε measures the size of direct CP violation in $K_L \to \pi\pi$ relative to the indirect CP violation which is described by ε_K (4.25).

Experimental Status: Experimentally, ε'/ε can be measured via the relation

$$1 - 6\ \mathrm{Re}(\varepsilon'/\varepsilon) \approx \left|\frac{\eta_{00}}{\eta_{+-}}\right|^2 , \tag{4.94}$$

where $\eta_{00} = \frac{A(K_L \to \pi^0\pi^0)}{A(K_S \to \pi^0\pi^0)}$ and $\eta_{+-} = \frac{A(K_L \to \pi^+\pi^-)}{A(K_S \to \pi^+\pi^-)}$. The average from measurements at NA48 [185] and KTeV [186, 187] yields

$$\varepsilon'/\varepsilon = (16.8 \pm 1.4) \cdot 10^{-4} , \tag{4.95}$$

making this channel the first experimental evidence for direct CP violation.

Theoretical Status and SM4 Evaluation: Unfortunately, the theoretical side cannot keep up with the experimental data. Above all, the calculation suffers from large uncertainties in the relevant hadronic parameters B_6 and B_8 (see below).

In the SM3, ε' is governed by QCD penguins but receives also an important destructively interfering contribution from electroweak penguins that is generally much more sensitive to NP than the QCD penguin contribution. Since electroweak penguin and box diagrams also enter rare K decays like $\mathrm{Br}(K_L \to \pi^0\nu\bar{\nu})$ and $\mathrm{Br}(K^+ \to \pi^+\nu\bar{\nu})$, strong correlations between ε'/ε and these decays can be expected, as shown for several models in [188–190]

In order to obtain ε'/ε in the SM4, we will adapt the formulae given in [190], which are based on [191] and yield

$$\varepsilon'/\varepsilon = \mathrm{Im}\lambda_c^{(K)} P_0 + \mathrm{Im}\lambda_t^{(K)} F_{\varepsilon'}(x_t) + \mathrm{Im}\lambda_{t'}^{(K)} F_{\varepsilon'}(x_{t'}) , \tag{4.96}$$

with

$$F_{\varepsilon'}(x) = P_0 + P_X X_0(x) + P_Y Y_0(x) + P_Z Z_0(x) + P_E E_0(x) . \tag{4.97}$$

While the loop functions X_0, Y_0, Z_0 and E_0 given in Appendix B arise from short distance physics, the coefficients P_i describe physics at scales $\mu \leq \mathcal{O}(m_t, M_W)$. They are given as

$$P_i = r_i^{(0)} + r_i^{(6)} R_6 + r_i^{(8)} R_8 \,. \tag{4.98}$$

The coefficients $r_i^{(j)}$ come from Wilson coefficients of the $\Delta S = 1$ weak effective Hamiltonian at NLO [152], their numerical values for different values of $\Lambda_{\rm QCD}$ can be found in [191].

From (4.96) and (4.98) one can see that ε'/ε depends crucially on the hadronic parameters R_6 and R_8, which are related to the matrix elements $B_6^{(1/2)}$ ($B_8^{(3/2)}$) of the dominant QCD (EW) penguin operator $\mathcal{Q}_6$ ($\mathcal{Q}_8$) by

$$R_6 \equiv B_6^{(1/2)} \left[\frac{121\text{MeV}}{m_s(mc) + m_d(mc)}\right]^2 , \quad R_8 \equiv B_8^{(3/2)} \left[\frac{121\text{MeV}}{m_s(mc) + m_d(mc)}\right]^2 . \tag{4.99}$$

In the strict large-N_C limit, $B_6^{(1/2)} = B_8^{(3/2)} = 1$, being compatible with lattice calculations which are however subject to large systematic uncertainties (s. [190] for further details and references). Altogether, we expect R_6 and R_8 to be in the ballpark of

$$R_8 \approx 1 \pm 0.5 \,, \qquad R_6 \approx 1 \pm 0.5 \,. \tag{4.100}$$

Hopefully, lattice calculations will provide better values [192] in the near future. Meanwhile, it appears to be the best strategy to be to study a set of different scenarios for R_6 and R_8, which we will do in our numerical analysis in Section 5.

4.2.5.3. CP-Violating B Decays into CP Eigenstates

Preliminaries

One special class of B_q decays is very auspicious with respect to the extraction of CP phases: transitions into CP eigenstates $|f\rangle$, satisfying

$$\mathcal{CP}|f\rangle = \eta_f |f\rangle \,, \tag{4.101}$$

with $\eta_f = \pm 1$ being the CP eigenvalue of f. The time-dependent CP asymmetries in these decays can be written as

$$\mathcal{A}_f(t) = S_f \sin(\Delta M_q t) - C_f \cos(\Delta M_q t) \,. \tag{4.102}$$

The CP asymmetries S_f and C_f are calculated as follows. One defines a complex quantity ξ_f,

$$\xi_f = e^{-2i\varphi_{B_q}^{\rm tot}} \frac{\bar{A}_f^q}{A_f^q} \,, \tag{4.103}$$

where $\varphi_{B_q}^{\rm tot}$ is the phase of the B_q-mixing amplitude $M_{12}^{B_q}$ and thus describes the "indirect" contribution to CP violation. Direct CP violation is characterized by the decay amplitudes A_f^q ($\bar{A}_f^q$) for $B_q(\overline{B_q}) \to f$, which can be calculated from the effective Hamiltonian relevant for $\Delta B = 1$ decays [152] in the following way

$$A_f^q = \langle f|\mathcal{H}_{\rm eff}|B_q\rangle \,, \quad \bar{A}_f^q = \langle f|\mathcal{H}_{\rm eff}|\overline{B_q}\rangle \,, \tag{4.104}$$

where the Wilson coefficients of the effective Hamiltonian depend on the electroweak theory while the matrix elements $\langle f|O_i|B_q(\overline{B_q})\rangle$ can be estimated, for instance, by means of QCD factorization [193]. We then find

$$S_f = \frac{2\mathrm{Im}(\xi_f)}{1+|\xi_f|^2}\,, \quad C_f = \frac{1-|\xi_f|^2}{1+|\xi_f|^2}\,. \tag{4.105}$$

Following [193], the SM3 contribution to the decay amplitudes of $\bar{b} \to \bar{q}'q'\bar{r}$ $(r = d, s)$ transitions can be written as a sum of two terms, $A_f^{\mathrm{SM}} = A_f^c + A_f^u$, with $A_f^c \propto V_{cb}^* V_{cr}$ and $A_f^u \propto V_{ub}^* V_{ur}$. Defining the ratio $a_f^u \equiv e^{-i\gamma}(A_f^u/A_f^c)$, we have

$$A_f^{\mathrm{SM}} = A_f^c \left(1 + a_f^u e^{i\gamma}\right)\,, \tag{4.106}$$

where the parameters a_f^u have been evaluated in the QCD factorization approach [5] [193,195, 196].

In the SM4, for simplicity, we follow the analysis in [193] which only takes into account the leading-order terms in α_s and neglects Λ/m_b corrections (except for so-called chirally enhanced terms). The modification of A_f in (4.106) due to 4G contributions can then be written as

$$A_f = A_f^c \left[1 + a_f^u e^{i\gamma} + \sum_i \left(b_{fi}^c + b_{fi}^u e^{i\gamma}\right) C_i^{\mathrm{NP}}(M_W)\right]\,, \tag{4.107}$$

where $C_i^{\mathrm{NP}}(M_W)$ are the NP contributions to the Wilson coefficients evaluated at the scale M_W. Defining the NP contributions to the master functions F_i given in Section 4.1.2.2 by

$$F_i = F_0^{\mathrm{SM}} + \Delta F_i\,, \tag{4.108}$$

the non-vanishing $C_i^{\mathrm{NP}}(M_W)$ relevant for $\bar{b} \to \bar{s}$ transitions are given as follows:

$$C_3^{\mathrm{NP}}(M_W) = \frac{\alpha}{6\pi}\frac{1}{\sin^2\theta_W}\left(2\Delta Y_{B_r} - \Delta X_{B_r}\right)\,, \tag{4.109a}$$

$$C_7^{\mathrm{NP}}(M_W) = \frac{\alpha}{6\pi}\,4\Delta Z_{B_r}\,, \tag{4.109b}$$

$$C_9^{\mathrm{NP}}(M_W) = \frac{\alpha}{6\pi}\left[4\Delta Z_{B_r} - \frac{2}{\sin^2\theta_W}\left(\Delta X_{B_r} + \Delta Y_{B_r}\right)\right]\,, \tag{4.109c}$$

$$C_{7\gamma}^{\mathrm{NP}}(M_W) = -\frac{1}{2}\Delta D'_{B_r}\,, \tag{4.109d}$$

$$C_{8G}^{\mathrm{NP}}(M_W) = -\frac{1}{2}\Delta E'_{B_r}\,. \tag{4.109e}$$

Here $\alpha = \alpha(M_W) = 1/127.9$ is the QED coupling constant and $\sin^2\theta_W = 0.231$. Having these formulae at hand, we can now study the most interesting CP-violating B decays in more detail.

[5] A critical discussion of the importance of power corrections and the potential size of long-distance final-state interactions in (4.106) can be found in [194]. As long as a model-independent prediction for these effects is lacking, we have to assign an irreducible theoretical error to the predictions for the a_f^u.

CP Asymmetries in the decays $B_d \to xK_s$ ($x = J/\psi, \phi, \eta'$)

The decays $B_d \to J/\psi K_s$, $B_d \to \phi K_s$ and $B_d \to \eta' K_s$ proceed at the quark level as $\bar{b} \to \bar{q}' q' \bar{s}$ ($q' = c, s, d, u$). Therefore, the coefficient $a_f^u \propto \frac{V_{ub}^* V_{us}}{V_{cb}^* V_{cs}}$ in (4.107) is Cabibbo-suppressed by $\mathcal{O}(\lambda^2)$.

Within the SM, it is predicted with good accuracy that the $|S_f|$ and C_f parameters are universal for all the transitions $\bar{b} \to \bar{q}' q' \bar{s}$. It turns out that $S_{\phi K_S} \simeq S_{\eta' K_S} \simeq S_{\psi K_S} \simeq \sin 2\beta$, with precise predictions given in Tables 1 and 6 of [75]. In particular, the SM3 predicts that $-\eta_f S_f \simeq \sin 2\beta$ and $C_f \simeq 0$. NP effects can contribute to[6]

(i) the B_d mixing amplitude [197],

(ii) the decay amplitudes $\bar{b} \to \bar{q} q \bar{s}$ ($q = s, d, u$) [197–199].

In case (i), the NP contribution shifts all S_f asymmetries away from $\sin 2\beta$ in a universal way, while the C_f asymmetries will still vanish. In case (ii), the various S_f and also the C_f asymmetries are, in general, different from their values in the SM3.

$B_d \to J/\psi K_S$: In the SM3, the cleanest CP-violating B_d decay is $B_d \to J/\psi K_s$, where a_f^u in (4.107) is negligible within a very good approximation, so

$$\xi_{\psi K_S}^{\rm SM3} = e^{-2i\beta}\,, \tag{4.110}$$

with $\beta = -{\rm Arg}(V_{td})$ (4.27) and therefore

$$S_{\psi K_S}^{\rm SM3} = \sin 2\beta\,. \tag{4.111}$$

In the SM4, there are two possible sources of deviation from this relation:

- The B_d mixing phase defined in (4.34),

$$2\varphi_{B_d}^{\rm tot} = {\rm Arg}(M_{12}^d) = 2{\rm Arg}(V_{td}^*) - {\rm Arg}(S_d) = 2\beta - \theta_{S_d}\,, \tag{4.112}$$

  is not longer determined by the single CKM matrix element V_{td}, but rather a combination of different matrix elements. It should also be emphasized that in the SM4, β differs from the SM3 value $\beta^{\rm SM3} \approx 21^\circ$ obtained from unitarity triangle (UT) analyses. As we will see, $\varphi_{B_d}^{\rm tot}$ will only slightly differ from β because of the experimental constraint on $S_{\psi K_S}$.

- In principle, sizable deviations can occur in $S_{\psi K_S}$ due to t' penguin pollution, especially for the case of large fourth-family mixing. We have evaluated these effects and found that possible corrections can be as large as 10%, dominated by hadronic uncertainties. So for our numerical analysis we are forced to take the formula of (4.35),

$$S_{\psi K_S} = \sin 2\varphi_{B_d}^{\rm tot}\,, \tag{4.113}$$

  and soften the experimental bounds on $S_{\psi K_S}$ appropriately.

[6] We assume that the asymmetry in the tree-level transition $\bar{b} \to \bar{c} c \bar{s}$ is not significantly affected by NP.

f	ϕK_s	$\eta' K_s$
b^c_{f3}	-46	-26
b^c_{f7}	22	3.8
b^c_{f9}	23	3.5
b^c_{f8G}	1.4	0.86

Table 4.1.: Hadronic parameters at $\mu = m_b$ taken from [193]. The parameters b^u_{fi} can be obtained via $b^u_{fi} = (|V_{ub}V^*_{us}|/|V_{cb}V^*_{cs}|)b^c_{fi}$.

$B_d \to \phi(\eta')K_S$: The theoretically rather clean asymmetries $S_{\phi K_S}$ and $S_{\eta' K_S}$ are measured to be

$$S_{\phi K_S} = 0.44 \pm 0.17, \qquad S_{\eta' K_S} = 0.59 \pm 0.07\,. \tag{4.114}$$

While $S_{\phi K_S}$ is found to be significantly smaller than the expected value of approximately 0.70 [196, 200, 201], $S_{\eta' K_S}$ is fully consistent with the expectations although on the low side. The parameters b^u_{fi} and b^c_{fi} calculated in [193] are collected for the ϕK_S and $\eta' K_S$ channels in Table 4.1. As the effects in $B \to X_s\gamma$ are small, we follow [193] and neglect $C_{7\gamma}$.

We note that within a very good approximation

$$A_f \approx A^c_f \left[1 + \sum_i b^c_{fi} C^{\rm NP}_i(M_W)\right] = A^c_f \left[1 + r_f \frac{\lambda^{(s)}_{t'}}{\lambda^{(s)}_t}\right], \tag{4.115}$$

where

$$r_{\phi K_S} = -0.248\; Y_0(x_{t'}) + 0.004\; X_0(x_{t'}) + 0.075\; Z_0(x_{t'}) - 0.7\; E'_0(x_{t'})\,, \tag{4.116}$$

$$r_{\eta' K_S} = -0.106\; Y_0(x_{t'}) + 0.034\; X_0(x_{t'}) + 0.012\; Z_0(x_{t'}) - 0.43\; E'_0(x_{t'})\,. \tag{4.117}$$

Thus, the departure of $S_{\phi K_S}$ and $S_{\eta' K_S}$ from $S_{\psi K_S}$ is governed by the common phase of $\lambda^{(s)}_{t'}/\lambda^{(s)}_t$ with the effect being larger in the case of $S_{\phi K_S}$. Denoting the final phase of A_f by φ_f, we find

$$S_f = -\eta_f \sin(2(\varphi^{\rm tot}_{B_d} + \varphi_f)), \tag{4.118}$$

where the CP parity of the final state $\eta_f = -1$ for both channels considered here. For $\varphi_f \neq 0$ the departure from $S_{\psi K_S}$ in (4.35) can be obtained.

It is known that going beyond leading order in the calculations of the b_f parameters, one would introduce a potentially sizable strong phase. We will comment on this issue in Section 5.1.5.

CP Asymmetries in $B_s \to J/\psi\phi$

In the SM3, the decay $B_s \to J/\psi\phi$ is a theoretically very clean way to extract the angle $\beta_s \equiv -{\rm Arg}(V_{ts})$ defined in (4.27), via the relation

$$S^{\rm SM3}_{\psi\phi} = -\sin 2\beta_s\,. \tag{4.119}$$

Including the fourth generation, the involved B_s mixing phase changes to

$$2\varphi^{\rm tot}_{B_s} = {\rm Arg}(M^s_{12}) = 2{\rm Arg}(V_{ts}) - {\rm Arg}(S_s) \equiv 2\beta_s - \theta^s_S\,, \tag{4.120}$$

where θ_S^s is defined in (4.14) and the CP asymmetry $S_{\psi\phi}$ reads

$$S_{\psi\phi} = -\sin 2\varphi_{B_s}^{\rm tot}\,, \tag{4.121}$$

which has already been anticipated in (4.35).

Again, β_s differs from its SM3 value $\beta_s^{\rm SM3} \approx -1^\circ$ obtained from UT analyses. The full angle $\varphi_{B_s}^{\rm tot}$ is expected to be very different from $\beta_s^{\rm SM3}$, in order to reproduce the data on $S_{\psi\phi}$ from CDF [202] and D0 [203], which are combined by HFAG [163] to

$$\varphi_{B_s}^{\rm tot} = -(0.39^{+0.18}_{-0.14}) \ \left[-(1.18^{+0.14}_{-0.18})\right]\,. \tag{4.122}$$

As we will see in Section 5.3, a big $S_{\psi\phi}$ will strongly correlate δ_{14} and δ_{24} as well as s_{14} and s_{24}.

4.2.5.4. $A_{\rm CP}(b \to s\gamma)$ in the SM4

The direct CP asymmetry in $B \to X_s\gamma$ decays $A_{\rm CP}(b \to s\gamma)$ [204–206] is predicted to be tiny in the SM3 but could be much larger in some of its extensions. Therefore $A_{\rm CP}(b \to s\gamma)$ is an attractive quantity to study, which has been analyzed recently in detail in the context of the flavor-blind MSSM (FBMSSM) [207] and supersymmetric flavor models [75]. As pointed out in [75, 207], it is interesting to consider the direct CP asymmetry in question together with the asymmetry $S_{\phi K_S}$ treated above.

If NP effects dominate over the SM3 contribution $A_{\rm CP}^{\rm SM}(b \to s\gamma) \simeq -0.5\%$, the following expression holds [205, 206],

$$\begin{aligned} A_{\rm CP}(b \to s\gamma) &\equiv \frac{\Gamma(B \to X_{\bar s}\gamma) - \Gamma(\overline{B} \to X_s\gamma)}{\Gamma(B \to X_{\bar s}\gamma) + \Gamma(\overline{B} \to X_s\gamma)} \\ &\simeq -\frac{1.23\ {\rm Im}[C_2 C_{7\gamma}] - 9.52\ {\rm Im}[C_{8G}^* C_{7\gamma}] + 0.10\ {\rm Im}[C_2 C_{8G}]}{|C_{7\gamma}|^2} - 0.5 \quad (\text{in } \%)\,, \end{aligned} \tag{4.123}$$

where we assumed a cut for the photon energy at $E_\gamma \simeq 1.8$GeV (see [205, 206] for details). In (4.123), the Wilson coefficients C_i are evaluated at the scale $\mu_{\rm eff}$ as given in (4.83). The Wilson coefficient C_2 is to a very good approximation independent of the 4G parameters and given by $C_2(\mu_{\rm eff}) \approx 1.14$. This treatment of QCD corrections is certainly an approximation and a full NNLO analysis would be much more involved. Yet, at present a NNLO analysis would clearly be premature.

4.3. Lepton Flavor Violation

4.3.1. Preliminaries

The lepton sector is in many ways different from the quark sector. Until the beginning of this century one could safely assume that neutrinos were massless and therefore transitions between fermion families were forbidden in the SM. But since the discovery of neutrino oscillations [30–32], we know that neutrinos do have masses and therefore lepton family number is not longer a conserved quantum number. However, the SM predicts only tiny branching ratios for lepton flavor violating (LFV) decays due to the small masses of the three known neutrinos (less than 1 eV). This is in good agreement with the experimental side, where no direct measurement of any lepton flavor violating process – except for neutrino oscillations – has been made so far. Nonetheless, the upper bounds obtained from these experiments provide valuable constraints on new physics such as the fourth generation, where especially the heavy fourth neutrino could increase LFV processes considerably. In this section we present the LFV observables which will be analyzed numerically in Section 5.4. The measured upper bounds on these processes will also be given there in Table 5.11.

4.3.2. Dipole Transitions ($\ell_a \to \ell_b\gamma$)

Effective Hamiltonian: The effective Hamiltonian relevant for the decays $\ell_a \to \ell_b\gamma$ can be obtained from the elementary vertex (A.17)

$\mathcal{H}_{\text{eff}}^{\ell_a\to\ell_b\gamma} = i$ 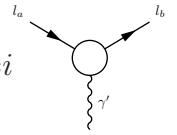

$$= -\frac{G_F}{\sqrt{2}}\frac{e}{8\pi^2}\lambda_{\nu_4}^{(\ell_a\ell_b)} H_0'(x_{\nu_4})\ \bar{\ell}_b\left[i\sigma^{\mu\nu}q^\nu m_{\ell_a}(1+\gamma_5)\right]\ell_a\,, \tag{4.124}$$

Branching Ratios: Having the effective Hamiltonian (4.124) at hand, it is a straightforward exercise to generalize the SM3 formulae [208] for the branching ratios

$$\text{Br}(\mu\to e\gamma) = \frac{3\alpha}{2\pi}\left|\lambda_{\nu_4}^{(\mu e)}\right|^2 H_0'(x_{\nu_4})^2\,, \tag{4.125a}$$

$$\text{Br}(\tau\to e\gamma) = \frac{3\alpha}{2\pi}\text{Br}(\tau^-\to\nu_\tau e^-\bar{\nu}_e)\left|\lambda_{\nu_4}^{(\tau e)}\right|^2 H_0'(x_{\nu_4})^2\,, \tag{4.125b}$$

$$\text{Br}(\tau\to \mu\gamma) = \frac{3\alpha}{2\pi}\text{Br}(\tau^-\to\nu_\tau \mu^-\bar{\nu}_\mu)\left|\lambda_{\nu_4}^{(\tau\mu)}\right|^2 H_0'(x_{\nu_4})^2\,. \tag{4.125c}$$

where the loop function $H_0'(x)$ is given in (B.4g) and the involved branching ratios of leptonic τ decays are [197]

$$\text{Br}(\tau^-\to\nu_\tau e^-\bar{\nu}_e) = (17.84\pm 0.05)\%\,, \tag{4.126a}$$

$$\text{Br}(\tau^-\to\nu_\tau \mu^-\bar{\nu}_\mu) = (17.36\pm 0.05)\%\,. \tag{4.126b}$$

In writing (4.125), we have neglected electroweak (EW) corrections and non-unitarity corrections in the PMNS matrix that affect the leptonic decays and have been recently discussed by Lacker and Menzel [209]. Similarly, we have neglected corrections $\sim \mathcal{O}(m_\mu^2/m_\tau^2)$, $\sim \mathcal{O}(m_e^2/m_\tau^2)$ and $\sim \mathcal{O}(m_e^2/m_\mu^2)$. These corrections amount to at most a few percent and would only be necessary in the presence of very accurate experimental branching ratios.

The important virtue of formulae (4.125) is that they allow for a direct determination of the ratios of the elements $|U_{e4}|$, $|U_{\mu 4}|$ and $|U_{\tau 4}|$, independently of the mass m_{ν_4}. In particular, we have

$$\frac{\mathrm{Br}(\tau \to \mu\gamma)}{\mathrm{Br}(\mu \to e\gamma)} = \left|\frac{U_{\tau 4}}{U_{e4}}\right|^2 \mathrm{Br}(\tau^- \to \nu_\tau \mu^- \bar{\nu}_\mu)\,, \tag{4.127}$$

$$\frac{\mathrm{Br}(\tau \to \mu\gamma)}{\mathrm{Br}(\tau \to e\gamma)} = \left|\frac{U_{\mu 4}}{U_{e4}}\right|^2 \frac{\mathrm{Br}(\tau^- \to \nu_\tau \mu^- \bar{\nu}_\mu)}{\mathrm{Br}(\tau^- \to \nu_\tau e^- \bar{\nu}_e)} \approx \left|\frac{U_{\mu 4}}{U_{e4}}\right|^2\,, \tag{4.128}$$

$$\frac{\mathrm{Br}(\tau \to e\gamma)}{\mathrm{Br}(\mu \to e\gamma)} = \left|\frac{U_{\tau 4}}{U_{\mu 4}}\right|^2 \mathrm{Br}(\tau^- \to \nu_\tau e^- \bar{\nu}_e)\,. \tag{4.129}$$

This would provide very important information about the involved PMNS matrix elements in the SM4 framework, once these processes have been measured.

4.3.3. Four-Lepton Transitions

4.3.3.1. The Decays $\tau^- \to \ell_b^- \ell_c^+ \ell_b^-$ ($\tau^- \to e^-\mu^+e^-$ and $\tau^- \to \mu^- e^+ \mu^-$)

The two decays $\tau^- \to e^-\mu^+e^-$ and $\tau^- \to \mu^- e^+ \mu^-$ are of $\Delta L = 2$ type and strongly suppressed in the SM.

Effective Hamiltonian: The effective Hamiltonians for the two decays are analogous to those of $\Delta F = 2$ processes. Taking the $\Delta F = 2$ vertex (A.6), one obtains

$$\mathcal{H}_{\mathrm{eff}}^{\tau \to \ell_b \bar{\ell}_c \ell_b} = i$$

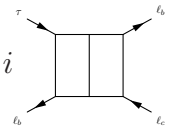

$$= \frac{G_F^2}{4\pi^2} \lambda_{\nu_4}^{(\tau \ell_b)} \lambda_{\nu_4}^{(\ell_b \ell_c)} S_0(x_{\nu_4})\ (\bar{\ell}_b \tau)_{\mathrm{V-A}} (\bar{\ell}_b \ell_c)_{\mathrm{V-A}}\,, \tag{4.130}$$

with the loop function $S_0(x)$ given in (B.1b).

Branching Ratios: The relevant branching ratios for the decays $\tau^- \to \ell_b^- \ell_c^+ \ell_b^-$ can be obtained by comparing (4.130) to the effective Hamiltonian of the tree level decay $\tau^- \to \nu_\tau e^- \bar{\nu}_e$,

$$\mathcal{H}_{\mathrm{eff}}^{\tau^- \to \nu_\tau e^- \bar{\nu}_e} = \frac{G_F}{\sqrt{2}} (\bar{\nu}_\tau \tau)_{\mathrm{V-A}} (\bar{e} \nu_e)_{\mathrm{V-A}}\,, \tag{4.131}$$

that yields the decay rate

$$\Gamma(\tau^- \to \nu_\tau e^- \bar{\nu}_e) = \frac{G_F^2 m_\tau^2}{192\pi^3}\,. \tag{4.132}$$

So we find for $\tau \to \ell_b \bar{\ell}_c \ell_b$

$$\mathrm{Br}(\tau \to \ell_b \bar{\ell}_c \ell_b) = \frac{m_\tau^5 \tau_\tau}{192\pi^3} \left(\frac{G_F^2 M_W^2}{4\pi^2}\right)^2 \left|\lambda_{\nu_4}^{(\tau\ell_b)} \lambda_{\nu_4}^{(\ell_b\ell_c)}\right|^2 S_0(x_{\nu_4})\,, \tag{4.133}$$

where $\ell_b \neq \ell_c \in \{\mu, e\}$, and we have included a factor 1/2 to take into account the presence of two identical fermions in the final state.

4.3.3.2. The Decays $\tau^- \to \ell_b^- \ell_c^+ \ell_c^-$ ($\tau^- \to \mu^- e^+ e^-$ and $\tau^- \to e^- \mu^+ \mu^-$)

The $\Delta L = 1$ decays $\tau^- \to \mu^- e^+ e^-$ and $\tau^- \to e^- \mu^+ \mu^-$ proceed basically in analogy to the decay $B \to X_s \ell^+ \ell^-$, only an additional box contribution has to be taken into account (last diagram in (4.134).

Effective Hamiltonian: In the absence of QCD corrections, the effective Hamiltonian can be written as

$\mathcal{H}_{\text{eff}}^{\tau\to\ell_b\bar{\ell}_c\ell_c} = i$ 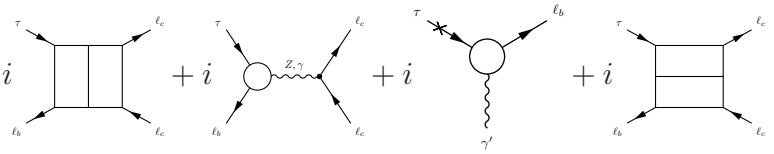 $+ i$ $+ i$ $+ i$

$$= -\frac{G_F}{\sqrt{2}} \lambda_{\nu_4}^{(\tau\ell_b)} \left[C_7^{(\tau\ell_b)} \mathcal{Q}_7^{(\tau\ell_b)} + C_9^{(\tau\ell_b)} \mathcal{Q}_9^{(\tau\ell_b)} + C_{10}^{(\tau\ell_b)} \mathcal{Q}_{10}^{(\tau\ell_b)}\right]\,, \tag{4.134}$$

with the three operators

$$\mathcal{Q}_7^{(\tau\ell_b)} = \frac{e}{8\pi^2} m_\tau \bar{\ell}_b \sigma^{\alpha\beta}(1+\gamma_5)\tau\ F_{\alpha\beta}\,, \tag{4.135a}$$

$$\mathcal{Q}_9^{(\tau\ell_b)} = (\bar{\ell}_b \tau)_{\mathrm{V-A}} (\bar{\ell}_c \ell_c)_{\mathrm{V}}\,, \tag{4.135b}$$

$$\mathcal{Q}_{10}^{(\tau\ell_b)} = (\bar{\ell}_b \tau)_{\mathrm{V-A}} (\bar{\ell}_c \ell_c)_{\mathrm{A}}\,. \tag{4.135c}$$

By virtue of the general formulae for the Wilson coefficients in (A.25), one then obtains

$$C_7^{(\tau\ell_b)} = -\frac{1}{2} H_0'(x_{\nu_4})\,, \tag{4.136a}$$

$$\tilde{C}_9^{(\tau\ell_b)} = (\frac{\alpha}{2\pi})^{-1} C_9 = \frac{1}{s_W^2}\left(\bar{Y}^{\ell_c}(x_{\nu_4}) - \frac{\lambda_{\nu_4}^{(\ell_c\ell_c)}}{4} S_0(x_{\nu_4})\right) - 4\bar{Z}^{(\nu)}(x_{\nu_4})\,, \tag{4.136b}$$

$$\tilde{C}_{10}^{(\tau\ell_b)} = (\frac{\alpha}{2\pi})^{-1} C_{10} = -\frac{1}{s_W^2}\left(\bar{Y}^{\ell_c}(x_{\nu_4}) - \frac{\lambda_{\nu_4}^{(\ell_c\ell_c)}}{4} S_0(x_{\nu_4})\right)\,. \tag{4.136c}$$

where the generalized gauge-independent loop functions defined in (4.4) have been adapted to the special case of ℓ_c in the fermion line and a neutrino in the loop:

$$\bar{Y}^{\ell_c}(x_{\nu_4}) = Y_0(x_{\nu_4}) + \lambda_{\nu_4}^{(\ell_c\ell_c)} F^{\nu\bar{\nu}}(x_{\nu_4}, x_{\nu_4})\,, \tag{4.137}$$

$$\bar{Z}^{(\nu)}(x_{\nu_4}) = C_0(x_{\nu_4}) + \frac{1}{4} H_0(x_{\nu_4}) \tag{4.138}$$

Here we neglected RGE running of α as well as operator mixing.

Branching ratios: In the following, we will consider the decay $\tau^- \to \mu^- e^+ e^-$, but of course the formulae for $\tau^- \to e^- \mu^+ \mu^-$ are easily obtained by just replacing e with μ and vice versa. Introducing

$$\hat{s} = \frac{(p_{\ell_c^+} + p_{\ell_c^-})^2}{m_\tau^2}\,, \qquad R^{\tau\mu}(\hat{s}) = \frac{\frac{d}{d\hat{s}}\Gamma(\tau^- \to \mu^- \ell_c^+ \ell_c^-)}{\Gamma(\tau^- \to \mu^- \bar{\nu}_b \nu_\tau)}\,, \tag{4.139}$$

and neglecting m_{ℓ_c} compared to m_τ, one finds for the differential decay rate $R^{\tau\tau}(\hat{s})$ [210]

$$R^{\tau\mu}(\hat{s}) = \frac{\alpha^2}{4\pi^2}(1-\hat{s})^2 \Bigg[(1+2\hat{s}) \left(|\tilde{C}_9^{\tau\mu}|^2 + |\tilde{C}_{10}^{\tau\mu}|^2 \right) + 4 \left(1 + \frac{2}{\hat{s}} \right) |C_7^{\tau\mu}|^2 + 12\,\mathrm{Re}(C_7^{\tau\mu} \tilde{C}_9^{\tau\mu *}) \Bigg]\,. \tag{4.140}$$

The branching ratio is then obtained by integrating over $\hat{s}$:

$$\mathrm{Br}(\tau^- \to \mu^- \ell_c^+ \ell_c^-) = \mathrm{Br}(\tau^- \to \mu^- \bar{\nu}_\mu \nu_\tau) \int_{4m_e^2/m_\tau^2}^1 R^{\tau\mu}(\hat{s})\, d\hat{s}\,, \tag{4.141}$$

We can perform the integral in (4.141) analytically, and finally arrive at

$$\frac{\mathrm{Br}(\tau^- \to \mu^- e^+ e^-)}{\mathrm{Br}(\tau^- \to \mu^- \bar{\nu}_\mu \nu_\tau)} = \frac{\alpha^2}{24\pi^2} \Bigg[3 \left(|\tilde{C}_{10}^{\tau\mu}|^2 + |\tilde{C}_9^{\tau\mu}|^2 \right) (1-z)^3 (1+z) - 8\,|C_7^{\tau\mu}|^2 (1-z) \left(8 - z - z^2 \right) + 24\,\mathrm{Re}(C_7^{\tau\mu} \tilde{C}_9^{\tau\mu *})\,(1-z)^3 - 48\,|C_7^{\tau\mu}|^2 \log(z) \Bigg]\,, \tag{4.142}$$

with $z \equiv \frac{4m_e^2}{m_\tau^2}$.

4.3.3.3. The Decays $\ell_a \to \ell_b^- \ell_b^+ \ell_b^-$ ($\mu^- \to e^- e^+ e^-$, $\tau^- \to \mu^- \mu^+ \mu^-$, $\tau^- \to e^- e^+ e^-$)

The third distinctive type of four-lepton transitions is represented by the three decays $\mu^- \to e^- e^+ e^-$, $\tau^- \to \mu^- \mu^+ \mu^-$ and $\tau^- \to e^- e^+ e^-$, in which the three outgoing leptons are of equal flavor.

Effective Hamiltonian:

$\mathcal{H}_{\mathrm{eff}}^{\ell_a \to \ell_b \bar{\ell}_b \ell_b} = i$ 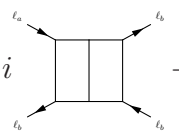 $+ i$ 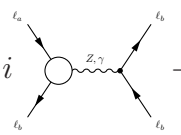 $+ i$ 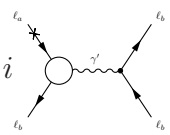

$$= -\frac{G_F}{\sqrt{2}} \lambda_{\nu_4}^{(\ell_a \ell_b)} \left[C_7^{(\ell_a \ell_b)} \mathcal{Q}_7^{(\ell_a \ell_b)} + C_9^{(\ell_a \ell_b)} \mathcal{Q}_9^{(\ell_a \ell_b)} + C_{10}^{(\ell_a \ell_b)} \mathcal{Q}_{10}^{(\ell_a \ell_b)} \right]\,, \tag{4.143}$$

with the three operators $\mathcal{Q}_7^{(\ell_a\ell_b)}, \mathcal{Q}_9^{(\ell_a\ell_b)}, \mathcal{Q}_{10}^{(\ell_a\ell_b)}$ given in (4.135), one obtains

$$C_7^{(\ell_a\ell_b)} = -H_0'(x_{\nu_4})\,, \tag{4.144a}$$

$$\tilde{C}_9^{(\ell_a\ell_b)} = (\frac{\alpha}{2\pi})^{-1} C_9 = \frac{2}{s_W^2}\bar{Y}^{\ell_c}(x_{\nu_4}) - 8\bar{Z}^{(\nu)}(x_{\nu_4})\,, \tag{4.144b}$$

$$\tilde{C}_{10}^{(\ell_a\ell_b)} = (\frac{\alpha}{2\pi})^{-1} C_{10} = -\frac{2}{s_W^2}\bar{Y}^{\ell_c}(x_{\nu_4})\,. \tag{4.144c}$$

The functions H_0', $\bar{Y}^{\ell_c}$ and $\bar{Z}^{(\nu)}$ are defined in (B.4g) and (4.4).

Branching Ratios: Inserting these loop functions into the formulae of [211] which have been corrected in [212, 213], one finds for the branching ratio

$$\begin{aligned}
\mathrm{Br}(\ell_a^- \to \ell_b^-\ell_b^+\ell_b^-) &= \frac{\Gamma(\ell_a^- \to \ell_b^-\ell_b^+\ell_b^-)}{\Gamma(\ell_a^- \to \ell_b^-\bar{\nu}_{\ell_b}\nu_{\ell_a})} \\
&= \frac{\alpha^2}{\pi^2}\left|\lambda_{\nu_4}^{(\ell_a\ell_b)}\right|^2 \mathrm{Br}(\ell_a^- \to \ell_b^-\bar{\nu}_{\ell_b}\nu_{\ell_a}) \\
&\quad\times\Bigg[3\bar{Z}^{(\nu)}(x_{\nu_4})^2 + 3\,\bar{Z}^{(\nu)}(x_{\nu_4})H_0'(x_{\nu_4}) + H_0'(x_{\nu_4})^2\left(\log\frac{m_{\ell_a}}{m_{\ell_b}} - \frac{11}{8}\right) \\
&\qquad + \frac{1}{2s_W^4}\bar{Y}^{\ell_b}(x_{\nu_4})^2 - \frac{2}{s_W^2}\bar{Z}^{(\nu)}(x_{\nu_4})\bar{Y}^{\ell_b}(x_{\nu_4}) - \frac{1}{s_W^2}H_0'(x_{\nu_4})\bar{Y}^{\ell_b}(x_{\nu_4})\Bigg]\,.
\end{aligned} \tag{4.145}$$

4.3.4. Semi-Leptonic τ Decays

Effective Hamiltonian for $\tau^- \to \mu^-\pi^0$:

$\mathcal{H}_{\text{eff}}^{\tau^-\to\mu^-\pi^0} = i$ 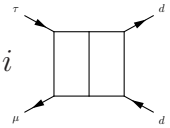 $+\,i$ 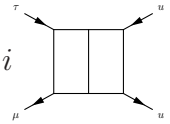 $+\,i$ 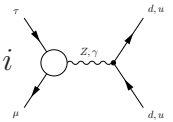

$$= \frac{G_F}{\sqrt{2}}\frac{\alpha}{2\pi s_W^2}\lambda_{\nu_4}^{\tau\mu}\left(\bar{X}^u(x_{\nu_4})(\bar{u}u)_{\mathrm{V-A}} - \bar{Y}^d(x_{\nu_4})(\bar{d}d)_{\mathrm{V-A}}\right)\otimes(\bar{\mu}\tau)_{\mathrm{V-A}}\,, \tag{4.146}$$

with the functions defined in (4.4)

$$\bar{X}^d(x_{\nu_4}) = X_0(x_{\nu_4}) + \sum_{j=t,t'}\lambda_j^{(dd)}F^{(-)}(x_{\nu_4}, x_j)\,, \tag{4.147}$$

$$\bar{Y}^u(x_{\nu_4}) = Y_0(x_{\nu_4}) - \lambda_{b'}^{(uu)}F^{(+)}(x_{\nu_4}, x_{b'})\,. \tag{4.148}$$

Branching Ratios: With the loop functions defined above and the pion decay constant $F_\pi \simeq 131\text{MeV}$ defined through

$$\langle 0|(\bar{u}u)_{V-A}|\pi^0\rangle = -\langle 0|(\bar{d}d)_{V-A}|\pi^0\rangle = \frac{F_\pi p_\pi^\mu}{\sqrt{2}}\,, \tag{4.149}$$

and neglecting suppressed pion and muon mass contributions of $\mathcal{O}(m_\pi^2/m_\tau^2)$ and $\mathcal{O}(m_\mu^2/m_\tau^2)$, we find

$$Br(\tau \to \mu\pi) = \frac{G_F^2\alpha^2 F_\pi^2 m_\tau^3 \tau_\tau}{128\pi^3 s_W^4}\, \left|\lambda_{\nu_4}^{(\tau\mu)}\right|^2 \left(\bar{X}^u(x_{\nu_4}) + \bar{Y}^d(x_{\nu_4})\right)^2\,, \tag{4.150}$$

with τ_τ and m_τ being the lifetime and mass of the decaying τ.

The generalization of (4.150) to the decays $\tau \to \mu\eta$ and $\tau \to \mu\eta'$ is in principle quite straightforward, although slightly obfuscated by mixing in the $\eta - \eta'$ system [210].

Due to the formulation of a new mixing scheme [214, 215], the understanding of $\eta - \eta'$ mixing has improved in the last decade. It provides two angles to relate the physical states $(\eta,\, \eta')$ to the octet and singlet states $(\eta_8,\, \eta_0)$, as

$$|\eta\rangle = \cos\theta_8|\eta_8\rangle - \sin\theta_0|\eta_0\rangle\,, \qquad |\eta'\rangle = \sin\theta_8|\eta_8\rangle + \cos\theta_0|\eta_0\rangle\,, \tag{4.151}$$

with

$$|\eta_8\rangle = \frac{1}{\sqrt{6}}(|\bar{u}u\rangle + |\bar{d}d\rangle - 2|\bar{s}s\rangle)\,, \qquad |\eta_0\rangle = \frac{1}{\sqrt{3}}(|\bar{u}u\rangle + |\bar{d}d\rangle + |\bar{s}s\rangle)\,. \tag{4.152}$$

In this mixing scheme, four independent decay constants are involved. Each of the two physical mesons $(P = \eta, \eta')$, in fact, has both octet $(a = 8)$ and singlet $(a = 0)$ components, defined by

$$\langle 0|(\bar{q}\frac{\lambda^a}{2}q)_{V-A}|P(p)\rangle = \frac{F_P^a p_\mu}{\sqrt{2}}\,, \tag{4.153}$$

where the $SU(3)$ generators λ^a satisfy the normalization convention $\text{Tr}[\lambda^a\lambda^b] = 2\delta^{ab}$. They are conveniently parameterized [214] in terms of the two mixing angles (θ_8, θ_0) and two basic decay constants (F_8, F_0), as

$$\begin{pmatrix} F_\eta^8 & F_\eta^0 \\ F_{\eta'}^8 & F_{\eta'}^0 \end{pmatrix} = \begin{pmatrix} F_8\cos\theta_8 & -F_0\sin\theta_0 \\ F_8\sin\theta_8 & F_0\cos\theta_0 \end{pmatrix}\,. \tag{4.154}$$

Working in this mixing scheme and generalizing the expression for the $\tau \to \mu\pi$ branching ratio in (4.150), one obtains

$$\text{Br}(\tau \to \mu\eta) = \frac{G_F^2\alpha^2 F_\pi^2 m_\tau^3 \tau_\tau}{128\pi^3 \sin^4\theta_W}\left|\lambda_4^{(\tau\mu)}\right|^2 \left(\frac{\cos\theta_8}{\sqrt{3}}\frac{F_8}{F_\pi}(\bar{X}^u + \bar{Y}^d) - \sqrt{\frac{2}{3}}\sin\theta_0\frac{F_0}{F_\pi}(\bar{X}^u - 2\,\bar{Y}^d)\right)^2\,, \tag{4.155a}$$

$$\text{Br}(\tau \to \mu\eta') = \frac{G_F^2\alpha^2 F_\pi^2 m_\tau^3 \tau_\tau}{128\pi^3 \sin^4\theta_W}\left|\lambda_4^{(\tau\mu)}\right|^2 \left(\frac{\sin\theta_8}{\sqrt{3}}\frac{F_8}{F_\pi}(\bar{X}^u + \bar{Y}^d) + \sqrt{\frac{2}{3}}\cos\theta_0\frac{F_0}{F_\pi}(\bar{X}^u - 2\,\bar{Y}^d)\right)^2\,, \tag{4.155b}$$

where the mixing is described in terms of octet and singlet decay constants F_8, F_0 and two mixing angles θ_8, θ_0 [214, 216–218]. Numerical input values are collected in Table 5.1.

4.3.5. Lepton-Flavor Violating B and K Decays

4.3.5.1. $K_{L,S} \to \mu e$ and $K_{L,S} \to \pi^0 \mu e$

The rare decay $K_L \to \mu e$ has been the object of intensive investigation due to its large effects in the Pati-Salam model [219]. In the SM3 it can proceed through box diagrams, but due to nearly degenerate neutrino masses, its calculated branching ratio is too tiny to be measured.

Effective Hamiltonian: Also in the SM4, $K_{L,S} \to \mu e$ proceeds through box diagrams, yielding the following effective Hamiltonian:

$$\mathcal{H}_{\rm eff}^{K_{L,S}\to\mu e} = i$$

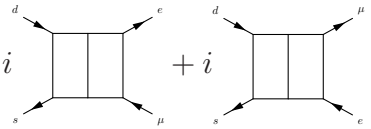

$$= \frac{G_F^2 M_W^2}{8\pi^2} \sum_{i=c,t,t'} \lambda_i^{(K)} S_0(x_i, x_{\nu_4}) \times \left[\lambda_{\nu_4}^{(\mu e)} (\bar{s}d)_{\rm V-A} (\bar{e}\mu)_{\rm V-A} + \lambda_{\nu_4}^{(\mu e)*} (\bar{s}d)_{\rm V-A} (\bar{\mu}e)_{\rm V-A}\right] + \text{h.c.}\,, \tag{4.156}$$

where the loop function S_0 is given in Appendix B.

Branching Ratios: Having the effective Hamiltonian (4.156) at hand, the branching ratio can be calculated with the help of formulae (XI.44) and (XXV.1) of [152]:

$$\begin{aligned} \text{Br}(K_L \to \mu e) &= \text{Br}(K_L \to \mu^+ e^-) + \text{Br}(K_L \to \mu^- e^+) \\ &= \frac{G_F^2 M_W^4}{8\pi^4} \text{Br}(K^+ \to \mu^+ \nu) \frac{\tau(K_L)}{\tau(K^+)} \frac{1}{|V_{us}|^2} \left|\lambda_{\nu_4}^{(\mu e)}\right|^2 \\ &\quad \times \left(\sum_{i=c,t,t'} \text{Re}(\lambda_i^{(K)}) S_0(x_i, x_{\nu_4}) \right)^2 , \end{aligned} \tag{4.157}$$

where the relevant measured quantities are given by [197, 220, 221]

$$\text{Br}(K^+ \to \mu^+ \nu) = (63.44 \pm 0.14)\%\,, \quad \frac{\tau(K_L)}{\tau(K^+)} = 4.117 \pm 0.019\,, \quad |V_{us}| = 0.225 \pm 0.001\,. \tag{4.158}$$

Note that in general the determination of $|V_{us}|$ from a SM3 fit of semileptonic K decays is not longer valid in the SM4. However, since a reanalysis of this fit in the context of the SM4 is clearly beyond the scope of the work, we use the above value for simplicity.

The branching ratio $\text{Br}(K_S \to \mu e)$ can be obtained from (4.157) by replacing [197]

$$\frac{\tau(K_L)}{\tau(K^+)} \to \frac{\tau(K_S)}{\tau(K^+)} = (7.229 \pm 0.014) \cdot 10^{-3}\,, \qquad \text{Re}(\lambda_i^{(K)}) \to \text{Im}(\lambda_i^{(K)})\,. \tag{4.159}$$

Due to the much shorter lifetime $\tau(K_S) \ll \tau(K_L)$, we expect the branching ratio $\text{Br}(K_S \to \mu e)$ to be two orders of magnitude smaller than $\text{Br}(K_L \to \mu e)$, unless $\text{Im}(\lambda_i^{(K)}) \gg \text{Re}(\lambda_i^{(K)})$.

The decay $K_L \to \pi^0 \mu e$ is again governed by the effective Hamiltonian in (4.156). However, the calculation of the branching ratio is done analogous to $K_L \to \pi^0 \nu\bar{\nu}$ [128]. Removing the overall factor 3 in $\mathrm{Br}(K_L \to \pi^0 \nu\bar{\nu})$, one finds

$$\begin{aligned}\mathrm{Br}(K_L \to \pi^0 \mu e) &\equiv \mathrm{Br}(K_L \to \pi^0 \mu^+ e^-) + \mathrm{Br}(K_L \to \pi^0 \mu^- e^+) \\ &= \frac{G_F^2 M_W^4}{8\pi^4} \mathrm{Br}(K^+ \to \pi^0 \mu^+ \nu) \frac{\tau(K_L)}{\tau(K^+)} \frac{1}{|V_{us}|^2} \left|\lambda_{\nu_4}^{(\mu e)}\right|^2 \\ &\quad \times \left(\sum_{i=c,t,t'} \mathrm{Im}(\lambda_i^{(K)}) S_0(x_i, x_{\nu_4}) \right)^2 , \end{aligned} \tag{4.160}$$

where the semi-leptonic branching ratio of $K^+ \to \pi^0 \mu^+ \nu$ is given by [197]

$$\mathrm{Br}(K^+ \to \pi^0 \mu^+ \nu) = (3.32 \pm 0.06)\% \,. \tag{4.161}$$

Note that this time $\mathrm{Im}(\lambda_i^{(K)})$ instead of $\mathrm{Re}(\lambda_i^{(K)})$ enters, due to the sign difference between

$$\langle \pi^0 | (\bar{d}s)_{V-A} | \bar{K}^0 \rangle = -\langle \pi^0 | (\bar{s}d)_{V-A} | K^0 \rangle \tag{4.162a}$$

and

$$\langle 0 | (\bar{d}s)_{V-A} | \bar{K}^0 \rangle = +\langle 0 | (\bar{s}d)_{V-A} | K^0 \rangle \,. \tag{4.162b}$$

The branching ratio for $K_S \to \pi^0 \mu e$ can be obtained from (4.160) by replacing

$$\frac{\tau(K_L)}{\tau(K^+)} \to \frac{\tau(K_S)}{\tau(K^+)} \,, \qquad \mathrm{Im}(\lambda_i^{(K)}) \to \mathrm{Re}(\lambda_i^{(K)}) \,. \tag{4.163}$$

4.3.5.2. $B_q \to \ell_c \ell_d$

The decays of neutral B mesons into two different charged leptons proceed basically in analogy to the $K_{L,S}$ decays discussed above.

Effective Hamiltonian: The effective Hamiltonian relevant for the decay $B_q \to \ell_c \ell_d$, where $q = d, s$ and $(\ell_c, \ell_d) = (\mu, e), (\tau, \mu), (\tau, e)$ is similar to (4.156)

$$\mathcal{H}_{\mathrm{eff}}^{B_q \to \ell_c \ell_d} = i$$

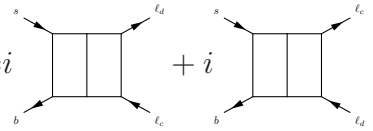

(4.164a)

$$\begin{aligned} &= \frac{G_F^2 M_W^2}{8\pi^2} \sum_{i=c,t,t'} \lambda_i^{(B_q)} S_0(x_i, x_{\nu_4}) \\ &\quad \times \left[\lambda_{\nu_4}^{(\ell_c \ell_d)} (\bar{b}q)_{\mathrm{V-A}} (\bar{\ell}_d \ell_c)_{\mathrm{V-A}} + \lambda_{\nu_4}^{(\ell_c \ell_d)*} (\bar{b}q)_{\mathrm{V-A}} (\bar{\ell}_c \ell_d)_{\mathrm{V-A}} \right] . \end{aligned} \tag{4.164b}$$

In contrast to the above section where the decaying mesons $K_{L,S}$ were mixtures of flavor eigenstates, now the decaying $B_q = \bar{b}q$ mesons are flavor eigenstates. The effective Hamiltonian for the respective anti-particles $\bar{B}_q = \bar{q}b$ is thus given by taking the hermitian conjugate,

$$\mathcal{H}_{\mathrm{eff}}^{\bar{B}_q \to \ell_c \ell_d} = \left(\mathcal{H}_{\mathrm{eff}}^{B_q \to \ell_c \ell_d} \right)^* . \tag{4.164c}$$

Branching Ratios: The branching ratios of B_q mesons to two different charged leptons are calculated analogously to the corresponding $K_{L,S}$ decays in the previous section. Taking into account that now the decaying mesons are flavor eigenstates, the branching ratios obtain a slightly different form:

$$\begin{aligned}\mathrm{Br}(B_d \to \ell_c \ell_d) = \mathrm{Br}(B_d \to \ell_c \ell_d) = \mathrm{Br}(B_d \to \ell_c^- \ell_d^+) + \mathrm{Br}(B_d \to \ell_c^+ \ell_d^-) = \\ = \frac{G_F^2 M_W^4}{16\pi^4 |V_{ub}|^2} \frac{\tau(B_d)}{\tau(B^+)} \mathrm{Br}(B^+ \to \ell_c^+ \nu_{\ell_c}) \left|\lambda_{\nu_4}^{(\ell_c \ell_d)}\right|^2 \\ \times \left| \sum_{i=c,t,t'} \lambda_i^{(d)} S_0(x_i, x_{\nu_4}) \right|^2 \qquad (4.165a)\end{aligned}$$

$$\begin{aligned}\mathrm{Br}(B_s \to \ell_c \ell_d) = \frac{G_F^2 M_W^4}{16\pi^4 |V_{ub}|^2} \frac{\tau(B_s)}{\tau(B^+)} \frac{M_{B_s}}{M_{B_d}} \frac{F_{B_s}^2}{F_{B_d}^2} \mathrm{Br}(B^+ \to \ell_c^+ \nu_{\ell_c}) \left|\lambda_{\nu_4}^{(\ell_c \ell_d)}\right|^2 \\ \times \left| \sum_{i=c,t,t'} \lambda_i^{(s)} S_0(x_i, x_{\nu_4}) \right|^2 , \qquad (4.165b)\end{aligned}$$

where ℓ_c and ℓ_d denote the two leptons in the final state with $m_{\ell_c} > m_{\ell_d}$. Along the lines of $\mathrm{Br}(K_L \to \mu e)$, we have normalized the branching ratios of $B_{d,s}$ by the corresponding branching ratios of B^+ leptonic decays, which are not very well measured yet [163, 222–224]

$$\mathrm{Br}(B^+ \to \tau^+ \nu_\tau) = (1.67 \pm 0.39) \cdot 10^{-4} , \qquad (4.166a)$$

$$\mathrm{Br}(B^+ \to \mu^+ \nu_\mu) < 6.6 \cdot 10^{-6} \qquad (90\%\ \mathrm{C.L.}) . \qquad (4.166b)$$

As soon as these measurements improve, this normalization will become very helpful. For the time being, we shall use the SM predictions for $\mathrm{Br}(B^+ \to \mu^+ \nu_\mu)$ and $\mathrm{Br}(B^+ \to \tau^+ \nu_\tau)$ [75,225] for our numerical analysis

$$\mathrm{Br}(B^+ \to \tau^+ \nu_\tau) = (0.8 \pm 0.12) \cdot 10^{-4} , \qquad (4.167a)$$

$$\mathrm{Br}(B^+ \to \mu^+ \nu_\mu) = (3.8 \pm 1.1) \cdot 10^{-7} . \qquad (4.167b)$$

The first value is on the lower side of experimental result, but still consistent within errors.

4.3.6. $\mu - e$ Conversion in Nuclei

Besides the decays $\mu \to e\gamma$ and $\mu^- \to e^- e^+ e^-$, the rate of $\mu - e$ conversion in nuclei provides the strongest bounds on mixing in the lepton sector. In particular, the experimental upper bound on $\mu - e$ conversion in $^{48}_{22}\mathrm{Ti}$ is given by [226]

$$\mathrm{R}(\mu\mathrm{Ti} \to e\mathrm{Ti}) < 4.3 \cdot 10^{-12} . \qquad (4.168)$$

In the near future, the J-PARC experiment PRISM/PRIME should reach a sensitivity of $\mathcal{O}(10^{-18})$ [227].

Conversion Rate: In analogy to [210], we use the general formula (58) of [211] to find the approximate conversion rate

$$\Gamma(\mu\mathrm{X}\to e\mathrm{X}) = \frac{G_F^2}{8\pi^4}\alpha^5\frac{Z_{\mathrm{eff}}^4}{Z}|F(q^2)|^2 m_\mu^5\left|\lambda_{\nu_4}^{(\mu e)}\right|^2 \tag{4.169}$$
$$\times\left[Z\left(4\bar{Z}^{(\nu)}(x_{\nu_4})+H_0'(x_{\nu_4})\right)-(2Z+N)\frac{\bar{X}^u(x_{\nu_4})}{s_W^2}+(Z+2N)\frac{\bar{Y}^d(x_{\nu_4})}{s_W^2}\right]^2,$$

where $\bar{X}^u$ and $\bar{Y}^d$ are defined in (4.4), and H_0' and $\bar{Z}^{(\nu)}$ are given in (B.4g) and (4.4d). Z and N denote the proton and neutron number of the nucleus, Z_{eff} has been determined in [228–231] and $F(q^2)$ is the nucleon form factor. In the case of $\mathrm{X} = {}^{48}_{22}\mathrm{Ti}$, one finds $Z_{\mathrm{eff}} = 17.6$ and $F(q^2\simeq -m_\mu^2)\simeq 0.54$ [232]. The $\mu-e$ conversion rate $\mathrm{R}(\mu\mathrm{X}\to e\mathrm{X})$ is then given by

$$\mathrm{R}(\mu\mathrm{X}\to e\mathrm{X}) = \frac{\Gamma(\mu\mathrm{X}\to e\mathrm{X})}{\Gamma_{\mathrm{capture}}^{\mathrm{X}}}, \tag{4.170}$$

with $\Gamma_{\mathrm{capture}}^{\mathrm{X}}$ being the μ capture rate of the element X. For titanium the experimental value is given by [233]

$$\Gamma_{\mathrm{capture}}^{\mathrm{Ti}} = (2.590\pm 0.012)\cdot 10^6\,\mathrm{s}^{-1}. \tag{4.171}$$

In this work, we will restrict our analysis to $\mu-e$ conversion in ${}^{48}_{22}\mathrm{Ti}$, for which the most stringent experimental upper bound exists and where the approximations entering (4.169) work very well. Further details can be found in [211, 232, 234].

4.3.7. Anomalous Magnetic Moment of the Muon

The anomalous magnetic moment of the muon $a_\mu = (g-2)_\mu/2$ is an excellent device for testing physics beyond the standard model. On the experimental side, it has been measured very precisely by the E821 experiment [235]

$$a_\mu^{\mathrm{exp}} = (11659208.0\pm 6.3)\cdot 10^{-10}. \tag{4.172}$$

This is to be compared to the SM prediction [236]

$$a_\mu^{\mathrm{SM3}} = a_\mu^{\mathrm{QED}} + a_\mu^{\mathrm{ew}} + a_\mu^{\mathrm{had}} = (11659180.4\pm 5.1)\cdot 10^{-10}, \tag{4.173}$$

which is 3.4σ below the experimental value. While the QED and electroweak contributions to a_μ^{SM3} can be calculated with high accuracy [237–239], the theoretical uncertainty mainly arises from the hadronic part, which has been calculated in [236, 240–242].

Although $(g-2)_\mu$ is not a lepton flavor violation observable in the strict sense, it shares some important properties with those. Especially its high sensitivity to intermediate new heavy particles makes it a very good test for new physics. Therefore studies of $(g-2)_\mu$ have been performed in all major NP scenarios, for instance in the MSSM [243, 244] or Little Higgs [210].

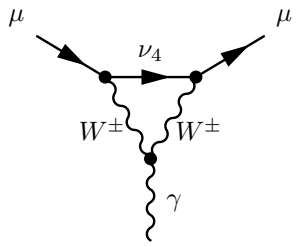

Figure 4.1.: Diagram contributing to $(g-2)_\mu$ in the SM4.

Calculation of a_μ: Starting from the muon-photon vertex function $\Gamma^\nu(p',p)$

$$\bar{\mu}(p')\Gamma^\nu(p',p)\mu(p) = \bar{\mu}(p')\left[\gamma^\nu F_V(q^2) + (p+p')^\nu F_M(q^2)\right]\mu(p)\,, \tag{4.174}$$

the anomalous magnetic moment of the muon a_μ can be extracted as

$$a_\mu = -2mF_M(0)\,. \tag{4.175}$$

For the study of new physics contributions, we split it into a standard model (SM3) and NP (SM4) part,

$$a_\mu = a_\mu^{\rm SM3} + a_\mu^{\rm SM4}\,. \tag{4.176}$$

The new contribution $a_\mu^{\rm SM4}$ is determined by the diagram shown in Figure 4.1. Following [210], the calculation of $a_\mu^{\rm SM4}$ yields

$$(a_\mu)_{\rm SM4} = -\frac{\sqrt{2}G_F}{8\pi^2} m_\mu^2\ \lambda_{\nu_4}^{\mu\mu}\ \tilde{L}_2(x_{\nu_4})\,, \tag{4.177}$$

where the function $\tilde{L}_2(x)$ is given in Appendix B.

Two comments are in order at this point:

1. Since $\tilde{L}_2(x_{\nu_4}) > 0$, the SM4 contribution tends to decrease a_μ, and therefore pushes it away from the experimental value.

2. After imposing the constraints from lepton universality and radiative decays, it will turn out that the SM4 contribution to a_μ is negligible compared to the theoretical uncertainties, and therefore the abovementioned negative effect does not play a role for our phenomenological analysis.

5. Numerical Analysis

5.1. Numerical Analysis of the Quark Sector

5.1.1. Preliminaries

For our numerical analysis, we construct a large number of random points in parameter space that are evenly distributed in all the mixing angles and phases. We keep only those points that satisfy all tree level CKM constraints at 2σ (it is not possible to bring $|V_{cs}| = 1.02 \pm 0.04$ within 1σ of its central value) and the experimental constraints on the $\Delta F = 2$ observables,

$$\varepsilon_K\,, \qquad \Delta M_K\,, \qquad \Delta M_q\,, \qquad \Delta M_d/\Delta M_s\,, \tag{5.1}$$

as well as the CP asymmetry $S_{\psi K_s}$ within 1σ and $\cos\varphi_{B_d}^{\rm tot} > 0$.

In order to compare our results to the experimental values, we calculate the propagated error from the corresponding hadronic parameters using Gaussian error propagation. We accept a point if it is at 1σ within its theoretical uncertainty compatible with the experimental value and its respective uncertainty.

One exception is the mass difference ΔM_K, which is very precisely measured but subject to LD contributions that are not well understood at present. Due to these uncertainties discussed at the end of Section 4.2.1.1, we can only demand $0.7 \leq \Delta M_K^{\rm SD}/\Delta M_K^{\rm exp} \leq 1.3$. Note that the contributions from the 4G quarks to the SD part of ΔM_K can exceed +30%. In this context we remark that the SM3 value of $|\varepsilon_K|$ also appears to be lower than the data [129]. However, in this case, LD contributions are estimated to be small [129, 131], and the cure of this anomaly can only come either from NP, or from significant changes in the input parameters like $|V_{cb}|$ and $|V_{ub}|$.

In addition to the $\Delta F = 2$ observables, we impose the following constraints from $\Delta F = 1$ observables:

$$\mathrm{Br}(B \to X_s \ell^+ \ell^-)_{\rm low.-int.}\,, \qquad \mathrm{Br}(B \to X_s \gamma)\,, \qquad \mathrm{Br}(K^+ \to \pi^+ \nu\bar{\nu})\,, \tag{5.2}$$

each at 4σ, not taking into account the theoretical errors. We note that a constraint comes also from the upper bound on $\mathrm{Br}(K_L \to \mu^+\mu^-)_{\rm SD}$ in (4.53).

Since ΔM_K poses no stringent bound on S_K, and S_K is correlated with X_K, Y_K etc., we chose to impose the experimental exclusion limits on various Kaon decays. For consistency reasons, as well as to eliminate highly tuned points, we also constrain $B_{s,d} \to \mu^+\mu^-$.

Obviously, the chance of a point to fulfil all constraints is much larger for small mixing angles than for larger ones. We therefore have not plotted all of the roughly 10 million points that we found for small mixing angles, but tried to distribute them as uniform as possible. For this reason, we thinned out densely populated parameter regions and finally took 2 million out of the valid points.

parameter	value		parameter	value	
$\sin^2\theta_W$	0.23122(15)	[103]	G_F	$1.16637(1)\cdot 10^{-5}\text{GeV}^{-2}$	[103]
α	1/137.035999084(51)	[103]	M_W	80.425(38) GeV	[103]
$\hat{B}_K$	0.725 ± 0.026	[130]	m_e	0.5110 MeV	[103]
F_{B_d}	(192.8 ± 9.9) MeV	[130]	m_μ	105.66 MeV	[103]
F_{B_s}	(238.8 ± 9.5) MeV	[130]	m_τ	1.77684(17) GeV	[103]
F_K	(155.8 ± 1.7) MeV	[130]	τ_τ	$290.6(1.0)\cdot 10^{-3}$ ps	[103]
F_π	130 ± 5 MeV	[103]	$m_c(m_c)$	(1.268 ± 0.009) GeV	[130, 245]
$\hat{B}_{B_d}$	1.26 ± 0.11	[130]	$m_t(m_t)$	(163.5 ± 1.7) GeV	[246]
$\hat{B}_{B_s}$	1.33 ± 0.06	[130]	M_{B_d}	5.2794(5) GeV	[103]
$\sqrt{\hat{B}_{B_d}}F_{B_d}$	(216 ± 15) MeV	[130]	M_{B_s}	5.3675(18) GeV	[103]
$\sqrt{\hat{B}_{B_s}}F_{B_s}$	(275 ± 13) MeV	[130]	ΔM_d	(0.507 ± 0.005) ps^{-1}	[201]
ξ	1.243 ± 0.028	[130]	ΔM_s	(17.77 ± 0.12) ps^{-1}	[201]
η_{cc}	1.51 ± 0.24	[247]	$\tau(B_d)$	(1.525 ± 0.009)ps	[103]
η_{tt}	0.5765 ± 0.0065	[138]	$\tau(B_s)$	(1.425 ± 0.041)ps	[103]
η_{ct}	0.47 ± 0.04	[248]	$\tau(B^+)$	1.638(11) ps	[103]
η_B	0.551 ± 0.007	[138, 249]	ΔM_K	$(5.292 \pm 0.009)\cdot 10^{-3}\text{ps}^{-1}$	[103]
F_8/F_π	1.28	(ChPT)	κ_ε	0.92 ± 0.02	[129]
F_0/F_π	1.18(4)		$\lvert\varepsilon_K\rvert$	$(2.228 \pm 0.011)\cdot 10^{-3}$	[103]
θ_8	$-22.2(1.8)^\circ$		$S_{\psi K_S}$	0.672 ± 0.024	[103]
θ_0	$-8.7(2.1)^\circ$	[250]			

Table 5.1.: Values of the input parameters used in our analysis. The tree level measurements of V_{CKM} can be found in Table 2.1

We would like to stress that (even without this procedure) the point density in our plots must not be understood as a probability density. The main information of the various correlation plots is contained in the *enveloping curve* for these points [251], without any preference for different points within this region. In order to obtain such enveloping curves, we have developed an algorithm which identifies the outermost corners of a given set of points.[1] By connecting the corners with a smooth curve, we are able to display correlations between the observables more clearly. We have performed this procedure for the most important correlations which are shown in Figs. 5.4, 5.9 and 5.10, as well as for the corresponding diagrams in Sec. 5.1.8.

In presenting the results of the global analysis, it will be useful to use a special color coding, in order to emphasize some aspects of the anatomy presented in the next section and to stress certain points that we found in the process of our numerical analysis:

- The large black point represents the SM3.
- Light blue and dark blue points stand for the results of our global analysis of the SM4

[1] This is highly nontrivial due to the large number of points and the possibility of concave enveloping polygons.

	BS1 (yellow)	BS2 (green)	BS3 (red)
$S_{\psi\phi}$	0.04 ± 0.01	0.04 ± 0.01	≥ 0.4
$\mathrm{Br}(B_s \to \mu^+\mu^-)$	$(2 \pm 0.2) \cdot 10^{-9}$	$(3.2 \pm 0.2) \cdot 10^{-9}$	$\geq 6 \cdot 10^{-9}$

Table 5.2.: Three scenarios for $S_{\psi\phi}$ and $\mathrm{Br}(B_s \to \mu^+\mu^-)$.

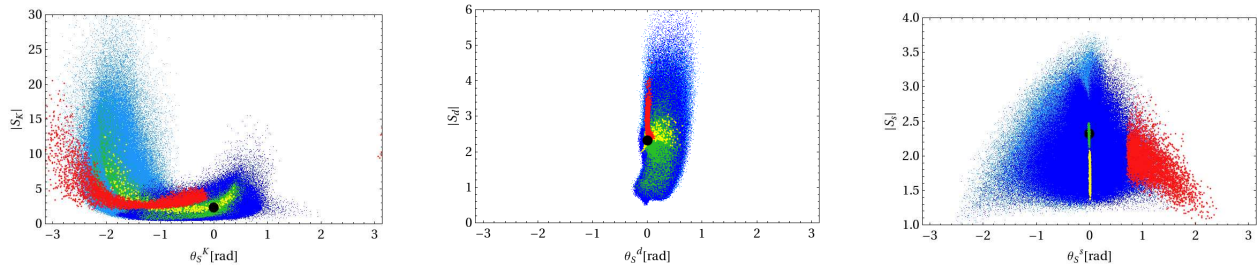

Figure 5.1.: The arguments θ_S^i of the functions S_i plotted against the absolute values $|S_i|$ for $i = K$ (left panel), $i = d$ (center panel) and $i = s$ (right panel).

with the following distinction: light blue stands for $\mathrm{Br}(K_L \to \pi^0\nu\bar{\nu}) > 2 \cdot 10^{-10}$ and dark blue for $\mathrm{Br}(K_L \to \pi^0\nu\bar{\nu}) \leq 2 \cdot 10^{-10}$. Note that the regions with light and dark blue points are not always exclusive but that the dark blue points are plotted above the light blue ones.

- The yellow, green and red colors represent the three scenarios for $S_{\psi\phi}$ and $\mathrm{Br}(B_s \to \mu^+\mu^-)$ that are shown in Table 5.2 and related to Step 2 of the anatomy.

5.1.2. Violation of Universality

Imposing the existing constraints from tree level determinations of the CKM matrix, electroweak precision observables and the existing data on the FCNC and CP violation observables, it is possible to significantly constrain the allowed ranges for the magnitudes and the phases of the master functions F_i introduced in Section 4.1.2.2. We recall that in the SM3, the master functions are real and independent of the meson system considered.

In Fig. 5.1 we show the allowed ranges in the planes $(\theta_S^i, |S_i|)$ for $i = K, d, s$. The flavor-universal SM3 value of $|S_i| = S_0(x_t)$ is indicated by a black dot. In Fig. 5.2, a similar analysis is done for the functions X_i. We observe that the flavor universality in question is significantly violated in a hierarchical manner:

- Concerning $|S_i|$, the largest effects are found for $|S_K|$, followed by $|S_d|$, and with the smallest effects found for $|S_s|$. This hierarchy is familiar from the LHT model and reflects the factor $1/\lambda_t^{(i)}$ in the definition of S_i with $|\lambda_t^{(K)}| \ll |\lambda_t^{(d)}| \leqslant |\lambda_t^{(s)}|$, as well as the fact that S_K is not as directly constrained through ε_K as S_d is through $S_{\psi K_s}$ and ΔM_d. In addition, as mentioned before, ΔM_K only poses a mild constraint.

- The departures of θ_S^i from zero are again largest in the K system. The strong preference for $\theta_S^K < 0$ is related — as seen through (4.26) — to the ε_K-anomaly in the SM3 [129], whose solution favors $\varphi_K > \bar{\beta} - \bar{\beta}_s$.

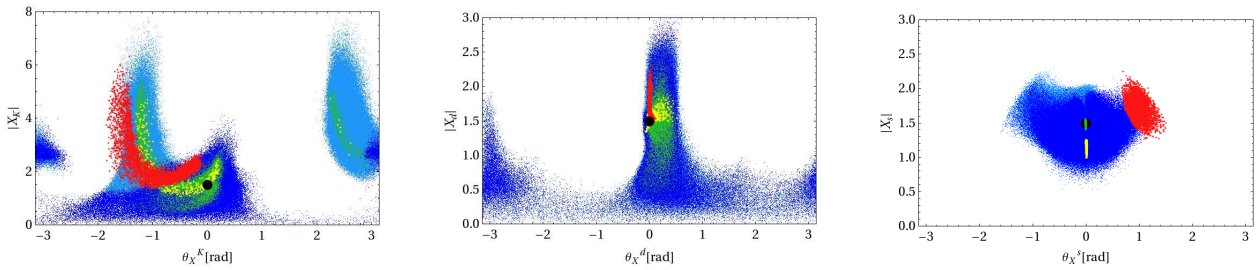

Figure 5.2.: The arguments θ_X^i of the functions X_i plotted against the absolute values $|X_i|$ for $i = K$ (left panel), $i = d$ (center panel) and $i = s$ (right panel).

- The phase θ_S^d is already rather constrained through $S_{\psi K_S}$, but a preference for $\theta_S^d > 0$ is clearly visible. This reflects the fact that for central values of $|V_{ub}|$, that are dominated by inclusive decays, the phase $\varphi_{B_d}^{\rm tot}$ is required to be smaller than $\bar{\beta}$, in order to fit $S_{\psi K_S}$ (see (4.112)).
- θ_S^s is much less constrained than θ_S^d, as the CP violation in the B_s system is experimentally basically unknown. The $S_{\psi\phi}$ anomaly at Tevatron, corresponding to the red points in Fig. 5.1, requires $\theta_S^s > 0$, as explicitly seen in (4.120) and (4.35) [129, 252].
- Even for no effects in $S_{\psi\phi}$ and $Br(B_s \to \mu^+\mu^-)$ (green points) the SM4 still allows for large effects in the kaon system.

Similar hierarchies in the violation of universality are observed in the case of the functions X_i, with the effects in X_s being smallest, not only in the magnitude, but also in its phase.

5.1.3. Correlations within the K System

$K_L \to \mu^+\mu^-$

We begin our analysis of rare K decays with the SD contribution to $K_L \to \mu^+\mu^-$, on which the bound is given in (4.53). It turns out that in the SM4 this bound can be strongly violated, and imposing it has an impact on the size of possible enhancements in other rare K decays. In order to see this transparently, let us define

$$T_Y \equiv \text{Br}(K_L \to \mu^+\mu^-)_{\rm SD} = 2.08 \cdot 10^{-9} \left(\frac{\text{Re}\lambda_c^{(K)}}{|V_{us}|} P_c(Y_K) + \frac{\text{Re}(\lambda_t^{(K)} Y_K)}{|V_{us}|^5} \right)^2 , \tag{5.3a}$$

$$T_X \equiv \text{Br}(K^+ \to \pi^+ \nu\bar{\nu}) - \frac{\kappa^+}{\kappa_L} \text{Br}(K_L \to \pi^0 \nu\bar{\nu}) = \kappa_+ \left(\frac{\text{Re}\lambda_c^{(K)}}{|V_{us}|} P_c(X) + \frac{\text{Re}(\lambda_t^{(K)} X_K)}{|V_{us}|^5} \right)^2 , \tag{5.3b}$$

with T_X entering the branching ratio $\text{Br}(K^+ \to \pi^+ \nu\bar{\nu})$ in (4.67a). In Fig. 5.3, we show T_X as a function of T_Y and find a strong correlation between these two quantities which could be anticipated on the basis of the analytic expressions for T_X and T_Y. As T_Y is constrained directly from above through (4.53), we obtain also an upper limit on T_X. Throughout our numerical analysis, we impose this bound.

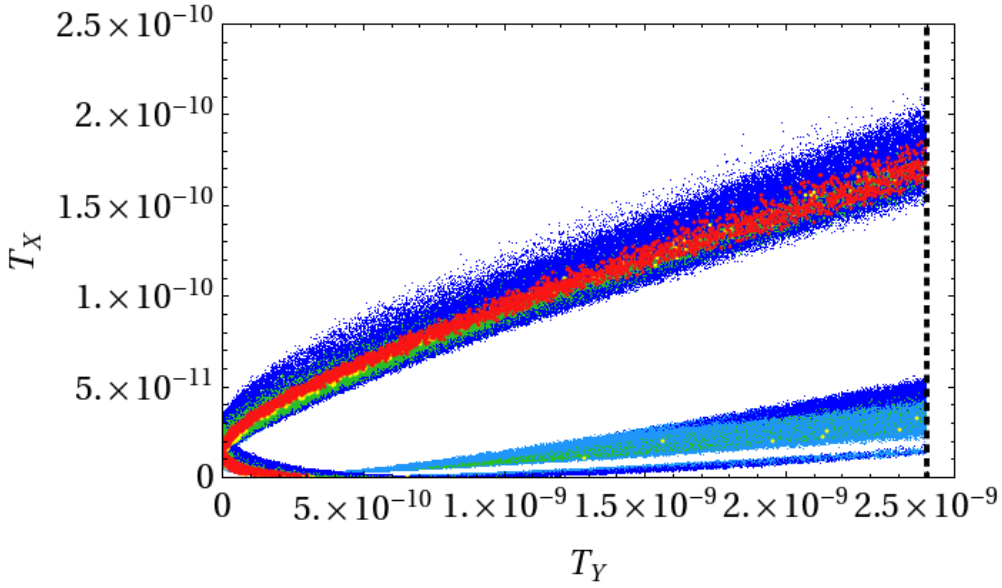

Figure 5.3.: T_X as a function of T_Y, as defined in (5.3). The vertical dashed red line represents the bound (4.53).

$K^+ \to \pi^+\nu\bar{\nu}$ and $K_L \to \pi^0\nu\bar{\nu}$

In Fig. 5.4, we show $\mathrm{Br}(K_L \to \pi^0\nu\bar{\nu})$ as a function of $\mathrm{Br}(K^+ \to \pi^+\nu\bar{\nu})$. The black point shows the central SM3 values of the branching ratios in question, and the shaded region corresponds to the experimental 1σ range for $\mathrm{Br}(K^+ \to \pi^+\nu\bar{\nu})$, with its central value indicated by the light vertical dashed line. Unless indicated otherwise, the meaning of dashed lines and shaded areas will be the same as described here throughout our analysis.

We observe that both branching ratios can be enhanced relative to the SM3 values in a spectacular manner. This is especially the case for $\mathrm{Br}(K_L \to \pi^0\nu\bar{\nu})$, which can reach values as high as 10^{-9}, that is by a factor of 40 larger than found in the SM3. $\mathrm{Br}(K^+ \to \pi^+\nu\bar{\nu})$ can be by a factor of 4 larger than in the SM3. We note that the Grossman-Nir (GN) [253] bound on $\mathrm{Br}(K_L \to \pi^0\nu\bar{\nu})$ can be saturated for all values of $\mathrm{Br}(K^+ \to \pi^+\nu\bar{\nu})$ shown in the plot. We also observe that large enhancements of $\mathrm{Br}(K_L \to \pi^0\nu\bar{\nu})$ imply necessarily enhancements of $\mathrm{Br}(K^+ \to \pi^+\nu\bar{\nu})$. The converse is obviously not true, but for $\mathrm{Br}(K^+ \to \pi^+\nu\bar{\nu}) > 1.7 \cdot 10^{-10}$ the $\mathrm{Br}(K_L \to \pi^0\nu\bar{\nu})$ is either below 10^{-10} or close to the GN bound and larger than $6 \cdot 10^{-10}$. For an earlier analysis of $K \to \pi\nu\bar{\nu}$, where large effects of 4G quarks can be found, see [45].

The pattern seen in Fig. 5.4 can be understood as follows. We distinguish two different branches in which enhancements of $\mathrm{Br}(K^+ \to \pi^+\nu\bar{\nu})$ are possible: The lower branch, on which $\mathrm{Br}(K_L \to \pi^0\nu\bar{\nu})$ does not depart by much from the SM3 values but $\mathrm{Br}(K^+ \to \pi^+\nu\bar{\nu})$ can be strongly enhanced, corresponds to the range of parameters for which the term T_X in (4.67a) dominates $\mathrm{Br}(K^+ \to \pi^+\nu\bar{\nu})$. But as we have seen above, T_X is efficiently constrained by the bound on $\mathrm{Br}(K_L \to \mu^+\mu^-)_{\mathrm{SD}}$, and consequently a stringent upper bound is put on $\mathrm{Br}(K^+ \to \pi^+\nu\bar{\nu})$ on this branch [2]. The upper branch, on which both $K \to \pi\nu\bar{\nu}$ branching ratios can be strongly enhanced, corresponds to the region of parameters for which T_X is

[2]The fact that the bound on $\mathrm{Br}(K_L \to \mu^+\mu^-)_{\mathrm{SD}}$ can have sizable impact on $\mathrm{Br}(K^+ \to \pi^+\nu\bar{\nu})$ has already been pointed out in [188]. See also [189].

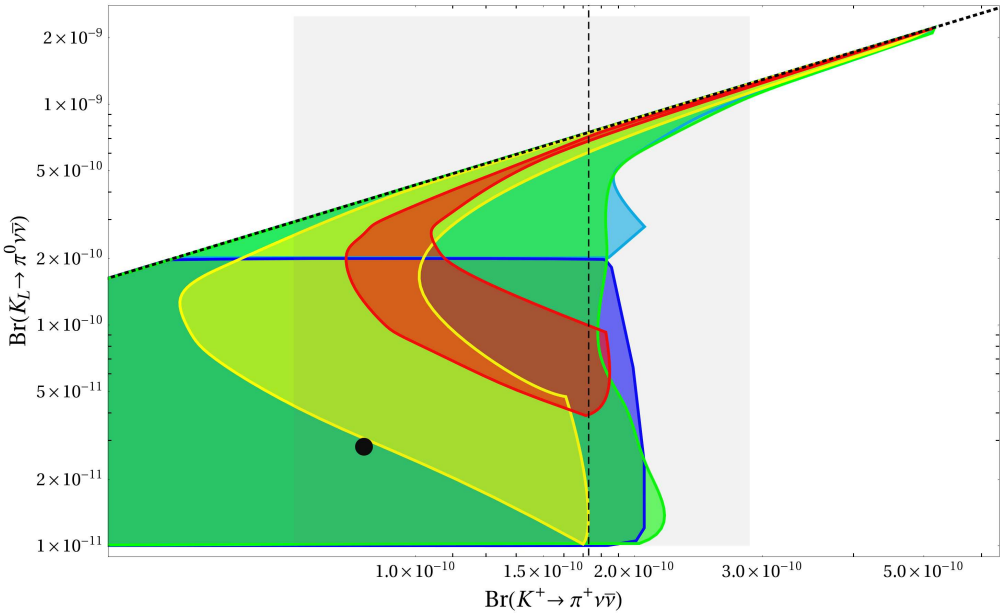

Figure 5.4.: $\mathrm{Br}(K_L \to \pi^0\nu\bar{\nu})$ as a function of $\mathrm{Br}(K^+ \to \pi^+\nu\bar{\nu})$. The dotted line corresponds to the model-independent GN bound.

subdominant and the first term in (4.67a) dominates $\mathrm{Br}(K^+ \to \pi^+\nu\bar{\nu})$. Comparing (4.67a) and (4.67b), we observe in this case a very strong correlation between $\mathrm{Br}(K_L \to \pi^0\nu\bar{\nu})_{\mathrm{SD}}$ and $\mathrm{Br}(K^+ \to \pi^+\nu\bar{\nu})$: their ratio is simply given by $\kappa_L/\kappa_+ \approx 4.3$ which is precisely the GN bound.

It is evident from this discussion that the upper branch, in contrast to the lower branch, is not affected by the bound on $\mathrm{Br}(K_L \to \mu^+\mu^-)$. In order to see how the latter bound affects other observables, we divide the points in Fig. 5.4 in two groups, with the ones corresponding to $\mathrm{Br}(K_L \to \pi^0\nu\bar{\nu}) > 2\cdot10^{-10}$ represented by *light blue* points.

In spite of the interesting pattern of deviations from the SM3 seen in Fig. 5.4, we conclude that on the basis of the present constraints the predictive power of the SM4 is limited, except that spectacular deviations from the SM3 are definitely possible, but suppressions cannot be excluded. We also note that even for large values of $S_{\psi\phi}$ and $\mathrm{Br}(B_s \to \mu^+\mu^-)$, represented by red points, large NP effects in both branching ratios are possible. In Fig. 5.5, we look closer at the latter feature. A large enhancement of both branching ratios is clearly possible as already seen in Fig. 5.4. Moreover, these plots look very different from those found in the LHT and RSc models [70–74].

In [254] the impact of ε_K on the correlation of $\mathrm{Br}(K_L \to \pi^0\nu\bar{\nu})$ and $\mathrm{Br}(K^+ \to \pi^+\nu\bar{\nu})$ was studied. It was argued that in the case of correlated phases in the NP contributions to $\Delta F = 2$ and $\Delta F = 1$ processes one naturally gets the observed two branched structure of the correlation. However even if this assumption is relaxed, the presence of additive NP contributions to ε_K implies

$$\theta_K^X \neq \bar{\beta} - \bar{\beta}_s \pm \frac{\pi}{2}\,, \tag{5.4}$$

and consequently the upper branch never reaches the GN bound. In the SM4 also $\mathrm{Im}\lambda_c^{(K)}$ is

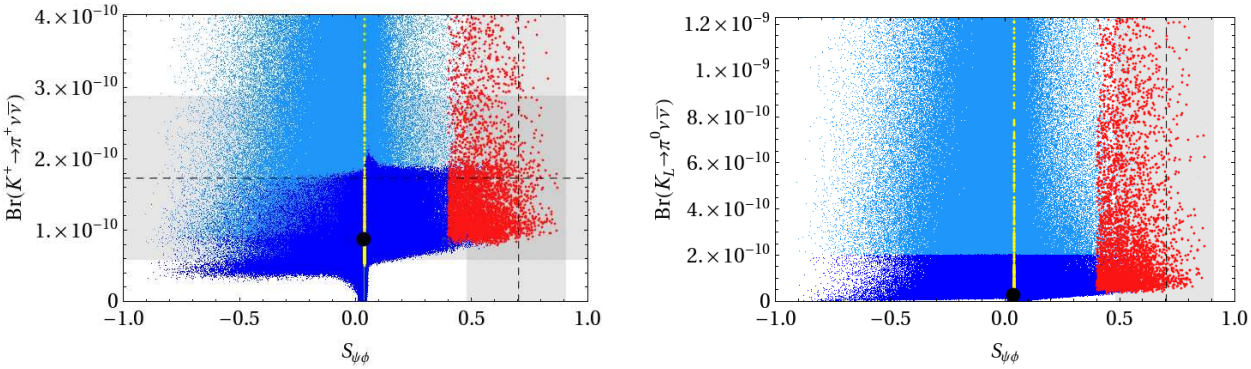

Figure 5.5.: $\mathrm{Br}(K^+ \to \pi^+\nu\bar{\nu})$ (left panel) and $\mathrm{Br}(K_L \to \pi^0\nu\bar{\nu})$ (right panel) as functions of the CP asymmetry $S_{\psi\phi}$.

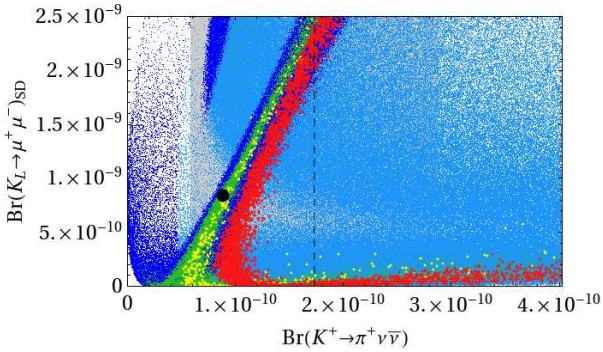

Figure 5.6.: The SD contribution to $\mathrm{Br}(K_L \to \mu^+\mu^-)$ as a function of $\mathrm{Br}(K^+ \to \pi^+\nu\bar{\nu})$.

affected and $|\mathrm{Im}\lambda_c^{(K)}| \gg \left(|\mathrm{Im}\lambda_c^{(K)}|\right)_{\mathrm{SM}}$ can compensate for large effects introduced through changes in $\lambda_t^{(K)}$ and through $\lambda_{t'}^{(K)}$. Effectively the SM4 is able to maximally violate the assumption of correlated new phases in ε_K and $K \to \pi\nu\bar{\nu}$ and the GN bound can be reached. The effects of $|\mathrm{Im}\lambda_c^{(K)}| \gg \left(|\mathrm{Im}\lambda_c^{(K)}|\right)_{\mathrm{SM}}$ on $\mathrm{Br}(K_L \to \pi^0\nu\bar{\nu})$ can be neglected, which is evident from the structure of (4.67a) and (4.67b).

$K_L \to \mu^+\mu^-$ and $K^+ \to \pi^+\nu\bar{\nu}$

In order to understand still better the structure of NP effects in Fig. 5.4, we show in Fig. 5.6 the correlation between $\mathrm{Br}(K_L \to \mu^+\mu^-)_{\mathrm{SD}}$ and $\mathrm{Br}(K^+ \to \pi^+\nu\bar{\nu})$. We observe that most points cluster around two branches corresponding to the two branches in Fig. 5.4. On one of them $\mathrm{Br}(K_L \to \mu^+\mu^-)_{\mathrm{SD}}$ is suppressed relative to the SM3 value while $\mathrm{Br}(K^+ \to \pi^+\nu\bar{\nu})$ can be large. On the second branch $\mathrm{Br}(K_L \to \mu^+\mu^-)_{\mathrm{SD}}$ can reach the upper limit at which point $\mathrm{Br}(K^+ \to \pi^+\nu\bar{\nu})$ is most likely in the ballpark of the central experimental value. Still, as seen in Fig. 5.6, other combinations of the values of both branching ratios cannot be excluded at present.

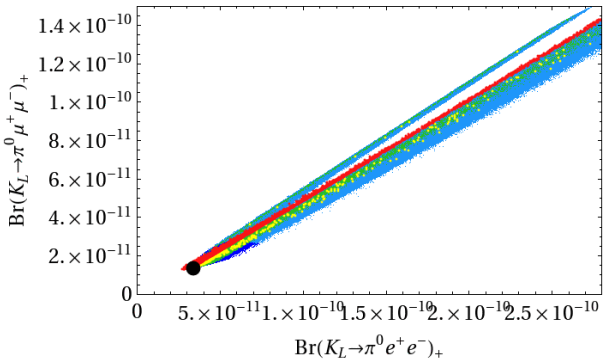

Figure 5.7.: $\mathrm{Br}(K_L \to \pi^0 e^+ e^-)$ as a function of $\mathrm{Br}(K_L \to \pi^0 \mu^+ \mu^-)$.

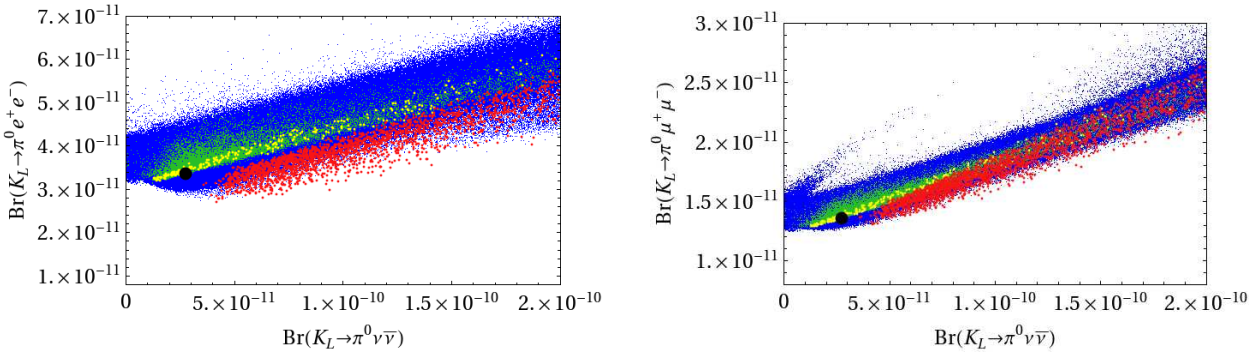

Figure 5.8.: $\mathrm{Br}(K_L \to \pi^0 e^+ e^-)_+$ as functions of $\mathrm{Br}(K_L \to \pi^0 \nu\bar{\nu})$ (left panel), $\mathrm{Br}(K_L \to \pi^0 \mu^+ \mu^-)_+$ as functions of $\mathrm{Br}(K_L \to \pi^0 \nu\bar{\nu})$ (right panel).

$K_L \to \pi^0 e^+ e^-$ vs. $K_L \to \pi^0 \mu^+ \mu^-$

In Fig. 5.7, we show the correlation between $\mathrm{Br}(K_L \to \pi^0 e^+ e^-)$ and $\mathrm{Br}(K_L \to \pi^0 \mu^+ \mu^-)$, also familiar from the LHT model [71]. We show only the "+" solution with the SM3 values given in (4.93a) and (4.93b). As expected, the allowed enhancements are not as pronounced as in the case of $K_L \to \pi^0 \nu\bar{\nu}$. However, they are still much larger than in the LHT model: one order of magnitude for both branching ratios with slightly larger effects for $K_L \to \pi^0 \mu^+ \mu^-$.

$K_L \to \pi^0 \ell^+ \ell^-$ vs. $K_L \to \pi^0 \nu\bar{\nu}$

In Fig. 5.8, we show a correlation between $\mathrm{Br}(K_L \to \pi^0 \ell^+ \ell^-)$ and $\mathrm{Br}(K_L \to \pi^0 \nu\bar{\nu})$ that has also been found in the LHT and RSc models [70–74]. The enhancement of one of the branching ratios implies automatically the enhancement of the other. We show only the results for $\mathrm{Br}(K_L \to \pi^0 \nu\bar{\nu}) \leqslant 2 \cdot 10^{-10}$, as the extrapolation to higher values is straightforward. The main message from this plot is that the enhancement of $\mathrm{Br}(K_L \to \pi^0 \nu\bar{\nu})$ can be much larger than the one of $\mathrm{Br}(K_L \to \pi^0 \ell^+ \ell^-)$, as already anticipated on the basis of analytic formulae.

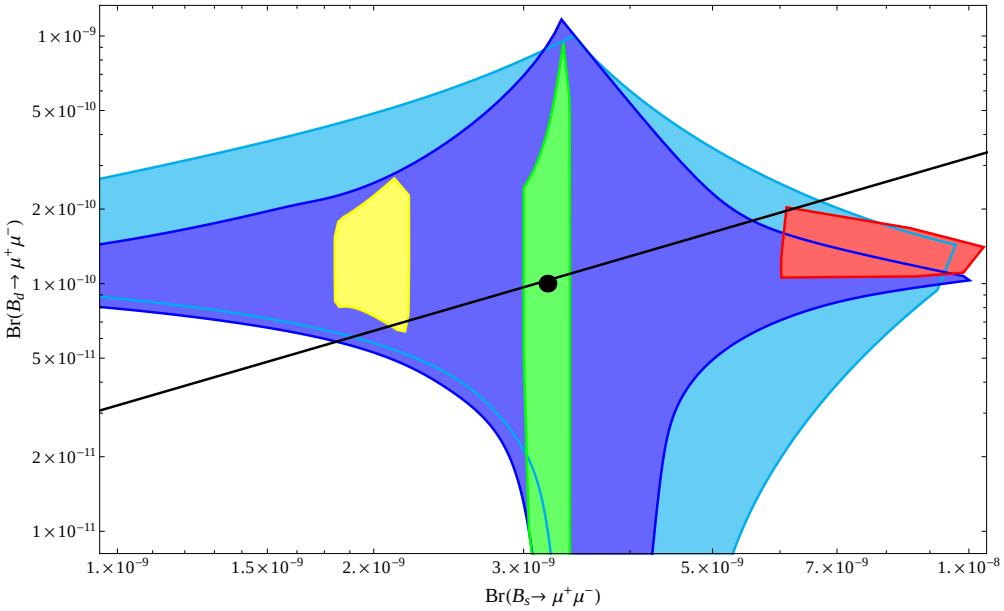

Figure 5.9.: $\mathrm{Br}(B_d \to \mu^+\mu^-)$ as a function of $\mathrm{Br}(B_s \to \mu^+\mu^-)$. The straight line depicts the "Golden Relation" of CMFV models as given in (4.59) with $r = 1$.

5.1.4. Correlations Involving the B System

$B_{s,d} \to \mu^+\mu^-$

In Fig. 5.9, we show $\mathrm{Br}(B_d \to \mu^+\mu^-)$ as a function of $\mathrm{Br}(B_s \to \mu^+\mu^-)$. The straight line in this plot represents the "Golden Relation" of CMFV models given in (4.59) with $r = 1$. We observe very strong departures from CMFV. We also observe that $\mathrm{Br}(B_d \to \mu^+\mu^-)$ can be as large as $8 \cdot 10^{-10}$ and $\mathrm{Br}(B_s \to \mu^+\mu^-)$ as large as $1 \cdot 10^{-8}$. The striking message from Fig. 5.9, reflecting the non-CMFV character of NP contributions, is that large enhancement of $\mathrm{Br}(B_s \to \mu^+\mu^-)$ implies SM3-like values of $\mathrm{Br}(B_d \to \mu^+\mu^-)$ and vice-versa.

In Fig. 5.10, we show $\mathrm{Br}(B_d \to \mu^+\mu^-)$ and $\mathrm{Br}(B_s \to \mu^+\mu^-)$ as functions of $S_{\psi\phi}$. The disparity between these plots shows the non-CMFV character of the NP contributions in the SM4. We observe a definite correlation between $\mathrm{Br}(B_s \to \mu^+\mu^-)$ and $S_{\psi\phi}$, thus, for a given value of $S_{\psi\phi}$, only a certain range for $\mathrm{Br}(B_s \to \mu^+\mu^-)$ is predicted. Moreover, with increasing $S_{\psi\phi}$ also $\mathrm{Br}(B_s \to \mu^+\mu^-)$ generally increases. In particular, for $S_{\psi\phi} > 0.4$, an enhancement of $\mathrm{Br}(B_s \to \mu^+\mu^-)$ is found. For $S_{\psi\phi} \approx 0.4$, we find that $\mathrm{Br}(B_s \to \mu^+\mu^-)$ can reach values as high as $7 \cdot 10^{-9}$. For larger values of $S_{\psi\phi}$, even higher values of $\mathrm{Br}(B_s \to \mu^+\mu^-)$ are possible. Interestingly, for SM3-like values of $S_{\psi\phi}$, the branching ratio $\mathrm{Br}(B_s \to \mu^+\mu^-)$ is more likely to be suppressed than enhanced.We conclude that a future measurement of $S_{\psi\phi}$ above 0.4 accompanied by $\mathrm{Br}(B_s \to \mu^+\mu^-)$ close to or below its SM3 value would put the SM4 into difficulties. From the right panel in Fig. 5.10 we can infer the following *soft* bounds

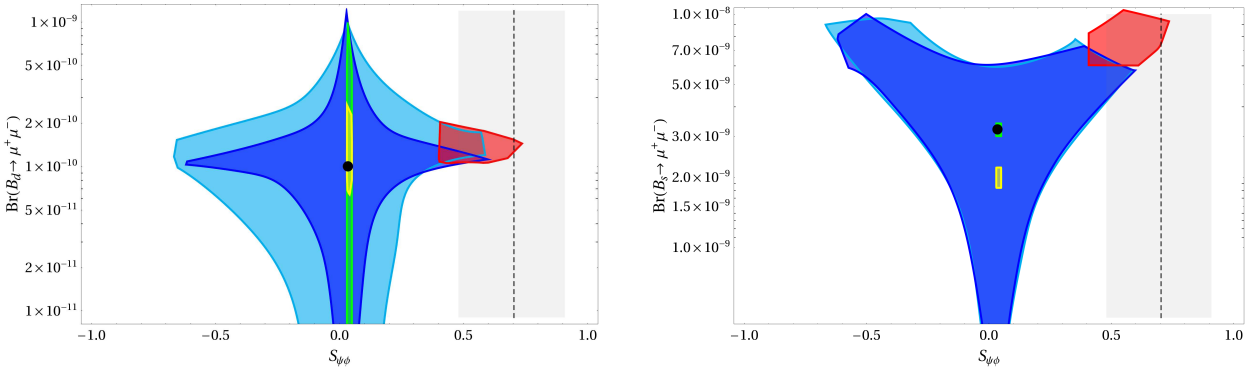

Figure 5.10.: $\mathrm{Br}(B_d \to \mu^+\mu^-)$ (left panel) and $\mathrm{Br}(B_s \to \mu^+\mu^-)$ (right panel) each as a function of $S_{\psi\phi}$.

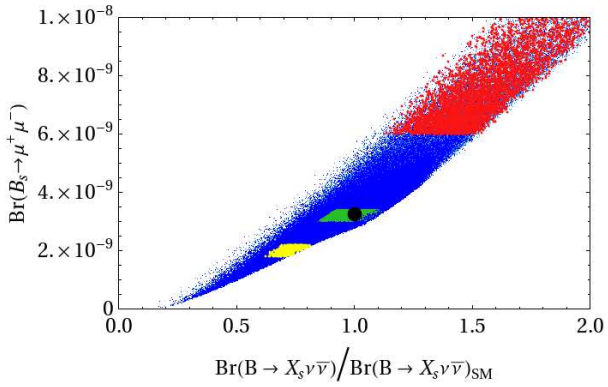

Figure 5.11.: $\mathrm{Br}(B_s \to \mu^+\mu^-)$ as a function of $\mathrm{Br}(B \to X_s\nu\bar{\nu})$.

on $\mathrm{Br}(B_s \to \mu^+\mu^-)$ as a function of $S_{\psi\phi}$

$$\mathrm{Br}(B_s \to \mu^+\mu^-) \leq \left(6 + \left(4 \cdot (S_{\psi\phi} - (S_{\psi\phi})_{\mathrm{SM}})\right)^4\right) \cdot 10^{-9}\,, \tag{5.5}$$

$$\mathrm{Br}(B_s \to \mu^+\mu^-) \geq \begin{cases} (-0.08 + S_{\psi\phi}) \cdot 10^{-8} & \text{for } S_{\psi\phi} > 0 \\ (-0.04 - S_{\psi\phi}) \cdot 10^{-8} & \text{for } S_{\psi\phi} < 0 \end{cases}\,. \tag{5.6}$$

In addition we find the global *soft* upper bound

$$\mathrm{Br}(B_s \to \mu^+\mu^-) \leq 1.3 \cdot 10^{-8}\,. \tag{5.7}$$

$B \to X_s\nu\bar{\nu}$ and $B_s \to \mu^+\mu^-$

Fig. 5.11 shows that $\mathrm{Br}(B \to X_s\nu\bar{\nu})$ is significantly correlated with $\mathrm{Br}(B_s \to \mu^+\mu^-)$. In particular, both branching ratios are most likely either simultaneously enhanced or simultaneously suppressed with respect to their SM3 values.

$B \to X_s\gamma$ and $B \to X_s\ell^+\ell^-$

In Fig. 5.12 we show $\mathrm{Br}(B \to X_s\gamma)$ versus $\mathrm{Br}(B \to X_s\ell^+\ell^-)_{q^2>14.4\mathrm{GeV}^2}$. This plot is self-explanatory and shows that enhancements of $S_{\psi\phi}$ and $\mathrm{Br}(B_s \to \mu^+\mu^-)$ (red points) are fully consistent with the experimental data for the two branching ratios shown in the plot. On the other hand the reduction of the experimental error on $\mathrm{Br}(B \to X_s\ell^+\ell^-)$ could have a

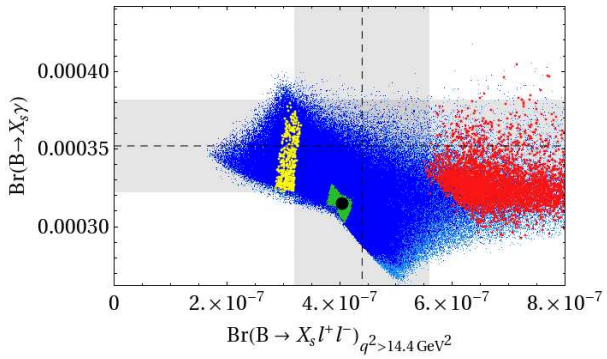

Figure 5.12.: $\mathrm{Br}(B \to X_s\gamma)$ as a function of $\mathrm{Br}(B \to X_s\ell^+\ell^-)_{q^2>14.4\mathrm{GeV}^2}$.

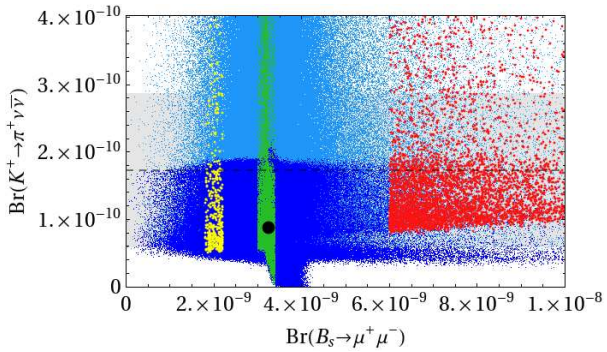

Figure 5.13.: $\mathrm{Br}(K^+ \to \pi^+\nu\bar{\nu})$ as a function of $\mathrm{Br}(B_s \to \mu^+\mu^-)$.

significant impact on the red points. We confirmed that the zero s_0 of the forward-backward asymmetry remains SM3-like. Variations up to 10% are possible, but since this is comparable with the theoretical errors (NLO calculation) we do not further discuss this issue here. See Section 4.2.4.2 for details.

$B_s \to \mu^+\mu^-$ vs. $K^+ \to \pi^+\nu\bar{\nu}$

In Fig. 5.13, we show $\mathrm{Br}(K^+ \to \pi^+\nu\bar{\nu})$ as a function of $\mathrm{Br}(B_s \to \mu^+\mu^-)$. The striking feature in this plot is the disparity of possible enhancements of both branching ratios relative to the SM3 values. While $\mathrm{Br}(K^+ \to \pi^+\nu\bar{\nu})$ can be strongly enhanced, as already seen in Figs. 5.4 and 5.5, the possible enhancement of $\mathrm{Br}(B_s \to \mu^+\mu^-)$ is more modest. We also conclude that there is no strong correlation between both branching ratios, so that they can be enhanced significantly at the same time, but this is not necessarily the case.

5.1.5. The CP Asymmetries $S_{\psi\phi}$, $S_{\phi K_S}$ and $A_{\mathrm{CP}}^{bs\gamma}$

As pointed out in [47], there is a strong correlation between the CP asymmetries $S_{\psi\phi}$ and $S_{\phi K_S}$ within the SM4. We show this correlation in the upper-left panel of Fig. 5.14. First of all, we observe that $S_{\psi\phi}$ can be as large as 0.8 although even larger values are possible. For $S_{\psi\phi} \approx 0.4$, the asymmetry $S_{\phi K_S}$ is strongly suppressed relative to $S_{\psi K_S}$ and in the ballpark of 0.4, close to its experimental central value represented by the horizontal dashed line. The analogous plot for $S_{\eta' K_S}$ is shown in the upper-right panel of Fig. 5.14. The suppression is

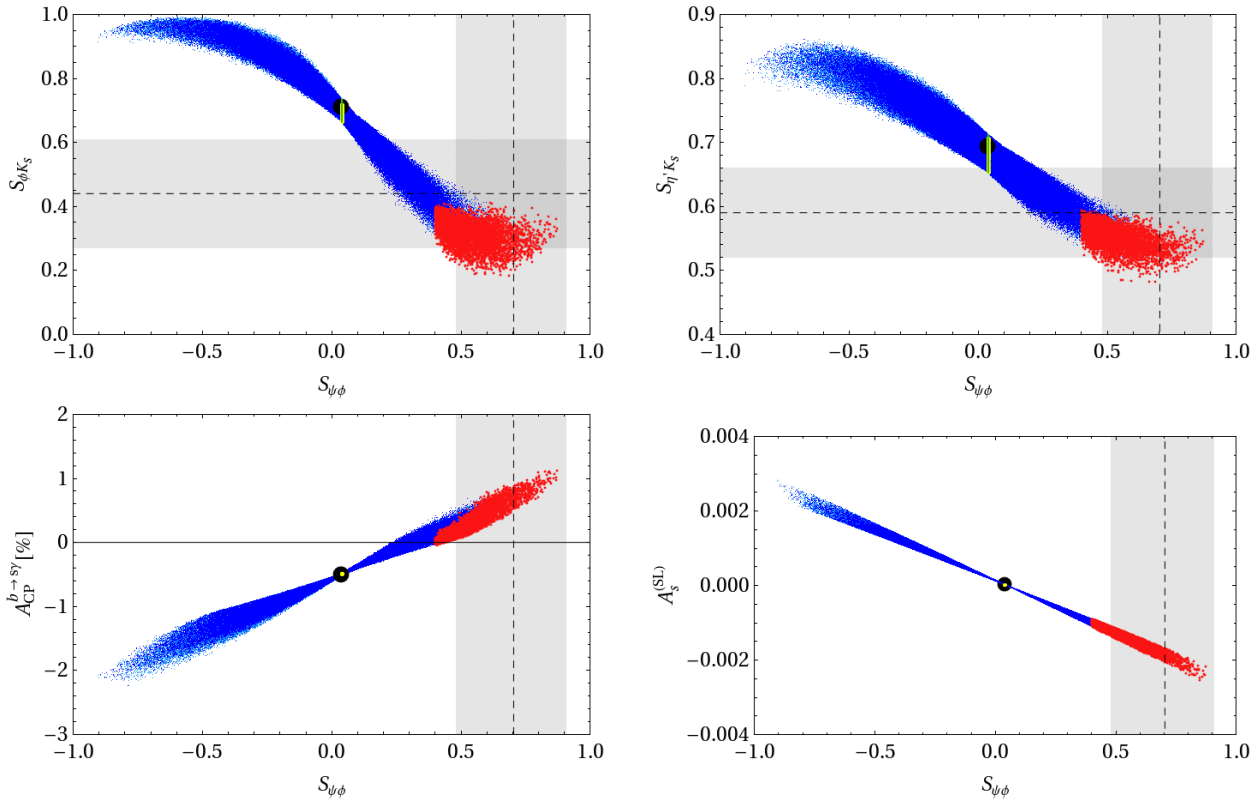

Figure 5.14.: The CP asymmetries $S_{\phi K_S}$ (upper-left panel), $S_{\eta' K_S}$ (upper-right panel), $A_{\rm CP}^{bs\gamma}$ (lower-left panel), A_{SL}^s (lower-right panel) shown as functions of $S_{\psi\phi}$.

now significantly weaker, and for $S_{\psi\phi} \approx 0.4$ one finds $S_{\eta' K_S} \approx 0.55$, in accordance with the data. The big black points represent the SM3 values of the asymmetries in question that are slightly above $S_{\psi K_S}$ [196, 200, 201].

Interestingly, for $S_{\psi\phi} \geq 0.6$ the values of $S_{\phi K_s}$ and $S_{\eta' K_s}$ predicted by the SM4 are below their central values indicated by data.

The correlation seen in the upper panels in Fig. 5.14 can easily be understood by noting that the ratio $\lambda_{t'}^{(s)}/\lambda_t^{(s)}$ and, in particular, its phase is responsible for departures of both, $S_{\psi\phi}$ and $S_{\phi K_S}$, from the SM3 predictions. A *positive* complex phase of this ratio implies the desired enhancement of $S_{\psi\phi}$ and, through (4.115) and (4.116), a *negative* phase $\varphi_{\phi K_S}$ of the decay amplitude $A_{\phi K_S}$. In turn, as seen in (4.118), $S_{\phi K_S}$ is suppressed relative to $S_{\psi K_S}$.

At this point some comments are in order

- The theoretical errors on (the real part of) the b_f parameters in (4.107) are of minor importance. We checked numerically that varying the b_f parameters by 10% yields only small effects on the studied correlations.

- On the other hand, sizable strong phases from non-factorizable final-state interactions may alter the *slope* for the predicted correlation between $S_{\phi K_S}$ and $S_{\psi\phi}$. This effect explains the difference between our result and the analysis by Soni et al. [47, 104], where the non-perturbative parameters are taken from [255], which is based on a phenomenological optimization of theory input in the context of the SM3.

The weaker suppression of $S_{\eta' K_S}$ originates in smaller values of non-perturbative parameters b_i as seen in Table 4.1. On the other hand, as pointed out in [75, 207] in the supersymmetric flavor models with exclusively left-handed currents and in the FBMSSM, the desire to explain the $S_{\phi K_S}$ anomaly implies automatically that $A_{\rm CP}^{bs\gamma}$ is much larger in magnitude than its SM3 value and has opposite sign. A qualitatively similar behavior is found in the SM4, but as $S_{\phi K_S}$ is strongly correlated with $S_{\psi\phi}$ and the latter asymmetry is theoretically cleaner, we prefer to show the correlation between $A_{\rm CP}^{bs\gamma}$ and $S_{\psi\phi}$. As seen in the lower-left panel of Fig. 5.14, for $S_{\psi\phi} \approx 0.5$ the asymmetry $A_{\rm CP}^{bs\gamma}$ reverses the sign but its magnitude is SM3-like. Larger effects are found for larger $|S_{\psi\phi}|$, in particular negative values of $S_{\psi\phi}$, which are however disfavored by Tevatron data. We conclude that $A_{\rm CP}^{bs\gamma}$ remains small also in the SM4, but the sign flip for large *positive* $S_{\psi\phi}$ could help to distinguish the SM4 from the SM3.

Finally, in the lower right panel of Fig. 5.14, we show the familiar correlation between A_{SL}^s and $S_{\psi\phi}$ [256]. The size of A_{SL}^s can be by an order of magnitude larger in the SM4 than in the SM3.

5.1.6. The Ratio ε'/ε

In Fig. 5.15, we show ε'/ε as a function of $S_{\psi\phi}$ for four different scenarios of the non-perturbative parameters R_6 and R_8: $(R_6, R_8) = (1.0, 1.0)$ (upper left panel), $(1.5, 0.8)$ (upper right panel), $(2.0, 1.0)$ (lower left panel) and $(1.5, 0.5)$ (lower right panel). Each set of points has the SM3 value indicated by a black dot. $\Lambda_{\overline{\rm MS}}$ has been set to 340 MeV. The non-perturbative parameters R_6 and R_8 are defined as

$$R_6 \equiv B_6^{(1/2)} \left[\frac{121 \text{ MeV}}{m_s(m_c) + m_d(m_c)}\right]^2, \qquad R_8 \equiv B_8^{(3/2)} \left[\frac{121 \text{ MeV}}{m_s(m_c) + m_d(m_c)}\right]^2. \tag{5.8}$$

As a general feature the SM4 can fit ε'/ε for all sets of non-perturbative parameters considered by us. However, the striking feature of these plots is the difficulty in reproducing the experimental data for ε'/ε within the SM4 when $S_{\psi\phi}$ is large and positive (red points) as suggested by the Tevatron data. Thus if the latter data will be confirmed ε'/ε can put the SM4 under pressure, unless R_6 is significantly larger than unity and R_8 sufficiently suppressed below one. This discussion demonstrates again that in order to use ε'/ε to constrain NP the knowledge of the parameters R_6 and R_8 has to be improved significantly. An analysis of ε'/ε in the 4G model has been presented in [45], where the hadronic uncertainties known from previous studies have been reemphasized. However, the direct impact of large $S_{\psi\phi}$ on ε'/ε has not been studied there.

It is then of interest to investigate what impact ε'/ε would have on our analysis when R_6 and R_8 were precisely known. To this end we introduce yet another coding in Table 5.3, this time for different values of R_6 and R_8. In Fig. 5.16 we show then the most interesting correlations, this time including also the ε'/ε-constraint. These are $S_{\phi K_S}$ vs. $S_{\psi\phi}$, $\text{Br}(B_s \to \mu^+\mu^-)$ vs. $S_{\psi\phi}$, $\text{Br}(K_L \to \pi^0\nu\bar{\nu})$ vs. $\text{Br}(K^+ \to \pi^+\nu\bar{\nu})$ and $\text{Br}(K_L \to \pi^0\nu\bar{\nu})$ vs. $S_{\psi\phi}$. These plots should be compared to the plots in Figs. 5.14, 5.10, 5.4 and 5.5 respectively, where the ε'/ε constraint has not been taken into account.

We observe the following striking features already anticipated on the basis of Fig. 5.15:

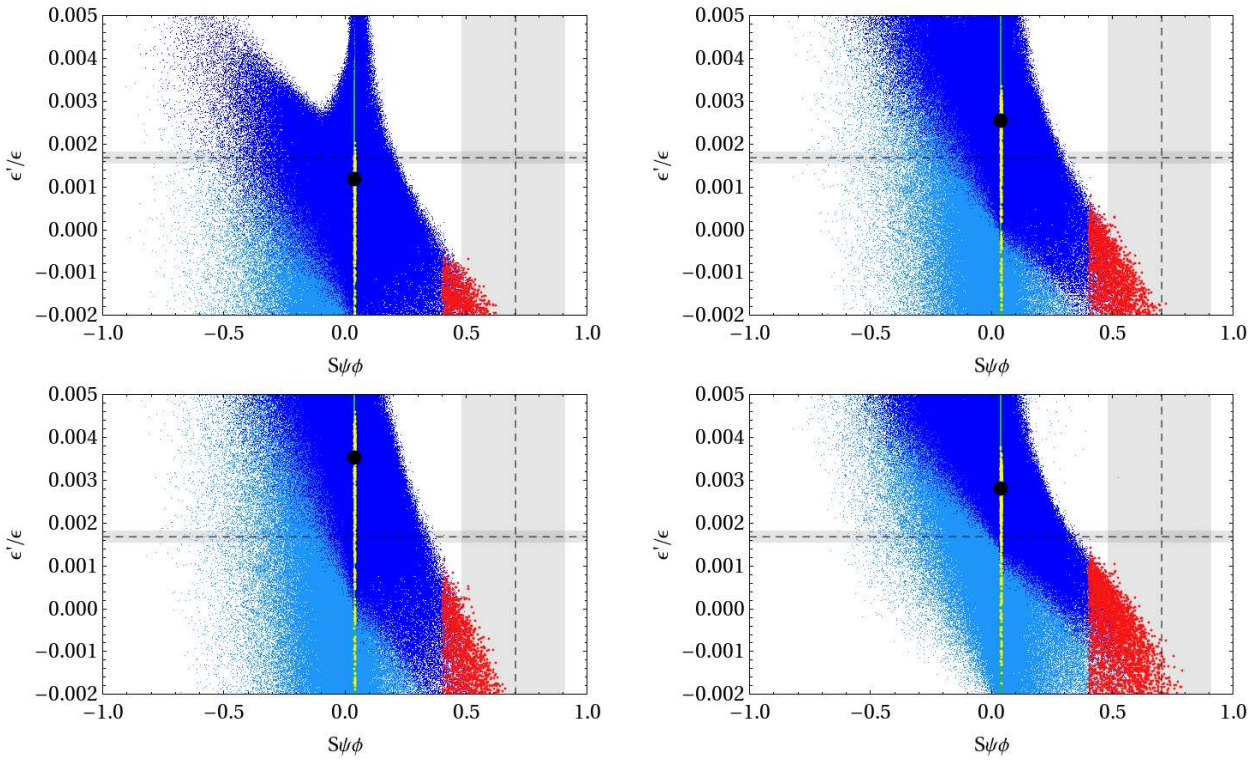

Figure 5.15.: ε'/ε as a function of the CP asymmetry $S_{\psi\phi}$ for four different scenarios of the non-perturbative parameters. $(R_6, R_8) = (1.0, 1.0)$ (upper left panel), $(1.5, 0.8)$ (upper right panel), $(2.0, 1.0)$ (lower left panel) and $(1.5, 0.5)$ (lower right panel).

R_6	R_8	
1.0	1.0	dark blue
1.5	0.8	purple
2.0	1.0	green
1.5	0.5	orange

Table 5.3.: Four scenarios for the parameters R_6 and R_8

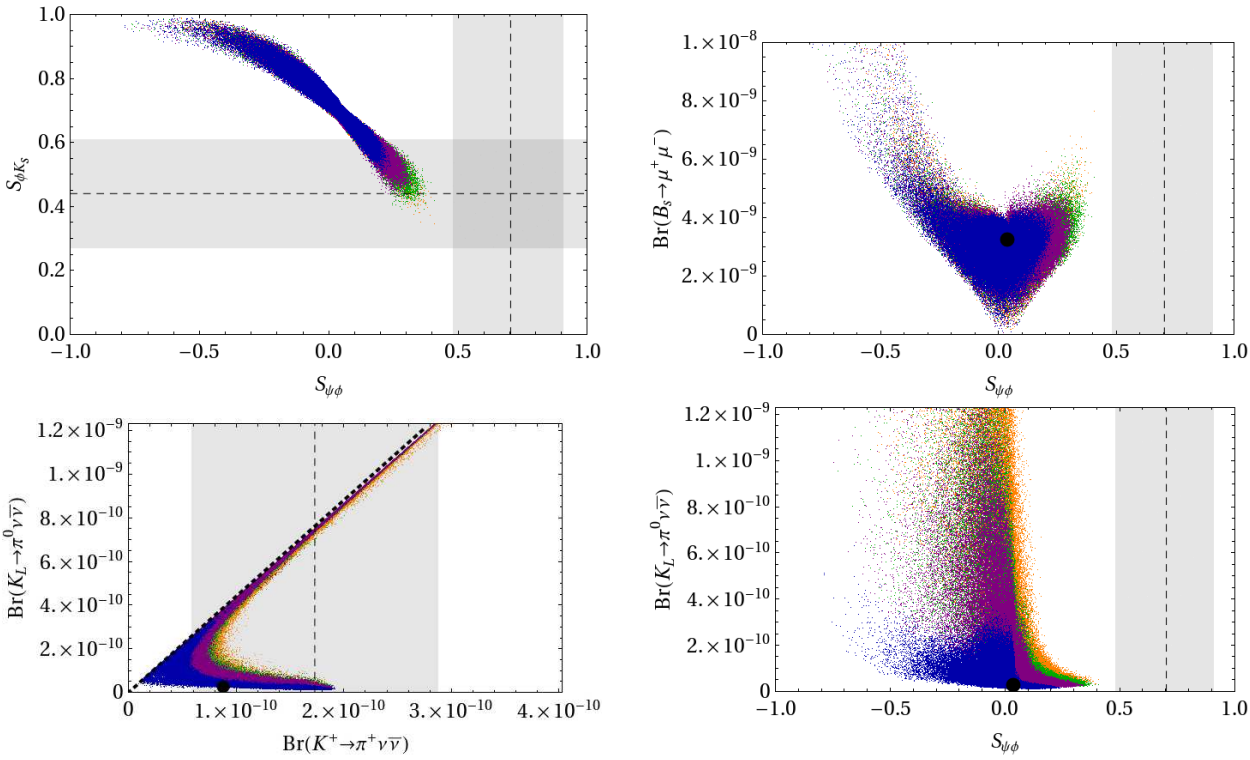

Figure 5.16.: Correlations including the ε'/ε-constraint (color coding according to Table 5.3) .

- $S_{\psi\phi}$ can be at most 0.4 and this upper bound is only reached for the green and orange points where the ratio $R_6/R_8 \geq 2$

- For the large N case $R_6 = R_8 = 1$ represented by dark blue points, we identify the following rough absolute bounds

$$S_{\psi\phi} \lesssim 0.25\,, \qquad \mathrm{Br}(K_L \to \pi^0\nu\bar{\nu}) \lesssim 4\cdot 10^{-10}\,,$$
$$\mathrm{Br}(K^+ \to \pi^+\nu\bar{\nu}) \lesssim 2\cdot 10^{-10}\,, \qquad \mathrm{Br}(B_s \to \mu^+\mu^-) \lesssim 4.9\cdot 10^{-9}\,,$$

  where in the last case $S_{\psi\phi} > 0$ has been assumed in accordance with CDF and D0 data.

- Weaker bounds are found for purple and in particular green and orange points where the role of electroweak penguins relative to QCD penguins in ε'/ε is suppressed and it is easier to have larger 4G effects in rare K and B decays, while still satisfying the ε'/ε constraint.

Finally we would like to remark that the enhancements of rare K decay branching ratios found here are larger than the bounds in [188] would suggest. This is related to the fact that in the SM4 the NP effects in neutral meson mixing can be significantly larger than assumed in [188], implying that the range for $\mathrm{Im}\lambda_t$ in the SM4 can be significantly larger than used in [188].

5.1.7. Violation of CKM Unitarity

From our discussion of unitarity of the matrix $V_{\rm SM4}$ in Section 2.2.1, we know that the 3×3 sub-matrix describing the 3G mixing is for non-vanishing mixing angles θ_{i4} necessarily non-unitary. A similar effect was observed also in the RS model with custodial protection [257]. In order to quantitatively describe the deviation from unitarity, we define

$$K^u \equiv V_{\rm CKM3} V_{\rm CKM3}^\dagger\,, \quad K^d \equiv V_{\rm CKM3}^\dagger V_{\rm CKM3} \tag{5.9}$$

which are generally different from the 3×3 unit matrix. In particular, we find

$$|K^u - \mathbb{1}|_{ij} = |V_{ib'} V_{jb'}^*|\,, \quad |K^d - \mathbb{1}|_{ij} = |V_{t'i} V_{t'j}^*|\,. \tag{5.10}$$

In Table 5.4, we collect the entries of $K^{u,d}$ and give the deviations from 3G unitarity in terms of the scaling of the mixing angles θ_{i4} for the benchmark scenarios introduced in Section 2.2.1. We see that, for several unitarity relations, the violation in the SM3 can be of the same size as the largest individual contribution from 3G mixing angles.

		$\lvert\mathbb{1}-K\rvert_{ij}$	(a) 431	(b) 211	(c) 231	(d) 321
$\underset{1}{\lvert V_{ud}\rvert^2} + \underset{\lambda^2}{\lvert V_{cd}\rvert^2} + \underset{\lambda^6}{\lvert V_{td}\rvert^2} =$	K^d_{11}	$\lvert V_{t'd}\rvert^2 \sim \lambda^{2n_1}$	λ^8	λ^4	λ^4	λ^6
$\underset{\lambda^2}{\lvert V_{us}\rvert^2} + \underset{1}{\lvert V_{cs}\rvert^2} + \underset{\lambda^4}{\lvert V_{ts}\rvert^2} =$	K^d_{22}	$\lvert V_{t's}\rvert^2 \sim \lambda^{2n_2}$	λ^6	λ^2	λ^6	λ^4
$\underset{\lambda^6}{\lvert V_{ub}\rvert^2} + \underset{\lambda^4}{\lvert V_{cb}\rvert^2} + \underset{1}{\lvert V_{tb}\rvert^2} =$	K^d_{33}	$\lvert V_{t'b}\rvert^2 \sim \lambda^{2n_3}$	λ^2	λ^2	λ^2	λ^2
$\underset{1}{\lvert V_{ud}\rvert^2} + \underset{\lambda^2}{\lvert V_{us}\rvert^2} + \underset{\lambda^6}{\lvert V_{ub}\rvert^2} =$	K^u_{11}	$\lvert V_{ub'}\rvert^2 \sim \lambda^{2n_1}$	λ^8	λ^4	λ^4	λ^6
$\underset{\lambda^2}{\lvert V_{cd}\rvert^2} + \underset{1}{\lvert V_{cs}\rvert^2} + \underset{\lambda^4}{\lvert V_{cb}\rvert^2} =$	K^u_{22}	$\lvert V_{cb'}\rvert^2 \sim \lambda^{2n_2}$	λ^6	λ^2	λ^6	λ^4
$\underset{\lambda^6}{\lvert V_{td}\rvert^2} + \underset{\lambda^4}{\lvert V_{ts}\rvert^2} + \underset{1}{\lvert V_{tb}\rvert^2} =$	K^u_{33}	$\lvert V_{tb'}\rvert^2 \sim \lambda^{2n_3}$	λ^2	λ^2	λ^2	λ^2
$\underset{\lambda}{V_{ud}V_{us}^*} + \underset{\lambda}{V_{cd}V_{cs}^*} + \underset{\lambda^5}{V_{td}V_{ts}^*} =$	K^d_{12}	$\lvert V_{t'd}V_{t's}^*\rvert \sim \lambda^{n_1+n_2}$	λ^7	λ^3	λ^5	λ^5
$\underset{\lambda^3}{V_{ud}V_{ub}^*} + \underset{\lambda^3}{V_{cd}V_{cb}^*} + \underset{\lambda^3}{V_{td}V_{tb}^*} =$	K^d_{13}	$\lvert V_{t'd}V_{t'b}^*\rvert \sim \lambda^{n_1+n_3}$	λ^5	λ^3	λ^3	λ^4
$\underset{\lambda^4}{V_{us}V_{ub}^*} + \underset{\lambda^2}{V_{cs}V_{cb}^*} + \underset{\lambda^2}{V_{ts}V_{tb}^*} =$	K^d_{23}	$\lvert V_{t's}V_{t'b}^*\rvert \sim \lambda^{n_2+n_3}$	λ^4	λ^2	λ^4	λ^3
$\underset{\lambda}{V_{ud}V_{cd}^*} + \underset{\lambda}{V_{us}V_{cs}^*} + \underset{\lambda^5}{V_{ub}V_{cb}^*} =$	K^u_{12}	$\lvert V_{ub'}V_{cb'}^*\rvert \sim \lambda^{n_1+n_2}$	λ^7	λ^3	λ^5	λ^5
$\underset{\lambda^3}{V_{ud}V_{td}^*} + \underset{\lambda^3}{V_{us}V_{ts}^*} + \underset{\lambda^3}{V_{ub}V_{tb}^*} =$	K^u_{13}	$\lvert V_{ub'}V_{tb'}^*\rvert \sim \lambda^{n_1+n_3}$	λ^5	λ^3	λ^3	λ^4
$\underset{\lambda^4}{V_{cd}V_{td}^*} + \underset{\lambda^2}{V_{cs}V_{ts}^*} + \underset{\lambda^2}{V_{cb}V_{tb}^*} =$	K^u_{23}	$\lvert V_{cb'}V_{tb'}^*\rvert \sim \lambda^{n_2+n_3}$	λ^4	λ^2	λ^4	λ^3

Table 5.4.: CKM unitarity relations and the amount by which they are broken in the SM4 in the four scaling scenarios introduced in Section 2.2.1. For comparison, in the first column we also give the scaling for the three individual terms on the l.h.s. of the relation.

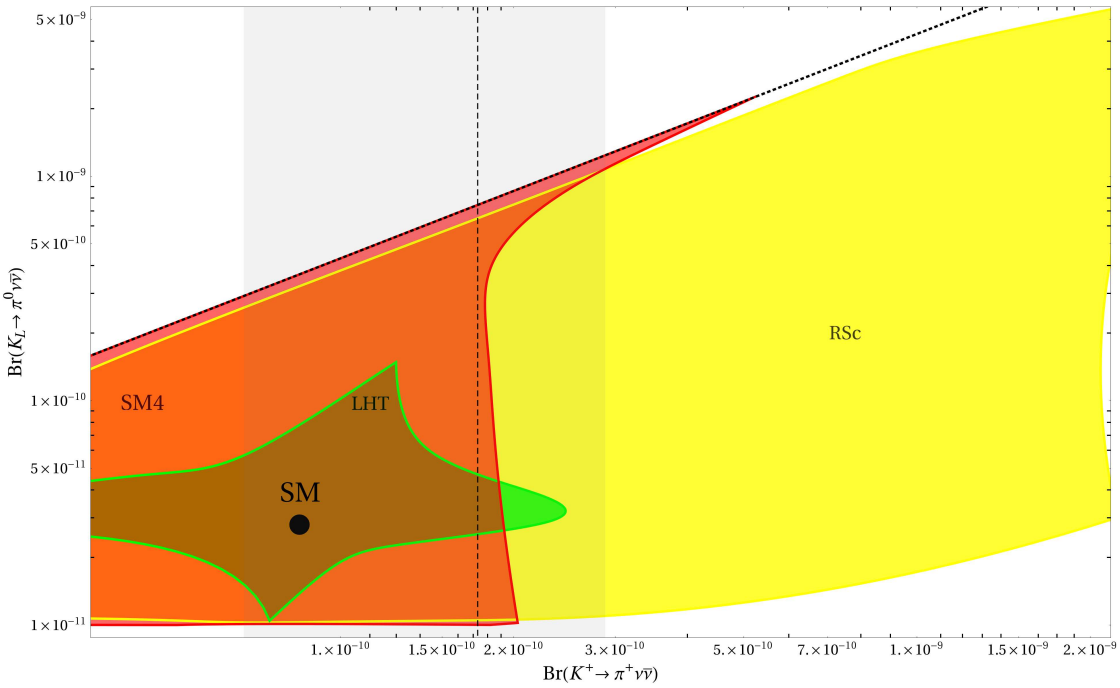

Figure 5.17.: Correlations between $\mathrm{Br}(K^+ \to \pi^+\nu\bar{\nu})$ and $\mathrm{Br}(K_L \to \pi^0\nu\bar{\nu})$ in several NP models. The effects of SUSY flavor models is very weak in the K-system and is therefore not plotted. The dotted line corresponds to the model-independent GN bound.

5.1.8. Patterns of Correlation and Comparison with other Models

In the course of this section, we have shown a number of correlations between various observables. This combined information can be very valuable since it provides a higher predictivity than the treatment of single quantities. It will allow us to exclude certain models once several of the involved observables are (better) measured, which should be the case for e.g. $\mathrm{Br}(B_{s,d} \to \mu^+\mu^-)$ and $S_{\psi\phi}$ already in the coming years.

In this section, we want to compare several predictions made by the SM4 with those from different NP models such as the Little Higgs model with T-parity (LHT) [70–72], the Randall-Sundrum model with custodial protection (RSc) [73, 74] and supersymmetric (SUSY) flavor models [75].It turns out that correlations characteristic for (C)MFV scenarios can be strongly violated in all of these scenarios.

Probably the most striking signature of the SM4, especially when compared to the LHT and SUSY flavor models, is the possibility of having simultaneously sizable NP effects in the K, B_d and B_s systems. We have already shown in Fig. 5.4 that the impact of a fourth generation can be truly spectacular in the K sector. Fig. 5.17 demonstrates that this statement holds also in the RSc model. In contrast, effects from the LHT model are still present but much smaller, while those from MSSM flavor models are strongly suppressed.

In the B system, represented by Figs. 5.18 and 5.19, the situation is totally different. In Fig. 5.18 we recognize that SUSY flavor models can generate simultaneously large positive effects in both $\mathrm{Br}(B_s \to \mu^+\mu^-)$ and $\mathrm{Br}(B_d \to \mu^+\mu^-)$. Conversely, in the SM4 and RSc

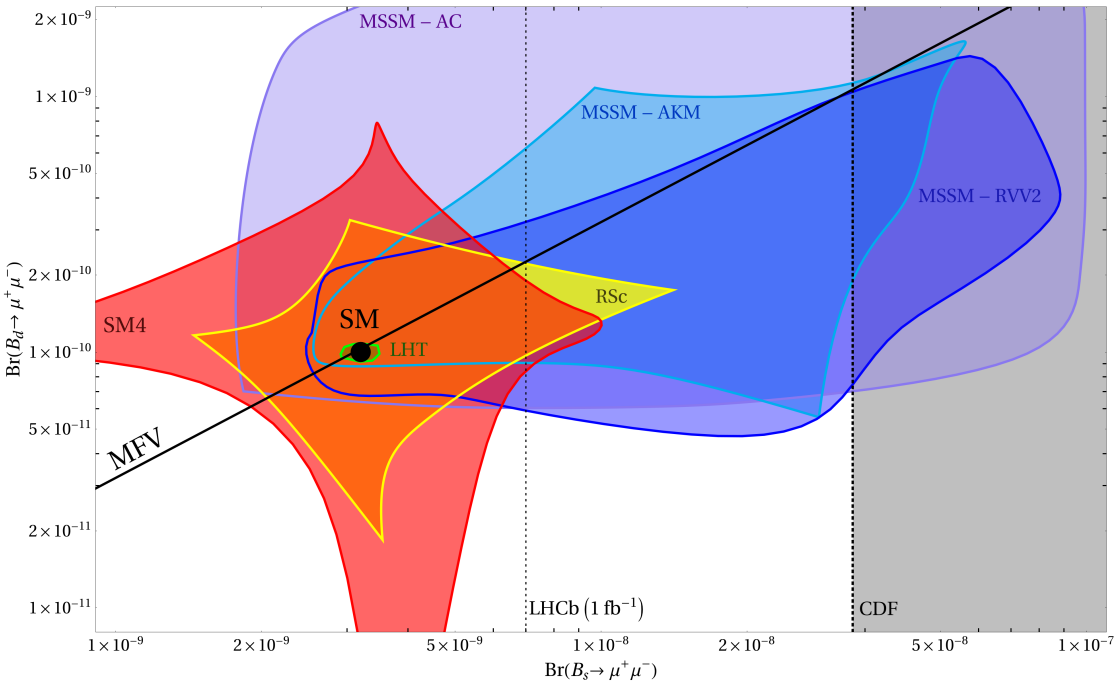

Figure 5.18.: Correlations between $\mathrm{Br}(B_s \to \mu^+\mu^-)$ and $\mathrm{Br}(B_d \to \mu^+\mu^-)$ in several NP models. The straight line depicts the "Golden Relation" of CMFV models as given in (4.59) with $r = 1$. The gray area is excluded by CDF measurements at 95% C.L. as stated in (4.61), while the vertical dotted line shows the predicted LHCb exlusion limit for 1 fb^{-1} of integrated luminosity as given in (4.62).

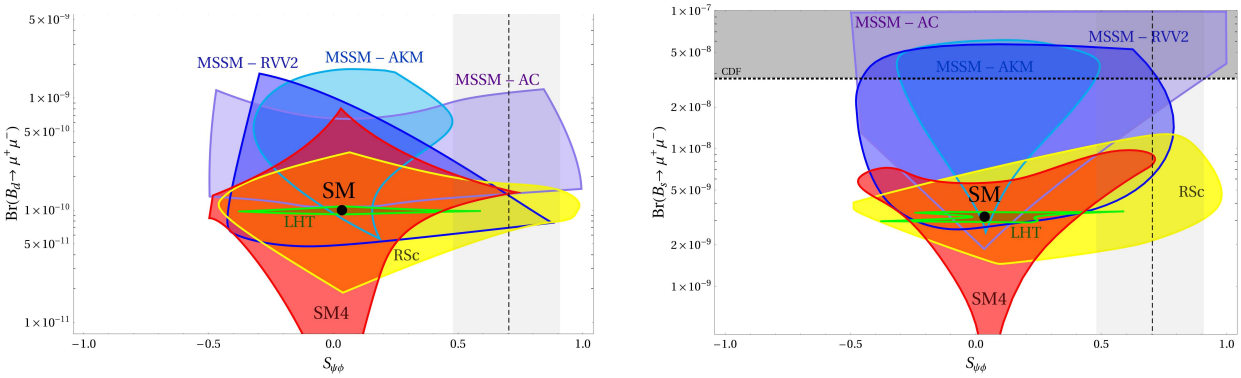

Figure 5.19.: Correlations between $S_{\psi\phi}$ and $\mathrm{Br}(B_d \to \mu^+\mu^-)$ (left panel), respectively $S_{\psi\phi}$ and $\mathrm{Br}(B_s \to \mu^+\mu^-)$ (right panel), for several NP scenarios.

large deviations from the SM (enhancements as well as suppressions) are permitted but mutually exclusive, while the LHT predicts only tiny effects. The differences between the two diagrams in Fig. 5.19 demonstrate the non-CMFV nature of the various NP models, which is particularly pronounced in the SM4.

The difference of SM4 flavor effects as compared to the other NP models can partially be traced back to the fact that the mass scales involved in the SM4 are generally significantly lower than in the LHT and in particular in the RSc. Another important source of deviations is the fact that in the SM4 the undetermined CKM matrix elements V_{td} and V_{ts} are not constrained by 3×3 unitarity and can obtain large enhancements as seen in (2.33). Finally, the non-decoupling of the new heavy fermions t' and b' plays a role – an effect which does not occur in the LHT, RSc and SUSY models.

5.2. Anatomy of the Quark Sector

5.2.1. Step 1: Parameter Scenarios

We begin the anatomy of the SM4 by analyzing the three scenarios for $|V_{ub}|$ and δ_{13} defined in Table 5.5. The three scenarios in question correspond to ones discussed in [75] and can be characterized as follows:

S1: $(\epsilon_K)_{\rm SM}$ is lower than the data, while $S_{\Psi K_S}$ and $\Delta M_d/\Delta M_s$ are compatible with experiment. The *orange* points in Fig. 5.20-5.22 correspond to the removal of this anomaly within the SM4.

S2: $(S_{\psi K_S})_{\rm SM}$ is above the data, while ϵ_K and $\Delta M_d/\Delta M_s$ are compatible with experiment. The *purple* points in Fig. 5.20-5.22 correspond to the removal of this anomaly within the SM4.

S3: $(\Delta M_d/\Delta M_s)_{\rm SM}$ is much higher than the data, while ϵ_K and $S_{\Psi K_S}$ are compatible with experiment. The *green* points in Fig. 5.20-5.22 correspond to the removal of this anomaly within the SM4.

The clear lessons from this analysis are the following:

- Due to the 4G contributions to ε_K and $S_{\psi K_S}$ in all scenarios simultaneous agreement with the data for these two observables can be achieved taking all existing constraints into account.

- However, only in scenario S1 values of $S_{\psi\phi}$ can be significantly enhanced and consequently $S_{\phi K_S}$ and $S_{\eta' K_S}$ significantly suppressed. As an example, we show in Fig. 5.21 (right panel) this situation by plotting $S_{\phi K_S}$ as a function of $S_{\psi\phi}$.

- As shown in Fig. 5.22, in all three scenarios significant enhancements of $\mathrm{Br}(K^+ \to \pi^+\nu\bar{\nu})$, $\mathrm{Br}(K_L \to \pi^0\nu\bar{\nu})$ and $\mathrm{Br}(K_L \to \mu^+\mu^-)$ are possible.

	S1 (orange)	S2 (purple)	S3 (green)
$\lvert V_{ub}\rvert$	0.0034 ± 0.00015	0.0043 ± 0.0001	0.0037 ± 0.0001
δ_{13}	$(66 \pm 2)°$	$(66 \pm 2)°$	$(84 \pm 2)°$

Table 5.5.: Three scenarios for the parameters s_{13} and δ_{13}

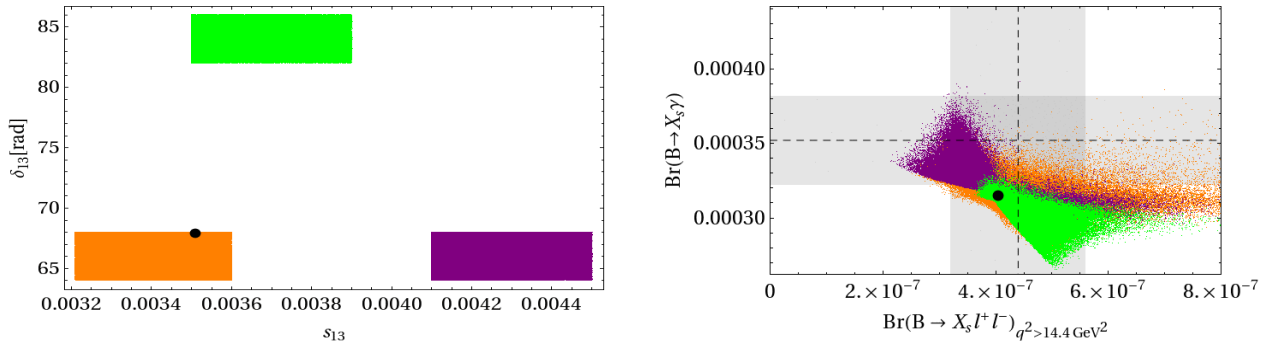

Figure 5.20.: We show the color coding of the tension scenarios (left panel) and $\mathrm{Br}(B \to X_s\gamma)$ vs. $\mathrm{Br}(B \to X_s\ell^+\ell^-)_{q^2>14.4\mathrm{GeV}^2}$ (right panel) for the tension scenarios defined in Tab. 5.5.

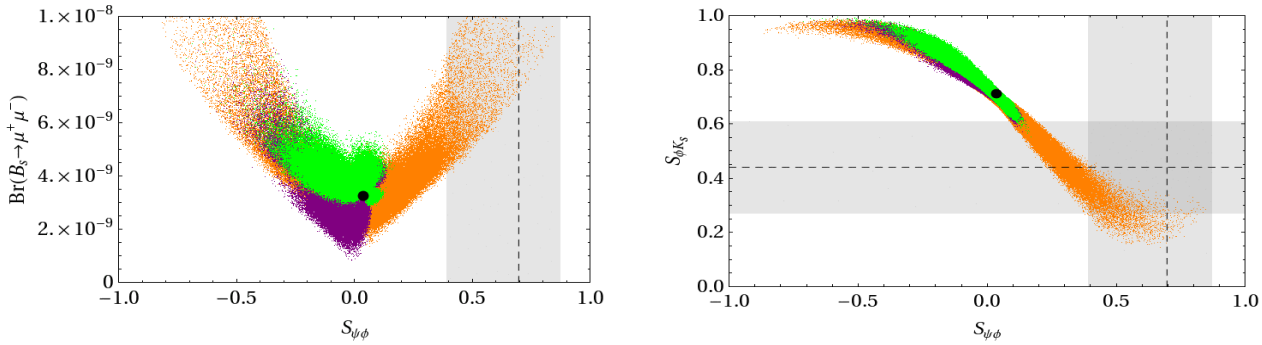

Figure 5.21.: We show $\mathrm{Br}(B_s \to \mu^+\mu^-)$ vs. $S_{\psi\phi}$ (left panel) and $S_{\phi K_s}$ vs. $S_{\psi\phi}$ (right panel) for the tension scenarios defined in Tab. 5.5. The color coding is defined in this table and can be read from the left panel of Fig. 5.20.

- On the other hand, as shown in the lower panel of Fig. 5.21 (right panel), the departure of $\mathrm{Br}(B_s \to \mu^+\mu^-)$ can be up to a factor of 4 for all three scenarios. However we found no points with large positive $S_{\psi\phi}$ for S2 and S3 which in turn puts a loose upper limit on $\mathrm{Br}(B_s \to \mu^+\mu^-)$ in these scenarios provided $S_{\psi\phi} > 0$.

5.2.2. Step 2: Anticipating LHCb Results

In the next three years, LHCb should be able to provide good data on $S_{\psi\phi}$ and $\mathrm{Br}(B_s \to \mu^+\mu^-)$. As we have seen in Fig. 5.10, a measurement of $S_{\psi\phi}$ above 0.5 accompanied by $\mathrm{Br}(B_s \to \mu^+\mu^-)_{\mathrm{exp}} \leq \mathrm{Br}(B_s \to \mu^+\mu^-)_{SM}$ would put the SM4 under pressure. Similarly for SM3-like values of $S_{\psi\phi}$, $\mathrm{Br}(B_s \to \mu^+\mu^-)$ can only be slightly enhanced over its SM3 value, and in fact a suppression of the latter branching ratio is more likely in this case.

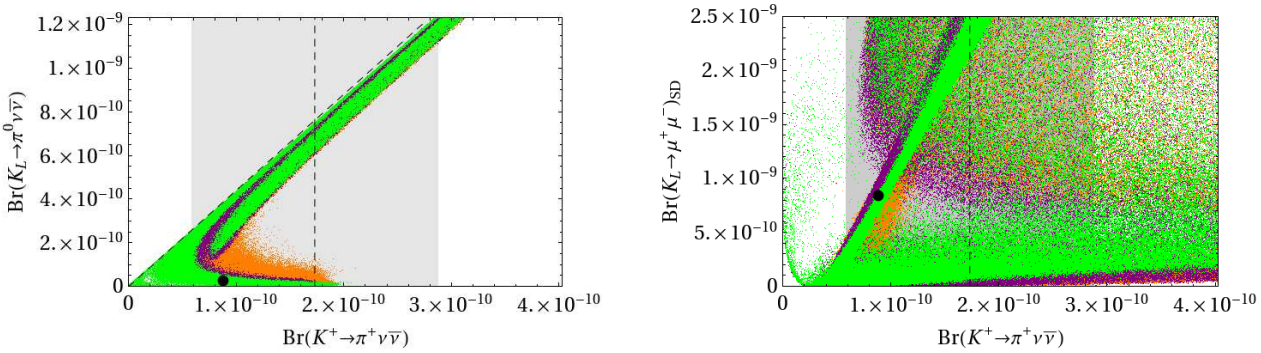

Figure 5.22.: We show $\mathrm{Br}(K_L \to \pi^0\nu\bar{\nu})$ vs. $\mathrm{Br}(K^+ \to \pi^+\nu\bar{\nu})$ (left panel) and $\mathrm{Br}(K_L \to \mu^+\mu^-)_{\rm SD}$ vs. $\mathrm{Br}(K^+ \to \pi^+\nu\bar{\nu})$ (right panel) for the tension scenarios defined in Tab. 5.5. The color coding is defined in the table and can be read of Fig. 5.20 left panel.

In view of this pattern, we considered three scenarios shown in Table 5.2 and asked what they would imply for other decays. The result of this exercise is shown in all plots of Section 5.1 where the three scenarios of Table 5.2 are exhibited in three different colors indicated in this table. Alternatively, the color coding can be conveniently inferred from Fig. 5.10. This results are self-explanatory and have been briefly discussed already in Section 5.1. Let us therefore only summarize our observations:

- As seen in Fig. 5.14, the $S_{\phi K_S}$ and $S_{\psi K_S}$ anomalies can only be explained in scenario BS3.
- Fig. 5.9 shows that in the BS1 and BS3 scenarios the branching ratio $\mathrm{Br}(B_d \to \mu^+\mu^-)$ remains SM3-like, while in scenario BS2 it can be enhanced by a factor of two.
- As seen in Figs. 5.4 and 5.6 in all three scenarios large NP effects in $\mathrm{Br}(K^+ \to \pi^+\nu\bar{\nu})$, $\mathrm{Br}(K_L \to \pi^0\nu\bar{\nu})$ and $\mathrm{Br}(K_L \to \mu^+\mu^-)$ are possible. Moreover in scenario BS3 they are particularly strongly correlated with each other.
- For large positive values of $S_{\psi\phi}$ the predicted value of ε'/ε is significantly below the data, unless the hadronic matrix elements of the electroweak penguins are sufficiently suppressed with respect to the large N result and the ones of QCD penguins enhanced.

This analysis shows that we will learn a lot about the SM4 when $S_{\psi\phi}$, $\mathrm{Br}(B_s \to \mu^+\mu^-)$, $\mathrm{Br}(K^+ \to \pi^+\nu\bar{\nu})$ and $\mathrm{Br}(K_L \to \pi^0\nu\bar{\nu})$ will be precisely known.

5.3. Determining the Matrix $V_{\rm SM4}$

5.3.1. Preliminaries

As discussed in previous sections, the mixing between the third and fourth generation is bounded by the electroweak precision data and cannot be significantly larger than s_{12}. Similarly, s_{14} and s_{24} are bounded by (2.29b). As a consequence, as can be explicitly seen by

the generalized Wolfenstein expansion for our benchmark scenarios (2.40–2.43), the relation between CKM parameters and the matrix elements $V_{us}, V_{cd}, V_{ub}, V_{cb}$,

$$\begin{aligned} s_{12} &= \lambda \simeq |V_{us}| \simeq |V_{cd}|\,, & s_{23} &= A\lambda^2 \simeq |V_{cb}|\,, \\ s_{13} &= A\lambda^3|z_\rho| \simeq |V_{ub}|\,, & \delta_{13} &= -\arg(z_\rho) \simeq -\arg(V_{ub})\,, \end{aligned} \tag{5.11}$$

are to a very good approximation unaffected by 4G contributions. Therefore the SM3 CKM parameters can be determined from the corresponding tree-level decays, practically without any NP pollution, with δ_{13} determined from $B \to DK$. In particular such a determination does not require the 3×3 CKM matrix to be unitary.[3] In the present Section we will further use (2.31) for the 4G mixing angles, in order to indicate how the $V_{\rm SM4}$ matrix can, in principle, be determined from future data.

A further comment on the determination of $\delta_{13} \approx \gamma$ is in order.

In the approximation of neglecting the phase of V_{cs} and V_{cb}, being real in the CKM convention, the $B_s \to D_s K$ complex in the SM3 measures directly a linear combination of the phase γ and the phase of B_s-mixing, where the latter can be extracted from $S_{\psi\phi}$. Analogous comments apply to $B_d \to D\pi$ decays. In the presence of 4G quarks, the phases in B_s and B_d mixing may change, but again they can be determined from the $S_{\psi\phi}$ and $S_{\psi K_S}$ asymmetries, respectively. The new feature, as seen in (2.12), are new phases of V_{cb} and V_{cs} induced by the presence of the 4G quarks. However, the imposition of tree-level and electroweak precision constraints implies that this NP pollution amounts to significantly less than 1° in the determination of δ_{13} and can be safely neglected. Analogous comments apply to other tree-level methods for the determination of δ_{13}.

The determination of the new parameters in the $V_{\rm SM4}$ matrix,

$$s_{14}\,, \qquad s_{24}\,, \qquad s_{34}\,, \qquad \delta_{14}\,, \qquad \delta_{24}\,, \tag{5.12}$$

is probably beyond the scope of flavor violating high-energy processes explored at the LHC and will have to be made through FCNC processes that, as in the SM3, appear first at the one-loop level due to the GIM mechanism at work. The accuracy of this determination will depend on

i) the precision of the relevant experimental data,

ii) the theoretical cleanliness of the observables involved (i.e. observables with small hadronic uncertainties should be favored),

iii) the potential size of NP contributions to the considered observable.

Clearly, the room for NP contributions to observables that are known already precisely will depend on the values of the CKM parameters in (5.11). In this context, let us recall the existing tension between the experimental values of ε_K and $S_{\psi K_S}$ within the SM3 that has been extensively discussed in [129, 252, 258, 259]. Whether the SM3 has a problem with ε_K,

[3] Needless to say, $|V_{us}|, |V_{ub}|, |V_{cb}|$ and δ_{13} can be determined from tree-level decays even in the absence of this approximation, but the relation to the fundamental parameters is less transparent and involves the 4G parameters.

$S_{\psi K_S}$ or both observables depends on the values in (5.11). In turn, this will have an impact on the determination of the new parameters in (5.12). In what follows, we will first make a list of observables that could help us in the future to determine the parameters (5.12), subsequently illustrating such determinations on a few examples. A more extensive general numerical analysis appears to us to be premature at present. On the other hand, as we will see in Section 5.3.3, new insight can be gained by examining the anatomy of different scaling scenarios for the mixing angles and their implications for various flavor observables.

5.3.2. Basic Observables

Among the FCNC observables that have already been measured, the values for

$$\varepsilon_K\,, \qquad \Delta M_d/\Delta M_s\,, \qquad S_{\psi K_S}\,, \qquad \mathrm{Br}\,(B\to X_s\gamma) \tag{5.13}$$

have presently the dominant impact on the allowed structure of the $V_{\rm SM4}$ matrix. Indeed, $S_{\psi K_S}$ is theoretically very clean (as discussed in Section 4.2.5), and the hadronic uncertainties in ε_K and $\Delta M_d/\Delta M_s$ are below 5% already now and are expected to be decreased further in the coming years through improved lattice calculations. Of particular interest in this decade will be the measurements of the branching ratios for

$$B_{s,d}\to\mu^+\mu^-\,, \qquad K^+\to\pi^+\nu\bar\nu\,, \qquad K_L\to\pi^0\nu\bar\nu\,, \qquad B\to X_s\nu\bar\nu\,, \tag{5.14}$$

and, very importantly, of the CP-violating observables

$$S_{\psi\phi}\,, \qquad S_{\phi K_S}\,, \qquad A_{\rm CP}(b\to s\gamma)\,. \tag{5.15}$$

In particular, various correlations between all these observables will significantly constrain the allowed range of the SM4 parameters and even have the power to exclude this NP scenario. Assuming that the SM4 will survive these new tests and having at hand all these measurements, it will be possible to determine the matrix $V_{\rm SM4}$. Indeed, let us note on the basis of the formulae of Section 4.1.2.2 that all these observables depend on six complex variables involving new parameters (see (2.20)),

$$\lambda_{t'}^{(K)}\,, \qquad \lambda_{t'}^{(s)}\,, \qquad \lambda_{t'}^{(d)}\,, \qquad \lambda_{t}^{(K)}\,, \qquad \lambda_{t}^{(s)}\,, \qquad \lambda_{t}^{(d)}\,, \tag{5.16}$$

that are not fully independent as, with (5.11) being fixed, they depend on the five parameters in (5.12). It is instructive to write down the expressions for $\lambda_{t^{(\prime)}}^{(i)}$ setting $c_{ij}=1$ and neglecting

higher-order terms in the Wolfenstein expansion, leading to

$$\begin{aligned}
\lambda_t^{(d)} = V_{tb}^* V_{td} &\approx -s_{13} e^{i\delta_{13}} - s_{14} s_{34} e^{i\delta_{14}} + s_{12} \left(s_{23} + s_{24} s_{34} e^{i\delta_{24}} \right) \\
&\approx -s_{13} e^{i\delta_{13}} + s_{12} s_{23} - \lambda_{t'}^{(d)} \,, && \text{(5.17a)} \\
\lambda_t^{(s)} = V_{tb}^* V_{ts} &\approx -s_{23} - s_{24} s_{34} e^{i\delta_{24}} \\
&\approx -s_{23} - \lambda_{t'}^{(s)} \,, && \text{(5.17b)} \\
\lambda_t^{(K)} = V_{ts}^* V_{td} &\approx \left(s_{23} + s_{24} s_{34} e^{-i\delta_{24}} \right) \\
&\quad \times \left(s_{13} e^{i\delta_{13}} + s_{14} s_{34} e^{i\delta_{14}} - s_{12} \left(s_{23} + s_{24} s_{34} e^{i\delta_{24}} \right) \right) \\
&\approx \lambda_t^{(s)*} \lambda_t^{(d)} \,, && \text{(5.17c)} \\
\lambda_{t'}^{(d)} = V_{t'b}^* V_{t'd} &\approx \left(s_{34} + s_{13} s_{14} e^{i(\delta_{13} - \delta_{14})} + s_{23} s_{24} e^{-i\delta_{24}} \right) \\
&\quad \times \left(e^{i\delta_{14}} s_{14} - e^{i\delta_{24}} s_{12} s_{24} - e^{i\delta_{13}} s_{13} s_{34} + s_{12} s_{23} s_{34} \right) \\
&\approx -e^{i\delta_{13}} s_{13} s_{34}^2 + s_{34} \left(s_{14} e^{i\delta_{14}} - s_{12} s_{24} e^{i\delta_{24}} \right) \\
&\quad + s_{14} s_{23} s_{24} e^{i(\delta_{1,4} - \delta_{24})} - s_{12} s_{23} \left(s_{24}^2 - s_{34}^2 \right) \,, && \text{(5.17d)} \\
\lambda_{t'}^{(s)} = V_{t'b}^* V_{t's} &\approx \left(s_{34} + s_{13} s_{14} e^{i(\delta_{13} - \delta_{14})} + s_{23} s_{24} e^{-i\delta_{24}} \right) \\
&\quad \times \left(e^{i\delta_{24}} s_{24} + e^{i\delta_{14}} s_{12} s_{14} - s_{23} s_{34} \right) \\
&\approx s_{12} s_{14} s_{34} e^{i\delta_{14}} + s_{24} s_{34} e^{i\delta_{24}} + s_{23} \left(s_{24}^2 - s_{34}^2 \right) \,, && \text{(5.17e)} \\
\lambda_{t'}^{(K)} = V_{t's}^* V_{t'd} &\approx \left(e^{-i\delta_{24}} s_{24} + e^{-i\delta_{14}} s_{12} s_{14} - s_{23} s_{34} \right) \\
&\quad \times \left(e^{i\delta_{14}} s_{14} - e^{i\delta_{24}} s_{12} s_{24} - e^{i\delta_{13}} s_{13} s_{34} + s_{12} s_{23} s_{34} \right) \\
&\approx s_{24} \left(-s_{12} s_{24} + s_{14} e^{i(\delta_{14} - \delta_{24})} \right) - s_{24} s_{34} e^{-i\delta_{24}} \left(-s_{12} s_{23} + s_{13} e^{i\delta_{13}} \right) \\
&\quad + \left(s_{12} s_{24} e^{i\delta_{24}} - s_{14} e^{i\delta_{14}} \right) \left(s_{23} s_{34} - s_{12} s_{14} e^{-i\delta_{14}} \right) \\
&\approx \frac{\lambda_{t'}^{(s)*} \lambda_{t'}^{(d)}}{|V_{t'b}|^2} \,. && \text{(5.17f)}
\end{aligned}$$

We observe that, in general, the variables $\lambda_{t^{(\prime)}}^{(K,s,d)}$ involve all 5 mixing parameters associated with the 4G in a rather complicated way. Some simplification arises if we assume a certain scaling of the mixing angles θ_{i4}, for instance with one of our benchmark scenarios of Section 2.2.1. Let us, as an example, study the case (2.41), for which the above equations

simplify as follows:

$$\begin{aligned}
\lambda_{t'}^{(s)} &\approx e^{i\delta_{24}} s_{24} s_{34} \equiv \sigma_{23}\,, \\
\lambda_{t'}^{(d)} &\approx s_{34}\left(s_{14} e^{i\delta_{14}} - s_{12} s_{24} e^{i\delta_{24}}\right) \equiv \sigma_{13} - s_{12}\sigma_{23} \\
\lambda_{t'}^{(K)} &\approx s_{24}\left(-s_{12} s_{24} + s_{14} e^{i(\delta_{14}-\delta_{24})}\right) = \frac{1}{s_{34}^2}\sigma_{23}^*\,(\sigma_{13} - s_{12}\sigma_{23}) \quad [= \frac{1}{s_{34}^2}\lambda_{t'}^{(s)*}\lambda_{t'}^{(d)}]\,, \\
\lambda_t^{(s)} &\approx -s_{23} - s_{24} s_{34} e^{i\delta_{24}} = -s_{23} - \lambda_{t'}^{(s)}\,, \\
\lambda_t^{(d)} &\approx -s_{13} e^{i\delta_{13}} - s_{14} s_{34} e^{i\delta_{14}} + s_{12}\left(s_{23} + s_{24} s_{34} e^{i\delta_{24}}\right) = -s_{13} e^{i\delta_{13}} + s_{12} s_{23} - \lambda_{t'}^{(d)}\,, \\
\lambda_t^{(K)} &\approx \left(s_{23} + s_{24} s_{34} e^{-i\delta_{24}}\right)\left(s_{13} e^{i\delta_{13}} + s_{14} s_{34} e^{i\delta_{14}} - s_{12}\left(s_{23} + s_{24} s_{34} e^{i\delta_{24}}\right)\right) \\
&= \left(s_{23} + \lambda_{t'}^{(s)*}\right)\left(s_{13} e^{i\delta_{13}} - s_{12} s_{23} + \lambda_{t'}^{(d)}\right)\,,
\end{aligned} \tag{5.18}$$

where the following two combinations of new parameters (5.12) have been introduced:

$$\sigma_{13} \equiv s_{14} s_{34} e^{i\delta_{14}}\,, \qquad \sigma_{23} \equiv s_{24} s_{34} e^{i\delta_{24}}\,. \tag{5.19}$$

For this particular case, we observe that

i) $\lambda_t^{(K)}$ and $\lambda_{t'}^{(K)}$ depend on σ_{13}, σ_{23} and s_{34}.

ii) $\lambda_t^{(d)}$ and $\lambda_{t'}^{(d)}$ depend on σ_{13} and σ_{23}.

iii) $\lambda_t^{(s)}$ and $\lambda_{t'}^{(s)}$ are sensitive to σ_{23} only. The determination of ΔM_s, $\mathrm{Br}(B_s \to \mu^+\mu^-)$ and $S_{\psi\phi}$ will thus play an important role in constraining these parameters. Moreover for $s_{24} \gtrsim s_{23} s_{34}$ and δ_{24} not too small, $S_{\psi\phi}$ should be much larger than its SM3 value $(S_{\psi\phi})_{SM} \approx 0.04$ as we have seen in Section 5.1.

In view of the many possibilities for theoretical parameters and phenomenological observables, we will in the following develop a general procedure that allows us to analyze future experimental data in a systematic manner. Let us first consider the plots in Fig. 5.23, which show correlations between various parameters of the SM4, on the basis of the three scenarios of Table 5.2. In particular,

- in the case of the scenario BS3 of Table 5.2, there is a strong correlation between s_{24} and s_{14} with $s_{24} \sim 4 s_{14}$ and s_{24} in the range

$$0.046 \leq s_{24} \leq 0.17\,. \tag{5.20}$$

- δ_{14} and δ_{24} are also very strongly correlated in the BS3 scenario with $\delta_{14} \approx \delta_{24} \approx 270^\circ \pm 20^\circ$.

- in the lower left panel of Fig. 5.23 one can see the strong correlation of s_{34} and $m_{t'}$ derived in Section 3.2.2.

In the following Section, we will analyze these correlations within specific scaling scenarios for the 4G mixing angles.

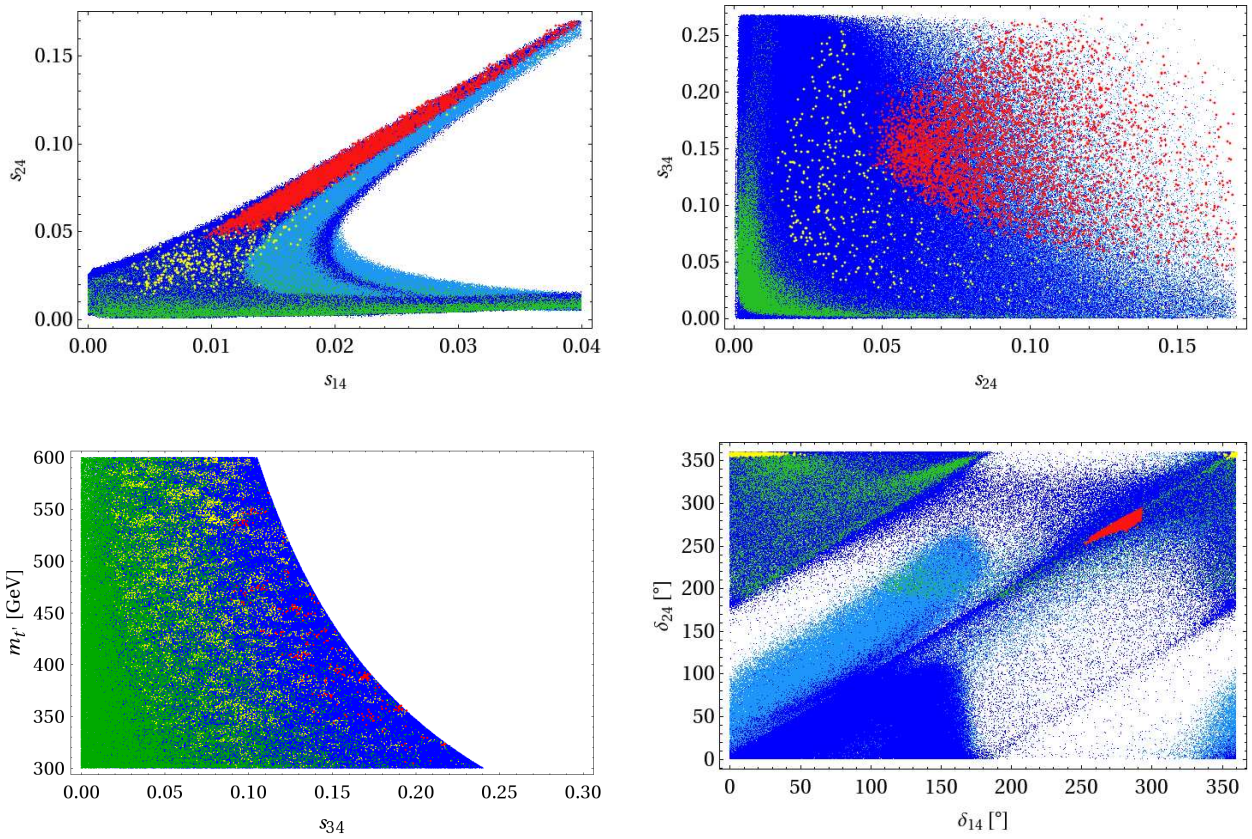

Figure 5.23.: Correlations between the new parameters for the parameter points used in our global analysis. The mixing angle s_{24} as a function of s_{14} (upper left panel), s_{34} as a function of s_{24} (upper right panel), $m_{t'}$ as a function of s_{34} (lower left panel) and δ_{24} as a function of δ_{14} (lower right panel). The color coding corresponds to scenarios of Table 5.2.

5.3.3. Anatomy of 4G Mixing Angles and CP Phases

As explained in Section 2.2.1, the 4G mixing matrix allows for different scalings of the 4G mixing angles θ_{14}, θ_{24} and θ_{34} with the Wolfenstein parameter $\lambda \ll 1$. Among the set of parameters that fulfil the present constraints on flavor observables, we may thus classify different subsets by calculating the exponents

$$(n_1, n_2, n_3) = \text{round}\left(\log_\lambda \left[\theta_{14}, \theta_{24}, \theta_{34}\right]\right) , \tag{5.21}$$

in (2.36) for $\lambda = s_{12} \ll 1$. Furthermore (see also Fig. 5.23), for a given set (n_1, n_2, n_3), the allowed values for the new CP phases δ_{14} and δ_{24} also exhibit a more or less strong correlation, which we will exploit to further distinguish different regions in the 4G parameter space. This enables us to identify a set of equivalence classes which – as we will illustrate – share certain characteristic features for the corresponding predictions for various flavor observables.

According to our discussion above, values (n_1, n_2, n_3) that do not fulfil the inequalities (2.39), from the theoretical point of view, should be considered as fine-tuned and will not be included in the subsequent discussion. (We convinced ourselves that we do not miss any of the observed phenomenological features by doing so.) For the remaining cases, we first identify – for a given scaling (n_1, n_2, n_3) – the allowed correlations between δ_{14} and δ_{24}, and then determine the assignment to one or the other equivalence class. Our procedure is summarised for the most prominent and representative examples in Table 5.6:

- Evidently, for small values of the n_i (i.e. large values of 4G mixing angles), one expects the largest deviations from the SM3 predictions. In fact, the most extreme case is characterized by example (2.41) from Section 2.2.1, with values $(n_1, n_2, n_3) = (2, 1, 1)$. As we already discussed, in this scenario the new 4G phases contribute at leading order to CP-violating observables, and therefore δ_{14} and δ_{24} are highly correlated and constrained. Separating the different relative and absolute signs of δ_{i4} enables us to classify the subsets $1a, 1b, 2a, 2b$ which show characteristic features in the selected set of observables shown in Tables 5.7 and 5.8. Similar correlations are found for the $(2, 2, 1)$ scenario.

- Decreasing the values of (some of) the mixing angles (i.e. increasing n_1, n_2, n_3), we observe that the correlations between the 4G phases become broader. Still, the values populate restricted areas in the δ_{24}–δ_{14} plane, which again allows to identify sub-classes with definite properties. A typical example is the case $(3, 2, 1)$ from our benchmark scenario (2.43). This scenario divides into two well-separated regions. Among one of them, we may (or may not) identify a subset of points as belonging to class 1a. This kind of arbitrariness is unavoidable (and expected), since the separation of points from scenario $(2, 2, 1)$ and $(3, 2, 1)$ is not clear-cut.

- For even smaller values of mixing angles, we observe for the cases $(3, 3, 1)$ and $(3, 3, 2)$ a separation into three sub-classes, where two classes (3a and 3b) can be considered as a continuation of those from the $(3, 2, 1)$ scenario, and class 4 is new.

- Considering $(4, 3, 1)$ (the benchmark scenario (2.40) discussed in Section 2.2.1) and $(4, 3, 2)$, the former classes 3b and 4 merge into one class 5 which already covers around

(n_1, n_2, n_3)	Correlation δ_{24} vs. δ_{14}	Assignment
$(2,1,1)$ $(2,2,1)$	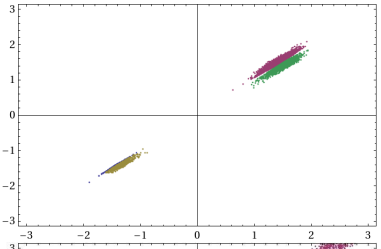	$\rightarrow \begin{cases} \text{class 1a: } \delta_{14} < \delta_{24} < \delta_{14} + \frac{\pi}{8}, & \delta_{24} < 0. \\ \text{class 1b: } \delta_{14} - \frac{\pi}{8} < \delta_{24} < \delta_{14}, & \delta_{24} < 0. \\ \text{class 2a: } \delta_{14} < \delta_{24} < \delta_{14} + \frac{\pi}{8}, & \delta_{24} > 0. \\ \text{class 2b: } \delta_{14} - \frac{\pi}{8} < \delta_{24} < \delta_{14}, & \delta_{24} > 0. \end{cases}$
$(3,2,1)$	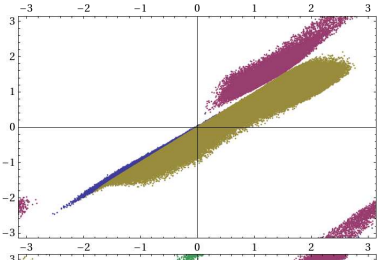	$\rightarrow \begin{cases} \text{class 1a: } \delta_{14} < \delta_{24} < \delta_{14} + \frac{\pi}{8}, & \delta_{24} < 0. \\ \text{class 2a/3a: } \delta_{14} < \delta_{24} < \delta_{14} + \frac{3\pi}{8}, & \delta_{24} > 0. \\ \text{class 3b: } \delta_{14} - \frac{3\pi}{8} < \delta_{24} < \delta_{14}. \end{cases}$
$(3,3,1)$ $(3,3,2)$	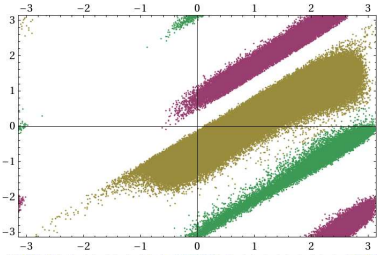	$\rightarrow \begin{cases} \text{class 3a: } \delta_{14} + \frac{\pi}{8} < \delta_{24} < \delta_{14} + \frac{\pi}{2}. \\ \text{class 3b: } \delta_{14} - \frac{3\pi}{4} < \delta_{24} < \delta_{14}. \\ \text{class 4: } \delta_{14} - \frac{9\pi}{8} < \delta_{24} < \delta_{14} - \frac{3\pi}{4}. \end{cases}$
$(4,3,1)$ $(4,3,2)$	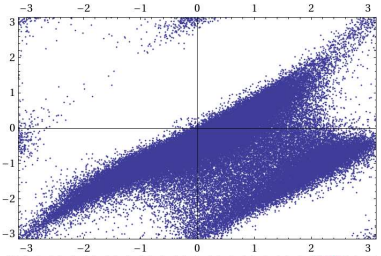	$\rightarrow \{ \text{class 5: } \delta_{14} - \frac{3\pi}{2} < \delta_{24} < \delta_{14} + \frac{\pi}{4}$
$(2,3,1)$	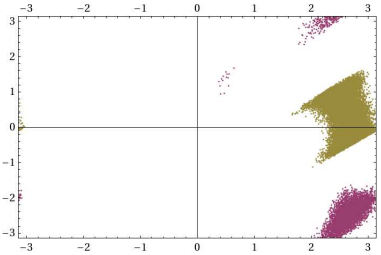	$\rightarrow \begin{cases} \text{class 6: } \delta_{14} + \frac{\pi}{8} < \delta_{24} < \delta_{14} + \frac{3\pi}{4}. \\ \text{class 7: } \delta_{14} - \frac{9\pi}{8} < \delta_{24} < \delta_{14} - \frac{\pi}{4}. \end{cases}$

Table 5.6.: Correlations between 4G phases for different scalings of 4G mixing angles (some selected examples). The constraints on the phases, of course, are understood to be periodic in units of 2π.

half of the δ_{24}-δ_{14} plane. Finally, for the scenario (2.42) with the scaling $(2, 3, 1)$, the former class 3a continues into class 6, while 3b and 4 merge into class 7, where the parameter space in the δ_{24}-δ_{14} plane is again somewhat more constrained.

Having identified the different sub-classes, we investigate the characteristic features for certain phenomenological observables in Tables 5.7-5.10. We see that each class can be distinguished from the others by at least one of the shown correlations: $\mathrm{Br}(B_s \to \mu^+\mu^-)$ vs. $S_{\psi\phi}$, $S_{\phi K_S}$ vs. $S_{\psi\phi}$, $\mathrm{Br}(b \to s\gamma)$ vs. $\mathrm{Br}(B \to X_s\ell\ell)$, $\mathrm{Br}(K_L \to \mu^+\mu^-)_{\mathrm{SD}}$ vs. $\mathrm{Br}(K^+ \to \pi^+\nu\bar{\nu})$ (The color coding is as defined in Table 5.2).

Turning the argument around, the observation of a combination of particular correlations in rare flavor processes can be translated into one or the other favored scenario for 4G mixing angles and CP phases. Only after a particular scaling scenario has been identified, the formulae for $\lambda_{t'}^{(K,d,s)}$ in (5.17f–5.17b) can be simplified, and we may (more or less) unambiguously determine the 4G mixing parameters from the future experimental data. We emphasize that, quite generally, such a procedure should be applied to the analysis of flavor parameters in NP models without MFV. In particular, without a specific theory of flavor at hand, the fact that certain scaling scenarios – like (2.40) – are represented by only a small number of points in the overall scan of parameter space, should not be taken as a signal for a small probability to observe the associated correlations in flavor observables.

Class	$10^8 \cdot \mathrm{Br}(B_s \to \mu^+\mu^-)$ vs. $S_{\psi\phi}$	$S_{\phi K_S}$ vs. $S_{\psi\phi}$	
1a:	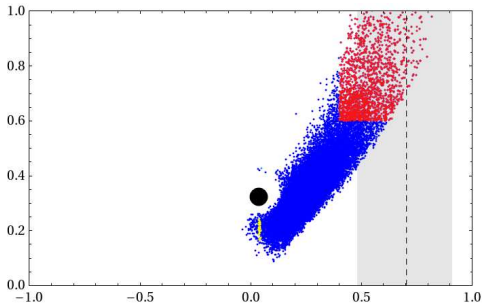	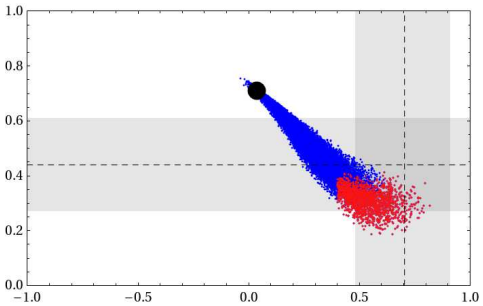	...
1b:	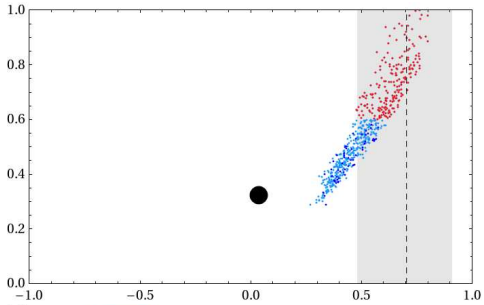	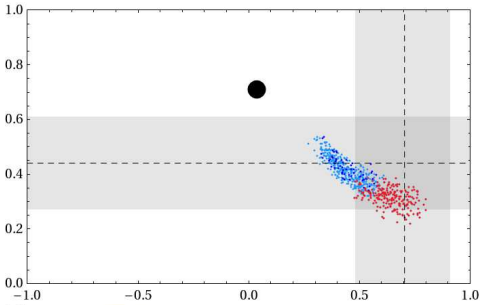	...
2a:	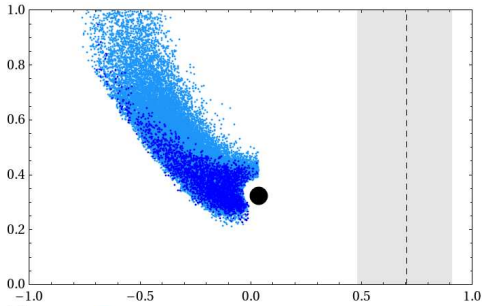	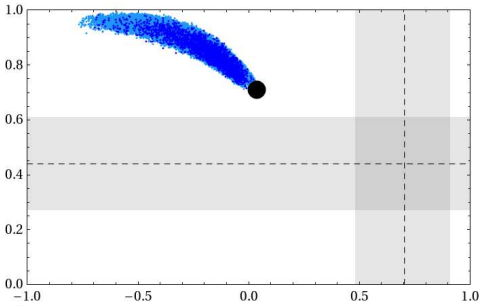	...
2b:	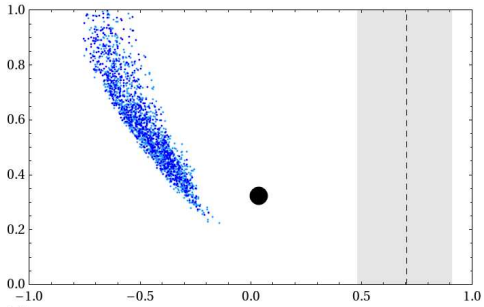	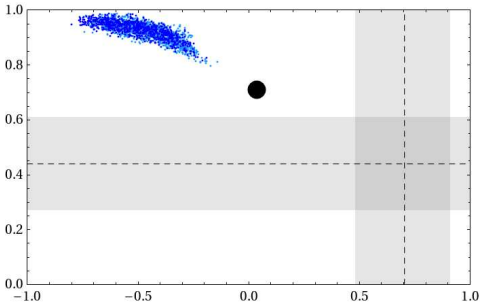	...
3a:	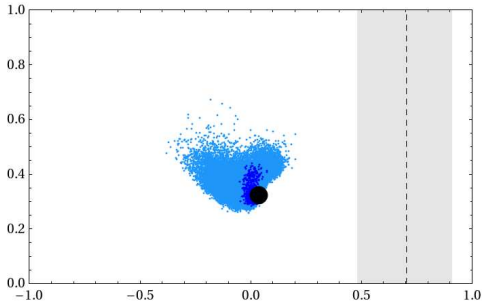	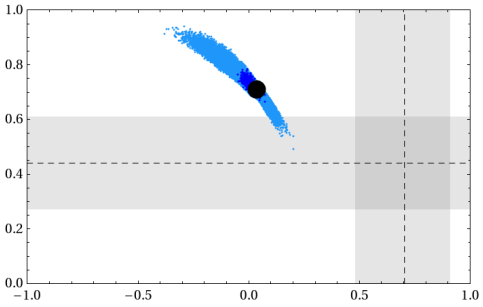	...
	...	...	

Table 5.7.: Selected correlations for classes identified in Table 5.6 (part 1 of 4). (The color coding is as defined in Table 5.2).

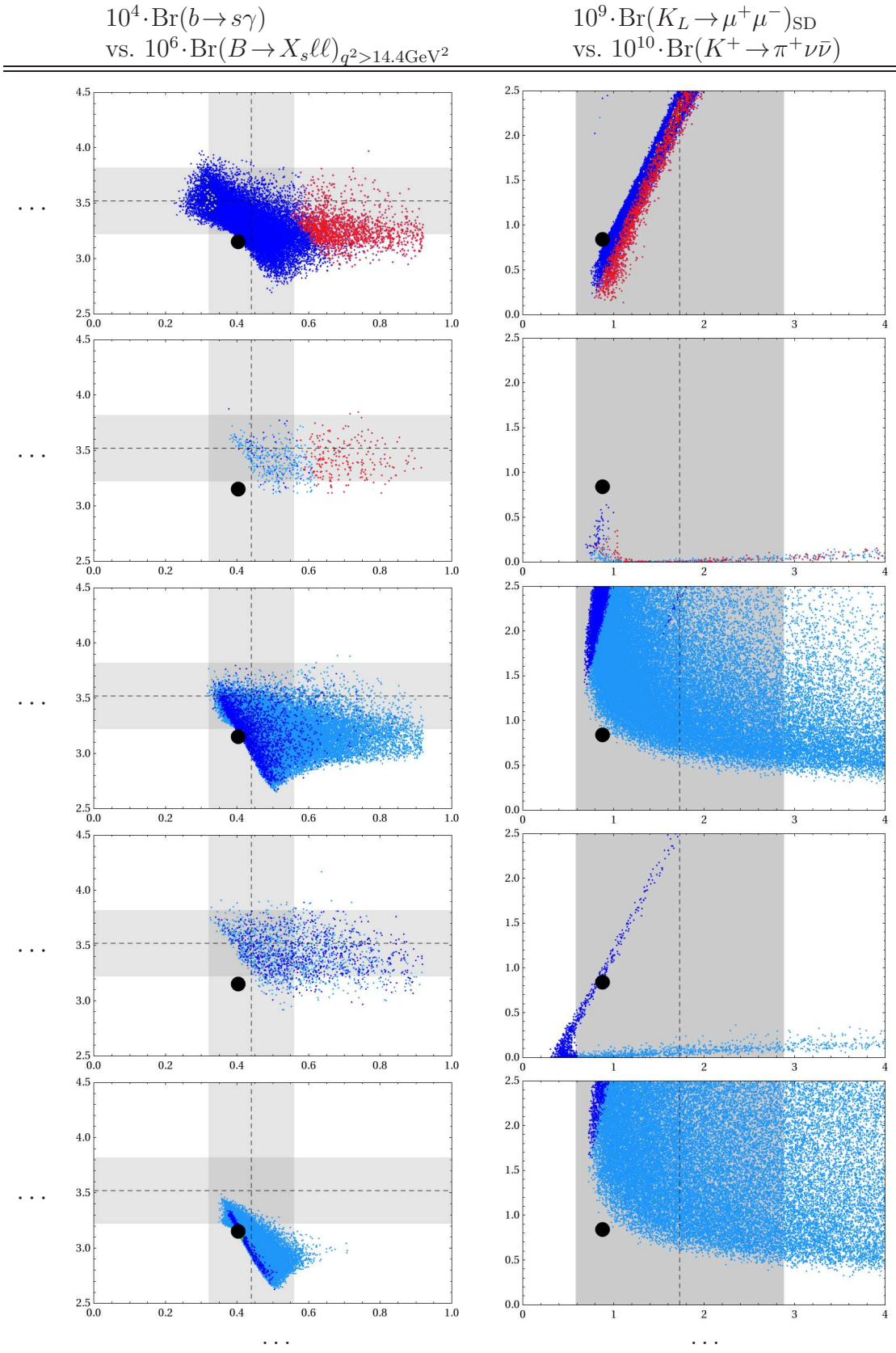

Table 5.8.: Selected correlations for classes identified in Table 5.6 (part 2 of 4).

Class	$10^8 \cdot \mathrm{Br}(B_s \to \mu^+\mu^-)$ vs. $S_{\psi\phi}$	$S_{\phi K_S}$ vs. $S_{\psi\phi}$	
	...	...	
3b:	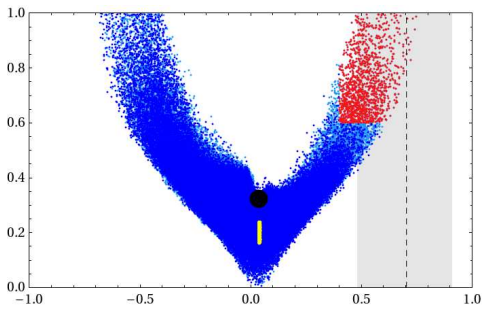	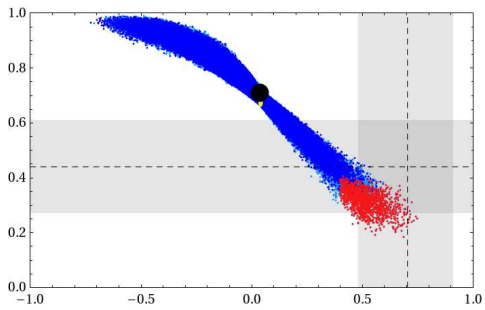	...
4:	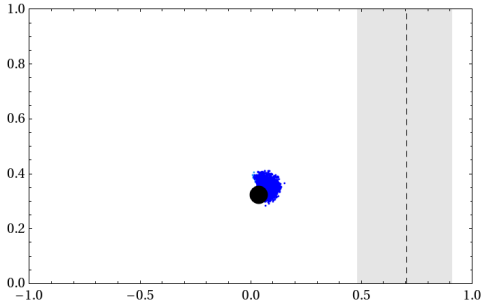	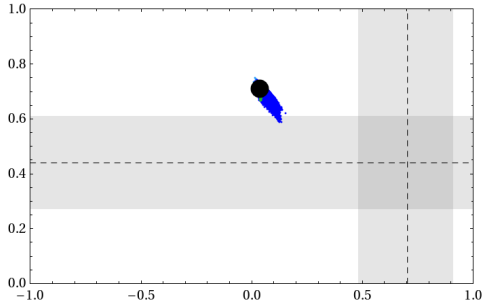	...
5:	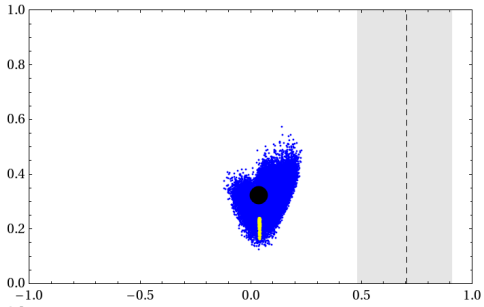	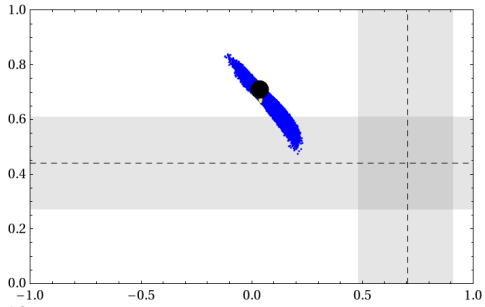	...
6:	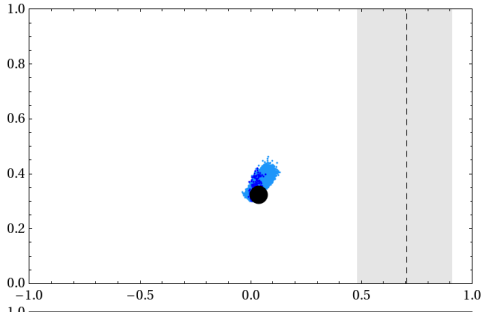	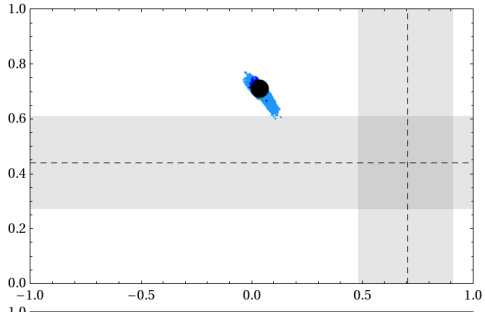	...
7:	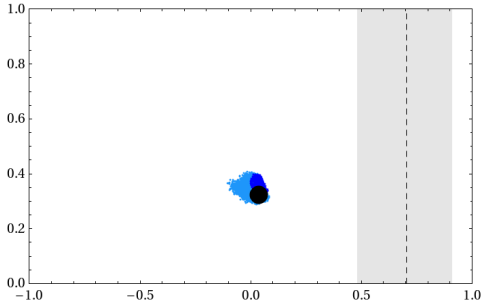	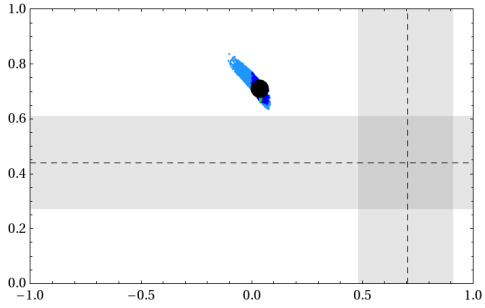	

Table 5.9.: Selected correlations for classes identified in Table 5.6 (part 3 of 4).

$10^4 \cdot \mathrm{Br}(b \to s\gamma)$ vs. $10^6 \cdot \mathrm{Br}(B \to X_s \ell\ell)_{q^2>14.4\mathrm{GeV}^2}$	$10^9 \cdot \mathrm{Br}(K_L \to \mu^+\mu^-)_{\mathrm{SD}}$ vs. $10^{10} \cdot \mathrm{Br}(K^+ \to \pi^+\nu\bar{\nu})$	Class
...	...	
...	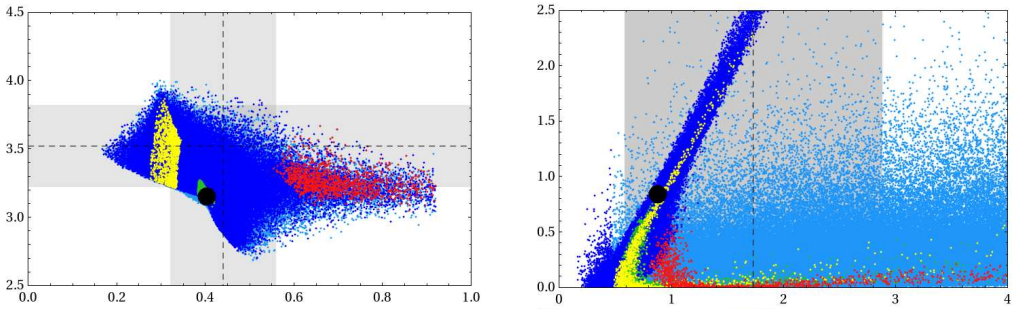	3b
...	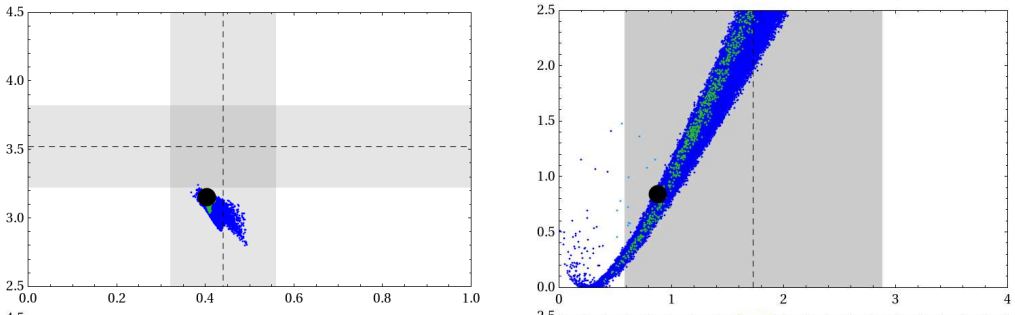	4
...	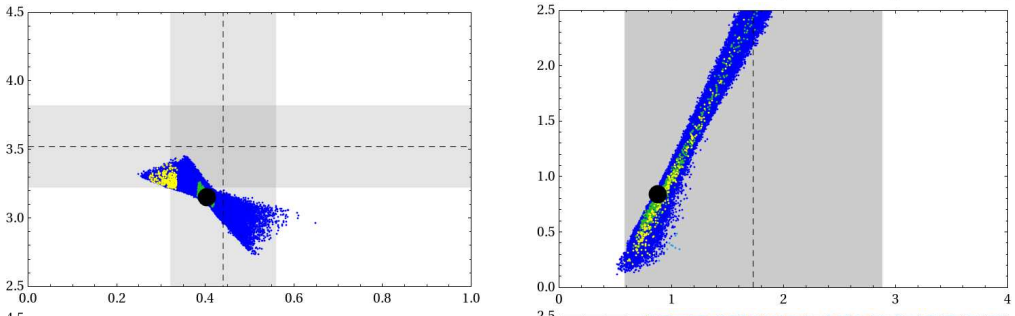	5
...	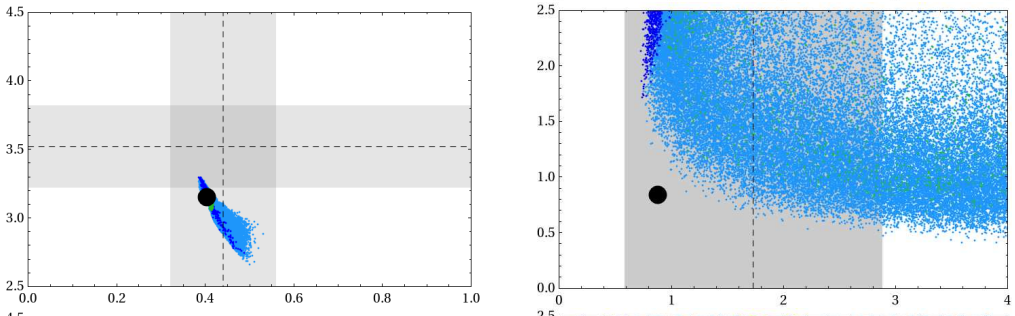	6
...	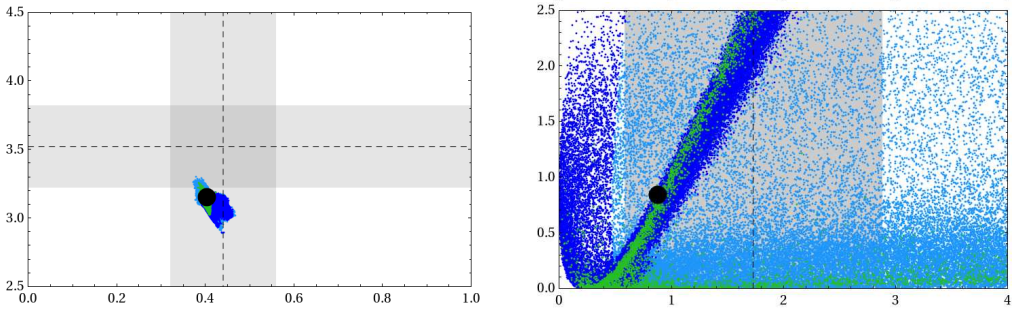	7

Table 5.10.: Selected correlations for classes identified in Table 5.6 (part 4 of 4).

5.4. Numerical Analysis of the Lepton Sector

5.4.1. Preliminaries

The analysis of LFV within the SM4 is rather simple due to the small number of free parameters as compared to other NP scenarios such as the general MSSM, the LHT and RS models. This also holds in comparison with the quark sector since the contributions of SM3 leptons in loops can be neglected, except when they are relevant in the context of the GIM mechanism.

Specifically, the processes $\ell_i \to \ell_j \gamma$ and the decays to three leptons are fully governed by the quantities

$$\lambda_{\nu_4}^{(\mu e)}\,, \qquad \lambda_{\nu_4}^{(\tau e)}\,, \qquad \lambda_{\nu_4}^{(\tau \mu)}\,, \qquad \lambda_{\nu_4}^{(ee)} = |U_{e\nu_4}|^2\,, \qquad \lambda_{\nu_4}^{(\mu\mu)} = |U_{\mu\nu_4}|^2\,, \tag{5.22}$$

and calculable functions of the neutrino mass m_{ν_4} which is bounded by direct measurements to $m_{\nu_4} \geq 90.3$ GeV (2.7). Therefore, strong correlations between the $\ell_i \to \ell_j \gamma$ and $\ell_i \to 3\ell_k$ decays are to be expected. While this expectation will be confirmed in the course of our numerical analysis, we will see that the possible ranges for various observables entering these correlations will still be rather large.

Semi-leptonic decays and $\mu - e$ conversion in nuclei involve also parameters in the quark sector that enter through box diagram contributions to the functions $\bar{X}^f$ and $\bar{Y}^f$ in (4.4). For the numerical analysis of these processes we used the points of our analysis in the quark sector (Sec. 5.1).

Our parameter points were generated using uniform random numbers, and we explicitly do not assign any statistical meaning to the point densities. We included the effect of a modified Fermi constant G_F due to the breaking of three-generation lepton-universality [209] and included the decays $\tau \to \mu\nu_\mu\nu_\tau$ and $\tau \to e\nu_e\nu_\tau$ to constrain the parameters. Contrary to [209] we do not find a significant effect of the $K_{3\ell}$ decays, but this is due to our much more conservative error treatment.

5.4.2. $\mu^- \to e^-\gamma$, $\mu^- \to e^-e^+e^-$ and $\mu - e$ Conversion

As pointed out by [209], the combination of results from leptonic τ decays and radiative μ decays efficiently constrains the involved PMNS parameters $|U_{e4}|$ and $|U_{\mu 4}|$. We show these bounds in Fig. 5.24, adding the constraint from $\mu - e$ conversion which turns out to be the most stringent one.

In Fig. 5.25 we show the correlation between $\mu \to e\gamma$ and $\mu^- \to e^-e^+e^-$ together with the experimental bounds on these decays. We observe:

- Both branching ratios can easily reach the present experimental bounds in a correlated manner.

- However, for a fixed value of either branching ratio, the respective other can still vary over one order of magnitude.

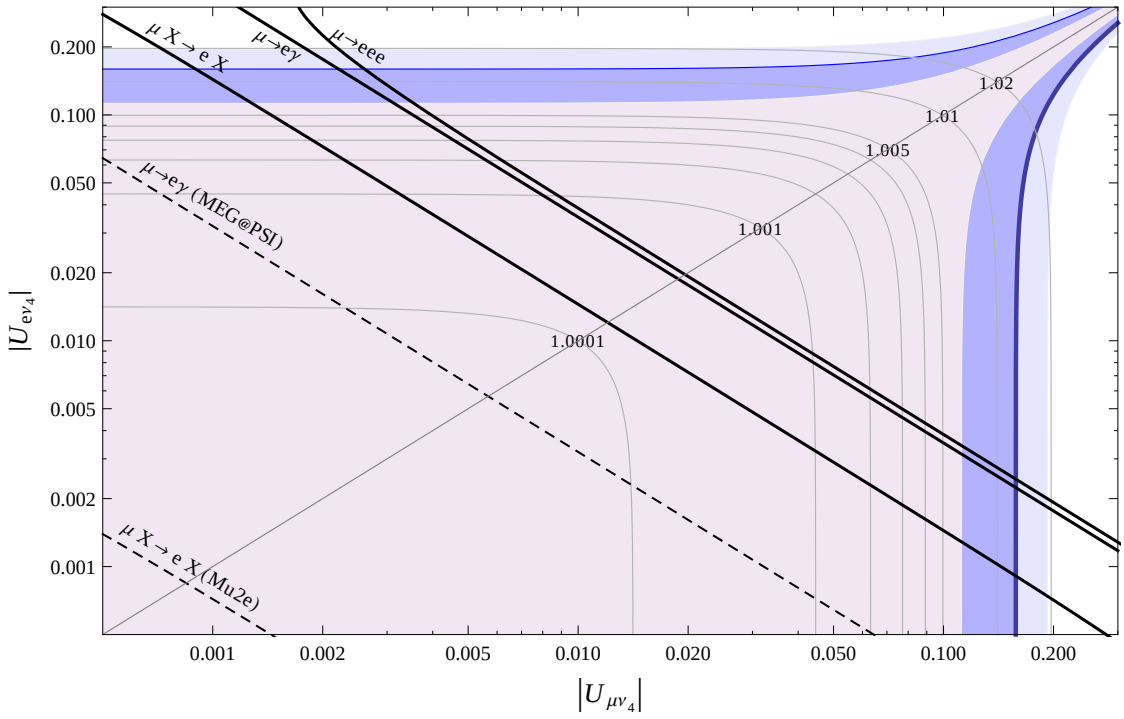

Figure 5.24.: Constraints on the allowed range of $|U_{e4}|$ and $|U_{\mu 4}|$ resulting from lepton universality (1σ/ $2\sigma/3\sigma$: purple/blue/light blue area, respectively) and the current experimental bounds on $\mu \to eee$, $\mu \to e\gamma$, and $\mu - e$ conversion (thick black lines). The contour lines indicate the ratio G_F^{SM4}/G_F^{SM3}, where G_F^{SM4} is the value of the Fermi constant extracted from muon lifetime measurement assuming 4 generations, and G_F^{SM3} is the usual SM3 Fermi constant (s. [209]).

Next, in Fig. 5.26 we show the correlation between the $\mu - e$ conversion rate in $^{48}_{22}$Ti and $\mathrm{Br}(\mu \to e\gamma)$, after imposing the existing constraints on $\mathrm{Br}(\mu \to e\gamma)$ and $\mathrm{Br}(\mu^- \to e^-e^+e^-)$. We observe that this correlation is weaker than the one in Fig. 5.25 as now also quark parameters enter the game. Still, for a given $\mathrm{Br}(\mu \to e\gamma)$ a sharp upper bound on the $\mu \to e$ conversion rate is identified. Furthermore, we find that the $\mu - e$ conversion rate in titanium is generally larger than the current experimental bound, but the bounds on both branching ratios can be simultaneously satisfied. Yet it is evident from this plot that lowering the upper bounds on both observables in the future will significantly reduce the allowed regions of the leptonic parameter space in the SM4.

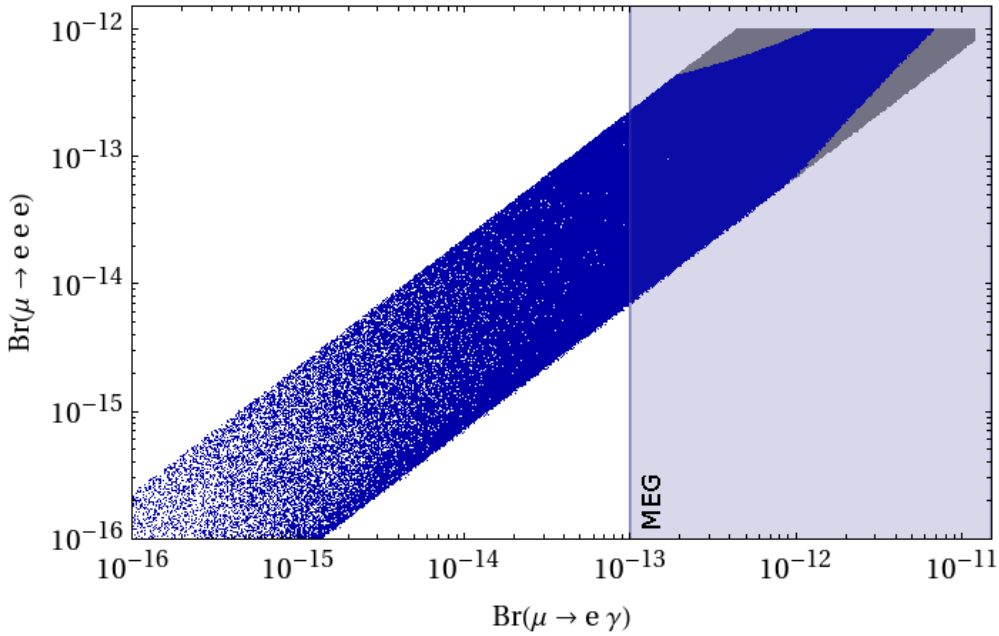

Figure 5.25.: Correlation between $\mathrm{Br}(\mu \to e\gamma)$ and $\mathrm{Br}(\mu^- \to e^-e^+e^-)$. Points that agree with the currently measured $\mu - e$ conversion rate in $^{48}_{22}$Ti (4.171) are shown in blue, while gray points violate this bound. The shaded area indicates the projected experimental bound on $\mathrm{Br}(\mu \to e\gamma)$ from the MEG experiment at PSI.

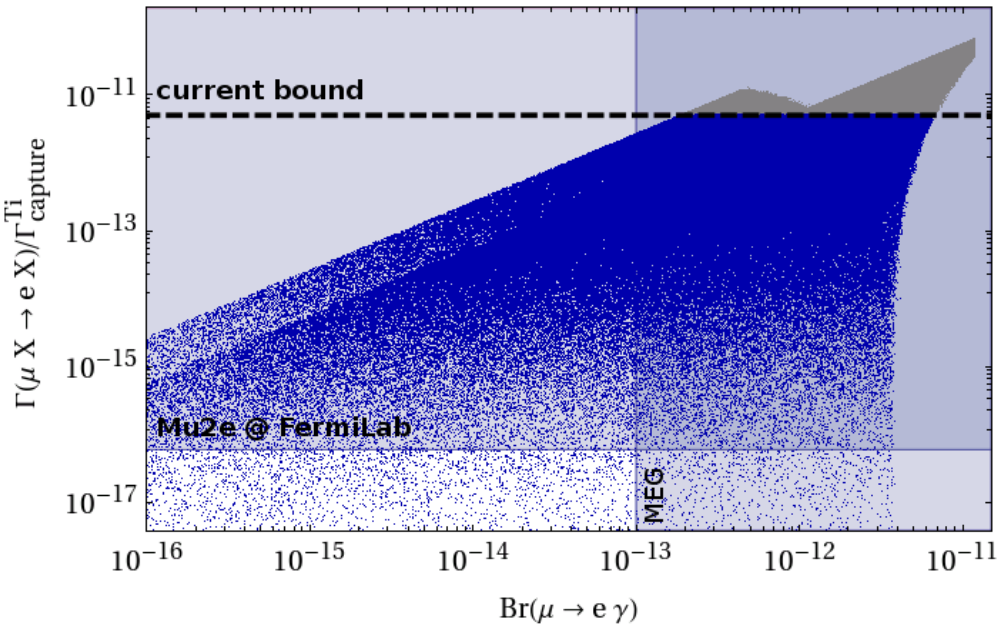

Figure 5.26.: Correlation between $\mathrm{Br}(\mu \to e\gamma)$ and $\mathrm{R}(\mu\mathrm{Ti} \to e\mathrm{Ti})$. The shaded areas indicate the expected future experimental bounds on both observables.

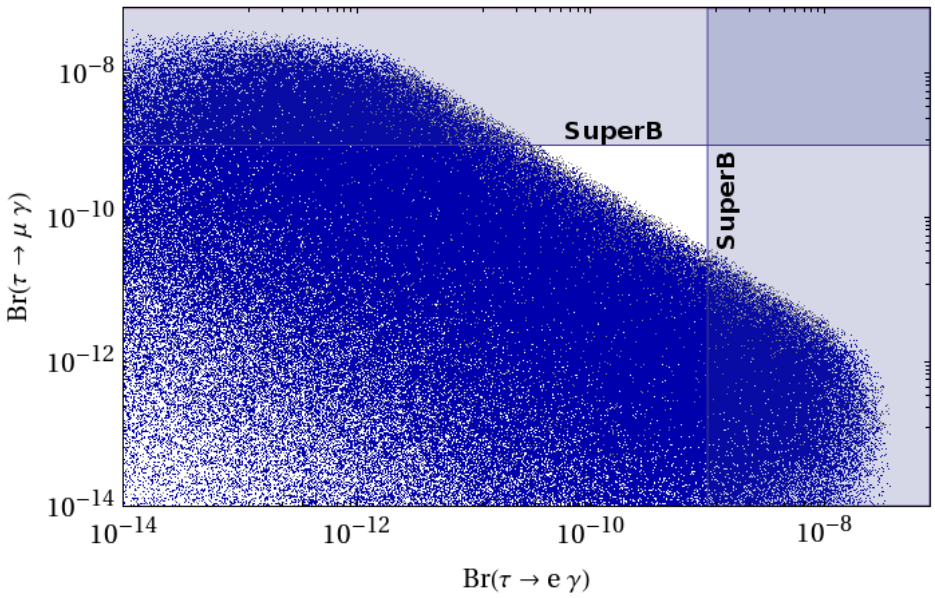

Figure 5.27.: Correlation between $\mathrm{Br}(\tau \to \mu\gamma)$ and $\mathrm{Br}(\tau \to e\gamma)$.

5.4.3. The Decays $\tau \to \mu\gamma$ and $\tau \to e\gamma$

In Fig. 5.27 we show the correlation between $\mathrm{Br}(\tau \to \mu\gamma)$ and $\mathrm{Br}(\tau \to e\gamma)$, imposing the experimental bounds on $\mu \to e\gamma$ and $\mu^- \to e^-e^+e^-$. We observe that they both can be individually as high as few times 10^{-8} and thus in the ball park of present experimental upper bounds. The maximal values however cannot be reached simultaneously, due to the $\mu \to e\gamma$ constraint. Thus finding both branching ratios at the $10^{-8} - 10^{-9}$ level will basically eliminate the SM4 scenario.

5.4.4. The Semi-Leptonic τ Decays $\tau \to (\mu\pi,\, \mu\eta,\, \mu\eta')$ and $\tau \to \mu\gamma$

In Fig. 5.28 we show $\mathrm{Br}(\tau \to \mu\pi)$ a function of $\mathrm{Br}(\tau \to \mu\gamma)$, imposing the constraints from $\mu \to e\gamma$ and $\mu^- \to e^-e^+e^-$. We find that $\mathrm{Br}(\tau \to \mu\pi)$ can reach values as high as the present experimental bounds from Belle and BaBar, which is in the ball park of 10^{-8}. It is evident from (4.150) and (4.155) that $\mathrm{Br}(\tau \to \mu\eta')$ and $\mathrm{Br}(\tau \to \mu\eta)$ are strongly correlated with $\mathrm{Br}(\tau \to \mu\pi)$, so we choose not to show the respective plots for these processes.

Completely analogous correlations can be found also for the corresponding decays $\tau \to e\pi, e\eta, e\eta'$ and $\tau \to e\gamma$. Indeed, this symmetry between the $\tau \to \mu$ and $\tau \to e$ systems turns out to be a general feature of the SM4, that can be found in all decays considered in the present work. We will return to this issue in Section 5.4.7.

An immediate consequence of these correlations is that the observation of a large $\tau \to \mu\gamma$ rate will immediately imply a large $\tau \to \mu\pi$ rate and vice versa. Still, for a fixed value of either branching ratio the second one can vary by almost an order of magnitude. Analogous statements apply to $\tau \to \mu(e)\eta$ and $\tau \to \mu(e)\eta'$.

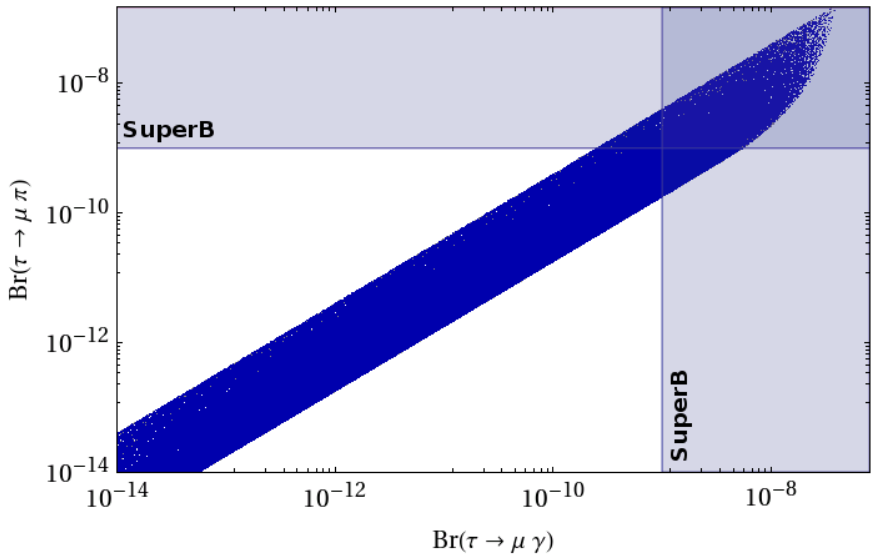

Figure 5.28.: Br($\tau \to \mu\pi$) as a function of Br($\tau \to \mu\gamma$)

5.4.5. $K_L \to \mu e$ and $K_L \to \pi^0 \mu e$

In Figs. 5.29 and 5.30 we show the results for Br($K_L \to \mu e$) and Br($K_L \to \pi^0 \mu e$) as functions of Br($\mu \to e\gamma$). Again strong correlations between these branching ratios are observed but the maximal values for Br($K_L \to \mu e$) and Br($K_L \to \pi^0 \mu e$) are by several orders of magnitude below the present experimental bounds.

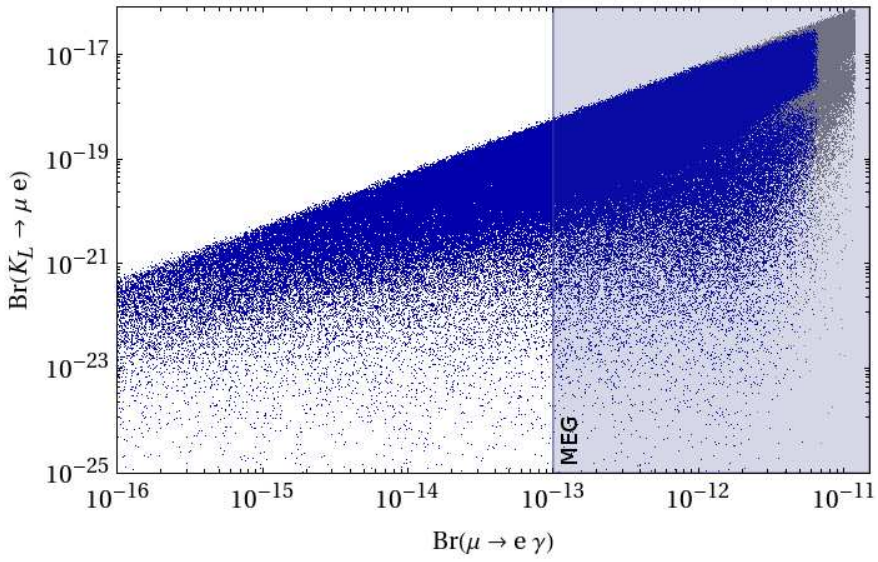

Figure 5.29.: Br($K_L \to \mu e$) as a function of Br($\mu \to e\gamma$). Colour coding defined in Fig. 5.25.

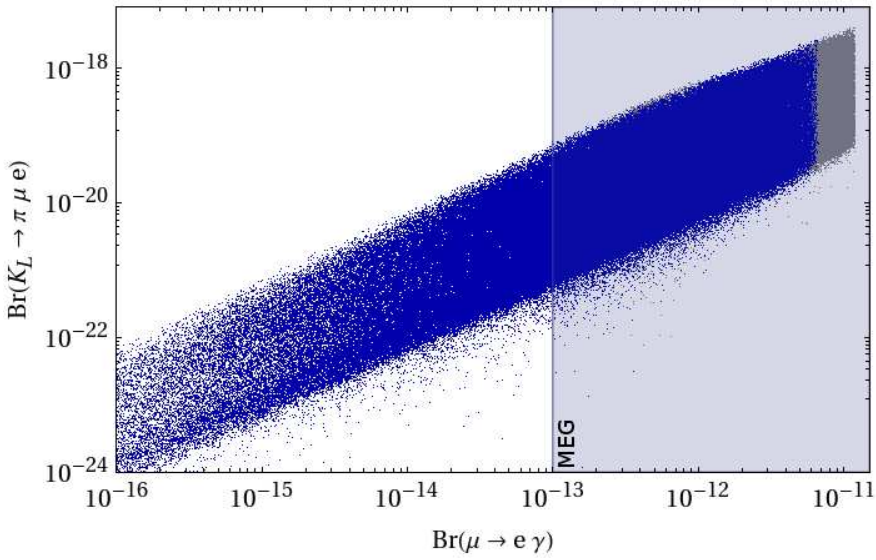

Figure 5.30.: $\mathrm{Br}(K_L \to \pi^0 \mu e)$ as a function of $\mathrm{Br}(\mu \to e\gamma)$. Colour coding defined in Fig. 5.25.

5.4.6. Upper Bounds

In Table 5.11 we show the maximal values obtainable in the SM4 for all branching ratios considered in the present work, together with the corresponding experimental bounds. We observe:

- The branching ratios for eleven of decays in this table can still come close to the respective experimental bounds and as we have seen in the previous plots they are correlated with each other.
- The remaining branching ratios are by several orders of magnitude below the present experimental bounds and if the SM4 is the whole story, these decays will not be seen in the foreseeable future.
- Comparing to the results obtained in the LHT model for a NP scale $f = 1\,\mathrm{TeV}$ [72,210], the SM4 allows for much larger branching ratios but the difference is much smaller for $f = 500\mathrm{GeV}$.

We have also investigated the effect of additionally imposing $\mathrm{R}(\mu\mathrm{Ti} \to e\mathrm{Ti}) < 5 \cdot 10^{-12}$ as a constraint, which we have chosen slightly above the experimental value $4.3 \cdot 10^{-12}$ in order to account for the involved theoretical uncertainties. We find that all maximal values collected in Table 5.11 depend only weakly on that constraint.

This finding justifies that we did not take into account this bound in our numerical analysis so far, as it has only a minor impact on the discussed observables. We would like to stress that the maximal values in Table 5.11 should only be considered as rough upper bounds. They have been obtained from scattering over the allowed parameter space of the model. In particular, no confidence level can be assigned to them. The same applies to the ranges given in Table 5.12 for the SM4 and the LHT model.

decay	maximal value	exp. upper bound
$\mu \to e\gamma$	$1.2 \cdot 10^{-11}$ $(6.8 \cdot 10^{-12})$	$1.2 \cdot 10^{-11}$ [260]
$\mu^- \to e^-e^+e^-$	$1.0 \cdot 10^{-12}$ $(1 \cdot 10^{-12})$	$1.0 \cdot 10^{-12}$ [261]
$\mathrm{R}(\mu\mathrm{Ti} \to e\mathrm{Ti})$	$6.6 \cdot 10^{-11}$ $(5 \cdot 10^{-12})$	$4.3 \cdot 10^{-12}$ [226]
$\tau \to e\gamma$	$3.9 \cdot 10^{-8}$ $(3.9 \cdot 10^{-8})$	$3.3 \cdot 10^{-8}$ [262]
$\tau \to \mu\gamma$	$3.9 \cdot 10^{-8}$ $(3.9 \cdot 10^{-8})$	$4.4 \cdot 10^{-8}$ [262]
$\tau^- \to e^-e^+e^-$	$7.5 \cdot 10^{-8}$ $(7.5 \cdot 10^{-8})$	$2.7 \cdot 10^{-8}$ [263]
$\tau^- \to \mu^-\mu^+\mu^-$	$7.4 \cdot 10^{-8}$ $(7.1 \cdot 10^{-8})$	$2.1 \cdot 10^{-8}$ [263]
$\tau^- \to e^-\mu^+\mu^-$	$5 \cdot 10^{-8}$ $(5 \cdot 10^{-8})$	$2.7 \cdot 10^{-8}$ [263]
$\tau^- \to \mu^-e^+e^-$	$5 \cdot 10^{-8}$ $(5 \cdot 10^{-8})$	$1.8 \cdot 10^{-8}$ [263]
$\tau^- \to \mu^-e^+\mu^-$	$4.7 \cdot 10^{-17}$ $(4.7 \cdot 10^{-17})$	$1.7 \cdot 10^{-8}$ [263]
$\tau^- \to e^-\mu^+e^-$	$4.9 \cdot 10^{-17}$ $(4.9 \cdot 10^{-17})$	$1.5 \cdot 10^{-8}$ [263]
$\tau \to \mu\pi$	$1.4 \cdot 10^{-7}$ $(1.4 \cdot 10^{-7})$	$5.8 \cdot 10^{-8}$ [264]
$\tau \to \mu\eta$	$2.5 \cdot 10^{-8}$ $(2.5 \cdot 10^{-8})$	$5.1 \cdot 10^{-8}$ [264]
$\tau \to \mu\eta'$	$2.9 \cdot 10^{-10}$ $(2.9 \cdot 10^{-8})$	$5.3 \cdot 10^{-8}$ [264]
$K_L \to \mu e$	$7.7 \cdot 10^{-17}$ $(3.3 \cdot 10^{-17})$	$4.7 \cdot 10^{-12}$ [265]
$K_L \to \pi^0\mu e$	$3.5 \cdot 10^{-18}$ $(2.1 \cdot 10^{-18})$	$6.2 \cdot 10^{-9}$ [266]
$B_d \to \mu e$	$2.4 \cdot 10^{-18}$ $(1.3 \cdot 10^{-18})$	$9.2 \cdot 10^{-8}$ [197]
$B_s \to \mu e$	$7.2 \cdot 10^{-17}$ $(4.0 \cdot 10^{-17})$	$6.1 \cdot 10^{-6}$ [267]
$B_d \to \tau e$	$1.4 \cdot 10^{-11}$ $(1.4 \cdot 10^{-11})$	$2.8 \cdot 10^{-5}$ [197]
$B_s \to \tau e$	$5.4 \cdot 10^{-10}$ $(5.4 \cdot 10^{-10})$	—
$B_d \to \tau\mu$	$1.4 \cdot 10^{-11}$ $(1.4 \cdot 10^{-11})$	$2.2 \cdot 10^{-5}$ [197]
$B_s \to \tau\mu$	$5.4 \cdot 10^{-10}$ $(5.4 \cdot 10^{-10})$	—

Table 5.11.: Maximal values for LFV decay branching ratios in the SM4, after imposing the constraints on $\mathrm{Br}(\mu \to e\gamma)$ and $\mathrm{Br}(\mu^- \to e^-e^+e^-)$. The numbers given in brackets are obtained after imposing the additional constraint $\mathrm{R}(\mu\mathrm{Ti} \to e\mathrm{Ti}) < 5 \cdot 10^{-12}$. The current experimental upper bounds are also given.

5.4.7. Patterns of Correlation and Comparison with other Models

In [72, 210] a number of correlations have been identified that allow to distinguish the LHT model from the MSSM. These results are recalled in Table 5.12. In the last column of this table we also show the results obtained in the SM4. We observe:

- For most of the ratios considered here the values found in the SM4 are significantly larger than in the LHT and by one to two orders of magnitude larger than in the MSSM.
- In the case of $\mu \to e$ conversion the predictions of the SM4 and the LHT model are very uncertain but finding said ratio to be of order one would favor the SM4 and the LHT model over the MSSM.
- Similarly, in the case of several ratios considered in this table, finding them to be of order one will choose the SM4 as a clear winner in this competition.

ratio	LHT	MSSM (dipole)	MSSM (Higgs)	SM4
$\frac{\mathrm{Br}(\mu^-\to e^-e^+e^-)}{\mathrm{Br}(\mu\to e\gamma)}$	$0.02\ldots1$	$\sim 6\cdot10^{-3}$	$\sim 6\cdot10^{-3}$	$0.06\ldots2.2$
$\frac{\mathrm{Br}(\tau^-\to e^-e^+e^-)}{\mathrm{Br}(\tau\to e\gamma)}$	$0.04\ldots0.4$	$\sim 1\cdot10^{-2}$	$\sim 1\cdot10^{-2}$	$0.07\ldots2.2$
$\frac{\mathrm{Br}(\tau^-\to \mu^-\mu^+\mu^-)}{\mathrm{Br}(\tau\to \mu\gamma)}$	$0.04\ldots0.4$	$\sim 2\cdot10^{-3}$	$0.06\ldots0.1$	$0.06\ldots2.2$
$\frac{\mathrm{Br}(\tau^-\to e^-\mu^+\mu^-)}{\mathrm{Br}(\tau\to e\gamma)}$	$0.04\ldots0.3$	$\sim 2\cdot10^{-3}$	$0.02\ldots0.04$	$0.03\ldots1.3$
$\frac{\mathrm{Br}(\tau^-\to \mu^-e^+e^-)}{\mathrm{Br}(\tau\to \mu\gamma)}$	$0.04\ldots0.3$	$\sim 1\cdot10^{-2}$	$\sim 1\cdot10^{-2}$	$0.04\ldots1.4$
$\frac{\mathrm{Br}(\tau^-\to e^-e^+e^-)}{\mathrm{Br}(\tau^-\to e^-\mu^+\mu^-)}$	$0.8\ldots2$	~ 5	$0.3\ldots0.5$	$1.5\ldots2.3$
$\frac{\mathrm{Br}(\tau^-\to \mu^-\mu^+\mu^-)}{\mathrm{Br}(\tau^-\to \mu^-e^+e^-)}$	$0.7\ldots1.6$	~ 0.2	$5\ldots10$	$1.4\ldots1.7$
$\frac{\mathrm{R}(\mu\mathrm{Ti}\to e\mathrm{Ti})}{\mathrm{Br}(\mu\to e\gamma)}$	$10^{-3}\ldots10^{2}$	$\sim 5\cdot10^{-3}$	$0.08\ldots0.15$	$10^{-12}\ldots26$

Table 5.12.: Comparison of various ratios of branching ratios in the LHT model [72], the MSSM without [212, 268] and with significant Higgs contributions [269, 270] and the SM4 calculated here.

6. Summary and Conclusions

In the present work we have performed a detailed analysis of the SM4, including the effects of direct measurements, electroweak precision tests and CP violation as well as quark and lepton flavor violation.

Concerning electroweak precision tests, the importance of non-oblique effects has been shown, leading to a upper bound on the mixing angle $s_{34} \leq 0.24$ ($m_{t'} = 300$ GeV) which is even stronger for larger t' masses. It has also been shown that the ranges for the possible mass splittings allowed by oblique parameters are much larger than stated before [39]. Particularly interesting is the case of nonvanishing s_{34}, for which degenerate masses are within the realms of possibility.

In the quark sector, we have studied a large number of FCNC and CP violation observables within the SM4. The most interesting results of this analysis are the following:

- All existing tensions in the UT fits can be removed within the SM4.
- As seen in Fig. 5.14, the attempt to explain the $S_{\psi\phi}$ anomaly implies the suppression of the CP asymmetries $S_{\phi K_S}$ and $S_{\eta' K_S}$ in agreement with the data.
- The same anomaly implies a sizable enhancement of $\mathrm{Br}(B_s \to \mu^+\mu^-)$ over the SM3 prediction although this effect is much more modest than in SUSY models. Yet, branching ratios as high as $8 \cdot 10^{-9}$ are certainly possible in the SM4, which is beyond the possible values obtained by the LHT model and the RSc model.
- Possible enhancements of $\mathrm{Br}(K^+ \to \pi^+\nu\bar{\nu})$ and $\mathrm{Br}(K_L \to \pi^0\nu\bar{\nu})$ over the SM3 values are much larger than in any other of the above mentioned NP models. Both branching ratios can reach as high as several 10^{-10} in the SM4. Moreover, the two branching ratios are strongly correlated and close to the GN bound, as seen in Fig. 5.4.
- In contrast to the LHT and RSc models, a high value of $S_{\psi\phi}$ does not preclude a sizable enhancements of $\mathrm{Br}(K^+ \to \pi^+\nu\bar{\nu})$, and $\mathrm{Br}(K_L \to \pi^0\nu\bar{\nu})$.
- NP effects in $K_L \to \pi^0\ell^+\ell^-$ and $K_L \to \mu^+\mu^-$ can be visibly larger than in the LHT and RSc models. In particular $\mathrm{Br}(K_L \to \mu^+\mu^-)_{\mathrm{SD}}$ can easily violate the existing bound of $2.5 \cdot 10^{-9}$. Imposition of this bound on top of other constraints results in a characteristic shape of the correlation between $\mathrm{Br}(K^+ \to \pi^+\nu\bar{\nu})$ and $\mathrm{Br}(K_L \to \pi^0\nu\bar{\nu})$ shown in Fig. 5.4.
- The magnitude of the CP asymmetry $A_{\mathrm{CP}}^{bs\gamma}$ remains small, but the desire to explain large values of $S_{\psi\phi}$ reverses its sign.
- Even in the presence of SM-like values for $S_{\psi\phi}$ and $\mathrm{Br}(B_s \to \mu^+\mu^-)$, large effects in the K-system are possible as illustrated by green points in numerous plots.

- For large positive values of $S_{\psi\phi}$ the predicted value of ε'/ε is significantly below the data, unless the hadronic matrix elements of the electroweak penguins are sufficiently suppressed with respect to the large N result and the ones of QCD penguins enhanced.

- We have also reemphasized [188,189] the important role ε'/ε will play in bounding rare K decay branching ratios once the relevant hadronic matrix elements in ε'/ε will be precisely known (see Sec. 5.1.6 for more details).

Other 4G effects in various observables and correlations between them can be found in numerous plots in Section 5.1. In particular, in Section 5.3 we have addressed the question of determining the SM4 parameters with the help of future measurements, employing various scenarios for the scalings of the 4G mixing matrix angles θ_{14}, θ_{24} and θ_{34}.

In the lepton sector, we have calculated branching ratios for a large number of lepton flavor violating decays within the SM4, taking into account all presently available constraints. Our main messages from this analysis are the following:

- The branching ratios for $\ell_i \to \ell_j\gamma$, $\tau \to \ell\pi$, $\tau \to \ell\eta^{(\prime)}$, $\mu^- \to e^-e^+e^-$, $\tau^- \to e^-e^+e^-$, $\tau^- \to \mu^-\mu^+\mu^-$, $\tau^- \to e^-\mu^+\mu^-$ and $\tau^- \to \mu^-e^+e^-$ can all still be as large as the present experimental upper bounds, but not necessarily simultaneously.

- The correlations between various branching ratios should allow to test this model. This is in contrast to the SM3, where all these branching ratios are unmeasurable.

- The rate for $\mu - e$ conversion in nuclei can also reach the corresponding upper bound.

- The pattern of the LFV branching ratios in the SM4 differs significantly from the one encountered in the MSSM and LHT, allowing to distinguish these two models with the help of LFV processes in a transparent manner, as can be seen from Table 5.12.

- The branching ratios for $K_L \to \mu e$, $K_L \to \pi^0\mu e$, $B_{d,s} \to \mu e$, $B_{d,s} \to \tau e$ and $B_{d,s} \to \tau\mu$ turn out to be by several orders of magnitude smaller than the present experimental bounds.

In summary, the SM4 offers very rich patterns of (lepton) flavor violation which can be tested already in the coming years – particularly through precise measurements of $S_{\psi\phi}$, $\mathrm{Br}(B_q \to \mu^+\mu^-)$, $\mathrm{Br}(K^+ \to \pi^+\nu\bar{\nu})$ and, later, $S_{\phi K_s}$, $S_{\eta' K_s}$ and $\mathrm{Br}(K_L \to \pi^0\nu\bar{\nu})$. Furthermore, precise measurements of the phase $\gamma \approx \delta_{13}$ will be important for this investigation. We close our detailed analysis with the following important question: Can the SM4 be excluded by precise measurements of FCNC processes? The answer is positive, provided large departures from the SM3 are observed with a different pattern of deviation from the SM3 predictions than found in our analysis. Let us just list three examples:

- Large values of $S_{\psi\phi} > 0.6$ accompanied with SM-like values of $\mathrm{Br}(B_s \to \mu^+\mu^-)$ will clearly disfavor the SM4 as the explanation of the $S_{\psi\phi}$ anomaly.

- Similarly, such large values accompanied by the observation of $S_{\phi K_s} \approx S_{\eta' K_s} \approx S_{\psi K_s}$ would also put the SM4 into difficulties.

- Finally, $S_{\psi\phi} > 0.3$ accompanied by the ε'/ε relevant $R_6 \approx R_8 \approx 1$ from future lattice calculations will disfavor SM4 by means of the measured ε'/ε.

It is evident from our analysis that apart from direct measurements and electroweak precision tests, FCNC processes will contribute in a profound manner to the search for the 4G quarks and leptons and, in the case of direct discovery, to the exploration of the structure of their weak mixings. We hope that our work will serve as a guideline to the analysis of future data from LHC and high-intensity experiments, and finally help to firmly establish or exclude the presence of a fourth sequential generation in nature.

A. Effective FCNC Vertices

In this section, we will give the formulae for generic effective FCNC vertices in the full theory. Once these are known, it is a rather simple exercise to calculate the effective Hamiltonians necessary for the calculation of flavor observables in Section 4.2.

The vertices are all calculated in t'Hooft-Feynman gauge ($\xi = 1$) and with Feynman rules obtained from "$i\mathcal{L}$", so they have to be multiplied by i in order to obtain their contribution to the effective Hamiltonian. For reasons of clarity we do not show the diagrams involving fictitious Higgs $\tilde{H}^\pm$ exchanges, but of course these have to be taken into account wherever a $W^\pm$ boson occurs.

In order to keep the expressions as general as possible, we will denote incoming and outgoing fermions (quarks or leptons) by a, b and c, d respectively. Where it is necessary to further specify the type of fermions, we will denote up- and down-type quarks by $u_i \in \{u, c, t, t'\}$ and $d_i \in \{d, s, b, b'\}$, charged leptons and neutrinos by $\ell_i \in \{e, \mu, \tau, \tau'\}$ and $\nu_i \in \{\nu_1, \nu_2, \nu_3, \nu_4\}$) respectively. For any of these fermions f, the squared fermion to W mass ratio will be denoted by $x_f = \frac{m_f^2}{M_W^2}$.

Furthermore, we use the generalized CKM and PMNS factors defined in (2.18,2.47):

$$\lambda_{u_i}^{(d_a d_b)} \equiv V_{u_i d_a} V_{u_i d_b}^* \,, \qquad \text{(A.1a)} \qquad \lambda_{d_i}^{(u_a u_b)} \equiv V_{u_b d_i} V_{u_a d_i}^* \,, \qquad \text{(A.1b)}$$

$$\lambda_{\nu_i}^{(\ell_a \ell_b)} \equiv U_{\ell_b \nu_i} U_{\ell_a \nu_i}^* \,, \qquad \text{(A.1c)} \qquad \lambda_{\ell_i}^{(\nu_a \nu_b)} \equiv U_{\ell_i \nu_a} U_{\ell_i \nu_b}^* \,. \qquad \text{(A.1d)}$$

obeying the unitarity relation

$$\sum_{i=1}^{4} \lambda_i^{(ab)} = \delta^{ab} \,. \qquad \text{(A.2)}$$

Finally, the sine and cosine of the Weinberg angle are denoted by $s_W \equiv \sin\theta_W$ and $c_W \equiv \cos\theta_W$.

A.1. Generic Effective Vertices

A.1.1. Generic Box Vertex

Basic Vertex:

Box diagrams occur in both $\Delta F = 2$ and $\Delta F = 1$ FCNC processes. Basically, there are two different types of such diagrams, depending on the relative sign σ of the weak isospins T_3 of

the two fermion lines. For equal T_3, i.e. $\sigma = +1$, the vertex is

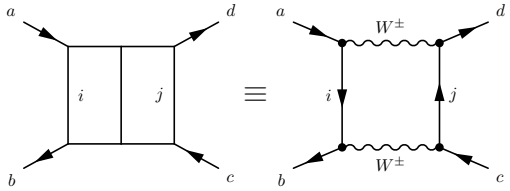

$$= -i\frac{G_F}{\sqrt{2}}\frac{\alpha}{2\pi s_W^2}\mathcal{S}\ \lambda_i^{(ab)}\lambda_j^{(cd)}\ B^{(+)}(x_i,x_j)\ \big(\bar{b}a\big)_{\mathrm{V-A}}\big(\bar{d}c\big)_{\mathrm{V-A}}\ , \tag{A.3}$$

while for different T_3, i.e. $\sigma = -1$

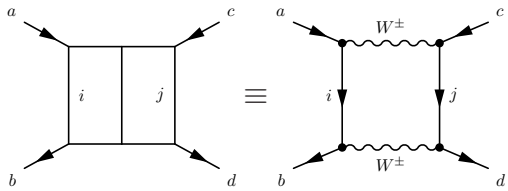

$$= -i\frac{G_F}{\sqrt{2}}\frac{\alpha}{2\pi s_W^2}\mathcal{S}\lambda_i^{(ab)}\lambda_j^{(cd)}\ B^{(-)}(x_i,x_j)\ \big(\bar{b}a\big)_{\mathrm{V-A}}\big(\bar{d}c\big)_{\mathrm{V-A}}\ , \tag{A.4}$$

where we introduced generalized box functions $B^{(\sigma)}$ defined by

$$B^{(+)}(x_i,x_j) = \frac{1}{4}\left[U(x_i,x_j) + \frac{x_i x_j}{4}U(x_i,x_j) - 2x_i x_j\tilde{U}(x_i,x_j)\right] = B^{\mu\bar{\mu}}(x_i,x_j)\,, \tag{A.5a}$$

$$B^{(-)}(x_i,x_j) = -\left[U(x_i,x_j) + \frac{x_i x_j}{16}U(x_i,x_j) + \frac{x_i x_j}{2}\tilde{U}(x_i,x_j)\right] = -4B^{\nu\bar{\nu}}(x_i,x_j)\,, \tag{A.5b}$$

with U and $\tilde{U}$ given in (B.3). For reasons of clarity, we have also shown the relations of $B^{(\sigma)}$ to the commonly used box functions $B^{\mu\bar{\mu}}$ and $B^{\nu\bar{\nu}}$ given in (B.1).

Summed Up Vertex in the SM4:

By summing over all loop fermions i, j, one obtains

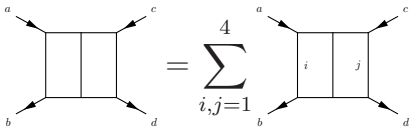

$$= -i\sum_{i,j=1}^{4}\frac{G_F}{\sqrt{2}}\frac{\alpha}{2\pi s_W^2}S\ \lambda_i^{(ab)}\lambda_j^{(cd)}\ B^{(\sigma)}(x_i,x_j)\ \big(\bar{b}a\big)_{\mathrm{V-A}}\big(\bar{d}c\big)_{\mathrm{V-A}}$$

$$\overset{\text{GIM}}{=} -i\frac{G_F}{\sqrt{2}}\frac{\alpha}{2\pi s_W^2}S\ \sum_{i=2}^{4}\lambda_i^{(ab)}\left(\delta^{cd}B_0^{(\sigma)}(x_i) + \sum_{j=2}^{4}\lambda_j^{(cd)}F^{(\sigma)}(x_i,x_j)\right)\ \times$$

$$\big(\bar{b}a\big)_{\mathrm{V-A}}\big(\bar{d}c\big)_{\mathrm{V-A}} \tag{A.6}$$

In the last step we have performed the GIM mechanism: Utilizing the unitarity of the 4×4 CKM/PMNS matrix (2.19), one can drop the $i=1$ contribution ($m_u, m_d, m_e, m_{\nu_1} \approx 0$) in the two sums and obtains the two loop functions $B_0^{(\sigma)}(x)$ and $F^{(\sigma)}(x_i, x_j)$

$$B_0^{(\sigma)}(x_i) = B^{(\sigma)}(x_i, 0) - B^{(\sigma)}(0,0) \tag{A.7a}$$

$$F^{(\sigma)}(x_i, x_j) = B^{(\sigma)}(x_i, x_j) - B^{(\sigma)}(x_i, 0) - B^{(\sigma)}(0, x_j) + B^{(\sigma)}(0,0) \tag{A.7b}$$

which are related to the loop functions $B_0(x_i)$, $F^{\mu\bar{\mu}}(x_i, x_j)$, $F^{\nu\bar{\nu}}(x_i, x_j)$ and $S_0(x_i, x_j)$ used for example in [67–69]

$$B_0^{(+)}(x_i) = -\frac{1}{4} B_0^{(-)}(x_i) = B_0(x_i) \tag{A.8a}$$

$$F^{(+)}(x_i, x_j) = -F^{\mu\bar{\mu}}(x_i, x_j) = \frac{1}{4} S_0(x_i, x_j) \tag{A.8b}$$

$$F^{(-)}(x_i, x_j) = 4F^{\nu\bar{\nu}}(x_i, x_j) \tag{A.8c}$$

A.1.2. Generic Z^0 Penguin Vertex

Basic Vertex:

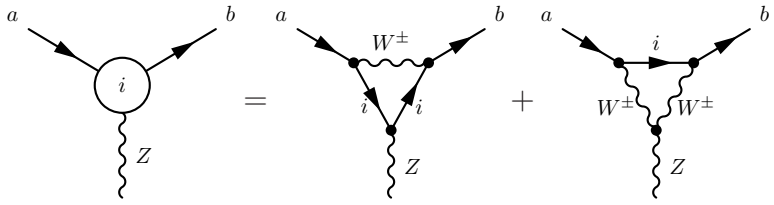

$$= +i\frac{G_F}{\sqrt{2}}\frac{e}{2\pi^2} M_Z^2 \frac{c_W}{s_W} \lambda_i^{(ab)} 2C_0(x_i) \left(\bar{b}\gamma_\mu(1-\gamma_5)a\right) , \tag{A.9}$$

with the loop function

$$C_0(x) = \frac{x}{8}\left[\frac{x-6}{x-1} + \frac{3x+2}{(x-1)^2}\log x\right] , \tag{A.10}$$

where we have dropped an (infinite) constant $c = -\frac{1}{\bar{\epsilon}}$ ($\overline{\text{MS}}$ scheme), which cancels due to the GIM mechanism.

Four-Fermion Vertex involving the Z^0-Penguin:

From (A.9) and the Feynman rules for Z^0-fermion-coupling follows

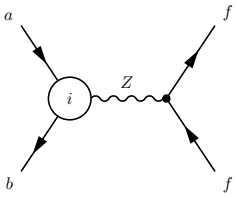

$$= -i\frac{G_F}{\sqrt{2}}\frac{\alpha}{2\pi s_W^2}\lambda_i^{(ab)} C_0(x_i) \times$$

$$\left(\bar{b}a\right)_{\mathrm{V-A}} \otimes \left[\left(\bar{f}f\right)_{\mathrm{V-A}} (T_3^f - Q_f s_W^2) - \left(\bar{f}f\right)_{\mathrm{V+A}} Q_f s_W^2\right], \quad \text{(A.11)}$$

(A.12)

where Q_f and T_3^f are the charge and weak isospin of the coupled fermion f, respectively.

A.1.3. Generic Photon Penguin Vertex

A.1.3.1. Off-Shell γ Penguin

Basic Vertex:

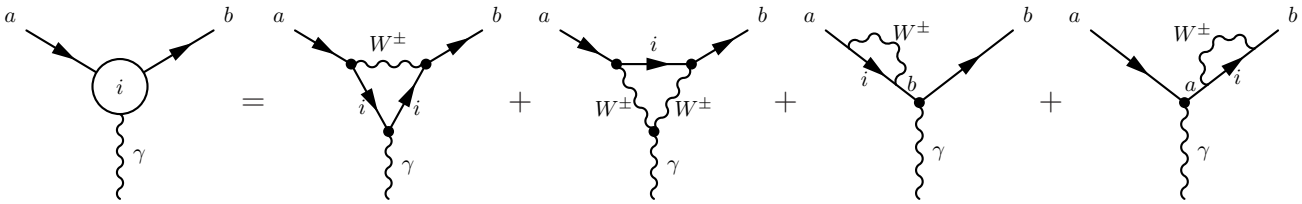

$$= -i\frac{G_F}{\sqrt{2}}\frac{e}{8\pi^2}\lambda_i^{(ab)} D^{(i)}(x_i)\; \bar{b}(q^2\gamma_\mu - q_\mu \not{q})(1-\gamma_5)a\,, \quad \text{(A.13)}$$

with the general off-shell γ penguin function

$$D^{(i)}(x) = Q_i\left(\frac{x\,(x^2+11x-18)}{12(x-1)^3} - \frac{(9x^2-16x+4)\log x}{6(x-1)^4}\right)$$
$$+ \frac{(-7x^2+x+12)\,x}{12(x-1)^3} - \frac{(x^2-10x+12)\,x^2\log x}{6(x-1)^4}\,. \quad \text{(A.14)}$$

For the different possible types fermions running in the loop, the function $D^{(i)}(x)$ becomes

$$D^{(i)}(x) = D_0(x) \qquad \text{for up-type quarks: } i \in \{u,c,t,t'\}\,, \quad \text{(A.15a)}$$

$$D^{(i)}(x) = H_0(x) \qquad \text{for neutrinos: } i \in \{\nu_1,\nu_2,\nu_3,\nu_4\}\,, \quad \text{(A.15b)}$$

where the SM functions on the right hand side are given in (B.4).

Four-Fermion Vertex Involving the Off-Shell γ-Penguin:

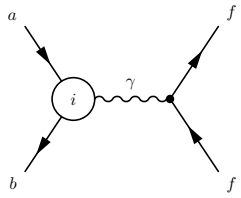

$$= + i\frac{G_F}{\sqrt{2}}\frac{\alpha}{2\pi}\ \lambda_i^{(ab)}\ D^{(i)}(x_i)\ Q_f\ \big(\bar{b}a\big)_{\mathrm{V-A}}\big(\bar{f}f\big)_{\mathrm{V}}\ , \tag{A.16}$$

A.1.3.2. On-Shell γ Penguin

Basic Vertex:

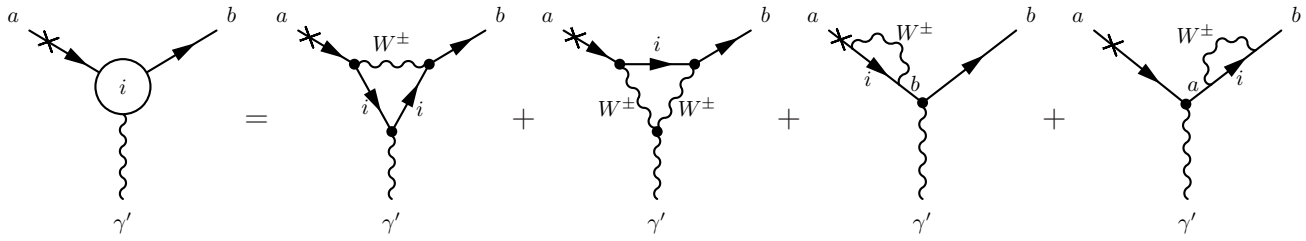

$$= +i\frac{G_F}{\sqrt{2}}\frac{e}{8\pi^2}\lambda_i^{(ab)}D'^{(i)}(x_i)\ \bar{b}(i\sigma_{\mu_\lambda}q^\lambda m_a(1+\gamma_5))a\,, \tag{A.17}$$

with the general on-shell γ penguin function

$$D'^{(i)}(x) = Q_i\left(\frac{(x^2-5x-2)\,x}{4(x-1)^3}+\frac{3x^2\log x}{2(x-1)^4}\right)+\frac{(2x^2+5x-1)\,x}{4(x-1)^3}-\frac{3x^3\log x}{2(x-1)^4}\,. \tag{A.18}$$

For the different possible types of loop fermions i, the function $D'^{(i)}$ becomes

$$D'^{(i)}(x) = D'_0(x) \qquad \text{for up-type quarks: } i\in\{u,c,t,t'\}\,,$$
$$D'^{(i)}(x) = H'_0(x) \qquad \text{for neutrinos: } i\in\{\nu_1,\nu_2,\nu_3,\nu_4\}\,,$$

where the SM functions on the right hand side are given in (B.4).

Four-Fermion Vertex Involving the On-Shell γ-Penguin:

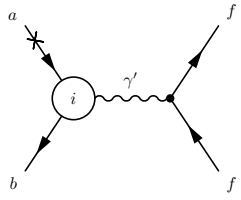

$$= -\,i\frac{G_F}{\sqrt{2}}\frac{\alpha}{2\pi}\ \lambda_i^{(ab)}\ D'^{(i)}(x_i)\ Q_f\frac{1}{q^2}\ \big(\bar{b}\,i\sigma_{\mu_\lambda}q^\lambda m_a(1+\gamma_5)\,a\big)\big(\bar{f}f\big)_{\mathrm{V}}\ , \tag{A.19}$$

(A.20)

A.1.4. Generic Gluon Penguin Vertex

Basic Vertex:

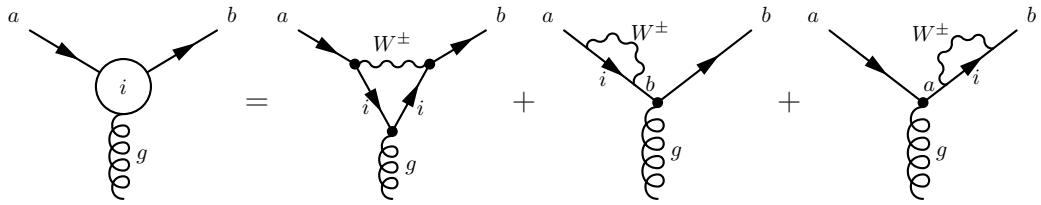

$$= -i\frac{G_F}{\sqrt{2}}\frac{e}{8\pi^2}\lambda_i^{(ab)} E_0(x_i)\ \bar{b}(q^2\gamma_\mu - q_\mu \not{q})(1-\gamma_5)a\,, \tag{A.21}$$

with the off-shell gluon penguin function $E_0(x)$ given in (B.4).

A.2. Wilson Coefficients and Gauge-Independent Loop Functions

In the following, we will give the Wilson coefficients for selected operators in the SM4. By comparison with the SM3 results, we are able to identify the corresponding gauge independent loop functions. The results of these calculations are used in Section 4.1.2.1.

A.2.1. Wilson Coefficients for $\Delta F = 2$ Four Fermion Operators

The general $\Delta F = 2$ [1] process $a\bar{b} \to \bar{a}b$ is governed by the effective Hamiltonian

$$\mathcal{H}_{\text{eff}}^{\Delta F=2} = i$$

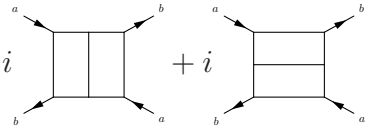

$$= \frac{G_F}{\sqrt{2}}\frac{\alpha}{2\pi s_W^2} C^{(\Delta F=2)} \mathcal{Q}^{(\Delta F=2)}\,, \tag{A.22}$$

with

$$\mathcal{Q}^{(\Delta F=2)} = (\bar{b}a)_{\text{V}-\text{A}}(\bar{b}a)_{\text{V}-\text{A}}\,. \tag{A.23}$$

The Wilson coefficient can easily be calculated from the value of the box diagram given in (A.6),

$$C^{(\Delta F=2)} = \frac{1}{2}\sum_{i,j=2}^{4} \lambda_i^{(ab)}\lambda_j^{(ab)} F^{(+)}(x_i, x_j)\,, \tag{A.24}$$

with the loop function $F^{(+)}$ given in (B.1c).

[1] here F can denote both quark- and lepton flavor

A.2.2. Wilson Coefficients for $\Delta F = 1$ Four Fermion Operators

For the general $\Delta F = 1$ process $a\bar{b} \to f\bar{f}$ ($f \neq a, b$), the relevant effective Hamiltonian reads

$$\mathcal{H}_{\text{eff}}^{\Delta F=1} = i$$ 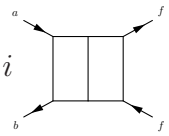 $$+ i$$ 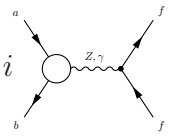

$$= \frac{G_F}{\sqrt{2}} \frac{\alpha}{2\pi s_W^2} \left[C_9^{(a\bar{b}\to f\bar{f})} \mathcal{Q}_9^{(a\bar{b}\to f\bar{f})} + C_{10}^{(a\bar{b}\to f\bar{f})} \mathcal{Q}_{10}^{(a\bar{b}\to f\bar{f})} \right] , \tag{A.25}$$

with

$$\mathcal{Q}_9^{(a\bar{b}\to f\bar{f})} = (\bar{b}a)_{\text{V}-\text{A}} (\bar{f}f)_{\text{V}} , \qquad \mathcal{Q}_{10}^{(a\bar{b}\to f\bar{f})} = (\bar{b}a)_{\text{V}-\text{A}} (\bar{f}f)_{\text{A}} . \tag{A.26}$$

The Wilson coefficients can then be calculated from (A.6,A.11,A.16):

$$C_9^{(a\bar{b}\to f\bar{f})} = \sum_{i=2}^{4} \lambda_i^{(ab)} \left(X_f^{(\sigma)}(x_i) - 4 Q_f s_W^2 \bar{Z}^{(i)}(x_i) \right) , \tag{A.27}$$

$$C_{10}^{(a\bar{b}\to f\bar{f})} = - \sum_{i=2}^{4} \lambda_i^{(ab)} X_f^{(\sigma)}(x_i) , \tag{A.28}$$

where the generalized gauge independent loop functions

$$X_f^{(\sigma)}(x_i) = 2T_3^f C_0(x_i) + B_0^{(\sigma)}(x_i) + \sum_{j=2}^{4} \lambda_j^{(ff)} F^{(\sigma)}(x_i, x_j) , \tag{A.29}$$

$$\bar{Z}^{(i)}(x_i) = C_0(x_i) + \frac{1}{4} D^{(i)}(x_i) , \tag{A.30}$$

have been introduced. In order to see the connection of $X^{(\sigma)}$ to the SM loop functions X_0 and Y_0 more clearly, we shall define yet another set of gauge independent loop functions

$$\bar{X}^f(x_i) \equiv X_f^{(-)}(x_i) = X_0(x_i) + \sum_{j=2}^{4} \lambda_j^{(ff)} F^{(-)}(x_i, x_j) , \tag{A.31}$$

$$\bar{Y}^f(x_i) \equiv -X_f^{(+)}(x_i) = Y_0(x_i) - \sum_{j=2}^{4} \lambda_j^{(ff)} F^{(+)}(x_i, x_j) . \tag{A.32}$$

In the case of vanishing mixing to the fourth generation, $\bar{X}^f$ and $\bar{Y}^f$ reduce to $X_0 \equiv C_0 - 4B_0$ and $Y_0 \equiv C_0 - B_0$, respectively, and therefore reproduce the SM results.

B. Reference: Loop Functions

For reasons of clarity, we shall summarize all loop functions used throughout this work:

Box Functions

$$S_0(x,y) = xy\left(\frac{(4-8y+y^2)\log y}{4(y-1)^2(y-x)} + (x \leftrightarrow y) - \frac{3}{4(x-1)(y-1)}\right), \tag{B.1a}$$

$$S_0(x) \equiv \lim_{y\to x} S_0(x,y) = \frac{x}{4}\,\frac{-4+15x-(12-6\log x)x^2+x^3}{(x-1)^3}, \tag{B.1b}$$

$$F^{(+)}(x,y) \equiv B^{(+)}(x,y) - B^{(+)}(0,y) - B^{(+)}(x,0) + B^{(+)}(0,0) = \frac{1}{4}S_0(x,y), \tag{B.1c}$$

$$F^{(-)}(x,y) \equiv B^{(-)}(x,y) - B^{(-)}(0,y) - B^{(-)}(x,0) + B^{(-)}(0,0), \tag{B.1d}$$

$$B_0^{(+)}(x) \equiv B^{(+)}(x,0) - B^{(+)}(0,0) = -\frac{1}{4}B_0^{(-)}(x) = B_0(x), \tag{B.1e}$$

with

$$B^{(+)}(x,y) = \frac{1}{4}\left[U(x,y) + \frac{xy}{4}U(x,y) - 2xy\tilde{U}(x,y)\right] = B^{\mu\bar{\mu}}(x,y), \tag{B.2a}$$

$$B^{(-)}(x,y) = -\left[U(x,y) + \frac{xy}{16}U(x,y) + \frac{xy}{2}\tilde{U}(x,y)\right] = -4B^{(\nu\bar{\nu})}(x,y), \tag{B.2b}$$

and

$$U(x_1,x_2) = \frac{x_1^2\log x_1}{(x_1-x_2)(1-x_1)^2} + \frac{x_2^2\log x_2}{(x_2-x_1)(1-x_2)^2} + \frac{1}{(1-x_1)(1-x_2)}, \tag{B.3a}$$

$$\tilde{U}(x_1,x_2) = \frac{x_1\log x_1}{(x_1-x_2)(1-x_1)^2} + \frac{x_2\log x_2}{(x_2-x_1)(1-x_2)^2} + \frac{1}{(1-x_1)(1-x_2)}. \tag{B.3b}$$

Penguin Functions

$$C_0(x) = \frac{x}{8}\left[\frac{x-6}{x-1} + \frac{3x+2}{(x-1)^2}\log x\right], \tag{B.4a}$$

$$D_0(x) = -\frac{4}{9}\log x + \frac{-19x^3+25x^2}{36(x-1)^3} + \frac{x^2(5x^2-2x-6)}{18(x-1)^4}\log x\,, \tag{B.4b}$$

$$E_0(x) = -\frac{2}{3}\log x + \frac{x^2(15-16x+4x^2)}{6(x-1)^4}\log x + \frac{x(18-11x-x^2)}{12(1-x)^3}\,, \tag{B.4c}$$

$$H_0(x) = \frac{x\,(-7x^2+x+12)}{12(x-1)^3} - \frac{x^2\,(x^2-10x+12)\log x}{6(x-1)^4}\,, \tag{B.4d}$$

$$D_0'(x) = \frac{(8x^3+5x^2-7x)}{12(x-1)^3} - \frac{(3x^3-2x^2)}{2(x-1)^4}\log x\,, \tag{B.4e}$$

$$E_0'(x) = \frac{3x^2}{2(x-1)^4}\log x + \frac{(x^3-5x^2-2x)}{4(x-1)^3}\,, \tag{B.4f}$$

$$H_0'(x) = \frac{x\,(2x^2+5x-1)}{4(x-1)^3} - \frac{3x^3\log x}{2(x-1)^4}\,, \tag{B.4g}$$

$$\tilde{L}_2(x) = -x\,\frac{2x^2-21x-1}{2(x-1)^3} - \frac{3x^3}{(x-1)^4}\log x\,. \tag{B.4h}$$

Gauge Invariant Loop Functions

$$X_0(x) = \frac{x}{8}\left[\frac{x+2}{x-1} + \frac{3x-6}{(x-1)^2}\,\log x\right], \tag{B.5a}$$

$$Y_0(x) = \frac{x}{8}\left[\frac{x-4}{x-1} + \frac{3x}{(x-1)^2}\log x\right], \tag{B.5b}$$

$$\begin{aligned} Z_0(x) = &-\frac{1}{9}\log x + \frac{18x^4-163x^3+259x^2-108x}{144(x-1)^3} \\ &+\frac{32x^4-38x^3-15x^2+18x}{72(x-1)^4}\log x\,, \end{aligned} \tag{B.5c}$$

List of Figures

Bibliography

[1] W. Pauli, *Personal memorandum*, 1931.

[2] F. Reines and C. Cowan, *Free anti-neutrino absorption cross-section. 1: Measurement of the free anti-neutrino absorption cross-section by protons*, *Phys.Rev.* **113** (1959) 273–279.

[3] S. Neddermeyer and C. Anderson, *Note on the nature of cosmic ray particles*, *Phys.Rev.* **51** (1937) 884–886.

[4] J. Street and E. Stevenson, *New evidence for the existence of a particle of mass intermediate between the proton and electron*, *Phys.Rev.* **52** (1937) 1003–1004.

[5] I. Rabi, *Cited in e.g. R.N. Cahn, G. Goldhaber, The Experimental Foundations of Particle Physics, Cambridge University Press, Cambridge, 1989, p. 52.*, .

[6] G. Danby *et al.*, *Observation of High-Energy Neutrino Reactions and the Existence of Two Kinds of Neutrinos*, *Phys. Rev. Lett.* **9** (1962) 36–44.

[7] L. Leprince$^-$Ringuet and M. L'Heritier, *Possible existence of a particle of mass 990 M(0) in cosmic radiation (in french)*, *Comptes Rend, Acad. Sci. Paris* **219** (1944) 618.

[8] R. Brown, U. Camerini, P. Fowler, H. Muirhead, C. Powell, *et al.*, *Observations with electron sensitive plates exposed to cosmic radiation*, *Nature* **163** (1949) 82.

[9] S. L. Glashow, J. Iliopoulos, and L. Maiani, *Weak Interactions with Lepton-Hadron Symmetry*, *Phys. Rev.* **D2** (1970) 1285–1292.

[10] **E598 Collaboration** Collaboration, J. Aubert *et al.*, *Experimental Observation of a Heavy Particle J*, *Phys.Rev.Lett.* **33** (1974) 1404–1406. Technical report 96.

[11] **SLAC-SP-017 Collaboration** Collaboration, J. Augustin *et al.*, *Discovery of a Narrow Resonance in e^+ e^- Annihilation*, *Phys.Rev.Lett.* **33** (1974) 1406–1408.

[12] B. Richter, *From the psi to Charm: The Experiments of 1975 and 1976*, *Rev.Mod.Phys.* **49** (1977) 251. Lecture delivered on occasion of presentation of 1976 Nobel Prizes in Physics.

[13] G. Goldhaber, F. Pierre, G. Abrams, M. Alam, A. Boyarski, *et al.*, *Observation in e^+ e^- Annihilation of a Narrow State at 1865-MeV/c**2 Decaying to $K\pi$ and $K\pi\pi\pi$*, *Phys.Rev.Lett.* **37** (1976) 255–259.

[14] M. L. Perl, G. Abrams, A. Boyarski, M. Breidenbach, D. Briggs, *et al.*, *Evidence for Anomalous Lepton Production in e^+ - e^- Annihilation*, *Phys.Rev.Lett.* **35** (1975) 1489–1492.

[15] S. Herb, D. Hom, L. Lederman, J. Sens, H. Snyder, *et al.*, *Observation of a Dimuon Resonance at 9.5-GeV in 400-GeV Proton-Nucleus Collisions*, *Phys.Rev.Lett.* **39** (1977) 252–255.

[16] **Pluto Collaboration** Collaboration, C. Berger *et al.*, *Observation of a Narrow Resonance Formed in e^+ e^- Annihilation at 9.46-GeV*, *Phys.Lett.* **B76** (1978) 243–245.

[17] **CDF Collaboration** Collaboration, F. Abe *et al.*, *Observation of top quark production in $\bar{p}p$ collisions*, *Phys.Rev.Lett.* **74** (1995) 2626–2631, [hep-ex/9503002].

[18] **D0 Collaboration** Collaboration, S. Abachi *et al.*, *Observation of the top quark*, *Phys.Rev.Lett.* **74** (1995) 2632–2637, [hep-ex/9503003].

[19] **DONUT Collaboration** Collaboration, B. Baller, *Direct observation of the tau neutrino*, *Nucl.Phys.Proc.Suppl.* **98** (2001) 43–47.

[20] P. H. Frampton, *Chiral dilepton model and the flavor question*, *Phys. Rev. Lett.* **69** (1992) 2889–2891.

[21] F. Pisano and V. Pleitez, *An SU(3) x U(1) model for electroweak interactions*, *Phys. Rev.* **D46** (1992) 410–417, [hep-ph/9206242].

[22] C. Promberger, S. Schatt, and F. Schwab, *Flavor changing neutral current effects and CP violation in the minimal 3-3-1 model*, *Phys. Rev.* **D75** (2007) 115007, [hep-ph/0702169].

[23] C. Promberger, S. Schatt, F. Schwab, and S. Uhlig, *Bounding the Minimal 331 Model through the Decay B —¿ X(s gamma)*, *Phys. Rev.* **D77** (2008) 115022, [0802.0949].

[24] G. S. Abrams *et al.*, *Initial Measurements of Z Boson Resonance Parameters in e^+ e^- Annihilation*, *Phys. Rev. Lett.* **63** (1989) 724.

[25] G. S. Abrams *et al.*, *Measurements of Z Boson Resonance Parameters in e^+ e^- Annihilation*, *Phys. Rev. Lett.* **63** (1989) 2173.

[26] **L3** Collaboration, B. Adeva *et al.*, *A Determination of the Properties of the Neutral Intermediate Vector Boson Z0*, *Phys. Lett.* **B231** (1989) 509.

[27] **ALEPH** Collaboration, D. Decamp *et al.*, *Determination of the Number of Light Neutrino Species*, *Phys. Lett.* **B231** (1989) 519.

[28] **OPAL** Collaboration, M. Z. Akrawy *et al.*, *Measurement of the Z0 Mass and Width with the OPAL Detector at LEP*, *Phys. Lett.* **B231** (1989) 530.

[29] **Super-Kamiokande** Collaboration, Y. Fukuda *et al.*, *Evidence for oscillation of atmospheric neutrinos*, *Phys. Rev. Lett.* **81** (1998) 1562–1567, [hep-ex/9807003].

[30] **SNO** Collaboration, Q. R. Ahmad *et al.*, *Measurement of the charged current interactions produced by B-8 solar neutrinos at the Sudbury Neutrino Observatory*, *Phys. Rev. Lett.* **87** (2001) 071301, [nucl-ex/0106015].

[31] **SNO** Collaboration, Q. R. Ahmad *et al.*, *Direct evidence for neutrino flavor transformation from neutral-current interactions in the Sudbury Neutrino Observatory*, *Phys. Rev. Lett.* **89** (2002) 011301, [nucl-ex/0204008].

[32] **Super-Kamiokande** Collaboration, S. Fukuda *et al.*, *Solar 8B and hep Neutrino Measurements from 1258 Days of Super-Kamiokande Data*, *Phys. Rev. Lett.* **86** (2001) 5651–5655, [hep-ex/0103032].

[33] J. Erler and P. Langacker, *Electroweak Model and Constraints on New Physics: in Review of Particle Physics (RPP 1998)*, *Eur. Phys. J.* **C3** (1998) 90–102.

[34] **Particle Data Group** Collaboration, J. Erler and P. Langacker, *Electroweak Model and Constraints on New Physics, in K. Hagiwara et al., Review of particle physics*, *Phys. Rev.* **D66** (2002) 010001.

[35] **Particle Data Group** Collaboration, J. Erler and P. Langacker, *Electroweak Model and Constraints on New Physics, in C. Amsler et al., Review of particle physics*, *Phys. Lett.* **B667** (2008) 1.

[36] M. Maltoni, V. A. Novikov, L. B. Okun, A. N. Rozanov, and M. I. Vysotsky, *Extra quark-lepton generations and precision measurements*, *Phys. Lett.* **B476** (2000) 107–115, [hep-ph/9911535].

[37] H.-J. He, N. Polonsky, and S. fang Su, *Extra families, Higgs spectrum and oblique corrections*, *Phys. Rev.* **D64** (2001) 053004, [hep-ph/0102144].

[38] J. Alwall *et al.*, *Is $V_{tb} \simeq 1$?*, *Eur. Phys. J.* **C49** (2007) 791–801, [hep-ph/0607115].

[39] G. D. Kribs, T. Plehn, M. Spannowsky, and T. M. P. Tait, *Four generations and Higgs physics*, *Phys. Rev.* **D76** (2007) 075016, [0706.3718].

[40] M. S. Chanowitz, *Bounding CKM Mixing with a Fourth Family*, *Phys. Rev.* **D79** (2009) 113008, [0904.3570].

[41] V. A. Novikov, A. N. Rozanov, and M. I. Vysotsky, *Once more on extra quark-lepton generations and precision measurements*, 0904.4570.

[42] P. H. Frampton, P. Q. Hung, and M. Sher, *Quarks and leptons beyond the third generation*, *Phys. Rept.* **330** (2000) 263, [hep-ph/9903387].

[43] B. Holdom *et al.*, *Four Statements about the Fourth Generation*, 0904.4698.

[44] A. Arhrib and W.-S. Hou, *Effect of fourth generation CP phase on $b \to s$ transitions*, *Eur. Phys. J.* **C27** (2003) 555–561, [hep-ph/0211267].

[45] W.-S. Hou, M. Nagashima, and A. Soddu, *Enhanced $K_L \to \pi^0 \nu\bar{\nu}$ from direct CP violation in $B \to K\pi$ with four generations*, *Phys. Rev.* **D72** (2005) 115007, [hep-ph/0508237].

[46] W.-S. Hou, M. Nagashima, and A. Soddu, *Large time$^-$dependent CP violation in B_s^0 system and finite D^0 - $\bar{D}^0$ mass difference in four generation standard model*, *Phys. Rev.* **D76** (2007) 016004, [hep-ph/0610385].

[47] A. Soni, A. K. Alok, A. Giri, R. Mohanta, and S. Nandi, *The Fourth family: A Natural explanation for the observed pattern of anomalies in B–CP asymmetries*, 0807.1971.

[48] J. A. Herrera, R. H. Benavides, and W. A. Ponce, *Flavor changing neutral currents with a fourth family of quarks*, *Phys. Rev.* **D78** (2008) 073008, [0810.3871].

[49] M. Bobrowski, A. Lenz, J. Riedl, and J. Rohrwild, *How much space is left for a new family of fermions?*, *Phys. Rev.* **D79** (2009) 113006, [0902.4883].

[50] G. Eilam, B. Melic, and J. Trampetic, *CP violation and the 4th generation*, *Phys. Rev.* **D80** (2009) 116003, [0909.3227].

[51] O. Eberhardt, A. Lenz, and J. Rohrwild, *Less space for a new family of fermions*, 1005.3505.

[52] M. Hashimoto, *Constraints on Mass Spectrum of Fourth Generation Fermions and Higgs Bosons*, 1001.4335.

[53] P. Q. Hung, *Minimal SU(5) resuscitated by long-lived quarks and leptons*, *Phys. Rev. Lett.* **80** (1998) 3000–3003, [hep-ph/9712338].

[54] W.-S. Hou, *CP Violation and Baryogenesis from New Heavy Quarks*, *Chin. J. Phys.* **47** (2009) 134, [0803.1234].

[55] Y. Kikukawa, M. Kohda, and J. Yasuda, *The strongly coupled fourth family and a first-order electroweak phase transition (I) Quark sector*, *Prog. Theor. Phys.* **122** (2009) 401–426, [0901.1962].

[56] R. Fok and G. D. Kribs, *Four Generations, the Electroweak Phase Transition, and Supersymmetry*, *Phys. Rev.* **D78** (2008) 075023, [0803.4207].

[57] B. Holdom, *Heavy quarks and electroweak symmetry breaking*, *Phys. Rev. Lett.* **57** (1986) 2496.

[58] C. T. Hill, M. A. Luty, and E. A. Paschos, *Electroweak symmetry breaking by fourth generation condensates and the neutrino spectrum*, *Phys. Rev.* **D43** (1991) 3011–3025.

[59] S. F. King, *Is electroweak symmetry broken by a fourth family of quarks?* , *Phys. Lett.* **B234** (1990) 108–112.

[60] G. Burdman and L. Da Rold, *Electroweak Symmetry Breaking from a Holographic Fourth Generation*, *JHEP* **12** (2007) 086, [0710.0623].

[61] P. Q. Hung and C. Xiong, *Renormalization Group Fixed Point with a Fourth Generation: Higgs-induced Bound States and Condensates*, 0911.3890.

[62] P. Q. Hung and C. Xiong, *Renormalization Group Fixed Point with a Fourth Generation: Solution to the hierarchy problem*, 0911.3892.

[63] B. Holdom, *Approaching a strong fourth family*, *Phys. Lett.* **B686** (2010) 146–151, [1001.5321].

[64] H.-S. Lee, Z. Liu, and A. Soni, *Neutrino dark matter candidate in fourth generation scenarios*, 1105.3490.

[65] G. Belanger, A. Pukhov, and G. Servant, *Dirac Neutrino Dark Matter*, *JCAP* **0801** (2008) 009, [0706.0526].

[66] G. Burdman, L. Da Rold, and R. D. Matheus, *The Lepton Sector of a Fourth Generation*, 0912.5219.

[67] A. J. Buras, B. Duling, T. Feldmann, T. Heidsieck, C. Promberger, and S. Recksiegel, *Patterns of Flavour Violation in the Presence of a Fourth Generation of Quarks and Leptons*, 1002.2126.

[68] A. J. Buras, B. Duling, T. Feldmann, T. Heidsieck, C. Promberger, and S. Recksiegel, *The Impact of a 4th Generation on Mixing and CP Violation in the Charm System*, *JHEP* **07** (2010) 094, [1004.4565].

[69] A. J. Buras, B. Duling, T. Feldmann, T. Heidsieck, and C. Promberger, *Lepton Flavour Violation in the Presence of a Fourth Generation of Quarks and Leptons*, *JHEP* **09** (2010) 104, [1006.5356].

[70] M. Blanke *et al.*, *Particle antiparticle mixing, ϵ_K, $\Delta(\Gamma(q))$, $A_{\rm SL}(q)$, $A_{\rm CP}(B_d \to \psi K_S)$, $A_{\rm CP}(B_s \to \psi\phi)$ and $B \to X_{s,d}\gamma$ in the littlest Higgs model with T-parity*, *JHEP* **12** (2006) 003, [hep-ph/0605214].

[71] M. Blanke *et al.*, *Rare and CP-Violating K and B Decays in the Littlest Higgs Model with T-Parity*, *JHEP* **01** (2007) 066, [hep-ph/0610298].

[72] M. Blanke, A. J. Buras, B. Duling, S. Recksiegel, and C. Tarantino, *FCNC Processes in the Littlest Higgs Model with T-Parity: a 2009 Look*, *Acta Phys. Polon. B* **41** (2010) 657, [0906.5454].

[73] M. Blanke, A. J. Buras, B. Duling, S. Gori, and A. Weiler, *$\Delta F = 2$ Observables and Fine$^-$Tuning in a Warped Extra Dimension with Custodial Protection*, *JHEP* **03** (2009) 001, [0809.1073].

[74] M. Blanke, A. J. Buras, B. Duling, K. Gemmler, and S. Gori, *Rare K and B Decays in a Warped Extra Dimension with Custodial Protection*, *JHEP* **03** (2009) 108, [0812.3803].

[75] W. Altmannshofer, A. J. Buras, S. Gori, P. Paradisi, and D. M. Straub, *Anatomy and Phenomenology of FCNC and CPV Effects in SUSY Theories*, *Nucl. Phys.* **B830** (2010) 17–94, [0909.1333].

[76] **CMS** Collaboration, *Search for a Heavy Bottom-like Quark in pp Collisions at sqrt(s) = 7 TeV*, 1102.4746.

[77] C. J. Flacco, D. Whiteson, and M. Kelly, *Fourth generation quark mass limits in CKM-element space*, 1101.4976.

[78] **CDF** Collaboration, J. Conway *et al.*, *CDF public conference note CDF/PUB/TOP/PUBLIC/10110*, 2010.

[79] **CDF** Collaboration, D. Whiteson *et al.*, *CDF public conference note CDF/PUB/TOP/PUBLIC/10243*, 2010.

[80] **CDF** Collaboration, T. Aaltonen *et al.*, *Search for New Bottomlike Quark Pair Decays $Q\bar{Q} \to (tW^{\mp})(\bar{t}W^{\pm})$ in Same^{-} Charge Dilepton Events*, *Phys. Rev. Lett.* **104** (2010) 091801, [0912.1057].

[81] **OPAL** Collaboration, G. Abbiendi *et al.*, *Precise determination of the Z resonance parameters at LEP: 'Zedometry'*, *Eur. Phys. J.* **C19** (2001) 587–651, [hep-ex/0012018].

[82] **L3 Collaboration** Collaboration, P. Achard *et al.*, *Search for heavy neutral and charged leptons in e^+e^- annihilation at LEP*, *Phys.Lett.* **B517** (2001) 75–85, [hep-ex/0107015].

[83] M. S. Chanowitz, M. A. Furman, and I. Hinchliffe, *Weak Interactions of Ultraheavy Fermions. 2*, *Nucl. Phys.* **B153** (1979) 402.

[84] N. Cabibbo, *Unitary symmetry and leptonic decays*, *Phys. Rev. Lett.* **10** (Jun, 1963) 531–533.

[85] M. Kobayashi and T. Maskawa, *CP-Violation in the Renormalizable Theory of Weak Interaction*, *Progress of Theoretical Physics* **49** (1973), no. 2 652–657.

[86] H. Fritzsch and J. Plankl, *The Mixing of Quark Flavors*, *Phys. Rev.* **D35** (1987) 1732.

[87] H. Harari and M. Leurer, *Recommending a Standard Choice of Cabibbo Angles and KM Phases for Any Number of Generations*, *Phys. Lett.* **B181** (1986) 123.

[88] A. A. Anselm, J. L. Chkareuli, N. G. Uraltsev, and T. A. Zhukovskaya, *On the Kobayashi-Maskawa model with four generations*, *Phys. Lett.* **B156** (1985) 102–108.

[89] J. C. Hardy and I. S. Towner, *Superallowed 0^+ to 0^+ nuclear beta decays: A new survey with precision tests of the conserved vector current hypothesis and the standard model*, *Phys. Rev.* **C79** (2009) 055502, [0812.1202].

[90] **Particle Data Group** Collaboration, E. Blucher and M. W.J., *V_{ud}, V_{us}, the Cabibbo Angle and CKM Unitarity, [Review of particle physics]*, *J. Phys.* **G37** (2010) 075021.

[91] **Particle Data Group** Collaboration, R. Kowalewski and T. Mannel, *Determination of v_{cb} and v_{ub}, [review of particle physics]*, *J. Phys.* **G37** (2010) 075021.

[92] **CHORUS** Collaboration, A. Kayis-Topaksu *et al.*, *Measurement of topological muonic branching ratios of charmed hadrons produced in neutrino induced charged-current interactions*, *Phys. Lett.* **B626** (2005) 24–34.

[93] **CLEO** Collaboration, D. Besson *et al.*, *Improved measurements of D meson semileptonic decays to pi and K mesons*, *Phys. Rev.* **D80** (2009) 032005, [0906.2983].

[94] **Belle** Collaboration, L. Widhalm *et al.*, *Measurement of $D_0 \to \pi\ell\nu(K\ell\nu)$ form factors and absolute branching fractions*, *Phys. Rev. Lett.* **97** (2006) 061804, [hep-ex/0604049].

[95] **BABAR** Collaboration, B. Aubert *et al.*, *Measurement of the hadronic form-factor in $D^0 \to K^- e^+ \nu_e$ 1*, *Phys. Rev.* **D76** (2007) 052005, [0704.0020].

[96] **Belle** Collaboration, L. Widhalm *et al.*, *Measurement of $B(D_s \to \mu\nu)$*, *Phys. Rev. Lett.* **100** (2008) 241801, [0709.1340].

[97] **CLEO** Collaboration, J. P. Alexander *et al.*, *Measurement of $BD_s^+ \to \ell^+\nu$ and the Decay Constant fD_s^+ From 600 /pb^{-1} of $e^\pm$ Annihilation Data Near 4170 MeV*, *Phys. Rev.* **D79** (2009) 052001, [0901.1216].

[98] **BABAR** Collaboration, B. Aubert *et al.*, *Measurement of the pseudoscalar decay constant f(D/s) using charm-tagged events in e^+ e^- collisions at s**(1/2) = 10.58-GeV*, *Phys. Rev. Lett.* **98** (2007) 141801, [hep-ex/0607094].

[99] **D0** Collaboration, V. M. Abazov *et al.*, *Observation of Single Top-Quark Production*, *Phys. Rev. Lett.* **103** (2009) 092001, [0903.0850].

[100] **CDF** Collaboration, T. Aaltonen *et al.*, *Search for single top quark production in pbar p collisions at sqrts=1.96 TeV in the missing transverse energy plus jets topology*, *Phys. Rev.* **D81** (2010) 072003, [1001.4577].

[101] **CKMfitter Group** Collaboration. http://ckmfitter.in2p3.fr/plots_ICHEP10/.

[102] H. Lacker, "Constraints on CKM matrix elements within a fourth generation." - talk given at 'Second Workshop on Beyond 3 Generation Standard Model - New Fermions at the Crossroads ov Tevatron and LHC Search', Taipeh, Taiwan, January 2010.

[103] **Particle Data Group** Collaboration, K. Nakamura *et al.*, *Review of particle physics*, *J. Phys.* **G37** (2010) 075021.

[104] A. Soni, A. K. Alok, A. Giri, R. Mohanta, and S. Nandi, *SM with four generations: Selected implications for rare B and K decays*, 1002.0595.

[105] L. Wolfenstein, *Parametrization of the Kobayashi-Maskawa Matrix*, *Phys. Rev. Lett.* **51** (1983) 1945.

[106] A. J. Buras, M. E. Lautenbacher, and G. Ostermaier, *Waiting for the top quark mass, $K^+ \to \pi^+ \nu\bar{\nu}$, $B_s^0 - \bar{B}_s^0$ mixing and CP asymmetries in B decays*, *Phys. Rev.* **D50** (1994) 3433–3446, [hep-ph/9403384].

[107] C. D. Froggatt and H. B. Nielsen, *Hierarchy of Quark Masses, Cabibbo Angles and CP Violation*, *Nucl. Phys.* **B147** (1979) 277.

[108] T. Feldmann and T. Mannel, *Minimal Flavour Violation and Beyond*, *JHEP* **02** (2007) 067, [hep-ph/0611095].

[109] C. Jarlskog, *Commutator of the Quark Mass Matrices in the Standard Electroweak Model and a Measure of Maximal CP Violation*, *Phys. Rev. Lett.* **55** (1985) 1039.

[110] C. Jarlskog, *A Basis Independent Formulation of the Connection Between Quark Mass Matrices, CP Violation and Experiment*, *Z. Phys.* **C29** (1985) 491–497.

[111] F. del Aguila and J. A. Aguilar-Saavedra, *Invariant formulation of CP violation for four quark families*, *Phys. Lett.* **B386** (1996) 241–246, [hep-ph/9605418].

[112] P. F. Harrison, D. H. Perkins, and W. G. Scott, *Tri-bimaximal mixing and the neutrino oscillation data*, *Phys. Lett.* **B530** (2002) 167, [hep-ph/0202074].

[113] J. Erler and P. Langacker, *Electroweak Physics*, *Acta Phys. Polon.* **B39** (2008) 2595–2610, [0807.3023].

[114] M. E. Peskin and T. Takeuchi, *A New constraint on a strongly interacting Higgs sector*, *Phys. Rev. Lett.* **65** (1990) 964–967.

[115] M. E. Peskin and T. Takeuchi, *Estimation of oblique electroweak corrections*, *Phys. Rev.* **D46** (1992) 381–409.

[116] C. P. Burgess, *The Effective use of precision electroweak measurements*, *Pramana* **45** (1995) S47–S71, [hep-ph/9411257].

[117] M. S. Chanowitz, M. A. Furman, and I. Hinchliffe, *Weak Interactions of Ultraheavy Fermions*, *Phys. Lett.* **B78** (1978) 285.

[118] O. Eberhardt, *Flavour and electroweak precision constraints on the existence of a fourth quark family*, Diploma Thesis, Universität Regensburg, 2010.

[119] T. Yanir, *Phenomenological constraints on extended quark sectors*, *JHEP* **06** (2002) 044, [hep-ph/0205073].

[120] J. Bernabeu, A. Pich, and A. Santamaria, *Top quark mass from radiative corrections to the $Z \to b$ anti-b decay*, *Nucl. Phys.* **B363** (1991) 326–344.

[121] B. A. Kniehl and J. H. Kuhn, *QCD Corrections to the Axial Part of the Z Decay Rate*, *Phys. Lett.* **B224** (1989) 229.

[122] B. A. Kniehl and J. H. Kuhn, *QCD Corrections to the Z Decay Rate*, *Nucl. Phys.* **B329** (1990) 547.

[123] **Particle Data Group** Collaboration, G. Cowan, *Statistics [review of particle physics]*, *J. Phys.* **G37** (2010) 075021.

[124] J. Erler and P. Langacker, *Precision Constraints on Extra Fermion Generations*, 1003.3211.

[125] K. G. Wilson, *Nonlagrangian models of current algebra*, *Phys. Rev.* **179** (1969) 1499–1512.

[126] A. J. Buras and R. Fleischer, *Quark mixing, CP violation and rare decays after the top quark discovery*, *Adv. Ser. Direct. High Energy Phys.* **15** (1998) 65–238, [hep-ph/9704376].

[127] G. Buchalla, A. J. Buras, and M. K. Harlander, *Penguin box expansion: Flavor changing neutral current processes and a heavy top quark*, *Nucl. Phys.* **B349** (1991) 1–47.

[128] A. J. Buras, *Weak Hamiltonian, CP violation and rare decays*, hep-ph/9806471.

[129] A. J. Buras and D. Guadagnoli, *Correlations among new CP violating effects in $\Delta F = 2$ observables*, *Phys. Rev.* **D78** (2008) 033005, [0805.3887].

[130] J. Laiho, R. S. Van de Water, and E. Lunghi, *Lattice QCD inputs to the CKM unitarity triangle analysis*, 0910.2928.

[131] A. J. Buras, D. Guadagnoli, and G. Isidori, *On ϵ_K beyond lowest order in the Operator Product Expansion*, 1002.3612.

[132] A. J. Buras and J. M. Gérard, *$1/N$ Expansion for Kaons*, *Nucl. Phys.* **B264** (1986) 371.

[133] J. Bijnens, J. M. Gérard, and G. Klein, *The $K_L - K_S$ mass difference*, *Phys. Lett.* **B257** (1991) 191–195.

[134] J.-M. Gerard, C. Smith, and S. Trine, *Radiative kaon decays and the penguin contribution to the Delta(I) = 1/2 rule*, *Nucl. Phys.* **B730** (2005) 1–36, [hep-ph/0508189].

[135] R. Gupta, T. Bhattacharya, and S. R. Sharpe, *Matrix elements of 4-fermion operators with quenched fermions*, *Phys. Rev.* **D55** (1997) 4036–4054, [hep-lat/9611023].

[136] **UKQCD** Collaboration, L. Lellouch and C. J. D. Lin, *Standard model matrix elements for neutral B meson mixing and associated decay constants*, *Phys. Rev.* **D64** (2001) 094501, [hep-ph/0011086].

[137] H.-W. Lin, S. Ohta, A. Soni, and N. Yamada, *Charm as a domain wall fermion in quenched lattice QCD*, *Phys. Rev.* **D74** (2006) 114506, [hep-lat/0607035].

[138] A. J. Buras, M. Jamin, and P. H. Weisz, *Leading and next-to-leading QCD corrections to ϵ parameter and $B^0 - \bar{B}^0$ mixing in the presence of a heavy quark*, *Nucl. Phys.* **B347** (1990) 491–536.

[139] S. Bethke, *The 2009 Wolrd Average of $\alpha_s(M_Z)$*, *Eur. Phys. J.* **C64** (2009) 689–703, [0908.1135].

[140] I. I. Bigi, M. Blanke, A. J. Buras, and S. Recksiegel, *CP Violation in $D^0 - \bar{D}^0$ Oscillations: General Considerations and Applications to the Littlest Higgs Model with T-Parity*, *JHEP* **07** (2009) 097, [0904.1545].

[141] W. Altmannshofer, A. J. Buras, and P. Paradisi, *A Lower Bound on hadronic EDMs from CP Violation in $D^0 - \bar{D}^0$ mixing in SUSY Alignment Models*, *Phys. Lett.* **B688** (2010), no. 2-3 202, [1001.3835].

[142] G. Buchalla and A. J. Buras, *The rare decays $K \to \pi\nu\bar{\nu}$, $B \to X\nu\bar{\nu}$ and $B \to \ell^+\ell^-$: An update*, *Nucl. Phys.* **B548** (1999) 309–327, [hep-ph/9901288].

[143] M. Misiak and J. Urban, *QCD corrections to FCNC decays mediated by Z-penguins and W-boxes*, *Phys. Lett.* **B451** (1999) 161–169, [hep-ph/9901278].

[144] M. Gorbahn and U. Haisch, *Charm quark contribution to $K_L \to \mu^+\mu^-$ at next-to-next-to-leading order*, *Phys. Rev. Lett.* **97** (2006) 122002, [hep-ph/0605203].

[145] G. Isidori and R. Unterdorfer, *On the short-distance constraints from $K_{L,S} \to \mu^+\mu^-$* , *JHEP* **01** (2004) 009, [hep-ph/0311084].

[146] A. J. Buras, *Relations between $\Delta M_{s,d}$ and $B_{s,d} \to \mu\bar{\mu}$ in models with minimal flavour violation*, *Phys. Lett.* **B566** (2003) 115–119, [hep-ph/0303060].

[147] J. Shigemitsu *et al.*, *Recent results on B mixing and decay constants from HPQCD*, 0910.4131.

[148] **CDF** Collaboration, T. Aaltonen *et al.*, *Search for $B_s^0 \to \mu^+\mu^-$ and $B_d^0 \to \mu^+\mu^-$ decays with $2fb^{-1}$ of $p\bar{p}$ collisions*, *Phys. Rev. Lett.* **100** (2008) 101802, [0712.1708].

[149] **D0** Collaboration, V. M. Abazov *et al.*, *Search for $B_s \to \mu^+\mu^-$ at D0*, *Phys. Rev.* **D76** (2007) 092001, [0707.3997].

[150] G. Punzi, *Flavour physics at the Tevatron*, 1001.4886.

[151] **LHCb** Collaboration, A. Perez-Calero, "Search for Rare Decays at LHCb with 0.2 and 1 fb^{-1}." - talk given at '22nd Rencontres de Blois', Blois, France, July 2010. http://confs.obspm.fr/Blois2010/Calero.pdf.

[152] G. Buchalla, A. J. Buras, and M. E. Lautenbacher, *Weak Decays Beyond Leading Logarithms*, *Rev. Mod. Phys.* **68** (1996) 1125–1144, [hep-ph/9512380].

[153] F. Mescia and C. Smith, *Improved estimates of rare K decay matrix-elements from K_{l3} decays*, *Phys. Rev.* **D76** (2007) 034017, [0705.2025].

[154] A. J. Buras, M. Gorbahn, U. Haisch, and U. Nierste, *Charm quark contribution to $K^+ \to \pi^+ \nu\bar{\nu}$ at next-to-next-to-leading order*, *JHEP* **11** (2006) 002, [hep-ph/0603079].

[155] J. Brod and M. Gorbahn, *Electroweak Corrections to the Charm Quark Contribution to $K^+ \to \pi^+ \nu\bar{\nu}$*, *Phys. Rev.* **D78** (2008) 034006, [0805.4119].

[156] G. Isidori, F. Mescia, and C. Smith, *Light-quark loops in $K \to \pi\nu\bar{\nu}$*, *Nucl. Phys.* **B718** (2005) 319–338, [hep-ph/0503107].

[157] **E949** Collaboration, A. V. Artamonov *et al.*, *New measurement of the $K^+ \to \pi^+ \nu\bar{\nu}$ branching ratio*, *Phys. Rev. Lett.* **101** (2008) 191802, [0808.2459].

[158] **E391a** Collaboration, J. K. Ahn *et al.*, *Search for the Decay $K_L^0 \to \pi^0 \nu\bar{\nu}$*, *Phys. Rev. Lett.* **100** (2008) 201802, [0712.4164].

[159] W. Altmannshofer, A. J. Buras, D. M. Straub, and M. Wick, *New strategies for New Physics search in $B \to K^* \nu\bar{\nu}$, $B \to K \nu\bar{\nu}$ and $B \to X_s \nu\bar{\nu}$ decays*, *JHEP* **04** (2009) 022, [0902.0160].

[160] M. Bartsch, M. Beylich, G. Buchalla, and D. N. Gao, *Precision Flavour Physics with $B \to K \nu\bar{\nu}$ and $B \to K \ell^+ \ell^-$*, *JHEP* **11** (2009) 011, [0909.1512].

[161] M. Bona *et al.*, *SuperB: A High-Luminosity Asymmetric e^+e^- Super Flavor Factory. Conceptual Design Report*, 0709.0451.

[162] G. Buchalla, G. Hiller, and G. Isidori, *Phenomenology of non-standard Z couplings in exclusive semileptonic $b \to s$ transitions*, *Phys. Rev.* **D63** (2001) 014015, [hep-ph/0006136].

[163] **Heavy Flavor Averaging Group** Collaboration, E. Barberio *et al.*, *Averages of b−hadron and c−hadron Properties at the End of 2007*, 0808.1297.

[164] M. Misiak *et al.*, *The first estimate of $B(\bar{B} \to X_s \gamma)$ at $O(\alpha_s^2)$*, *Phys. Rev. Lett.* **98** (2007) 022002, [hep-ph/0609232].

[165] A. Ali, T. Mannel, and T. Morozumi, *Forward backward asymmetry of dilepton angular distribution in the decay $b \to s \ell^+ \ell^-$*, *Phys. Lett.* **B273** (1991) 505–512.

[166] G. Burdman, *Short distance coefficients and the vanishing of the lepton asymmetry in $B \to V\ell^+\ell^-$*, *Phys. Rev.* **D57** (1998) 4254–4257, [hep-ph/9710550].

[167] M. Beneke, T. Feldmann, and D. Seidel, *Systematic approach to exclusive $B \to V\ell^+\ell^-, V\gamma$ decays*, *Nucl. Phys.* **B612** (2001) 25–58, [hep-ph/0106067].

[168] A. J. Buras, R. Fleischer, S. Recksiegel, and F. Schwab, *Anatomy of prominent B and K decays and signatures of CP-violating new physics in the electroweak penguin sector*, *Nucl. Phys.* **B697** (2004) 133–206, [hep-ph/0402112].

[169] A. J. Buras and M. Münz, *Effective Hamiltonian for $B \to X_s e^+ e^-$ beyond leading logarithms in the NDR and HV schemes*, *Phys. Rev.* **D52** (1995) 186–195, [hep-ph/9501281].

[170] H. M. Asatrian, K. Bieri, C. Greub, and A. Hovhannisyan, *NNLL corrections to the angular distribution and to the forward-backward asymmetries in $b \to X_s\ell^+\ell^-$*, *Phys. Rev.* **D66** (2002) 094013, [hep-ph/0209006].

[171] A. Ghinculov, T. Hurth, G. Isidori, and Y. P. Yao, *The rare decay $B \to X_s\ell^+\ell^-$ to NNLL precision for arbitrary dilepton invariant mass*, *Nucl. Phys.* **B685** (2004) 351–392, [hep-ph/0312128].

[172] C. Bobeth, P. Gambino, M. Gorbahn, and U. Haisch, *Complete NNLO QCD analysis of $\bar{B} \to X_s\ell^+\ell^-$ and higher order electroweak effects*, *JHEP* **04** (2004) 071, [hep-ph/0312090].

[173] T. Huber, T. Hurth, and E. Lunghi, *Logarithmically Enhanced Corrections to the Decay Rate and Forward Backward Asymmetry in $\bar{B} \to X_s\ell^+\ell^-$*, *Nucl. Phys.* **B802** (2008) 40–62, [0712.3009].

[174] **BABAR** Collaboration, B. Aubert *et al.*, *Measurement of the $B \to X_s\ell^+\ell^-$ branching fraction with a sum over exclusive modes*, *Phys. Rev. Lett.* **93** (2004) 081802, [hep-ex/0404006].

[175] **Belle** Collaboration, M. Iwasaki *et al.*, *Improved measurement of the electroweak penguin process $B \to X_s\ell^+\ell^-$*, *Phys. Rev.* **D72** (2005) 092005, [hep-ex/0503044].

[176] G. D'Ambrosio, G. Ecker, G. Isidori, and J. Portoles, *The decays $K \to \pi\ell^+\ell^-$ beyond leading order in the chiral expansion*, *JHEP* **08** (1998) 004, [hep-ph/9808289].

[177] G. Buchalla, G. D'Ambrosio, and G. Isidori, *Extracting short-distance physics from $K_{L,S} \to \pi^0 e^+ e^-$ decays*, *Nucl. Phys.* **B672** (2003) 387–408, [hep-ph/0308008].

[178] G. Isidori, C. Smith, and R. Unterdorfer, *The rare decay $K_L \to \pi^0\mu^+\mu^-$ within the SM*, *Eur. Phys. J.* **C36** (2004) 57–66, [hep-ph/0404127].

[179] S. Friot, D. Greynat, and E. De Rafael, *Rare kaon decays revisited*, *Phys. Lett.* **B595** (2004) 301–308, [hep-ph/0404136].

[180] F. Mescia, C. Smith, and S. Trine, *$K_L \to \pi^0 e^+ e^-$ and $K_L \to \pi^0 \mu^+ \mu^-$: A binary star on the stage of flavor physics*, *JHEP* **08** (2006) 088, [hep-ph/0606081].

[181] J. Prades, *ChPT Progress on Non-Leptonic and Radiative Kaon Decays*, *PoS* **KAON** (2008) 022, [0707.1789].

[182] A. J. Buras, M. E. Lautenbacher, M. Misiak, and M. Münz, *Direct CP violation in $K_L \to \pi^0 e^+ e^-$ beyond leading logarithms*, *Nucl. Phys.* **B423** (1994) 349–383, [hep-ph/9402347].

[183] **KTeV** Collaboration, A. Alavi-Harati *et al.*, *Search for the Rare Decay $K_L \to \pi^0 e^+ e^-$*, *Phys. Rev. Lett.* **93** (2004) 021805, [hep-ex/0309072].

[184] **KTEV** Collaboration, A. Alavi-Harati *et al.*, *Search for the Decay $K_L \to \pi^0 \mu^+ \mu^-$*, *Phys. Rev. Lett.* **84** (2000) 5279–5282, [hep-ex/0001006].

[185] **NA48** Collaboration, J. R. Batley *et al.*, *A precision measurement of direct CP violation in the decay of neutral kaons into two pions*, *Phys. Lett.* **B544** (2002) 97–112, [hep-ex/0208009].

[186] **KTeV** Collaboration, A. Alavi-Harati *et al.*, *Measurements of Direct CP Violation, CPT Symmetry, and Other Parameters in the Neutral Kaon System*, *Phys. Rev.* **D67** (2003) 012005, [hep-ex/0208007].

[187] **KTeV** Collaboration, E. T. Worcester, *The Final Measurement of ϵ'/ϵ from KTeV*, 0909.2555.

[188] A. J. Buras and L. Silvestrini, *Upper bounds on $K \to \pi\nu\bar{\nu}$ and $K_L \to \pi^0 e^+ e^-$ from ε'/ε and $K_L \to \mu^+ \mu^-$*, *Nucl. Phys.* **B546** (1999) 299–314, [hep-ph/9811471].

[189] A. J. Buras, G. Colangelo, G. Isidori, A. Romanino, and L. Silvestrini, *Connections between ε'/ε and rare kaon decays in supersymmetry*, *Nucl. Phys.* **B566** (2000) 3–32, [hep-ph/9908371].

[190] M. Blanke, A. J. Buras, S. Recksiegel, C. Tarantino, and S. Uhlig, *Correlations between ϵ'/ϵ and rare K decays in the littlest Higgs model with T–parity*, *JHEP* **06** (2007) 082, [0704.3329].

[191] A. J. Buras and M. Jamin, *ϵ'/ϵ at the NLO: 10 years later*, *JHEP* **01** (2004) 048, [hep-ph/0306217].

[192] N. H. Christ, *Theoretical strategies for ϵ'/ϵ*, 0912.2917.

[193] G. Buchalla, G. Hiller, Y. Nir, and G. Raz, *The pattern of CP asymmetries in $b \to s$ transitions*, *JHEP* **09** (2005) 074, [hep-ph/0503151].

[194] H.-Y. Cheng, C.-K. Chua, and A. Soni, *Effects of Final-state Interactions on Mixing-induced CP Violation in Penguin-dominated B Decays*, *Phys. Rev.* **D72** (2005) 014006, [hep-ph/0502235].

[195] M. Beneke and M. Neubert, *Flavor-singlet B decay amplitudes in QCD factorization*, *Nucl. Phys.* **B651** (2003) 225–248, [hep-ph/0210085].

[196] M. Beneke, *Corrections to* $\sin(2\beta)$ *from CP asymmetries in* $B^0 \to (\pi^0, \rho^0, \eta^0, \eta', \omega, \phi)K_S$ *decays*, *Phys. Lett.* **B620** (2005) 143–150, [hep-ph/0505075].

[197] **Particle Data Group** Collaboration, C. Amsler *et al.*, *Review of particle physics*, *Phys. Lett.* **B667** (2008) 1.

[198] D. London and A. Soni, *Measuring the CP angle beta in hadronic* $b \to s$ *penguin decays*, *Phys. Lett.* **B407** (1997) 61–65, [hep-ph/9704277].

[199] Y. Grossman and M. P. Worah, *CP asymmetries in B decays with new physics in decay amplitudes*, *Phys. Lett.* **B395** (1997) 241–249, [hep-ph/9612269].

[200] M. Artuso *et al.*, *B, D and K decays*, *Eur. Phys. J.* **C57** (2008) 309–492, [0801.1833].

[201] **Heavy Flavor Averaging Group (HFAG)** Collaboration, E. Barberio *et al.*, *Averages of b-hadron properties at the end of 2006*, 0704.3575. Updates available on http://www.slac.stanford.edu/xorg/hfag.

[202] **CDF** Collaboration, T. Aaltonen *et al.*, *First Flavor-Tagged Determination of Bounds on Mixing-Induced CP Violation in* $B_s^0 \to J/\psi\phi$ *Decays*, *Phys. Rev. Lett.* **100** (2008) 161802, [0712.2397].

[203] **D0** Collaboration, V. M. Abazov *et al.*, *Measurement of* B_s^0 *mixing parameters from the flavor-tagged decay* $B_s^0 \to J/\psi\phi$, *Phys. Rev. Lett.* **101** (2008) 241801, [0802.2255].

[204] J. M. Soares, *CP violation in radiative b decays*, *Nucl. Phys.* **B367** (1991) 575–590.

[205] A. L. Kagan and M. Neubert, *Direct CP violation in* $B \to X_s\gamma$ *decays as a signature of new physics*, *Phys. Rev.* **D58** (1998) 094012, [hep-ph/9803368].

[206] A. L. Kagan and M. Neubert, *QCD anatomy of* $B \to X_s\gamma$ *decays*, *Eur. Phys. J.* **C7** (1999) 5–27, [hep-ph/9805303].

[207] W. Altmannshofer, A. J. Buras, and P. Paradisi, *Low Energy Probes of CP Violation in a Flavor Blind MSSM*, *Phys. Lett.* **B669** (2008) 239–245, [0808.0707].

[208] G. Altarelli, L. Baulieu, N. Cabibbo, L. Maiani, and R. Petronzio, *Muon Number Nonconserving Processes in Gauge Theories of Weak Interactions*, *Nucl. Phys.* **B125** (1977) 285.

[209] H. Lacker and A. Menzel, *Simultaneous Extraction of the Fermi constant and PMNS matrix elements in the presence of a fourth generation*, 1003.4532.

[210] M. Blanke, A. J. Buras, B. Duling, A. Poschenrieder, and C. Tarantino, *Charged Lepton Flavour Violation and $(g-2)_\mu$ in the Littlest Higgs Model with T-Parity: a clear Distinction from Supersymmetry*, *JHEP* **05** (2007) 013, [hep-ph/0702136].

[211] J. Hisano, T. Moroi, K. Tobe, and M. Yamaguchi, *Lepton-Flavor Violation via Right-Handed Neutrino Yukawa Couplings in Supersymmetric Standard Model*, *Phys. Rev.* **D53** (1996) 2442–2459, [hep-ph/9510309].

[212] J. R. Ellis, J. Hisano, M. Raidal, and Y. Shimizu, *A new parametrization of the seesaw mechanism and applications in supersymmetric models*, *Phys. Rev.* **D66** (2002) 115013, [hep-ph/0206110].

[213] E. Arganda and M. J. Herrero, *Testing supersymmetry with lepton flavor violating tau and mu decays*, *Phys. Rev.* **D73** (2006) 055003, [hep-ph/0510405].

[214] R. Kaiser and H. Leutwyler, *Pseudoscalar decay constants at large N_c*, hep-ph/9806336.

[215] T. Feldmann and P. Kroll, *Flavor symmetry breaking and mixing effects in the eta gamma and eta-prime gamma transition form-factors*, *Eur.Phys.J.* **C5** (1998) 327–335, [hep-ph/9711231].

[216] R. Kaiser and H. Leutwyler, *Large N_c in chiral perturbation theory*, *Eur. Phys. J.* **C17** (2000) 623–649, [hep-ph/0007101].

[217] T. Feldmann, P. Kroll, and B. Stech, *Mixing and decay constants of pseudoscalar mesons*, *Phys. Rev.* **D58** (1998) 114006, [hep-ph/9802409].

[218] T. Feldmann, *Quark structure of pseudoscalar mesons*, *Int. J. Mod. Phys.* **A15** (2000) 159–207, [hep-ph/9907491].

[219] J. C. Pati and A. Salam, *Unified Lepton-Hadron Symmetry and a Gauge Theory of the Basic Interactions*, *Phys. Rev.* **D8** (1973) 1240–1251.

[220] M. Antonelli *et al.*, *An evaluation of $|V_{us}|$ and precise tests of the Standard Model from world data on leptonic and semileptonic kaon decays*, 1005.2323.

[221] M. Antonelli *et al.*, *Flavor Physics in the Quark Sector*, 0907.5386.

[222] **Belle** Collaboration, I. Adachi *et al.*, *Measurement of $B \to \tau^- \bar{\nu}_\tau$ Decay With a Semileptonic Tagging Method*, 0809.3834.

[223] **BABAR** Collaboration, B. Aubert *et al.*, *A Search for $B^+ \to \ell^+ \nu_\ell$ Recoiling Against $B^- \to D^0 \ell^- \bar{\nu} X$*, *Phys. Rev.* **D81** (2010) 051101, [0809.4027].

[224] **BABAR** Collaboration, B. Aubert *et al.*, *Search for the rare leptonic decay $B^+ \to \mu^+ \nu_\mu$*, *Phys. Rev. Lett.* **92** (2004) 221803, [hep-ex/0401002].

[225] **UTfit** Collaboration, M. Bona *et al.*, *An Improved Standard Model Prediction Of $Br(B \to \tau\nu)$ And Its Implications For New Physics*, *Phys. Lett.* **B687** (2010) 61–69, [0908.3470].

[226] **SINDRUM II.** Collaboration, C. Dohmen *et al.*, *Test of lepton flavor conservation in $\mu \to e$ conversion on titanium*, *Phys. Lett.* **B317** (1993) 631–636.

[227] **PRISM/PRIME working group** Collaboration, Y. Mori *et al.*, *LOI at J-PARC 50-GeV PS, LOI-25*, *http://psux1.kek.jp/ jhf-np/LOIlist/LOIlist.html*.

[228] J. C. Sens, *Capture of negative muons by nuclei*, *Phys. Rev.* **113** (Jan, 1959) 679–687.

[229] K. W. Ford and W. J. G., *Calculated properties of μ-mesonic atoms*, *Nucl. Phys.* **35** (1962) 295–302.

[230] R. Pla and J. Bernabeu, *Nuclear Size Effect in Muon Capture*, *An. Fis.* **67** (1971) 455.

[231] H. C. Chiang, E. Oset, T. S. Kosmas, A. Faessler, and J. D. Vergados, *Coherent and incoherent (μ^-, e^-) conversion in nuclei*, *Nucl. Phys.* **A559** (1993) 526–542.

[232] J. Bernabeu, E. Nardi, and D. Tommasini, *$\mu - e$ conversion in nuclei and Z' physics*, *Nucl. Phys.* **B409** (1993) 69–86, [hep-ph/9306251].

[233] T. Suzuki, D. F. Measday, and J. P. Roalsvig, *Total nuclear capture rates for negative muons*, *Phys. Rev.* **C35** (1987) 2212.

[234] R. Kitano, M. Koike, and Y. Okada, *Detailed calculation of lepton flavor violating muon electron conversion rate for various nuclei*, *Phys. Rev.* **D66** (2002) 096002, [hep-ph/0203110].

[235] **Muon G-2** Collaboration, G. W. Bennett *et al.*, *Final report of the muon E821 anomalous magnetic moment measurement at BNL*, *Phys. Rev.* **D73** (2006) 072003, [hep-ex/0602035].

[236] K. Hagiwara, A. D. Martin, D. Nomura, and T. Teubner, *Improved predictions for g-2 of the muon and $\alpha_{\rm QED}(M_Z^2)$*, *Phys. Lett.* **B649** (2007) 173–179, [hep-ph/0611102].

[237] M. Passera, *Precise mass-dependent QED contributions to leptonic g-2 at order α^2 and α^3*, *Phys. Rev.* **D75** (2007) 013002, [hep-ph/0606174].

[238] A. Czarnecki, W. J. Marciano, and A. Vainshtein, *Refinements in electroweak contributions to the muon anomalous magnetic moment*, *Phys. Rev.* **D67** (2003) 073006, [hep-ph/0212229].

[239] A. Czarnecki, *A Finer constant*, *Nature* **442** (2006) 516–517.

[240] M. Davier, *The hadronic contribution to (g-2)(mu)*, *Nucl. Phys. Proc. Suppl.* **169** (2007) 288–296, [hep-ph/0701163].

[241] J. F. de Troconiz and F. J. Yndurain, *The hadronic contributions to the anomalous magnetic moment of the muon*, *Phys. Rev.* **D71** (2005) 073008, [hep-ph/0402285].

[242] J. Bijnens and J. Prades, *The hadronic light-by-light contribution to the muon anomalous magnetic moment: Where do we stand?*, *Mod. Phys. Lett.* **A22** (2007) 767–782, [hep-ph/0702170].

[243] S. Heinemeyer, W. Hollik, and G. Weiglein, *Electroweak precision observables in the minimal supersymmetric standard model*, *Phys. Rept.* **425** (2006) 265–368, [hep-ph/0412214].

[244] D. Stockinger, *The muon magnetic moment and supersymmetry*, *J. Phys.* **G34** (2007) R45–R92, [hep-ph/0609168].

[245] **HPQCD** Collaboration, I. Allison *et al.*, *High-Precision Charm-Quark Mass from Current-Current Correlators in Lattice and Continuum QCD*, *Phys. Rev.* **D78** (2008) 054513, [0805.2999].

[246] **Tevatron Electroweak Working Group** Collaboration, *Combination of CDF and D0 Results on the Mass of the Top Quark*, 0903.2503.

[247] S. Herrlich and U. Nierste, *Enhancement of the $K_L - K_S$ mass difference by short distance QCD corrections beyond leading logarithms*, *Nucl. Phys.* **B419** (1994) 292–322, [hep-ph/9310311].

[248] S. Herrlich and U. Nierste, *Indirect CP violation in the neutral kaon system beyond leading logarithms*, *Phys. Rev.* **D52** (1995) 6505–6518, [hep-ph/9507262].

[249] G. Buchalla, *Renormalization of $\Delta(B) = 2$ transitions in the static limit beyond leading logarithms*, *Phys. Lett.* **B395** (1997) 364–368, [hep-ph/9608232].

[250] R. Escribano and J.-M. Frere, *Study of the $\eta - \eta'$ system in the two mixing angle scheme*, *JHEP* **06** (2005) 029, [hep-ph/0501072].

[251] R. Royber and H. Hodson, *The Royber-Hodson-Plots*. Thienemann Verlag, 2005.

[252] E. Lunghi and A. Soni, *Possible Indications of New Physics in B_d -mixing and in $\sin(2\beta)$ Determinations*, *Phys. Lett.* **B666** (2008) 162–165, [0803.4340].

[253] Y. Grossman and Y. Nir, *$K_L \to \pi^0 \nu\bar{\nu}$ beyond the Standard Model*, *Phys. Lett.* **B398** (1997) 163–168, [hep-ph/9701313].

[254] M. Blanke, *Insights from the Interplay of $K \to \pi\nu\bar{\nu}$ and ε_K on the New Physics Flavour Structure*, 0904.2528.

[255] M. Beneke and M. Neubert, *QCD factorization for $B \to PP$ and $B \to PV$ decays*, *Nucl. Phys.* **B675** (2003) 333–415, [hep-ph/0308039].

[256] Z. Ligeti, M. Papucci, and G. Perez, *Implications of the measurement of the $B_s^0 - \bar{B}_s^0$ mass difference*, *Phys. Rev. Lett* **97** (2006) 101801, [hep-ph/0604112].

[257] A. J. Buras, B. Duling, and S. Gori, *The Impact of Kaluza-Klein Fermions on Standard Model Fermion Couplings in a RS Model with Custodial Protection*, *JHEP* **09** (2009) 076, [0905.2318].

[258] A. J. Buras and D. Guadagnoli, *On the consistency between the observed amount of CP violation in the K and B_d systems within minimal flavor violation*, *Phys. Rev.* **D79** (2009) 053010, [0901.2056].

[259] E. Lunghi and A. Soni, *Hints for the scale of new CP-violating physics from B-CP anomalies*, *JHEP* **08** (2009) 051, [0903.5059].

[260] **MEGA** Collaboration, M. L. Brooks *et al.*, *New Limit for the Family-Number Non-conserving Decay $\mu^+ \to e^+\gamma$*, *Phys. Rev. Lett.* **83** (1999) 1521–1524, [hep-ex/9905013].

[261] **SINDRUM** Collaboration, U. Bellgardt *et al.*, *Search for the Decay $\mu^+ \to e^+e^+e^-$*, *Nucl. Phys.* **B299** (1988) 1.

[262] **BABAR** Collaboration, B. Aubert *et al.*, *Searches for Lepton Flavor Violation in the Decays $\tau \to e\gamma$ and $\tau \to \mu\gamma$*, *Phys. Rev. Lett.* **104** (2010) 021802, [0908.2381].

[263] K. Hayasaka *et al.*, *Search for Lepton Flavor Violating τ Decays into Three Leptons with 719 Million Produced $\tau^+\tau^-$ Pairs*, *Phys. Lett.* **B687** (2010) 139–143, [1001.3221].

[264] S. Banerjee, *Searches for lepton flavor violating decays $\tau^\pm \to \ell^\pm\gamma$, $\tau^\pm \to \ell^\pm P^0$ (where $\ell^- = e^-$, μ^-, and $P^0 = \pi^0$, η, η') at B-factories: Status and combinations*, hep-ex/0702017.

[265] **BNL** Collaboration, D. Ambrose *et al.*, *New limit on muon and electron lepton number violation from $K_L^0 \to \mu^\pm e^\mp$ decay*, *Phys. Rev. Lett.* **81** (1998) 5734–5737, [hep-ex/9811038].

[266] K. Arisaka *et al.*, *Search for the lepton-family number violating decays $K_L \to \pi^0\mu^\pm e^\mp$*, *Phys. Lett.* **B432** (1998) 230–234.

[267] **CDF** Collaboration, F. Abe *et al.*, *Search for the decays B_s^0, $B_d^0 \to e^\pm\mu^\mp$ and Pati-Salam leptoquarks*, *Phys. Rev. Lett.* **81** (1998) 5742–5747.

[268] A. Brignole and A. Rossi, *Anatomy and phenomenology of μ τ lepton flavour violation in the MSSM*, *Nucl. Phys.* **B701** (2004) 3–53, [hep-ph/0404211].

[269] P. Paradisi, *Higgs-mediated $\tau \to \mu$ and $\tau \to e$ transitions in II Higgs doublet model and supersymmetry*, *JHEP* **02** (2006) 050, [hep-ph/0508054].

[270] P. Paradisi, *Higgs-mediated $e \to \mu$ transitions in II Higgs doublet model and supersymmetry*, *JHEP* **08** (2006) 047, [hep-ph/0601100].

[271] T. Feldmann, C. Promberger, and S. Recksiegel, *Characterising New Physics Models by Effective Dimensionality of Parameter Space*, 1009.5283.

Danksagung

Ich möchte diese letzte Seite dazu nutzen, meine Dankbarkeit gegenüber all jenen auszudrücken, die mich während der Zeit der Promotion und darüber hinaus begleitet und unterstützt haben.

Ganz besonders bedanke ich mich bei:

- Andrzej Buras für sein Vertrauen, die offene und humorvolle Art, mit der er an seinem Lehrstuhl für eine optimale Arbeitsatmosphäre sorgte, und für die unzähligen Hilfen bei der Erstellung dieser Arbeit.
- Der 4G-Arbeitsgruppe, bestehend aus Andrzej, Björn, Stefan, Thorsten und Tillmann, deren Teil ich sein durfte. Zusammen haben wir, in unterschiedlicher Besetzung, vier Papiere veröffentlicht [67–69, 271], welche die Grundlage dieser Arbeit bilden. Ganz besonderer Dank gebührt dabei Thorsten Feldmann, der mich lange Zeit betreut hat, für die große Unterstützung und engelsgleiche Geduld!
- Allen anderen Kollegen vom Lehrstuhl T31, die mich insgesamt vier Jahre begleitet haben, insbesondere meinem langjährigen Zimmergenossen Tillmann für die vertrauensvolle Zusammenarbeit und seine große Hilfe bei der Erstellung dieser Arbeit. Auch möchte ich Wolfi, Björn, Moni und Stefan für ihre Hilfsbereitschaft bei der Bereitstellung der Vergleichsdaten danken.
- Meinen Eltern für ihre unerschütterliche Liebe und unermüdliche Unterstützung, nicht nur in materieller sondern auch und vor allem in ideeller Form.
- Meiner Freundin Jasmin, dafür dass sie so viel Freude und Sinn in mein Leben bringt.

Ihr habt es mir ermöglicht, dass ich mich heute in dieser privilegierten Lage befinde. Dafür gebührt Euch allen mein tief empfundener Dank.